8-2013

Thermal and photochemical reactions of large metallaborane clusters and functionalizations of boron nitride nanosheets

Pei Ma

Abstract

Thermal and photochemical reactions of large metallaborane clusters and functionalizations of boron nitride nanosheets

Pei Ma
Syracuse University, August 2013

The thermal and photochemical pathways of several metallaborane compounds and the functionalization of boron nitride nanosheets have been investigated. The nanosheets have potential applications in Dye Sensitized Solar Cells.

Chapters 1 and 3 describe the thermal and photochemical pathways for two metalladecaboranes, [*nido*-6-$Mn(CO)_3B_9H_{13}$][NMe_4] (**1.1**) and [6-(η^5-C_5Me_5)-*nido*-6-RhB_9H_{13}] (**3.1**). Isomerization or cage closure reactions were observed depending on the reaction conditions and the transition metal employed. Characterized products include the first *nido*-5 metalladecaborane and a *hypercloso*-metalladecaborane containing a group 7 transitional metal, [*hypercloso*-$Mn(CO)_3B_9H_9$][NMe_4] (**1.3**) and [*arachno*-B_9H_{14}][NMe_4] (**1.4**), respectively. Other findings include the facile acid catalyzed cyclic oxonium functionalization of complex **1.1**, the role of complex **3.1** as the catalyst for the [2+2+2] cycloadditions of terminal alkynes, and the formation of *hypercloso*-rhodadecaborane **3.3** which is the first *hypercloso*-metalladecaborane containing the metal rhodium.

Chapter 2 describes investigations of the photochemical reactions between metallaboranes and unsaturated molecules. The complex **1.1** was found to photoreact with both terminal and internal alkynes to afford the carborane with general formula [7-R-8-R'-7,8-*nido*-$C_2B_9H_{10}$][NMe_4] (**2**) in good yield. This represents a novel method for generating the substituted *nido*-C_2B_9 complex. Besides alkynes, the investigation of the photoreactions of other unsaturated species with the complex **1.1** were found to generate the [*arachno*-B_9H_{14}]$^-$ (**2.4**) and [*nido*-B_9H_{12}]$^-$ (**2.5**) anions in different

relative ratios, depending on the nature of the unsaturated molecules. The complex **1.1** was also found to act as an efficient catalyst for isocyanate cyclodimerization under photo-irradiation conditions, representing the first example of a metallaborane complex to catalyse the cyclodimerization of isocyanate.

In Chapter 4, an effective and simple noncovalent functionalization and solubilization of boron nitride nanosheets (BNNSs) has been achieved by using polythiophene or polyvinylpyrrolidone as a functionalization polymer with BNNSs. The BNNSs form strong $\pi - \pi$ stacking interactions with the polythiophenes and were found to act as a bandgap tuning tool for polythiophene derivatives. A BNNS-polythiophne-TiO_2 hybrid nanomaterial was achieved by the covalent binding between TiO_2 nanoparticle surfaces and the BNNS-polythiophene unit containing a carboxylic acid functional group. This nanomaterial was then further incorporated into a Dye Sensitized Solar Cells (DSSCs) and the observed enhancement of the performance of the cells is discussed.

Thermal and photochemical reactions of large metallaborane clusters and functionalizations of boron nitride nanosheets

By

Pei Ma

B.S., Tianjin University, 2007
M.S., Syracuse University, 2013

Dissertation

Submitted in partial fulfillment of the requirements for the
degree of Doctor of Philosophy in Chemistry
in the Graduate School of Syracuse University

Syracuse University

August 2013

I would like to dedicate this thesis to my loving parents.

Acknowledgements

I would like to express my sincere thanks to my advisor Dr. James T. Spencer. I've learned so much from him over the years, and I've greatly enjoyed the fascinating Boron chemistry he introduced to me. I thank him for his support, valuable guidance and constant encouragement. I am infinitely grateful for his helps and advices during my stay at his lab as a graduate student. I would also like to thank my committee members Dr. Michael B. Sponsler, and Dr. Philip N. Borer for their helpful discussions and support of my research.

I would like to acknowledge Dr. Deborah Kerwood for her assistance in acquiring the NMR data and Tiffany Smith, and members of Dr. Jon Zubieta's research group, for obtaining the crystallographic data.

I would like to acknowledge the Department of Chemistry of Syracuse University for allowing me to carry out my research. I also thanks all members of my research group, as well as Faculty and Staff of the Department of Chemistry, for their friendly accommodation.

At last, I would like to express my deepest thanks to my parents, without whom my life would not be possible. I thank them for the love, support and encouragements.

Table of Contents

List of Tables

List of Figures

List of Compounds

1.1 [*nido*-6-$Mn(CO)_3B_9H_{13}$][NMe_4]

1.2 [*nido*-5-$Mn(CO)_3B_9H_{13}$][NMe_4]

1.3 [*hypercloso*-$Mn(CO)_3B_9H_9$][NMe_4]

1.4 [*arachno*-B_9H_{14}][NMe_4], [*arachno*-B_9H_{14}]$^-$

1.5 [*nido*-B_9H_{12}][NMe_4], [*nido*-B_9H_{12}]$^-$

1.6 [2-$(CH_2)_4O$-*nido*-6-$Mn(CO)_3B_9H_{12}$]

1.7 [2-$O(CH_2CH_2)_2O$-*nido*-6-$Mn(CO)_3B_9H_{12}$]

1.8 [2-$(CH_2)_4O$-*nido*-6-$Re(CO)_3B_9H_{12}$]

2 [7-R-8-R'-7,8-*nido*-$C_2B_9H_{10}$][NMe_4]

2a [7- n-C_4H_9-7, 8-*nido*-$C_2B_9H_{11}$][NMe_4]

2b [7, 8-Et_2-7, 8-*nido*-$C_2B_9H_{10}$][NMe_4]

2c [7- n-C_3H_7-7, 8-*nido*-$C_2B_9H_{11}$][NMe_4]

2d [7- PhC_2H_4-7, 8-*nido*-$C_2B_9H_{11}$][NMe_4]

2e [7- $SiMe_3$-7, 8-*nido*-$C_2B_9H_{11}$][NMe_4]

2f [7-$C_5H_5FeC_5H_4$-7,8-*nido*-$C_2B_9H_{11}$][NMe_4]

2f' [7-$C_5H_5FeC_5H_4$-7,8-*nido*-$C_2B_9H_{11}$]K

2g [7-C_6H_5-7,8-*nido*-$C_2B_9H_{11}$][NMe_4]

2.1 1,2-μ-$C_6H_4(CH_2)_2$-3-Ph-1,2-$C_2B_{11}H_{10}$

2.2 [1-$C_5H_5FeC_5H_4$-1,2-*closo*-$C_2B_{10}H_{11}$]

2.3 [KB_9H_{14}]

2.4 [*arachno*-B_9H_{14}]$^-$

2.5 [*nido*-B_9H_{12}][NMe_4], [*nido*-B_9H_{12}]$^-$

2.6 $[Co(CO)_3B_{10}H_{12}][NMe_4]$

2.7 *ortho*-$C_2B_{10}H_{12}$

2.8 $[nido\text{-}7,8\text{-}C_2B_9H_{12}]^-$

2.9 $[nido\text{-}7,8\text{-}C_2B_9H_{11}]^{2-}$

2.10 $[closo\text{-}1,2\text{-}Et_2\text{-}1,2\text{-}C_2B_{10}H_{10}]$

2.11 1,3-diphenyl-urea ($C_{13}H_{12}N_2O$)

3.1 $[6\text{-}(\eta^5\text{-}C_5Me_5)\text{-}nido\text{-}6\text{-}RhB_9H_{13}]$

3.2 $[5\text{-}(\eta^5\text{-}C_5Me_5)\text{-}nido\text{-}5\text{-}RhB_9H_{11}\text{-}7\text{-}(PMe_2Ph)_2]$

3.3 $[hypercloso\text{-}(\eta^5\text{-}C_5Me_5)RhB_9H_9]$

3.4 $[nido\text{-}5\text{-}(\eta^5\text{-}C_5Me_5)RhB_9H_{13}]$

3.5 $[(PPh_3)_2HIrB_9H_{13}]$

3.6 $[(PPh_3)(Ph_2PC_6H_4)HIrB_9H_{12}]$

3.7 $[(PPh_3)(Ph_2PC_6H_4)HIrB_9H_8]$

3.8 $[hypercloso\text{-}2,5\text{-}(OEt)_2\text{-}(\eta^5\text{-}C_5Me_5)RhB_9H_7]$

3.9 $[hypercloso\text{-}2,3,5\text{-}(OEt)_3\text{-}(\eta^5\text{-}C_5Me_5)RhB_9H_6]$

3.10 $[hypercloso\text{-}2,3,4,5\text{-}(OEt)_4\text{-}(\eta^5\text{-}C_5Me_5)RhB_9H_5]$

4.1 Poly[3-(4-carboxybutyl)thiophene-2,5-diyl] (PCBT)

4.2 Poly(3-hexylthiophene-2,5-diyl) (H3PT)

4.3 Poly(3-thiophenezoic acid) (PTPA)

4.4 Poly(3-thiophene acetic acid) (P3TAA)

List of Abbreviations

AANS	Acid-Assisted Nucleophilic Substitution
BNCT	Boron neutron capture therapy
BNNSs	Boron nitride nanosheets
BNNTs	Boron nitride nanotubes
CNTs	Carbon nanotubes
COSY	Correlation spectroscopy
CVD	Chemical vapor deposition
DCM	Dichloromethane
DFT	Density functional theory
DMSO	Dimethyl sulfoxide
DSD	Diamond-square-diamond
DSSCs	Dye Sensitized Solar Cells
EINS	Electrophile-Induced Nucleophilic Substitution
FTIR	Fourier transform infrared spectroscopy
GC-MS	Gas chromatographymass spectrometry
h-BN	Hexagonal boron nitride
H3PT	Poly(3-hexylthiophene-2,5-diyl)
I-V	Current-voltage curve
IPA	Isopropyl alcohol
MCPs	Metallacyclopentadiene compounds
MLCT	Metal-to-ligand charge-transfer
NMR	Nuclear magnetic resonance

ORTEP	Oak Ridge Thermal Ellipsoid Plot Program
P3TAA	Poly(3-thiophene acetic acid)
PCBT	Poly[3-(4-carboxybutyl)thiophene-2,5-diyl]
PCE	Power conversion efficiency
PEG	Poly(ethylene glycol)
PT	Polythiophene
PTPA	Poly(3-thiophenezoic acid)
PVP	Polyvinylpyrrolidone
r.t.	Room temperature
SEM	Scanning electron microscope
SEPs	Skeleton electron pairs
SL	Spectator ligands
TEM	Transmission electron microscopy
THF	Tetrahydrofuran
TLC	Thin layer chromatography
UV-Vis	Ultravioletvisible spectroscopy

Chapter 1

Chemistry of a Manganadecaborane [*nido*-6-$Mn(CO)_3B_9H_{13}$][NMe_4] (1.1)

1.1 Introduction

1.1.1 Thermal Versus Photochemical Pathways of Manganadecaborane 1.1

The 10-vertex metallaboranes are among the best-represented complexes in polyhedral metallaborane chemistry.[1] The *nido*-ten-vertex borane structure and numbering system is given in Figure 1. Replacement of BH units at the 1, 2, 5, or 6 positions give the corresponding *nido*-1, *nido*-2, *nido*-5 or *nido*-6 metalladecaborane complexes (Figure 1). Although the number of known *nido*-6-metalladecaboranes is over 60 in the literature,[1,2] other substitution of *nido*-metalladecaboranes are relatively rare.[1] To our knowledge, there are only 14 compounds known complexes that fall within the *nido*-5-metalladecaboranes category (Table 1).[1] Such metalladecaboraness are known for iron, cobalt, rhodium, iridium, ruthenium, and osmium.[1,3] Of these, seven have been characterized by single crystal X-ray diffraction studies (Table 1). In contrast, *nido*-2-metalladecaboranes are known for ruthenium, cobalt and iron[4] whereas the *nido*-1-metalladecaborane structure is only known for ruthenium.[4]

Besides the *nido*-structures, 10-vertex metalladecaboranes can also form a C_{3v} *hypercloso* geometry (Figure 2). There has been theoretical interest in closed deltahedral metallaboranes of the general formulation LMB_9H_9 (LM = metal center plus *exo*-polyhedral ligands) because of their apparent contravention of the Wade-Mingos cluster-geometry and electron-counting rules.[12–15] A conventional cluster count of

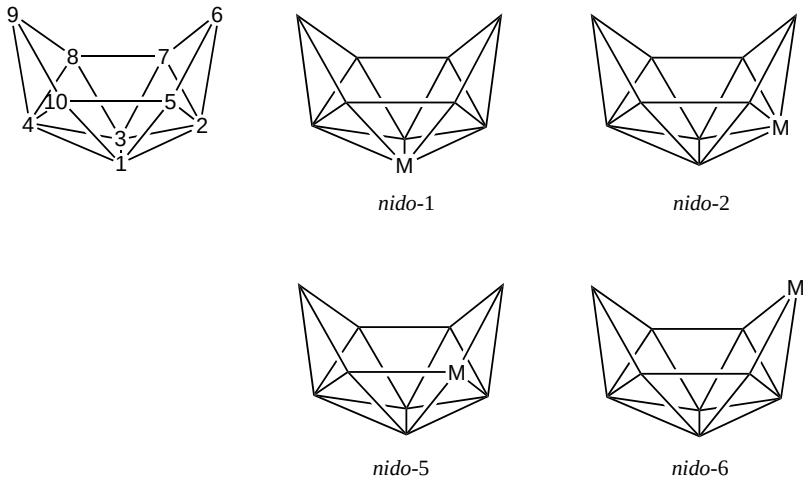

Figure 1: *Nido*-10-vertex decaborane clusters numbering system (vertex represents a BH or BH_2).

Table 1: Known *nido*-5 Metalladecaboranes

Entry	X-ray structure
$[(Me_3C_6H_3)FeB_9H_{13}]$	Yes[5]
$[(C_5H_5)CoB_9H_{13}]$	Yes[6]
$[(C_5Me_5)CoB_9H_{13}]$	
$[(Me_2C_2B_3H_5)CoB_9H_{12}$-1-(THF)]	Yes[7]
$[(Et_2C_2B_3H_5)CoB_9H_{12}$-1-(THF)]	Yes[8]
$[(Et_2C_2B_4H_4)CoB_9H_{12}$-1-(THF)]	
$[(PPh_3)(Ph_2PC_6H_4)HIrB_9H_{12}$	Yes[1]
$[(PPh_3)(Ph_2PC_6H_4)HIrB_9H_{10}$-2-7-$(PPh_3)]$	Yes[9]
$[(PPh_3)(Ph_2PC_6H_4)HIrB_9H_9Cl(PPh_3)]$	
$[(C_6Me_6)RuB_9H_{13}]$	
$[(C_5Me_5)RhB_9H_{13}]$	
$[(C_6Me_6)OsB_9H_{13}]$	
$[(C_5Me_5)IrB_9H_{13}]$	
$[(C_5Me_5)RhB_9H_{11}$-7-$(PMe_2Ph)_2]$	Yes[10]
$[(C_6Me_6)RuB_9H_{11}$-7-$(PMe_2Ph)_2]$[11]	

$2\times9+2 = 20$ leaves it two electrons short of a $2n+2 = 2\times10+2 = 22$ ($n = 10$, which is the vertex number) *closo* electron count with a geometry that is based on a C_{3v} 1:3:3:3 stack that differs from the D_{4d} antiprismatic structure expected for a conventional *closo*-species (Figure 2). There are two possibilities regarding the geometry of this type of metallaboranes proposed in literature: *hypercloso* versus *isocloso*. On the basis of electron counting arguments and by comparison to the known compounds, Baker[12] suggested that these complexes contain two skeletal electrons fewer than their *closo*-counterparts and are thus best regarded as *hypercloso*-metallaboranes. On the other hand, Kennedy and co-workers[13] treated the metal fragment as a four orbital-four electron donor toward cluster bonding so that the metal fragment donates an additional electron pair. This brings the skeleton electron pairs (SEPs) count of the cluster to n+1, that is 2n+2 skeletal electron count. Since number of SEPs is the same as that of the *closo*-structure, they considered these clusters to be the isomer of the *closo*-structure, hence the name *isocloso*. Johnston and Mingos showed,[14] using molecular orbital calculations employing the extended Huckel method, that the distortions from *closo* to *hypercloso* increases the connectivity of the metal atom with borane and provides additional stability. They further pointed out that, since these compounds with n SEPs are electron-deficient with respect to the corresponding *closo*-structures with an n+1 SEPs, the term *hypercloso* is more appropriate. In recent years, Jemmis and coworkers[15] explored the structural and electronic relationship of 9-, 10-, 11-, and 12-vertex *closo* and *hypercloso* (*isocloso*)- metallaboranes using DFT calculations. Their calculation also showed that n vertex *hypercloso* structures need only n skeleton electron pairs and thus favoured the *hypercloso* term. Here, we use the *hypercloso* terminology to describe this geometry.

The studies of these species are, however, inhibited by the paucity of high yield routes for their synthesis. Similar to the *nido*-5-metalladecaboranes, there are only

ten experimentally characterized compounds in the *hypercloso*-metalladecaborane structural category (Table 2).[2,5,16–20]

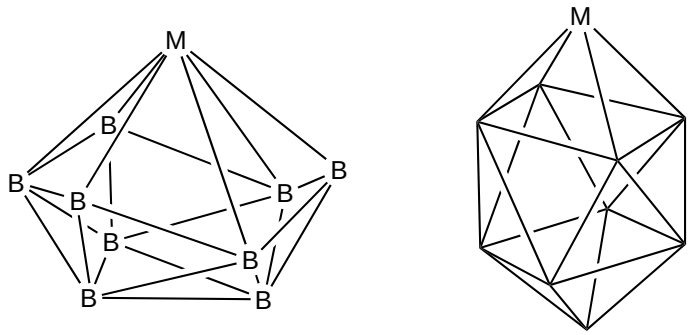

Figure 2: *Hypercloso*-metalladecaborane(left) and *closo*-metalladecaborane(right) geometries.

Table 2: Known *hypercloso*-metalladecaboranes

Entry	X-ray structure
$[(PPh_3)(Ph_2PC_6H_4)HIrB_9H_8]$	Yes[2]
$[(PMe_3)_2HIrB_9H_9]$	
$[(C_8H_{12})IrB_9H_9]$	
$[(C_6Me_6)RuB_9H_9]$	
$[(pcym)RuB_9H_9]^a$	Yes[18]
$[(PPh_3)ClHRuB_9H_7(PPh_3)_2]$	Yes[20]
$[(C_6Me_6)(PhNH)RuB_9H_8]$	Yes[19]
$[(C_6Me_6)(PhNH)_2RuB_9H_7]$	
$[(C_6Me_6)(PhNH)_3RuB_9H_6]$	
$[(PPh_3)RuB_9H_9\{RuCl_2(PPh_3)_2\}_2]$	Yes[17]
$[C_6(CH_3)_3FeB_9H_9]$	

[a] pcym is the benzenoid species *para*-cymene

In considering the large number of known *nido*-6-metalladecaboranes,[1] it is very unusual that only a small number of either *nido*-5- or *hypercloso*-metalladecaboranes have been reported and further that no known *nido*-5- or *hypercloso*-metalladecaboranes are known from metals other than the group 8 and 9 metals (Figure 3).

During our investigation reported here of the chemical behavior of metalladecaboranes under thermal and photochemical conditions, we found that under

3	4	5	6	7	8	9	10	11	12
Scandium 21 **Sc** 44.96	Titanium 22 **Ti** 47.88	Vanadium 23 **V** 50.94	Chromium 24 **Cr** 52.00	Manganese 25 **Mn** 54.94	Iron 26 **Fe** 55.85	Cobalt 27 **Co** 58.93	Nickel 28 **Ni** 58.69	Copper 29 **Cu** 63.55	Zinc 30 **Zn** 65.39
Yttrium 39 **Y** 88.91	Zirconium 40 **Zr** 91.22	Niobium 41 **Nb** 92.91	Molybdenum 42 **Mo** 95.94	Technetium 43 **Tc** (98)	Ruthenium 44 **Ru** 101.07	Rhodium 45 **Rh** 102.91	Palladium 46 **Pd** 106.42	Silver 47 **Ag** 107.87	Cadmium 48 **Cd** 112.41
Lutetium 71 **Lu** 174.97	Hafnium 72 **Hf** 178.49	Tantalum 73 **Ta** 180.95	Tungsten 74 **W** 183.84	Rhenium 75 **Re** 186.21	Osmium 76 **Os** 190.23	Iridium 77 **Ir** 192.22	Platinum 78 **Pt** 195.08	Gold 79 **Au** 196.97	Mercury 80 **Hg** 200.59
Lawrencium 103 **Lr** (262)	Rutherfordium 104 **Rf** (267)	Dubnium 105 **Db** (268)	Seaborgium 106 **Sg** (271)	Bohrium 107 **Bh** (272)	Hassium 108 **Hs** (270)	Meitnerium 109 **Mt** (276)	Darmstadtium 110 **Ds** (281)	Roentgenium 111 **Rg** (280)	Copernicium 112 **Cn** (285)

Figure 3: Metals reported in known *nido*-5-metallodecaboranes.

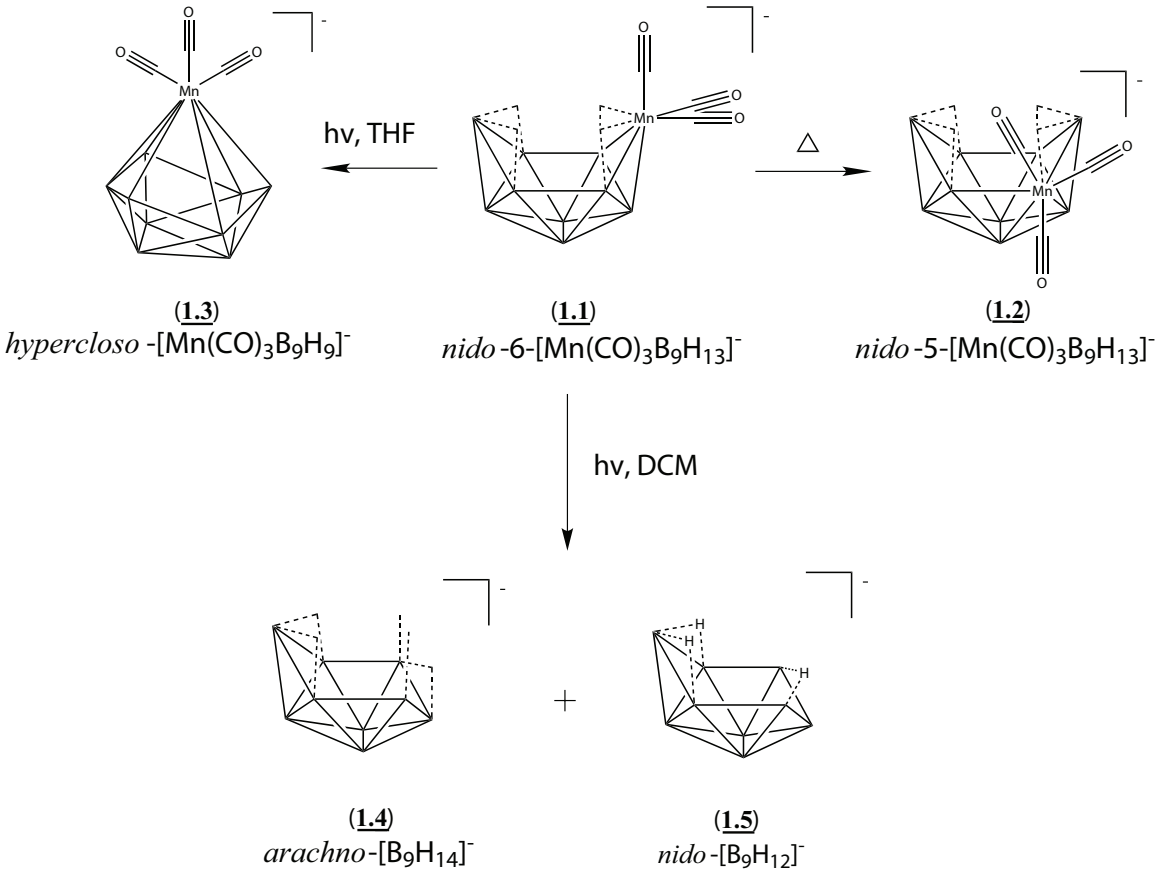

Figure 4: Thermal and photochemical conversion of complex **1.1** (each vertex represents a BH or BH_2 unit).

thermal conditions, the *nido*-6 manganadecaborane [*nido*-6-$Mn(CO)_3B_9H_{13}$][NMe_4] (**1.1**)[21] undergoes isomerization to previously unknown *nido*-5-metalladecaborane: the [*nido*-5-$Mn(CO)_3B_9H_{13}$][NMe_4] (**1.2**). Under UV irradiation, however, the complex **1.1** is either converted into the *hypercloso*-manganadecaborane [*hypercloso*-$Mn(CO)_3B_9H_9$][NMe_4] (**1.3**) (Figure 4) or to the mono polyhedral anions [*arachno*-B_9H_{14}][NMe_4] (**1.4**) and [*nido*-B_9H_{12}][NMe_4] (**1.5**) depending on the solvent employed (Figure 4, some preliminary results of the photochemical conversion in THF was reported before by our group[22]).

Herein, we describe the synthesis and structural characterization of the new *nido*-5-metalladecaborane, complex **1.2**, together with the photolytic synthesis of the *hypercloso*-manganadecaborane, **1.3**. The photolytic pathways from metallaborane **1.1** to boron cluters **1.4** and **1.5** are also discussed. Although both ^{11}B NMR and ^{1}H NMR spectra were presented in the original paper, no structural characterization via X-ray diffraction studies were reported for the starting manganadecaborane **1.1**.[21] We also, therefore, examined this compound with X-ray diffraction techniques and compared its structure with that of its 5-substituted isomer **1.2**.

To our knowledge, the manganese containing complexes **1.2** and **1.3** are the first *nido*-5-metalladecaborane and *hypercloso*-metalladecaboranes reported containing a Group 7 transition metal. The photogenerated *hypercloso*-manganadecaborane also presents a rare example of photochemically generated *hypercloso*-metalladecaborane. It suggests that photochemistry may be an alternative pathway for experimentally realizing the synthesis of metal inserted decaboranes of this type.

1.1.2 Functionalization of Manganadecaborane 1.1 using Cyclic Oxonium Derivatives

The high stability of polyhedral boron hydrides opens the way to their practical use in various fields. In recent years, there has been growing interest in boron cluster

compounds chemistry.[23,24] These compounds have found applications in fields such as catalysts,[25–27] nuclear waste processing,[28,29] microelectronics, non-linear optics,[30–33] medicine,[34] stationary phase in HPLC,[35] molecular imaging,[36–38] Hydrogen Storage Metal Organic Frameworks (HSMOF),[39,40] redox-couple in Dye Sensitized Solar Cells (DSSCs),[41] and as building blocks for self-assembled monolayers on metal surfaces.[42]

However, to realize their full potential for these and other applications, the development of functionalization methods are required. To appreciate the important role of the functionalization of these species, an illustrative example would be "click chemistry". In 2001, Sharpless and coworkers introduced the concept of "click chemistry" that refers to facile, efficient, selective and versatile chemical transformations that leads to a single reaction product.[43,44] This has become one of the most visible trends in contemporary synthesis chemistry.[45] Numerous examples of the versatile utilization and modification of these reactions have been seen since its introduction.[46] They include applications to surfaces,[47] materials,[48] polymers and macromolecules,[49] pharmaceuticals[50] and in bioconjugates.[51] Similarly, the development of new and convenient ways of functionalizing metallaboranes will greatly promote the utilization of them in both fundamental and practical applications.

In 2000, nucleophilic ring-opening of cyclic oxonium derivatives of the *closo*-dodecaborate anion $[B_{12}H_{12}]^{2-}$ was proposed to be a new synthetic methodology for the preparation of a wide spectrum of the $[B_{12}H_{12}]^{2-}$ functional derivatives.[52] The general scheme employed in this method is shown in Figure 5. Since then, this methodology has also been applied to the synthesis of functional derivatives of cobalt bis(dicarbollide) [3,3-Co(1,2-$C_2B_9H_{11})_2]^-$,[28,53,54] and *closo*-decaborate $[B_{10}H_{10}]^{2-}$.[55,56]

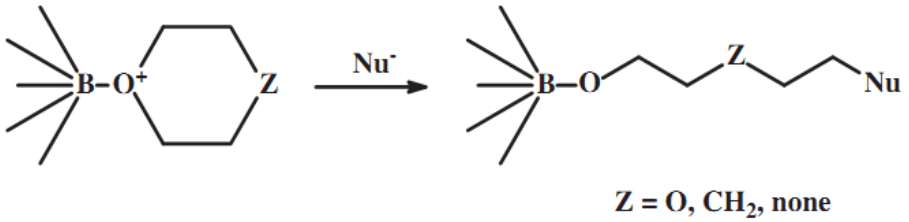

Figure 5: General scheme of the oxonium ring disclosure in boron hydride derivatives.[57]

In order to expand the scope of this strategy, we used the manganadecaborane (**1.1**) as a model compound and studied its functionalization utilizing this methodology. We, therefore, describe here the syntheses of the cyclic oxonium manganadecaborane derivatives **1.6** and **1.7** together with their potential applications for the synthesis of functionalized manganadecaboranes. We also report the crystal structure of a rhenium analog of the complex **1.6**, the [2-$(CH_2)_4$O-*nido*-6-Re$(CO)_3B_9H_{12}$] (**1.8**) (Figure 6).

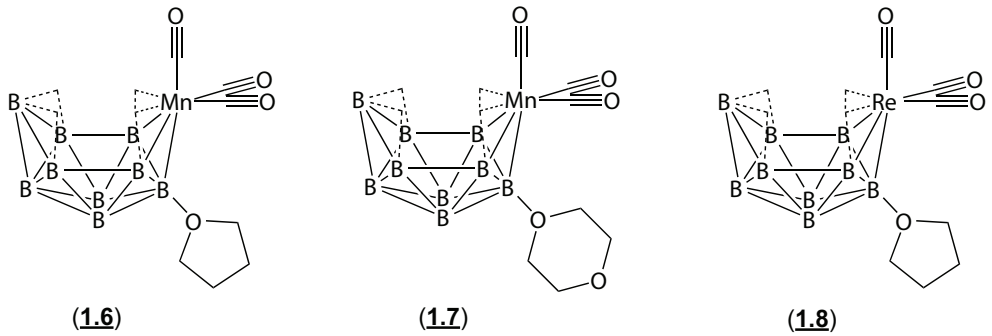

Figure 6: Structures of complexes **1.6**, **1.7** and **1.8**.

1.2 Experimental

1.2.1 Physical Measurements

All NMR spectra were recorded on a Bruker Avance 300 MHz NMR equipped with a 5 mm OXI probe. The ^{11}B NMR spectra were recorded at 96.3 MHz and were referenced at 96.3 MHz. Spectra were referenced to BBr_3 at +40.0 ppm (relative to BF_3Et_2O at $\delta = 0.0$ ppm) with positive chemical shifts indicating downfield resonances. Typical ^{11}B NMR acquisition parameters employed were a relaxation delay of 0.1 ms and a 90° pulse of 10 μs. As previously described, an absolute-value-mode COSY pulse sequence[58] was used to generate the t_1, t_2 data matrix (relaxation delay $-(\pi/2) - t_1 - (\pi/2) - t_2$ in which t_1 was incremented by the inverse of the sweep width in the F_1 dimension and t_2 was the usual acquisition time in a 1D experiment). The t_1, t_2 matrix was collected as 1024×256 data points. Data processing involved the application of a dc offset and first-point correction, shifted sine bell apodization, zero filling, Fourier transformation, and a magnitude calculation to give the 512×512 2D ^{11}B-^{11}B $\{^1H\}$ spectrum.[59,60] Proton (^{1}H) NMR spectra were recorded at 300.15 MHz with chemical shifts referenced to an internal standard of tetramethylsilane at δ=0.0 ppm. Carbon (^{13}C) NMR spectra were obtained at 77.47 MHz. Unit resolution mass spectra were obtained on a Hewlett Packard model 5989B gas chromatograph/mass spectrometer (GC/MS) using an ionization potential of between 11 and 70 eV. FT-IR spectra in the range of 400 to 4000 cm^{-1} were measured on a Mattson Galaxy 2020 spectrometer and were referenced to the 1602.8 cm^{-1} band of polystyrene. The spectra were observed as KBr mulls and are reported in cm^{-1}. UV-Vis spectral data were collected on a Cary 1 UV-Vis spectrophotometer in a quartz cell. All photoreactions were carried out under a medium pressure mercury vapor lamp (ACE GLASS, Model: Hanovia, 7825-34, IMMERSION LAMP, Medium Pressure, 450 watt).

1.2.2 Materials

All solvents employed were reagent grade or better. Tetrahydrofuran (THF) and hexane were distilled from potassium metal prior to use. TLC plates were purchased from Fisher Scientific. The *nido*-decaborane(14) ($B_{10}H_{14}$), was purchased from the Callery Chemical Company and was purified by vacuum sublimation at 40 °C prior to use. Appropriate care was taken in handling the boron hydrides under inert atmosphere conditions.[61] All reactions were done in an inert atmosphere unless otherwise noted. Deuterated NMR solvents were purchased from Cambridge Isotope Laboratories, Inc. and dried over molecular sieves before use, unless otherwise noted. All other commercially available reagents were used as received. The manganadecaborane **1.1** ([*nido*-6-$Mn(CO)_3B_9H_{13}$][NMe_4]) was synthesized by a modified literature procedure.[21]

1.2.3 Synthesis

[*Nido*-6-$Mn(CO)_3B_9H_{13}$][NMe_4] (**1.1**) $Mn(CO)_5Br$ (1.38 g, 5.00 mmol) and freshly prepared $K[B_9H_{14}]$[62] (0.75 g, 5.00 mmol) were heated to reflux in 50 mL Tetrahydrofuran(THF) for 1.5 h. After cooling to room temperature, the solvent was removed by distillation under vacuum until only a dark red oil remained. To this mixture 1.5 g of NMe_4Cl in 50 mL of distilled water was then added. The resultant precipitate was collected and applied to a silica column (10 × 1 cm). Using dichloromethane/hexane (9:1) as eluting solvent a red band was collected. The product was recrystallized from dichloromethane/heptane (3:1) and then washed with hexane to give 0.6 g (yield 52%) of complex **1.1** as a red crystalline material. The ^{11}B NMR spectrum is essentially identical to the data in reported work.[21]

[*Nido*-5-$Mn(CO)_3B_9H_{13}$][NMe_4] (**1.2**) Complex **1.1** (0.10 g, 0.30 mmol) in 10 mL of sodium-dried mesitylene was refluxed under dry nitrogen for 1 hr. After cooling to r.t., the solvent was removed on the vacuum line. The residue was then chromatographed on a 10 × 1 cm column of silica gel, eluting with chloroform. A

fast-moving orange-brown band was collected. After solvent removal, this orange-brown was recrystallized from its saturated solution in dichloromethane-ethanol (2:1) and then washed with cold hexane to give 0.09 g of [*nido*-5-$Mn(CO)_3B_9H_{13}$][NMe_4] (**1.2**) (yield 90%). ^{11}B NMR (CD_2Cl_2), δ (ppm): +23.7 (d, 1B, B(6), J_{BH}=130 Hz), +20.3 (d, 1B, B(1), J_{BH}=115 Hz), +10.8 (d, 1B, B(3), J_{BH}=136 Hz), +0.5 (d, 4B, B(7,9,8,10), J_{BH}=125 Hz), -24.7 (d, 1B, B(2), J_{BH}=128 Hz), -35.3 (d, 1B, B(4), J_{BH}=147 Hz). FTIR (cm^{-1}): 2524.9 (B-H), 2013.8, 1935.1 (MCO), 1698.2. ^{1}H (CD_2Cl_2), δ(ppm): -0.27 (4H), 1.20 (3H), 1.29 (1H), 2.09 (12H), 2.15 (1H), 2.61 (1H), 2.85 (2H), 3.81 (1H).

[***Hypercloso*-$Mn(CO)_3B_9H_9$][NMe_4]** (**1.3**) 0.02 g (0.06 mmol) of complex (**1.1**) in 2 mL degassed THF was placed in a quartz NMR tube under dry nitrogen. The solution was then irradiated in a quartz photochemical reactor for 10 min. Partial of the starting material was converted to complex **1.3**, as indicated by NMR. ^{11}B NMR (CD_2Cl_2), δ (ppm): +110.0 (d,3B,B(2,3,4), J_{BH}=153 Hz), +28.4(d,3B,B(8,9,10), J_{BH}=135 Hz), -14.8(d, 3B, B(5,6,7), J_{BH}=139 Hz). Longer time of irradiation leaded all boron containing compounds to degradation.

[***Arachno*-B_9H_{14}][NMe_4]** (**1.4**) and [***nido*-B_9H_{12}][NMe_4]** (**1.5**): Complex (**1.1**) (0.02 g, 0.08 mmol) in 2 mL dichloromethane (DCM) was placed in a NMR tube. The solution was irradiated in a quartz photochemical reactor for 20 min. The main product in the solution after the irradiation was the complex **1.4**, as indicated by the ^{11}B NMR data. ^{11}B NMR for complex **1.4** (CD_2Cl_2, δ (ppm), s=singlet, d=doublet): -7.16 (d, 3B, J_{BH}=134 Hz), -20.05 (d, 3B, J_{BH}=128 Hz), -22.99(d, 3B, J_{BH}=133 Hz). The ^{11}B NMR spectra of complex **1.4** are essentially identical to literature values for the complex [KB_9H_{14}],[62] although the ^{11}B NMR spectra for complex **1.5** was not resolved due to the low concentration. It was identified as complex **1.5** through the comparison of its ^{11}B NMR with literature compounds.[63]

[2-$(CH_2)_4$O-*nido*-6-$(CO)_3B_9H_{12}$] (**1.6**) Concentrated HCl (10 mL) and 37% aqueous formaldehyde (10 mL, 0.14 mol) were added dropwise to a well stirred solution of 0.95 g (2.9 mmol) complex **1.1** in 25 mL of tetrahydrofuran and the reaction mixture was stirred at room temperature for 10 min. The solvent was distilled off under vacuum from the reaction mixture and the residue was chromatographed on silica gel column (10 × 1 cm) and eluted with DCM/hexane (v/v = 3/2). After drying *in vacuo*, it gave 0.84 g (90%) of the product **1.6**. ^{11}B NMR (CD_2Cl_2, δ (ppm)): +12.34 (d, 2B J_{BH}=143 Hz), +9.47 (d, 2B J_{BH}=133 Hz), +0.16 (d, 1B J_{BH}=133 Hz), -2.43 (d, 2B J_{BH}=132 Hz), -4.38 (d, 1B J_{BH}=139 Hz), -34.3 (d, 1B J_{BH}=134 Hz). The ^{11}B NMR spectrum are essentially identical to the data reported previously.[21]

[2-O$(CH_2CH_2)_2$O-*nido*-6-Mn$(CO)_3B_9H_{12}$] (**1.7**) 1,4-dioxane (0.7 mL, 5.5 mmol), concentrated HCl (10 mL) and 37% aqueous formaldehyde (10 mL, 0.14 mol) were added dropwise to a well stirred solution of 0.95 g (2.9 mmol) complex **1.1** in 25 mL of dichloromethane. The reaction mixture was stirred at room temperature for 15 min. The solvent was distilled off under vacuum from the reaction mixture and the residue was chromatographed on silica gel column (10 × 1 cm) with ethyl acetate as eluent. After drying *in vacuo*, 0.84 g (86%) of the product **1.7** was isolated. ^{11}B NMR (CD_2Cl_2), δ (ppm): 14.7(d, 2B, J_{BH}=133 Hz), 11.74(s, 1B), 4.34(d, 1B, J_{BH}=135 Hz), -1.92 (s, 4B), -34.437 (d, 1B, J_{BH}=135 Hz).

[2-$(CH_2)_4$O-*nido*-6-Re$(CO)_3B_9H_{12}$] (**1.8**) $Re(CO)_5Br$ (2.03 g, 5.00 mmol), tetrahydrofuran (0.40 mL, 5.00 mmol) and freshly prepared $K[B_9H_{14}]$[62] (0.75 g, 5.00 mmol) were heated to reflux in 50 mL toluene for 1.5 h under nitrogen. After cooling to room temperature, the solvent was removed by distillation under vacuum until only a dark red oil remained. The residue was then applied to a silica column (10 × 1 cm). A red band was collected using dichloromethane/hexane (8:1) as eluting solvent. The product was recrystallized from dichloromethane/heptane (3:1) and then washed with

hexane to give 0.72 g (yield 32%) of complex **1.8** as brown-black crystals. The ^{11}B NMR spectrum is essentially identical to that previously reported.[21]

1.2.4 X-ray Crystallographic Studies

Crystallographic studies of compounds **1.1** and **1.2** were completed. The X-ray crystal structure of **1.7** and a determination of the analogous structure of **1.8** were also carried out. Structure for **1.6**, originally determined in 1973 by Lott and coworkers,[64] was also redetermined for purposes of direct comparison with the complex **1.7**.

Suitable crystals of **1.1**, **1.2**, **1.6**, **1.7** and **1.8** were grown either from the slow evaporation of concentrated dichloromethane (1,4-dioxane for **1.7**) solutions or by using either slow vapor or solution diffusion methods. Suitable crystals were selected under a microscope, attached to a glass fiber, and immediately placed in the low temperature nitrogen stream of the diffractometer.[65] Crystallographic data for all compounds was collected on a Bruker KAPPA APEX DUO diffractometer using Mo-K_α radiation ($\lambda = 0.71073$ Å) with a APEX II CCD system.[66] All data collections were taken at low temperature (90 K). The data were corrected for Lorentz and polarization effects,[67] and adsorption corrections were made using *SADABS*.[68] Structures were solved by direct methods. Refinements for each structure were carried out using the SHELXTL[69] crystallographic software. Following assignment of all non-hydrogen atoms, the models were refined against F^2 first using isotropic and then using anisotropic thermal displacement parameters. The hydrogen atoms were introduced in calculated positions and then refined isotropically. Neutral atom scattering coefficients along with anomalous dispersion corrections were taken from the International Tables, Vol. C.

The molecular structures of the compounds **1.1** together with **1.2**, **1.6** together with **1.7**, and **1.8** are shown in Figure 7, Figure 10 and Figure 12, respectively. For the corresponding crystallographic details, see Table 3, Table 8 and Table 11, respectively.

Table 3: Crystallographic Data for Compounds **1.1** and **1.2**.

	1.1	**1.2**
empirical formula	$MnB_9H_{25}C_7O_3N$	$MnB_9H_{25}C_7O_3N$
formula weight	323.51	323.51
crystal system	orthorhombic	monoclinic
space group	Pnnm	$P2_1/c$
a (Å)	7.9777(16)	8.1221(6)
b (Å)	14.618(3)	15.5394(11)
c (Å)	14.618(3)	14.0640(10)
α (°)	90	90(2)
β (°)	90	97.9330(10)
γ (°)	90	90
V (Å^3)	1737.5(6)	1758.1(2)
Z	8	4
T (K)	90(2)	296(2)
D_{calc} (g/cm^3)	1.221	1.222
$F(000)$	656	672
crystal size (mm^3)	$0.17 \times 0.1 \times 0.06$	$0.12 \times 0.08 \times 0.04$
θ range (deg)	1.95 to 28.28	2.53 to 32.26
index ranges	-3≤h≤10, -19≤k≤12, -18≤l≤19	-12≤h≤12, -23≤k≤23, -21≤l≤21
goodness of fit (GOF)	1.138	1.105
no. of reflns collected	9823	31352
no. of independent reflns	2229 [R(int) = 0.0438]	6207 [R(int) = 0.0331]
no. of parameters	107	194
wavelength (Å)	0.71073	0.71073
final R indices [I > $2\sigma(I)$]	$R_1 = 0.0944$ $wR_2 = 0.2743$	$R_1 = 0.0442$ $wR_2 = 0.1438$
final R indices (all data)	$R_1 = 0.1053$ $wR_2 = 0.2807$	$R_1 = 0.0587$ $wR_2 = 0.1538$
largest diff. peak and hole ($e^-/\AA^3$)	2.002 and -0.945	0.971 and -0.317

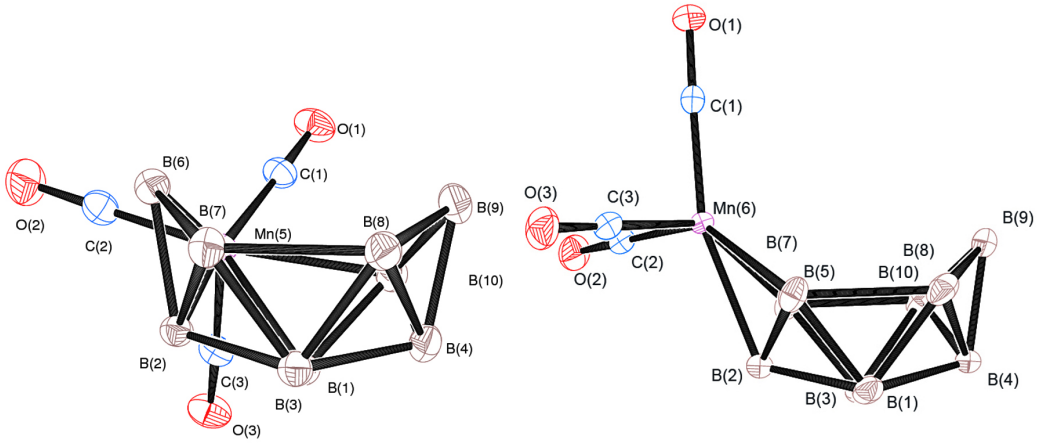

Figure 7: ORTEP drawings of the crystallographically-determined molecular structures of complexes [*nido*-6-$Mn(CO)_3B_9H_{13}$][NMe_4](**1.1**) (right) and [*nido*-5-$Mn(CO)_3B_9H_{13}$][NMe_4](**1.2**) (left) as determined in their $[NMe_4]^+$ salt. Hydrogen atoms are omitted for clarity, and thermal ellipsoids are drawn with 50% probability.

Table 4: Selected Bond Distances(Å) for Complex **1.2** with estimated standard deviations in parentheses.

bond	distance	bond	distance
Mn(5)-B(10)	2.342(2)	Mn(5)-C(1)	1.806(2)
Mn(5)-B(6)	2.160(2)	O(1)-C(1)	1.147(3)
Mn(5)-B(1)	2.222(2)	O(2)-C(2)	1.150(3)
Mn(5)-B(2)	2.256(2)	O(3)-C(3)	1.150(2)
B(1)-B(10)	1.760(3)	B(3)-B(8)	1.752(3)
B(1)-B(3)	1.787(3)	B(3)-B(4)	1.762(3)
B(1)-B(2)	1.803(3)	B(4)-B(9)	1.721(3)
B(1)-B(4)	1.826(3)	B(4)-B(8)	1.784(3)
B(2)-B(6)	1.749(3)	B(4)-B(10)	1.799(3)
B(2)-B(3)	1.788(3)	B(6)-B(7)	1.809(3)
B(2)-B(7)	1.797(3)	B(7)-B(8)	1.965(3)
B(3)-B(7)	1.750(3)	B(8)-B(9)	1.805(3)
B(9)-B(10)	1.807(3)		

Table 5: Selected Bond Angles (°) for Complex **1.2** with estimated standard deviations in parentheses.

angle	value	angle	value
C(1)-Mn(5)-C(3)	94.69(9)	C(1)-Mn(5)-B(1)	124.41(9)
C(1)-Mn(5)-C(2)	91.30(9)	C(3)-Mn(5)-B(1)	78.87(8)
C(3)-Mn(5)-C(2)	89.65(9)	C(2)-Mn(5)-B(1)	142.95(9)
C(1)-Mn(5)-B(6)	124.04(8)	B(6)-Mn(5)-B(1)	85.68(8)
C(3)-Mn(5)-B(6)	140.05(9)	C(1)-Mn(5)-B(2)	161.72(8)
C(2)-Mn(5)-B(6)	80.90(9)	C(3)-Mn(5)-B(2)	98.71(8)
C(2)-Mn(5)-B(2)	101.11(9)	B(6)-Mn(5)-B(2)	46.59(8)
C(1)-Mn(5)-B(10)	81.99(9)	B(1)-Mn(5)-B(2)	47.48(8)
C(3)-Mn(5)-B(10)	96.96(9)	B(1)-Mn(5)-B(10)	45.26(8)
C(2)-Mn(5)-B(10)	170.92(9)	B(6)-Mn(5)-B(10)	97.75(8)
B(2)-Mn(5)-B(10)	84.09(8)		
B(10)-B(1)-Mn(5)	70.99(11)	B(1)-B(2)-Mn(5)	65.27(9)
B(3)-B(1)-Mn(5)	116.57(12)	B(2)-B(6)-Mn(5)	69.59(10)
B(2)-B(1)-Mn(5)	67.25(9)	B(7)-B(6)-Mn(5)	117.05(12)
B(4)-B(1)-Mn(5)	122.41(13)	B(1)-B(10)-Mn(5)	63.75(10)
B(6)-B(2)-Mn(5)	63.81(9)	B(4)-B(10)-Mn(5)	117.54(13)
B(3)-B(2)-Mn(5)	114.90(12)	B(9)-B(10)-Mn(5)	120.12(13)
B(7)-B(2)-Mn(5)	113.02(12)		
B(6)-B(2)-B(3)	111.08(15)	B(3)-B(7)-B(8)	55.93(11)
B(6)-B(2)-B(7)	61.32(12)	B(9)-B(8)-B(7)	119.20(15)
B(3)-B(2)-B(7)	58.42(12)	B(4)-B(9)-B(8)	60.75(13)
B(6)-B(2)-B(1)	114.07(15)	B(8)-B(9)-B(10)	105.82(16)
B(3)-B(4)-B(8)	59.21(12)	B(1)-B(10)-B(9)	108.82(16)
B(1)-B(10)-B(4)	61.72(13)	B(8)-B(4)-B(1)	105.65(15)
B(9)-B(4)-B(1)	109.69(16)	B(3)-B(4)-B(1)	59.73(12)
O(1)-C(1)-Mn(5)	176.05(18)	O(2)-C(2)-Mn(5)	179.1(2)
O(3)-C(3)-Mn(5)	177.47(19)		

Table 6: Selected Bond Distances(Å) for Complex **1.1** with estimated standard deviations in parentheses.

bond	distance	bond	distance
Mn(6)-B(5)	2.230(6)	B(5)-B(10)	2.025(9)
Mn(6)-B(2)	2.218(8)	B(2)-B(5)	1.796(8)
Mn(6)-C(1)	1.775(8)	B(3)-B(9)	1.714(12)
B(1)-B(2)	1.772(10)	B(9)-B(10)	1.773(9)
B(1)-B(5)	1.764(9)	B(2)-B(4)	1.772(13)
B(2)-B(10)	1.758(9)	O(1)-C(1)	1.169(10)
B(3)-B(10)	1.790(8)	O(2)-C(2)	1.149(7)
B(2)-B(3)	1.791(10)		

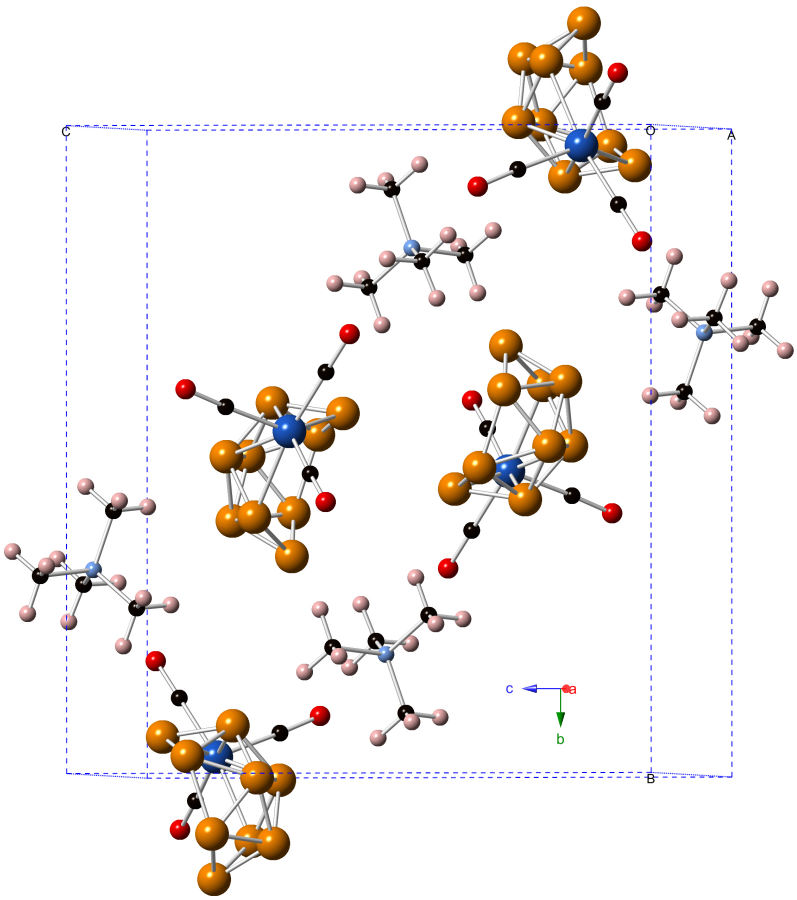

Figure 8: Partial packing diagram and unit cell of the crystal structure of complex **1.2**.

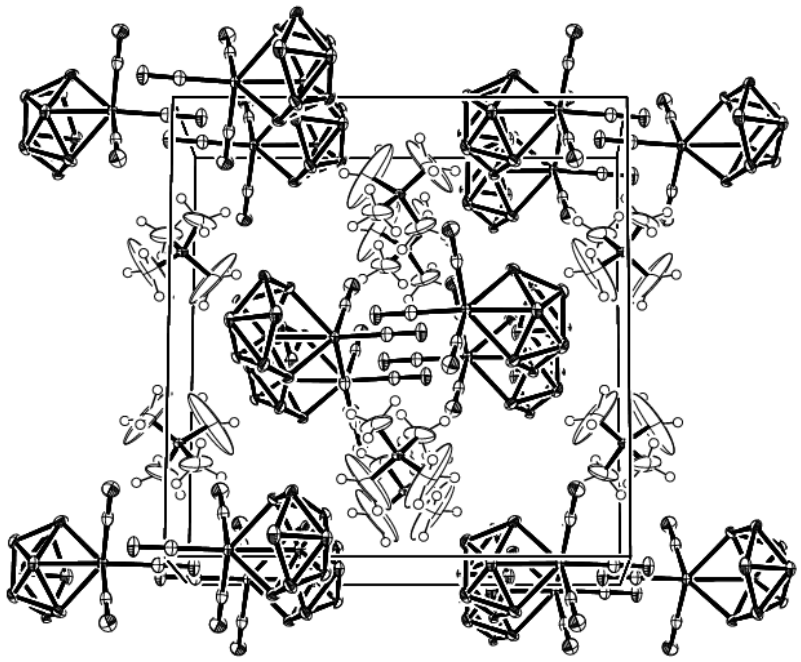

Figure 9: Partial packing diagram and unit cell of the crystal structure of complex **1.1**.

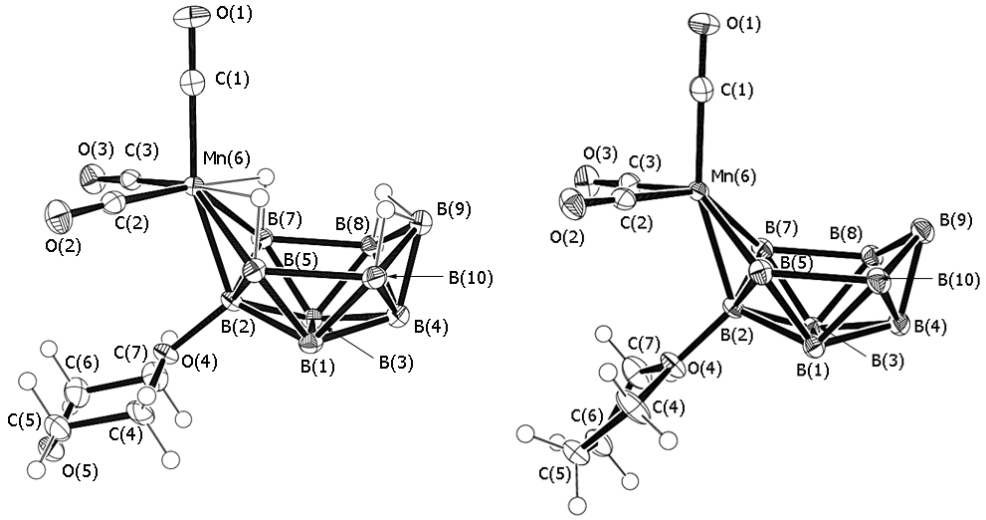

Figure 10: ORTEP drawing of the crystallographically-determined molecular structures of complexes [2-$O(CH_2CH_2)_2O$-*nido*-6-$Mn(CO)_3B_9H_{12}$](**1.7**) (on left) and [2-$(CH_2)_4O$-*nido*-6-$Mn(CO)_3B_9H_{12}$] (**1.6**) (on right). Hydrogen atoms are omitted for clarity, and thermal ellipsoids are drawn with 50% probability.

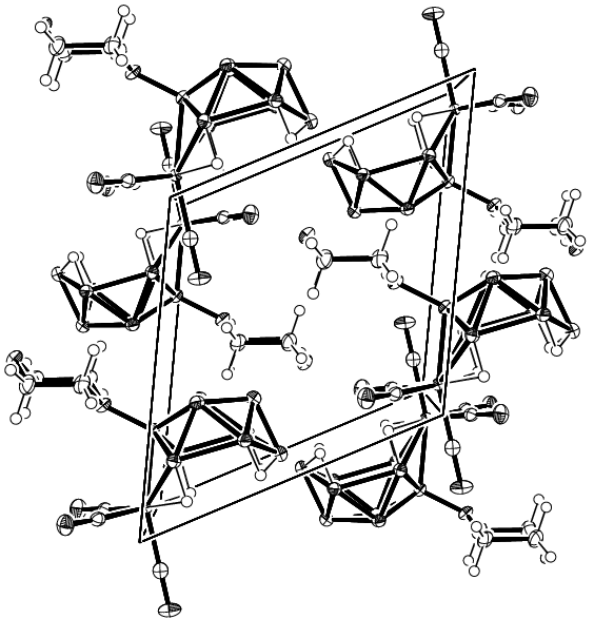

Figure 11: Partial packing diagram and unit cell of the crystal structure of complex **1.6**.

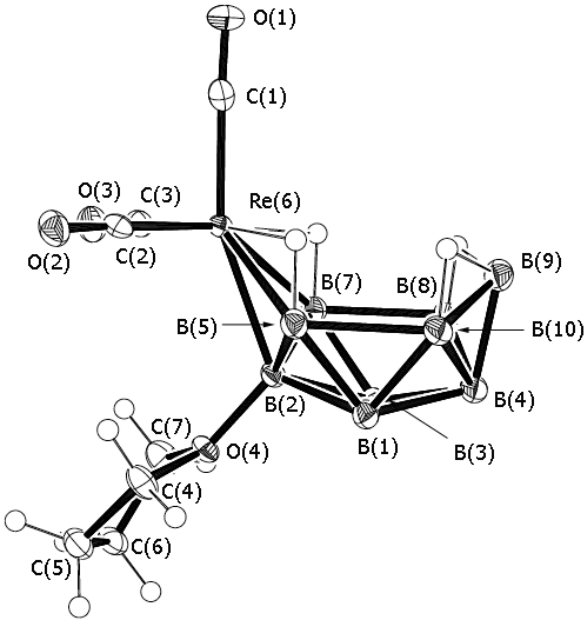

Figure 12: ORTEP drawing of the crystallographically-determined molecular structure of [2-$(CH_2)_4$O-*nido*-6-Re$(CO)_3B_9H_{12}$](**1.8**). Hydrogen atoms are omitted for clarity, and thermal ellipsoids are drawn with 50% probability.

Table 7: Selected Bond Angles(°) for Complex **1.1** with estimated standard deviations in parentheses.

angle	value	angle	value
C(1)-Mn(6)-C(2)	92.2(2)	C(1)-Mn(6)-B(5)	122.6(2)
C(2)-Mn(6)-C(3)	91.4(4)	C(2)-Mn(6)-B(5)	83.2(2)
C(1)-Mn(6)-B(1)	162.3(3)	B(1)-Mn(6)-B(5)	47.6(2)
C(2)-Mn(6)-B(1)	100.1(2)	B(5)-Mn(6)-B(7)	81.7(3)
B(2)-B(5)-Mn(6)	119.5(4)	B(10)-B(5)-Mn(6)	122.5(3)
B(1)-B(5)-Mn(6)	65.8(3)	B(5)-B(1)-Mn(6)	66.5(3)
B(1)-B(2)-B(3)	114.5(4)	B(3)-B(9)-B(8)	61.7(3)
B(1)-B(2)-B(5)	61.0(3)	B(10)-B(9)-B(8)	106.1(6)
B(3)-B(2)-B(10)	60.6(4)	B(9)-B(3)-B(10)	60.7(3)
B(5)-B(2)-B(10)	70.2(4)	B(9)-B(3)-B(2)	110.0(5)
B(10)-B(2)-B(4)	107.6(3)	B(10)-B(3)-B(8)	104.7(6)
B(5)-B(2)-B(4)	108.9(3)	B(10)-B(3)-B(2)	58.8(4)
B(1)-B(2)-B(4)	60.0(2)	B(9)-B(3)-B(4)	110.0(5)
B(3)-B(2)-B(4)	60.3(3)	B(2)-B(3)-B(4)	59.3(5)
B(3)-B(9)-B(10)	61.7(3)	B(2)-B(10)-B(9)	108.8(5)
B(2)-B(10)-B(3)	60.6(4)	B(2)-B(5)-B(10)	54.8(3)
B(9)-B(10)-B(3)	57.5(4)	B(1)-B(5)-B(10)	104.4(4)
B(2)-B(10)-B(5)	55.0(3)	B(2)-B(1)-B(5)	60.0(5)
B(9)-B(10)-B(5)	117.6(4)	B(4)-B(1)-B(5)	107.5(5)
B(3)-B(10)-B(5)	107.1(4)	B(2)-B(1)-B(5)	59.3(3)
B(2)-B(5)-B(1)	59.7(4)	B(5)-B(1)-B(7)	108.7(6)
O(1)-C(1)-Mn(6)	178.3(7)	O(2)-C(2)-Mn(6)	179.6(6)

Table 8: Crystallographic Data for Compounds **1.7** and **1.6**.

	1.7	**1.6**
empirical formula	$C_7H_{20}B_9MnO_5$	$C_7H_{20}B_9MnO_4$
formula weight	336.46	320.46
crystal system	monoclinic	triclinic
space group	$P2_1/m$	P1
a (Å)	8.8922(12)	7.1440(7)
b (Å)	10.9815(14)	9.6333(9)
c (Å)	9.3490(12)	12.2768(12)
α (°)	90	73.814(2)
β (°)	118.011(3)	75.000(2)
γ (°)	90	86.724
V (Å^3)	805.98(18)	783.65(13)
Z	2	2
T (K)	90(2)	296(2)
D_{calc} (g/cm^3)	1.386	1.249
$F(000)$	344	300
crystal size (mm^3)	0.15 ×0.10 × 0.10	NA
θ range (deg)	2.47 to 25.67	1.79 to 26.37
index ranges	-10≤h≤10	-7≤h≤8
	-13≤k≤13	-12≤h≤12
	-11≤l≤11	-15≤h≤15
goodness of fit (GOF)	1.101	1.050
no. of reflns collected	7025	10011
no. of independent reflns	1625 [R(int) = 0.0298]	3192 [R(int) = 0.0197]
no. of parameters	118	190
wavelength (Å)	0.71073	0.71073
final R indices [I > $2\sigma(I)$]	$R_1 = 0.0402$	$R_1 = 0.0457$
	$wR_2 = 0.1219$	$wR_2 = 0.1462$
final R indices (all data)	$R_1 = 0.0471$	$R_1 = 0.0489$
	$wR_2 = 0.1266$	$wR_2 = 0.1495$
largest diff. peak and hole (e$^-$/Å^3)	0.925 and -0.231	1.200 and -0.468

Table 9: Selected Bond Distances(Å) for Complexes **1.7** and **1.6** with estimated standard deviations in parentheses.

bond	distance	
	1.7	**1.6**
Mn(6)-B(5)	2.223(3)	2.239(3)
Mn(6)-B(2)	2.179(4)	2.193(3)
Mn(6)-B(7)	2.223(3)	2.223(3)
Mn(6)-C(1)	1.823(4)	1.807(3)
Mn(6)-C(2)	1.797(3)	1.800(3)
Mn(6)-C(3)	1.797(3)	1.802(3)
B(1)-B(2)	1.767(5)	1.768(4)
B(1)-B(5)	1.781(4)	1.769(5)
B(4)-B(10)	1.789(4)	1.790(5)
B(4)-B(9)	1.723(6)	1.718(5)
B(1)-B(10)	1.749(4)	1.741(4)
B(1)-B(3)	1.787(6)	1.785(4)
B(5)-B(10)	2.032(4)	2.034(5)
B(2)-B(5)	1.772(4)	1.777(4)
B(9)-B(10)	1.785(4)	1.784(5)
B(1)-B(4)	1.788(5)	1.786(4)
O(1)-C(1)	1.136(5)	1.144(4)
O(2)-C(2)	1.146(3)	1.141(4)
B(2)-O(4)	1.553(5)	1.522(3)
O(4)-C(4)	1.473(3)	1.454(3)
O(5)-C(5)	1.417(4)	NA
C(4)-C(5)	1.511(4)	1.508(4)
C(4)-H	0.9900	0.9700

Table 10: Selected Bond Angles(°) for Complexes **1.7** and **1.6** with estimated standard deviations in parentheses.

angle	value		angle	value	
	1.7	**1.6**		**1.7**	**1.6**
C(1)-Mn(6)-C(2)	92.84(12)	91.83(13)	C(1)-Mn(6)-B(5)	123.07(11)	121.63(13)
C(2)-Mn(6)-C(3)	89.82(17)	89.82(13)	C(2)-Mn(6)-B(5)	143.46(12)	146.15(12)
C(1)-Mn(6)-B(2)	162.27(17)	161.39(13)	B(2)-Mn(6)-B(5)	47.45(9)	47.26(11)
C(2)-Mn(6)-B(2)	99.66(11)	101.79(12)	B(5)-Mn(6)-B(7)	82.86(16)	82.63(12)
B(2)-B(5)-Mn(6)	64.95(16)	65.01(14)	B(1)-B(5)-Mn(6)	119.06(18)	118.78(19)
B(10)-B(5)-Mn(6)	122.00(17)	121.49(17)	B(5)-B(2)-Mn(6)	67.60(16)	67.73(14)
B(1)-B(2)-B(3)	60.8(2)	60.63(18)	B(1)-B(2)-B(5)	60.43(16)	59.88(18)
B(3)-B(1)-B(10)	107.62(15)	107.8(2)	B(5)-B(1)-B(10)	70.29(18)	70.79(19)
B(10)-B(1)-B(4)	60.76(19)	60.97(19)	B(5)-B(1)-B(4)	119.5(2)	120.5(2)
B(3)-B(1)-B(4)	60.01(12)	60.28(18)	B(4)-B(9)-B(10)	61.30(18)	61.44(19)
B(10)-B(9)-B(8)	105.7(3)	105.7(2)	B(9)-B(4)-B(10)	61.07(18)	61.07(19)
B(4)-B(10)-B(9)	57.6(2)	57.48(18)	B(5)-B(10)-B(1)	55.59(16)	55.24(17)
B(9)-B(10)-B(1)	109.0(2)	108.7(2)	B(2)-B(5)-B(10)	102.8(2)	103.1(2)
B(9)-B(10)-B(5)	117.3(2)	117.6(2)	B(4)-B(10)-B(5)	107.4(2)	107.5(2)
B(2)-B(5)-B(1)	59.65(19)	59.81(18)	B(1)-B(5)-B(10)	54.12(15)	53.97(16)
B(2)-B(1)-B(5)	59.92(17)	60.31(18)	B(3)-B(1)-B(5)	108.93(14)	109.2(2)
B(10)-B(4)-B(1)	58.53(17)	58.29(18)	B(1)-B(10)-B(4)	60.7(2)	60.75(18)
B(2)-B(1)-B(10)	115.7(2)	116.8(2)	B(1)-B(4)-B(9)	110.1(3)	109.7(2)
B(2)-B(1)-B(4)	112.9(2)	113.8(2)	B(2)-B(1)-B(3)	59.61(12)	59.68(17)
B(1)-B(4)-B(3)	60.0(2)	59.82(17)	B(5)-B(2)-B(7)	112.3(3)	111.8(2)
O(1)-C(1)-Mn(6)	179.8(4)	178.9(3)	O(2)-C(2)-Mn(6)	177.2(2)	178.5(3)
O(5)-C(5)-C(4)	111.3(3)	NA	O(4)-C(4)-C(5)	107.4(2)	105.2(2)

Table 11: Crystallographic Data for Complex **1.8**.

	1.8
empirical formula	$C_7H_{20}B_9ReO_4$
formula weight	451.66
crystal system	Triclinic
space group	P1
a (Å)	7.0840(4)
b (Å)	9.6979(6)
c (Å)	12.5788(7)
α (°)	73.5790(10)
β (°)	75.5520(10)
γ (°)	87.066(2)
V (Å^3)	802.53(8)
Z	2
T (K)	90(2)
D_{calc} (g/cm^3)	1.836
$F(000)$	412
crystal size (mm^3)	$0.20 \times 0.10 \times 0.08$
θ range (deg)	2.19 to 25.02
index ranges	-8≤h≤8, -11≤k≤11, -14≤l≤14
goodness of fit (GOF)	1.069
no. of reflns collected	8776
no. of independent reflns	2822 [R(int) = 0.0135]
no. of parameters	202
wavelength (Å)	0.71073
final R indices [I > $2\sigma(I)$]	$R_1 = 0.0184$,w$R_2 = 0.0508$
final R indices (all data)	$R_1 = 0.0199$,w$R_2 = 0.0522$
largest diff. peak and hole (e$^-$/Å^3)	1.034 and -0.608

Table 12: Selected Bond Distances(Å) for Complex **1.8** with estimated standard deviations in parentheses.

bond	distance	bond	distance
Re(6)-B(5)	2.357(5)	O(1)-C(1)	1.149(6)
Re(6)-B(2)	2.342(5)	O(2)-C(2)	1.153(6)
Re(6)-C(1)	1.941(5)	B(2)-O(4)	1.526(5)
Re(6)-C(2)	1.920(5)	O(4)-C(4)	1.479(5)
B(1)-B(2)	1.772(7)	B(2)-B(5)	1.798(7)
B(1)-B(3)	1.793(7)	B(4)-B(9)	1.719(7)
B(1)-B(4)	1.798(7)	B(4)-B(10)	1.797(7)
B(1)-B(5)	1.777(7)	B(9)-B(10)	1.798(7)
B(1)-B(10)	1.743(7)	B(5)-B(10)	2.052(7)

Table 13: Selected Bond Angles (°) for Complex **1.8** with estimated standard deviations in parentheses.

angle	value	angle	value
C(1)-Re(6)-C(2)	89.77(18)	C(1)-Re(6)-B(5)	144.17(18)
C(2)-Re(6)-C(3)	89.88(18)	C(2)-Re(6)-B(5)	84.94(18)
C(1)-Re(6)-B(2)	103.44(17)	B(2)-Re(6)-B(5)	45.00(16)
C(2)-Re(6)-B(2)	105.00(17)	B(5)-Re(6)-B(7)	78.79(17)
B(2)-B(5)-Mn(6)	67.0(2)	B(1)-B(5)-Mn(6)	120.7(3)
B(10)-B(5)-Mn(6)	122.3(3)	B(5)-B(2)-Mn(6)	68.0(2)
B(1)-B(2)-B(3)	60.9(3)	B(1)-B(2)-B(5)	59.7(3)
B(3)-B(1)-B(10)	107.5(3)	B(5)-B(1)-B(10)	71.3(3)
B(10)-B(1)-B(4)	61.0(3)	B(5)-B(1)-B(4)	120.9(4)
B(3)-B(1)-B(4)	59.7(3)	B(4)-B(9)-B(10)	61.4(3)
B(10)-B(9)-B(8)	106.1(4)	B(9)-B(4)-B(10)	61.5(3)
B(4)-B(10)-B(9)	57.1(3)	B(5)-B(10)-B(1)	57.1(3)
B(9)-B(10)-B(1)	108.7(4)	B(2)-B(5)-B(10)	102.3(3)
B(9)-B(10)-B(5)	117.5(3)	B(4)-B(10)-B(5)	107.6(3)
B(2)-B(5)-B(1)	59.4(3)	B(1)-B(5)-B(10)	53.5(2)
B(2)-B(1)-B(5)	60.9(3)	B(3)-B(1)-B(5)	109.4(3)
B(10)-B(4)-B(1)	58.0(3)	B(1)-B(10)-B(4)	61.0(3)
B(2)-B(1)-B(10)	117.4(4)	B(1)-B(4)-B(9)	109.7(4)
B(2)-B(1)-B(4)	113.2(4)	B(2)-B(1)-B(3)	59.4(3)
B(1)-B(4)-B(3)	60.0(3)	B(5)-B(2)-B(7)	113.3(3)
O(1)-C(1)-Re(6)	178.0(4)	O(2)-C(2)-Re(6)	178.3(4)
O(4)-C(4)-C(5)	101.8(4)		

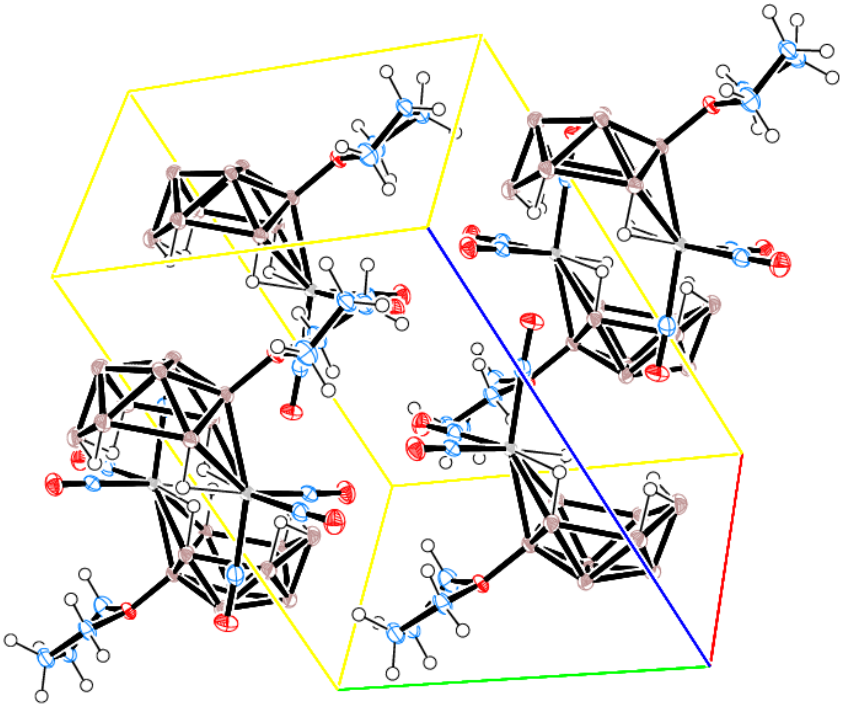

Figure 13: Partial packing diagram and unit cell of the crystal structure of complex **1.8**

1.3 Results and Discussion

1.3.1 Chemical Versus Photochemical Pathways of Manganadecaborane 1.1

The complex **1.1** ([*nido*-6-$Mn(CO)_3B_9H_{13}$][NMe_4]) was first reported by Lott and Gaines.[21,64] However, the chemistry of this complex has not been explored beyond its synthesis. Specifically, we were interested in exploring the relationship between thermal and photochemical pathways for this species. We found that under thermal conditions, **1.1** undergoes isomerization to [*nido*-5-$Mn(CO)_3B_9H_{13}$][NMe_4] (**1.2**) while upon UV irradiation **1.1** was converted into the *hypercloso*-borane [*hypercloso*-$Mn(CO)_3B_9H_9$][NMe_4] (**1.3**), with the loss of two equivalents of dihydrogen (H_2). The *nido*- and *hypercloso*-configurations for these structures are shown in Figure 1 and Figure 2, respectively. Both compounds **1.1** and **1.2** have 14 skeleton electrons whereas the *hypercloso* **1.3** has four fewer electrons. These reactions will be discussed in the following sections.

[*Nido*-5-$Mn(CO)_3B_9H_{13}$][NMe_4] (1.2)

The manganadecaborane **1.2** was prepared by refluxing the manganadecaborane **1.1** in mesitylene at 175 °C for 1 hour as shown in equation (1.1). This conversion was found to be almost quantitative within an hour. This compound was found to be stable at 175 °C towards isomerization as monitored by ^{11}B NMR.

$$[nido\text{-}6\text{-}Mn(CO)_3B_9H_{13}][NMe_4] \longrightarrow [nido\text{-}5\text{-}Mn(CO)_3B_9H_{13}][NMe_4] \qquad (1.1)$$

Several synthetic procedures have been previously reported for the synthesis of *nido*-5-metalladecaboranes as shown in Table 2. One method involves a conversion from a *nido*-6 to *nido*-5 metalladecaborane. For example,

Bown and coworkers have shown that the passage of dioxygen through a solution of [6-(η^6-C_6Me_6)-*nido*-6-IrB_9H_{13}] resulted in its complete conversion to [5-(η^6-C_6Me_6)-*nido*-5-IrB_9H_{13}] over 75 min with some decomposition as monitored by NMR. spectroscopy.[3] The authors did not mention, however, the mechanism for this isomerization. Similarly, the reaction of [6-(η^5-C_5Me_5)-*nido*-6-RhB_9H_{13}] with an excess of PMe_2Ph in dichloromethane solution at room temperature yielded the air-stable red-orange [5-(η^5-C_5Me_5)-*nido*-5-RhB_9H_{11}-7-$(PMe_2Ph)_2$] complex with a yield of 35%.[10] The direct synthesis method has also been reported. For example, [5-(η^5-C_5H_5)-*nido*-5-CoB_9H_{13}] was isolated from the reaction of NaB_5H_8, $CoCl_2$, and NaC_5H_5 in THF at temperatures below $-20\,^{\circ}C$.[70] The ruthenium, rhodium, and osmium species were also prepared by the direct reaction between [$RuCl_2(\eta^6$-$C_6Me_6)_2$], [$RhCl_2(\eta^6$-$C_5Me_5)_2$], or [$OsCl_2(\eta^6$-$C_6Me_6)_2$] and the [*nido*-$B_{10}H_{13}]^-$ anion in dichloromethane solution.[3]

In the [*nido*-5-$Mn(CO)_3B_9H_{13}NMe_4$] (**1.2**) case, however, none of previously employed synthetic methods were found to work. This may imply that conditions for the formation of each *nido*-5-metalladecaboranes depend on individual compound's properties.

Elevated temperature-induced isomerization is not unusual in carborane chemistry. For example, in 1963, Grafstein and Dvorak first reported the thermal isomerization of *o*-carborane to *m*-carborane at 450 °C.[71] A year later, the higher temperature (approximately 600 °C and above) rearrangement of *m*-carborane to the *para*-isomer was described by Papetti and Heying.[72] In metalladecaborane chemistry, thermolytic transformation has also been studied. For example, Bould and coworkers[2] reported that the *nido*-metalladecaboranes [$(PPh_3)_2HIrB_9H_{13}$] or [$(PPh_3)(Ph_2PC_6H_4)HIrB_9H_{12}$], when heated in solution at approximately 80°C, quantitatively loses dihydrogen to form [$(PPh_3)(Ph_2PC_6H_4)HIrB_9H_8$]. However, *nido*-6 to *nido*-5 metalladecaborane transformations are unprecedented. The high temperature induced isomerization for

metalladecaboranes may present one alternative route for the synthesis of other *nido*-5-metalladecaboranes.

The progress of the thermal isomerization reaction of complex **1.1** was monitored by ^{11}B NMR spectroscopy (Figure 14). To assign the ^{11}B resonances of the new compound to specific boron atoms, a 2-D ^{11}B-^{11}B COSY spectrum were performed (Figure 15). The ^{11}B-^{11}B COSY cross-correlations were essentially identical to those previously reported for the cobalt analogue *nido*-$[(C_5Me_5)CoB_9H_{13}]$.[73] Simple stick representations of the ^{11}B spectra of the two *nido*-manganadecaborane compounds [*nido*-6-$Mn(CO)_3B_9H_{13}$][NMe_4] (**1.1**) and [*nido*-5-$Mn(CO)_3B_9H_{13}$][NMe_4] (**1.2**), along with $B_{10}H_{14}$ for comparison, are shown in Figure 16. The differences in compounds **1.1** and **1.2** can be clearly seen in the NMR data. While spectrum of **1.1** is very close to that of $B_{10}H_{14}$, compound **1.2** has two peaks that are shifted downfield to around +20 ppm. The spectrum of compound **1.2** reveals a 1:1:1:4:1:1 pattern of resonances in the region 30 to -40 ppm.

Figure 17 shows the relative intensities and chemical shifts in the ^{11}B NMR spectra of the complex **1.2**, together with the ^{11}B NMR spectra data for some other *nido*-5 metalladecaboranes: $[(C_6Me_6)RuB_9H_{13}]$, $[(C_5Me_5)RhB_9H_{13}]$, $[(C_6Me_6)OsB_9H_{13}]$, $[(C_5Me_5)IrB_9H_{13}]$, $[(Me_3C_6H_3)FeB_9H_{13}]$, and $[(C_5Me_5)CoB_9H_{13}]$[3] for comparison. From the comparisons, it can be observed that the location and pattern of ^{11}B NMR spectrum of **1.2** agrees well with other known *nido*-5-metalladecaborane compounds. For example, the B6, B1 and B2, B4 resonances are located at similar range with other *nido*-5-metalladecaboranes. Nonetheless, one noticeable difference observed is the pattern of B7-B10 resonance. Almost all the other *nido*-5-metalladecaboranes have separated resonances for B7-B10 that lie between −8 to +8 ppm whereas [*nido*-5-$Mn(CO)_3B_9H_{13}NMe_4$] (**1.2**) shows only one peak for B7-B10 at +0.5 ppm. Considering the molecular structure similarities of these nido-5-metalladecaboranes, the single very broad resonance for B7-B10 in **1.2** can be explained as overlaps of

these boron resonances. If this explanation is true, then the actual NMR pattern can be regarded as a 1:1:1:1:1:1:1:1:1:1 pattern with no equivalent boron atoms. This agrees well with the proposed *nido*-5-metalladecaborane structure.

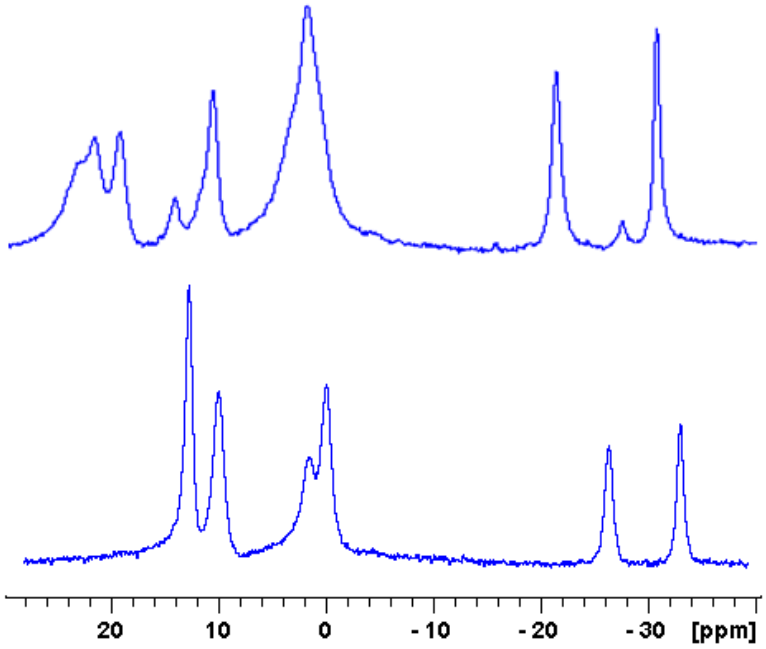

Figure 14: ^{11}B NMR spectra monitoring of the thermal conversion of complex **1.1** (Bottom, before reaction; Top, after reaction).

The IR spectra of the complex **1.2** shows υ_{CO} stretching bands at 2013.8 and 1935.1 cm^{-1} as compared with the data for **1.1**: 2025, 2060, 2005 cm^{-1}.[21] Both **1.1** and **1.2** have cluster B-H stretching bands in their IR spectra at around 2500 cm^{-1}.

UV-Vis spectra of the two *nido*-manganadecaborane isomers are shown in Figure 18. Both compound **1.1** and **1.2** have strong absorption peaks at 314 nm, while **1.2** shows a significant blue shift at 433 nm compared with 462 nm of **1.1**. Based on previously reported spectroscopic studies of manganese tricarbonyl complexes,[74] we have tentatively assigned the absorption peaks. The intense absorption around 315 nm is thought to be from intraligand (IL) transitions ($\pi-\pi^{\star}$). The less intense and lower-energy absorptions are assigned to a metal-to-ligand charge-transfer (MLCT)

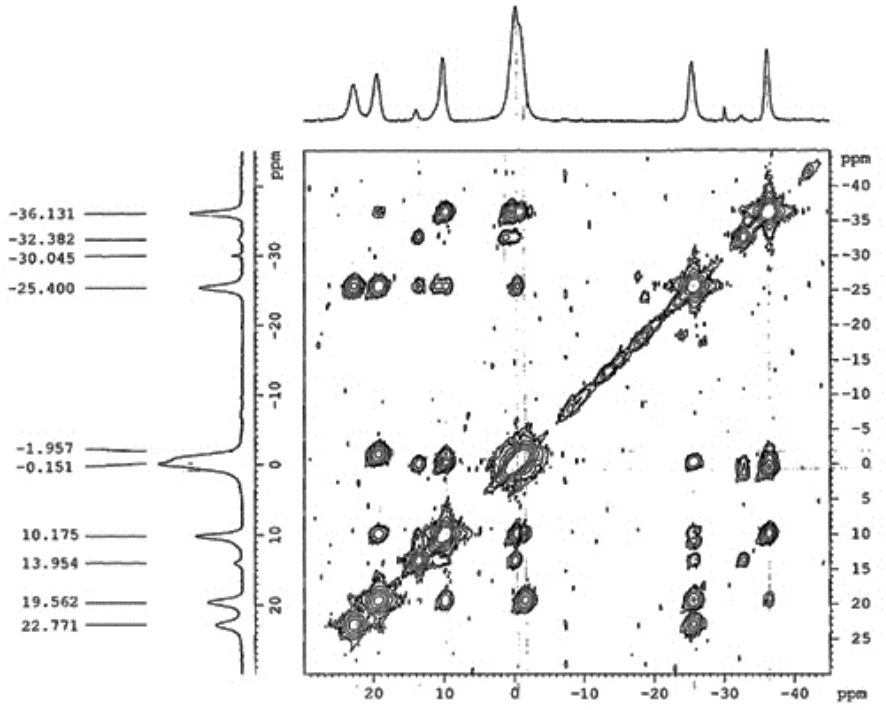

Figure 15: 2D ^{11}B-^{11}B $\{^{1}$H$\}$ COSY NMR spectrum of the complex **1.2**.

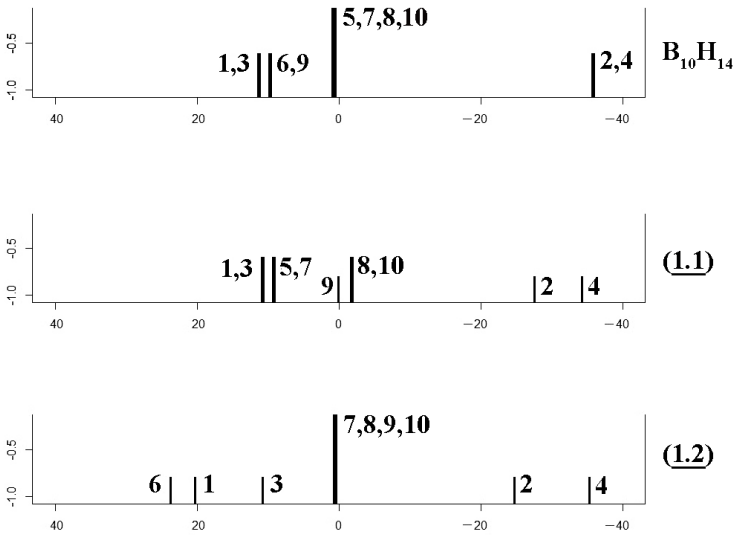

Figure 16: Stick representation of the ^{11}B NMR spectra of decaborane, complex **1.1**, and complex **1.2**.

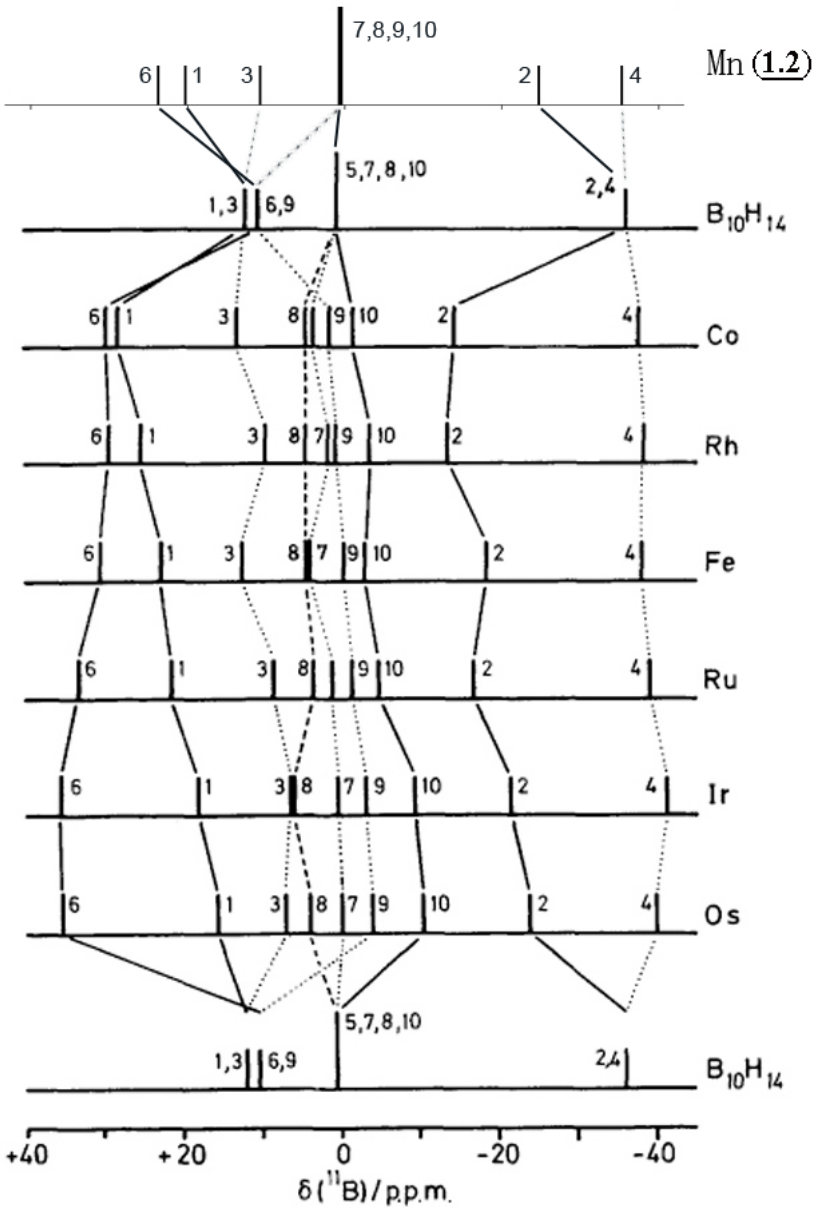

Figure 17: Stick representation of chemical shifts and other *nido*-5 metalladecaboranes comparison.[3]

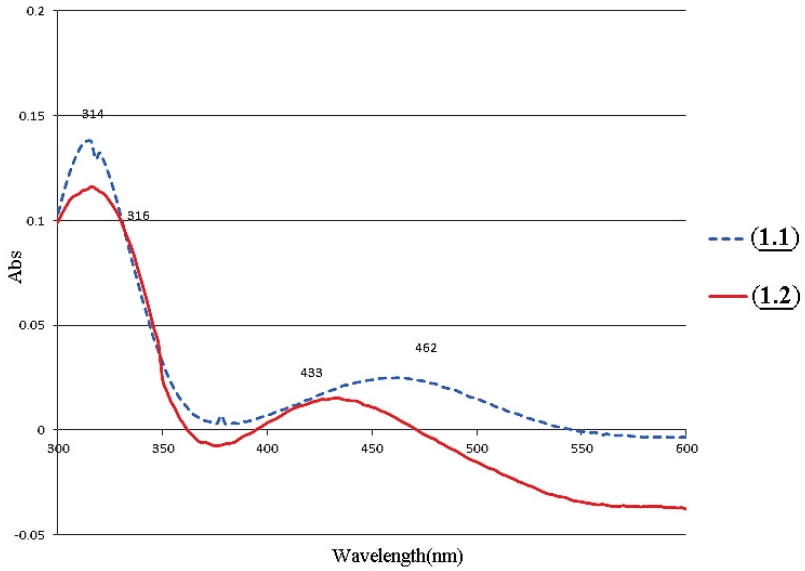

Figure 18: UV-Vis Spectra of [*nido*-6-$(CO)_3$-6-$MnB_9H_{13}NMe_4$] (**1.1**) and [*nido*-5-$(CO)_3$-5-$MnB_9H_{13}NMe_4$] (**1.2**).

π(Mn) - $\pi^\star$(ligand) transition. Comparing the absorption spectra of **1.2** with **1.1**, the blue shift can be explained as due to the lowest $\pi^\star$ orbital of $B_9H_{13}^{2-}$ ligand is higher in **1.2** compared with that in **1.1**. This can be explained by the more symmetric molecular structure of complex **1.1** compared with **1.2**.

[*Hypercloso*-$Mn(CO)_3B_9H_9$][NMe_4] (1.3)

[*Hypercloso*-$Mn(CO)_3B_9H_9$][NMe_4] (**1.3**) was prepared photochemically from the UV irradiation of complex **1.1** in dry and degassed THF.

Various synthetic procedures have been reported for the preparation of *hypercloso*-metalladecaboranes. Bould and coworkers[2] reported that either *nido*-[$(PPh_3)_2HIrB_9H_{13}$] or *nido*-[$(PPh_3)(Ph_2PC_6H_4)HIrB_9H_{12}$], when heated in solution at ca. 80°C, quantitatively lose dihydrogen to form [$(PPh_3)(Ph_2PC_6H_4)HIrB_9H_8$]. Crook[20] first reported that the reaction between [$RuCl_2(PPh_3)_3$] and the *arachno*-$[B_9H_{14}]^-$ anion in dichloromethane solution at ambient temperature yields *arachno*-

$[(PPh_3)ClHRuB_9H_7(PPh_3)_2]$ as an orange crystalline, somewhat air-sensitive solid in an isolable yield of ca. 40%. The reaction also gives an interesting *hypercloso*-tri-ruthenium species formulated as $[(PPh_3)RuB_9H_9\{RuCl_2(PPh_3)_2\}_2]$.[17] Reaction of SMe_2 with $[C_6Me_6RuB_9H_{13}]$ in refluxing toluene has also been found to give the ten-vertex *hypercloso* species $[C_6Me_6RuB_9H_9]$ in 75-80% yield.[16] The reaction of $[C_6Me_6RuB_9H_9]$ with aniline $[PhNH_2]$ gives a variety of B-phenylamino *hypercloso*-derivatives: $[(C_6Me_6)(PhNH)RuB_9H_8]$, $[(C_6Me_6)(PhNH)_2RuB_9H_7]$, and $[(C_6Me_6)(PhNH)_3RuB_9H_6]$.[19] The reaction of thermally generated iron atoms with decaborane(14) and mesitylene under rotary metal atom conditions gives *hypercloso*-$[C_6(CH_3)_3FeB_9H_9]$ with less than 1% yield.[5] The compound *hypercloso*-$[(pcym)RuB_9H_9]$ has been isolated by chromatography as a minor by-product (less than 1%) from the reaction of the *arachno*-$[B_9H_{14}]^-$ anion with $[\{(pcym)RuCl_2\}_2]$ that gives *nido*-$[(pcym)RuB_9H_{13}]$.[18] A photochemical pathway for the formation of a *hypercloso*-metalladecaborane is, however, unprecedented.

The compound **1.3** was characterized by ^{11}B NMR spectra. The far downfield resonance at around 100 ppm is diagnostic for the *hypercloso*-structure. Figure 19 represents the relative intensities and chemical shifts in the ^{11}B NMR spectra of **1.3**, together with the ^{11}B NMR data for known *hypercloso*-metalladecaborane containing Ir,[2] Ru,[20] Fe.[5] From the figure, all the spectra have a 1:1:1 ratio of intensities and more importantly, the locations of the three resonances are very similar to each other among all these *hypercloso*-metalladecaboranes. For example, ^{11}B NMR data of $[C_6(CH_3)_3FeB_9H_9]$[5] shows three resonance at 106.5 (178), 27.7 (144) and −11.4 (148) with relative area 3:3:3. These similarities of the spectrum indicate a similar metallaborane cage configuration.

Like other *hypercloso*-metalladecaboranes, the ^{11}B NMR spectra of **1.3** (Figure 19) shows three doublets of equal intensity with two of the doublets shifted to low field. The doublet at very low field, +110 ppm, is highly indicative of low-coordinate boron

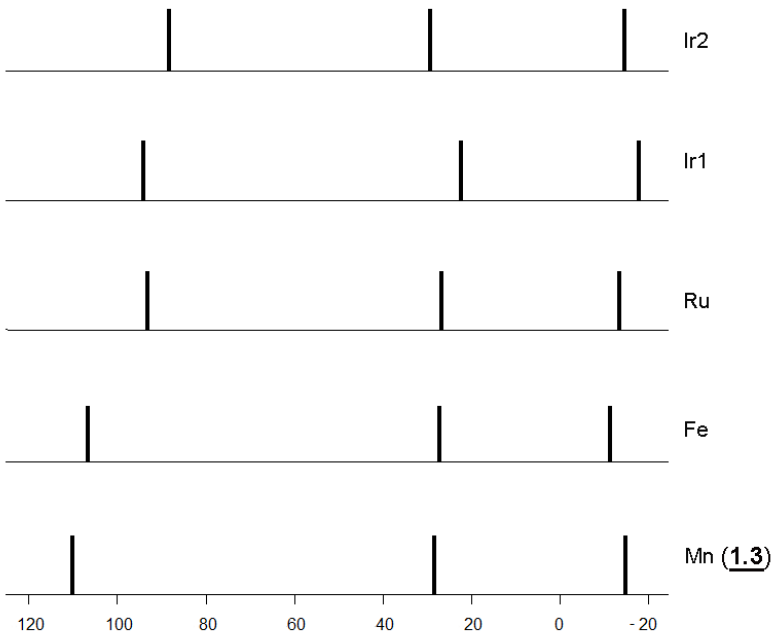

Figure 19: Stick representation of ^{11}B NMR spectra chemical shifts comparison for *hypercloso*-metalladecaboranes (Data for literature compounds adapted from references 2, 5, 20).

atoms directly bonded to a metal and are, therefore, assigned to the four-coordinate B2, B3, and B4 borons in Figure 20. The doublet at +28.4 ppm is assigned to boron atoms B5, B6, and B7, which are also bonded to the metal but which are in five-coordinate positions. The remaining resonance at -14.8 ppm is, therefore, assigned to B8, B9, and B10.

The ^{11}B NMR data of *hypercloso*-metalladecaboranes for complex **1.3** indicates that the complex has a 3-fold axis, strongly supporting the proposed C_{3v} symmetry structure shown in Figure 20. The 1:3:3:3 stack geometry approximates to an ideal C_{3v} symmetry with the manganese atom occupying the unique axial position on the threefold cluster axis. The B_9 unit has a *hexahapto*-chair configuration with respect to the manganese atom. The compound, therefore, can be regarded as a complex between a *hexahapto*-tetradentate $[B_9H_9]^{4-}$ anion and a manganese metal center.

For the compound **1.3**, similar to both compounds **1.1**[21] and **1.2**, the manganese acts as a formal Mn^{1+} center and the metal carbonyl fragment donates 2 electrons and 3 orbitals toward cluster bonding, whereas each B-H vertex donates 2 electrons and 3 orbitals to the bonding orbital. The total 20 electrons in bonding orbital bring the skeleton electron pairs (SEPs) count of the cluster to n where $n = 10$, which is one SEPs fewer than its *closo*-counterparts. This agrees with electron counting of known *hypercloso*-metallaboranes and supported by previous theoretical work.[15]

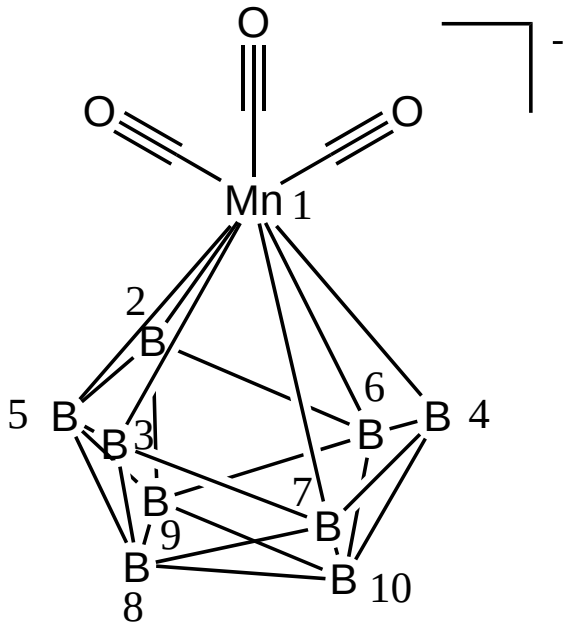

Figure 20: Proposed structure of photochemical reaction product **1.3**.

[*Arachno*-B_9H_{14}][NMe_4] (**1.4**) and [*nido*-B_9H_{12}][NMe_4] (**1.5**)

In contrast to its chemical behavior in THF, it was found that while under photolytic condition in dried dichloromethane compound **1.1** is converted to the tetradecahydrononaborate(1−) anion **1.4** by extrusion of the Mn metal center. Concomitant with the formation of this *arachno* anion **1.4** there is also some 2,5:6,10:8,10-tri-μ-hydro-nonahydro-*nido*-nonaborate(1−) **1.5** present in the reaction mixture.

Both the compounds **1.4** and **1.5** were characterized by ^{11}B NMR spectra and by comparison of the data with these literature compounds (Figure 21).[62,63] The relative positions, intensities, and BH coupling constants are all consistent with the literature values. Using the ^{11}B NMR data, the ratio of the amounts for compounds **1.4** and **1.5** was estimated as 10:1.

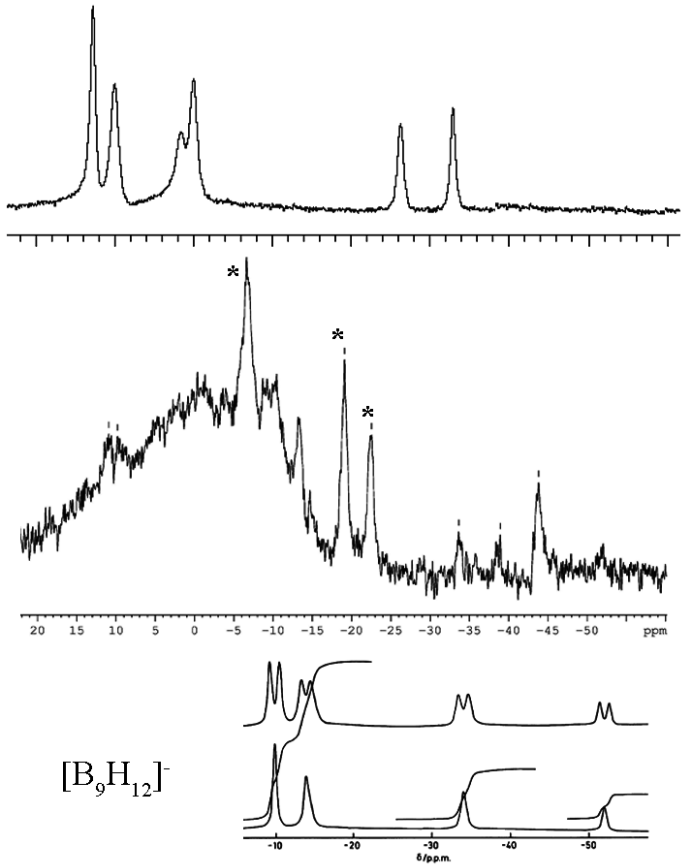

Figure 21: Photolysis monitoring of complex **1.1** in DCM (Top: ^{11}B NMR spectra of the complex **1.1** in DCM, middle: ^{11}B NMR spectra of the solution after photolysis in DCM, $*$ shows the peaks for complex **1.4**, and bottom: literature data for complex **1.5**.[63])

1.3.2 Molecular Structural Description

[*nido*-5-$Mn(CO)_3B_9H_{13}$][NMe_4] (**1.2**)

The bonding electron count for **1.2** is similar to that for **1.1**. The structure of the complex **1.2** can be viewed as a formal Mn^{1+} metal carbonyl complex coordinated to one $[B_9H_{13}]^{2-}$ ligand. From the 1D and 2D ^{11}B NMR spectra, its structure was proposed as a *nido*-5-metalladecaborane. Single-crystal X-ray crystallography confirmed its structure.

The compound **1.2** was isolated as reddish purple, air-stable, crystalline solid. Two views of the determined molecular structure are given in Figure 22 and important bond distances and angles are given in Table 4 and Table 5, respectively. The structure can be envisioned as being derived from a decaborane(14) structure in which an $Mn(CO)_3$ unit occupies the cage vertex 5-position (equivalent to 7, 8, and 10). The unit cell of crystalline **1.2** contains a pair of 5- and 7-substituted molecules (Figure 8), and references to the 5-Mn also apply to the equivalent 7-position isomer.

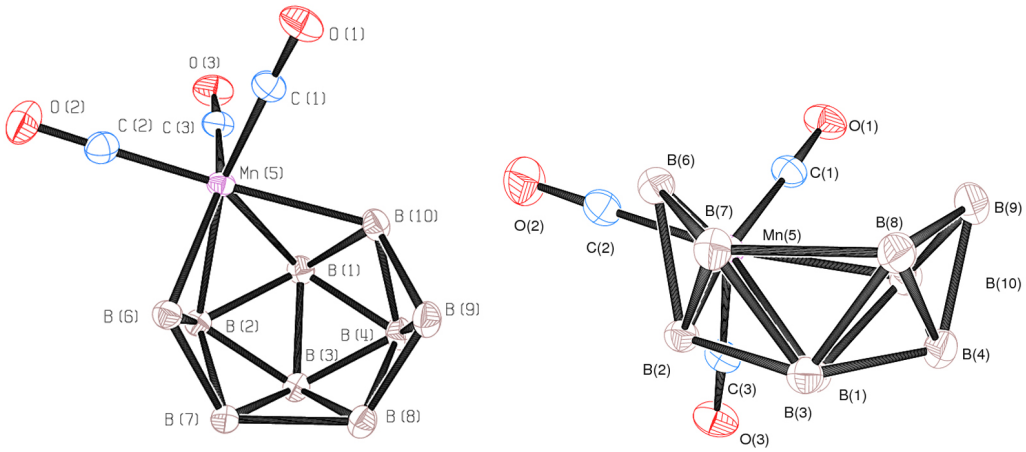

Figure 22: Two ORTEP drawing views of the molecular structure of [*nido*-5-$Mn(CO)_3B_9H_{13}$][NMe_4] (**1.2**) showing the crystallographic labeling scheme as determined in its $[NMe_4]^+$ salt (Hydrogen atoms and cation molecules are omitted for clarity and thermal ellipsoids are drawn with 50% probability).

In the structure **1.2**, the manganese atom is bound to boron atoms B6, B2, B1, and B10, with an average manganese-boron distance of 2.245(2) Å. This compares to an average iron-boron distance of 2.145 Å in $[(Me_3C_6H_3)FeB_9H_{13}]$[75] and cobalt-boron distance of 2.107(6) Å in $[(C_5Me_5)CoB_9H_{13}]$ (Figure 23 and Table 14).[5] The four borons bound to the manganese are approximately planar and this is also similar to the four boron atoms in the complex $[(Me_3C_6H_3)FeB_9H_{13}]$.[75] Two of the Mn-B distances, 2.26 (Mn-B2) and 2.34 (Mn-B10) Å, and are slightly longer than any previous reported manganese-boron distance in MnB_9 cluster (average 2.22(2) Å, maximum is 2.237 Å).[1] This is almost as large as the largest manganese-boron distance in all reported manganese-borane clusters (2.356(9) Å for MnB_3).[1]

The bonding of the manganese to the carbonyl ligands appears normal with the average manganese-carbon distance at 1.807(2) Å. All hydrogens were located by difference Fourier methods, and the complex was shown to have four bridging hydrogens on the open face of the cage. In *nido*-5 metalladecaboranes $[(Me_3C_6H_3)FeB_9H_{13}]$,[75] $[(C_5Me_5)CoB_9H_{13}]$,[5] and the compound **1.1**,[70] three of these hydrogens are boron-boron bridging, B6-B7, B8-B9, and B9-B10, while the fourth is boron-manganese bridging, B6-Mn. The intracage distances for **1.2**, $[(Me_3C_6H_3)FeB_9H_{13}]$,[75] $[(C_5Me_5)CoB_9H_{13}]$,[5] and $B_{10}H_{14}$[76] are listed in Table 14.

The analogy between the *nido*-5 metalladecaborane structure and $B_{10}H_{14}$[76] was demonstrated by comparison of crystallographic bond distances. However, compared to $[(Me_3C_6H_3)FeB_9H_{13}]$,[75] and $[(C_5Me_5)CoB_9H_{13}]$,[5] complex **1.2** shows variations at B1-B2, B1-B4, B2-B6, B6-B7, and B8-B9 where the manganadecaborane distances are respectively 0.00293, 0.0523, 0.0343, 0.0473, and 0.0433 Å longer than those in $B_{10}H_{14}$.[76] This is an average 0.036 Å longer than that observed in $B_{10}H_{14}$. While $[(Me_3C_6H_3)FeB_9H_{13}]$,[75] and $[(C_5Me_5)CoB_9H_{13}]$[5] have similar intracage boron-boron distances (Table 14) and they are closes analogues to $B_{10}H_{14}$, the complex **1.2** presents a somewhat distorted boron cluster cage. Although the exact reason is unclear, this

distortion difference can be partially explained by the different *exo*-polyhedral ligands: carbonyl group versus the arene groups.

Table 14: Boron-boron and metal-boron distances comparisons (Å).

	5-MnB_9	5-FeB_9	5-CoB_9	$B_{10}H_{14}$
B(1)-B(10)	1.760(3)	1.744(7)	1.767(7)	1.754
B(1)-B(3)	1.787(3)	1.780(6)	1.746(7)	1.772
B(1)-B(2)	1.803(3)	1.765(6)	1.768(7)	1.774
B(1)-B(4)	1.826(3)	1.794(6)	1.765(7)	1.774
B(2)-B(6)	1.749(3)	1.723(7)	1.749(8)	1.715
B(2)-B(3)	1.788(3)	1.778(6)	1.754(8)	1.782
B(2)-B(7)	1.797(3)	1.784(6)	1.777(9)	1.787
B(3)-B(7)	1.750(3)	1.749(7)	1.734(8)	1.758
B(3)-B(8)	1.752(3)	1.732(7)	1.743(8)	1.758
B(3)-B(4)	1.762(3)	1.749(6)	1.743(8)	1.782
B(4)-B(9)	1.721(3)	1.695(6)	1.712(8)	1.715
B(4)-B(8)	1.784(3)	1.751(6)	1.763(8)	1.787
B(4)-B(10)	1.799(3)	1.779(6)	1.776(7)	1.785
B(6)-B(7)	1.809(3)	1.977(6)	1.95(1)	1.973
B(8)-B(9)	1.805(3)	1.778(7)	1.784(9)	1.762
B(9)-B(10)	1.807(3)	1.791(7)	1.779(7)	1.788
B(7)-B(8)	1.965(3)	1.977(6)	1.95(1)	1.973
M-B(6)[a]	2.160(2)	2.077(5)	2.072(6)	1.788
M-B(1)	2.222(2)	2.118(4)	2.082(5)	1.754
M-B(2)	2.256(2)	2.143(4)	2.091(5)	1.785
M-B(10)	2.342(2)	2.241(5)	2.183(5)	1.973

[a] M stands for Metal or boron

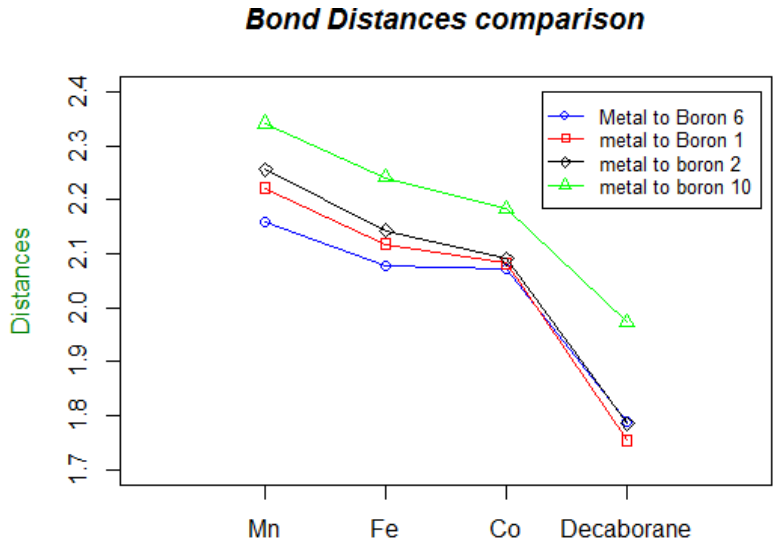

Figure 23: Plot of metal-boron distances for *nido*-5 Mn,Fe,Co and decaborane (Å).

[*Nido*-6-$Mn(CO)_3B_9H_{13}$][NMe_4] (**1.1**)

In order to compare the structural features of the two isomers, **1.1** and **1.2**, the structure of **1.1** was also studied by X-ray diffraction. Two views of the molecular structure of **1.1** are given in Figure 24 and selected interatomic bond distances and bond angles for **1.1** appear in Table 6 and Table 7, respectively. All bond distances are comparable with 2-position B(2) substituted structure [2-C_4H_8O-*nido*-6-$(CO)_3$-6- MnB_9H_{12}] (**1.6**),[64] as can been seem from Table 15. The largest bond distance difference between complex **1.1** and **1.6** in Table 15 is 0.022(2) Å for Mn-B2. This difference is clearly due to the THF substitution on the B2. The angles and distances for the remainder of the B_9 cage are very similar to those reported in $B_{10}H_{14}$.[76]

The molecular structures of compounds **1.1** and **1.2** are shown in Figure 7. Table 16 shows the selected bond distances in these two compounds. The manganese atom in **1.1** is bound to boron atoms B5, B2 and B7 with distances of 2.237(5), 2.196(6) and 2.237(5) Å respectively. These are comparable with the manganese-boron distance in **1.6**.[64] However, when compared with those in **1.2**, they are on average 0.0213 Å shorter. As the result of the metal substitution pattern, the B9 cages in **1.1** and

1.2 show structural differences. Notable differences include B1-B2, B1-B4, B8-B9 and B9-B10, which are 0.031, 0.035, 0.031, and 0.033 Å shorter in **1.1** than in **1.2** respectively. B7-B8 in **1.1** is also 0.061 Å longer than that in **1.2**.

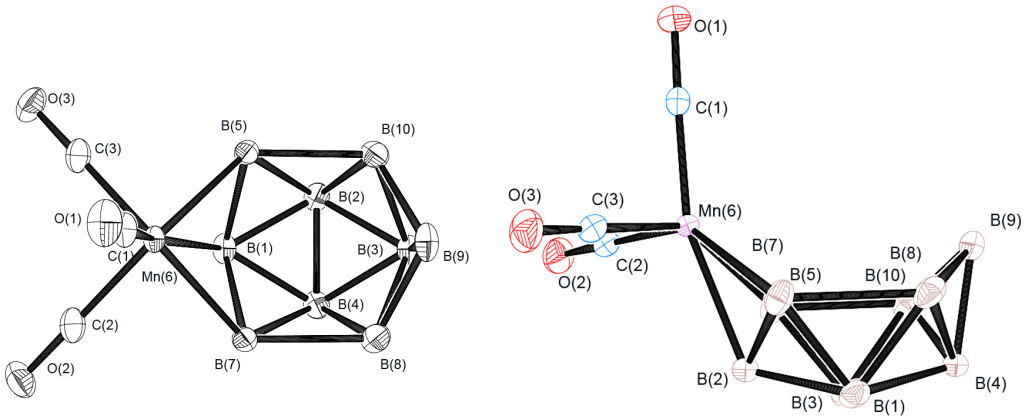

Figure 24: Two ORTEP drawing views of the molecular structure of [*nido*-6-$Mn(CO)_3B_9H_{13}$][NMe_4] (**1.1**) showing the crystallographic labelling scheme as determined in its $[NMe_4]^+$ salt (Hydrogen atoms and cation molecules are omitted for clarity and thermal ellipsoids are drawn with 50% probability).

Table 15: Selected bond distances (Å) comparison between compounds **1.1** and **1.6**.

	(**1.1**)	(**1.6**)
Mn-C3	1.793(5)	1.775(8)
Mn-B5	2.237(5)	2.230(6)
Mn-B2	2.196(6)	2.218(8)
Mn-B7	2.237(5)	2.230(6)
B2-B1	1.766(3)	1.772(10)

Table 16: Boron-boron distances (Å) comparisons between compounds (**1.2**) and (**1.1**).

	(**1.2**)	(**1.1**)
B(1)-B(10)	1.760(3)	1.758(9)
B(1)-B(3)	1.787(3)	1.773(9)
B(1)-B(2)	1.803(3)	1.772(10)
B(1)-B(4)	1.826(3)	1.791(10)
B(2)-(6)[a]	1.749(3)	2.218(8)
B(2)-B(3)	1.788(3)	1.791(10)
B(2)-B(7)	1.797(3)	1.796(8)
B(3)-B(7)	1.750(3)	1.764(9)
B(3)-B(8)	1.752(3)	1.758(9)
B(3)-B(4)	1.762(3)	1.758(9)
B(4)-B(9)	1.721(3)	1.714(12)
B(4)-B(8)	1.784(3)	1.790(8)
B(4)-B(10)	1.799(3)	1.790(8)
(6)-B(7)	1.809(3)	2.230(6)
B(8)-B(9)	1.805(3)	1.773(9)
B(9)-B(10)	1.807(3)	1.773(9)
B(7)-B(8)	1.965(3)	2.025(9)
(5)-B(6)	2.160(2)	2.230(6)
(5)-B(1)	2.222(2)	1.764(9)
(5)-B(2)	2.256(2)	1.796(8)
(5)-B(10)	2.342(2)	2.025(9)

[a] number alone means Boron or Mn atom

1.3.3 Mechanism Discussion

The thermal and solvent dependent photochemical pathways of the metalladecaborane complex **1.1** show a rich chemistry about the metalladecaborane containing a group 7 metal. Considerations regarding the origins for these transformations may help guiding our understanding of similar polyhedral metallaborane species.

Thermal Isomerization

Although the framework rearrangement of borane and carboranes are well known and documented in literature,[77–84] the question arises as to what type of skeletal rearrangement process will enable the observed change for the *nido*-6 to *nido*-5 manganadecaborane isomerization to occur. A process that can account for the observed isomerization in a straightforward manner is the vertex-swing mechanism which was previously proposed for the formation of several *nido*-5-iridadecaborane compounds.[9] The isomerization of compound **1.1** to **1.2**, therefore, can be reasonably rationalized in terms of the vertex swing of a BH group from B(9) as follows. If the B(9) vertex is first moved to connect across the 6, 7, 8 position (or the enantiomeric 6, 5, 10 position), then this will effect the observed isomerization(Figure 25). The enantiomers are shown in the crystal unit cell (Figure 8).

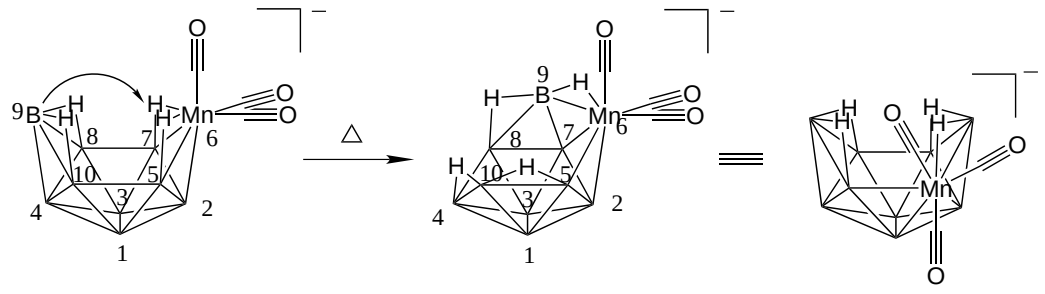

Figure 25: Vertex swing mechanism (B9 moves to form one of the enantiomers).

It should be noted that although the above isomerization can be rationalized on the basis of vertex swing mechanism, the actual processes by which the isomerization may

be accomplished may be far more complex. Other mechanisms may also be possible for the isomerization process. For example, the pentagonal-belt rotation was proposed by Larry G. Sneddon and coworkers for the isomerization of 6-CH_3-5,6,9-$C_3B_7H_{10}$ to 5-CH_3-5,6,9-$C_3B_7H_{10}$ and studied by carbon-13 labelling investigations.[85] The actual isomerization contains 6 individual DSD (diamond-square-diamond) steps to reach the final product.[77] In the formation of complex **1.2**, the starting manganadecaborane **1.1** may be converted to an intermediate which undergoes the pentagonal-belt rotation thus leads to its isomer (Figure 26).

Nonetheless, compared with the pentagonal belt rotation mechanism, the vertex swing isomerization mechanism has the advantage in that it involves the minimum number of atom migration steps.

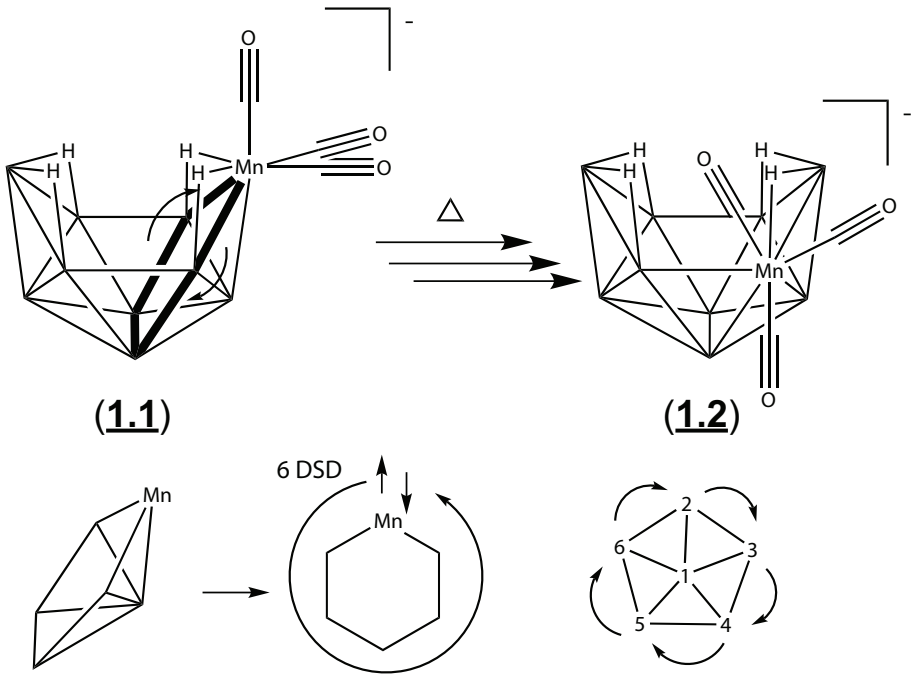

Figure 26: Pentagonal-belt rotation mechanism involving DSD steps.[85]

Photoelimination of Hydrogens to Complex 1.3

The photolysis of manganadecaborane **1.1** in THF to form the *hypercloso*-manganadecaborane **1.3** is shown by the equation (1.2):

$$[\mathrm{Mn(CO)_3B_9H_{13}NMe_4}] \xrightarrow{h\nu} [\mathrm{Mn(CO)_3B_9H_9NMe_4}] + 2\,\mathrm{H_2} \qquad (1.2)$$

The loss of two molecules of dihydrogen during the cluster-closure reaction presumably involves a number of intermediate steps. The first hydrogen loss should be initiated by the photochemical irradiation to generate a $2e^-$ vacant site at the Mn, as we will see later.[86] A solvent THF molecule presumably plays an important role at this stage to stabilize this intermediate. The unsaturated manganese center may then initiate the cage closure with the elimination of the second hydrogen molecule. Therefore, the most reasonable path for the cluster closure for the complex **1.1**, as shown in Figure 27, is *via* the photo initiated loss of dihydrogen, followed by a movement of the 6 vertex toward the B(5,10,9) corner of the cluster together with a rearrangement of the bridging hydrogen atoms. It would then proceed *via* the loss of two further hydrogen atoms, continuing via the *isonido*-intermediate to the final *hypercloso*-product **1.3** (Figure 27).[2]

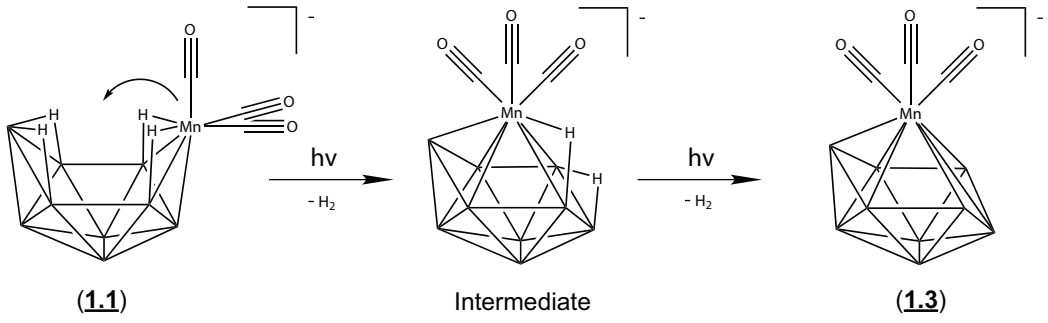

Figure 27: Proposed *nido*-6 to *hypercloso*-manganadecaborane pathway.

Photolytic Extrusion of Manganese Center

The photolysis of compound **1.1** in DCM affords the *arachno*-anion **1.4** and a small amount of the *nido* anion **1.5**. Compared with the photoelimination of hydrogen and cage rearrangement observed in **1.1** to give the *hypercloso*-complex **1.3** in THF, the generation of complex **1.4** and **1.5** here illustrates that solvent can greatly influence a photochemical reaction course.

This difference can be rationalized by the inability of DCM molecule to undergo a replacement reaction of a cage vertex hydrogen compared with the THF molecule. This substitution presumably is a key step to stabilize the intermediate. The failure of DCM to undergo this substitution in a cage closure pathway to a *hypercloso*-structure prevents product formation. Although we have not been able to characterize the manganese degradation product completely from the reaction mixture, the reaction can be thought as a demetallation or decomplexation reaction of the borane ligand from the manganese carbonyl center. This type of photo-induced decomplexation reaction has been well studied in organometallic chemistry including in the arene chromium tricarbonyl and arene manganese tricarbonyl systems.[87–94]

1.3.4 Synthesis of Cyclic Oxonium Derivatives of Manganadecaborane **1.1**

We were interested in finding convenient methods to functionalize the manganadecaborane **1.1** to extend its reaction chemistry. Previous approaches for synthesizing tetrahydrofuran derivatives of the complex **1.1** were reported by D.F.Gaines and co-workers in 1974.[21] They reported three routes for the oxidation of complex **1.1** to afford complex **1.6**. These routes include: a room-temperature reaction in THF for several days with the presence of iodine; refluxing in THF for 1 hour; and the reaction at room temperature in THF with $HgCl_2$. The yields found for the product

1.6 were 15.2%, 10.6%, and 26%, respectively. Unfortunately, the low yields limited their further studies.

In recent years, interest has been paid to exploring additional functionalization methods. For example, Sharpless and coworkers introduced the concept of "click" chemistry to promote the use of efficient, selective and versatile chemical reactions in synthetic chemistry.[43] With the great potential of metallaborane and boron containing cluster compounds for various applications, a straightforward functionalization method for metallaboranes would greatly benefit their further research and applications.

In recent years, nucleophilic ring-opening of cyclic oxonium derivatives of the *closo*-dodecaborate anion $[B_{12}H_{12}]^{2-}$ was proposed to be a new synthetic methodology for the preparation of a wide spectrum of its functional derivatives. This approach has great potential for the modification of various types of organic and bioorganic molecules and the synthesis of compounds that could be used in different fields from the treatment of nuclear wastes to the treatment of cancer.[95]

Nonetheless, this approach has been mainly studied for $[C_2B_9H_{12}]^-$, $[B_{12}H_{12}]^{2-}$,[3,3-Co(1,2-$C_2B_9H_{11})_2]^-$, and $[B_{10}H_{10}]^{2-}$. We, therefore, briefly investigated the application of this approach for the manganadecaborane **1.1**.

Syntheses of Manganadecaborane Cyclic Oxonium Derivatives 1.6 and 1.7

The cyclic oxonium derivatives of compound **1.1** were synthesized according to similar procedure as for the $[C_2B_9H_{12}]^-$ anion by the treatment of the parent anion with acetaldehyde (formaldehyde) in a mixture of toluene, aqueous hydrochloric acid and the corresponding cyclic ether.[96] We have found that both tetrahydrofuran and 1,4-dioxane react with the metalladecaborane **1.1** in the presence of hydrochloric acid and formaldehyde to yield the derivatives **1.6** and **1.7**, respectively (Figure 28). The transformations were almost quantitative, and both reactions completed within 5 to 10 min.

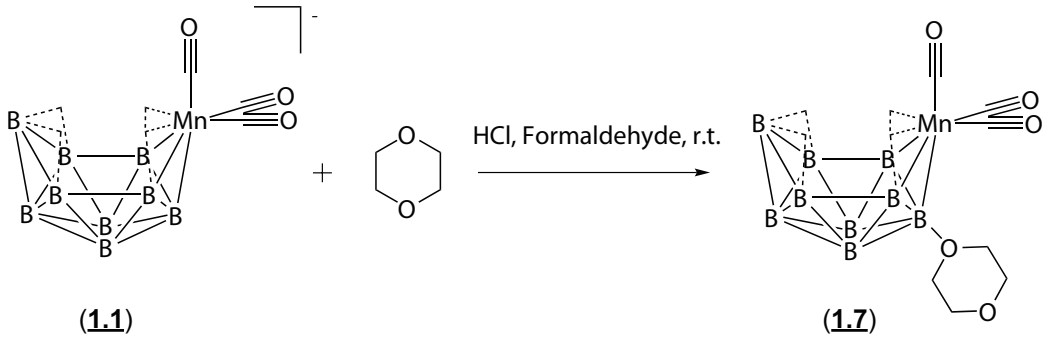

Figure 28: Synthesis of 1,4-dioxane derivative **1.7**.

Both compounds **1.6** and **1.7** were characterized by ^{11}B NMR spectroscopy. The main advantages of this synthetic method over the previously published reactions[21] are high yield of the product and high reproducibility.

The structures of both derivatives **1.6** and **1.7** were determined by single-crystal X-ray diffraction. Although the crystal structure of compound **1.6** has been reported before,[64] we report here the redetermination of its crystal along with the structure of compound **1.7** (Figure 10) for comparison. The crystal data and structural refinement parameters are presented in Table 8 and selected atomic distances and angles are given in Table 9 and Table 10, respectively.

The difference between **1.6** and **1.7** is the mode of substitution group on B2. The structure **1.7** is symmetric with the 1,4-dioxane ring attached to the boron cluster having a chair conformation (Figure 10). The interatomic distances B-O_{ox} (1.553 Å), O_{ox}-C (1.473 Å), and O-C (1.417 Å) fall within the range of equivalent distances for known 1,4-dioxane derivatives of other polyhedral boron hydrides.[97] On the other hand, the THF group for compound **1.6** is slightly twisted, thus causing the structure of the **1.6** to have reduced symmetry (Figure 10).

The influence of the different substitution groups on the polyhedral skeleton are of interest. The distances of B2-Mn6, B2-B1 and B2-B5 in structure **1.6** are 2.193(3), 1.768(4) and 1.777(4) Å, respectively. The corresponding distances in structure **1.7**

are 2.179(4), 1.767(5) and 1.772(4) Å, respectively. These values are not significantly different from each other except that the B2-Mn6 for structure **1.6** is slightly longer than that of **1.7** (0.026 Å longer). Nonetheless, this small difference possibly will not affect their chemical reactivity. From a comparison of the atomic distances and angles shown in Table 9 and Table 10, the boron cluster skeletons in both structures are very similar.

Mechanism Discussions

The described cyclic oxonium functionalization method is based on the hydridic properites of hydrogen atoms in polyhedral boron hydrides. The first stage of the reaction presumably involves the primary attack of the proton from the Bronsted acids, resulting in the highly unstable intermediate. This intermediate then eliminates a hydride and electrophile to form a carbocation-like centre on the boron atom, which is then subjected to attack by a cyclic ether species (Figure 29).[95,97] This mechanism is therefore described as Acid-Assisted Nucleophilic Substitution (AANS) and is a special case of the Electrophile-Induced Nucleophilic Substitution (EINS).[97]

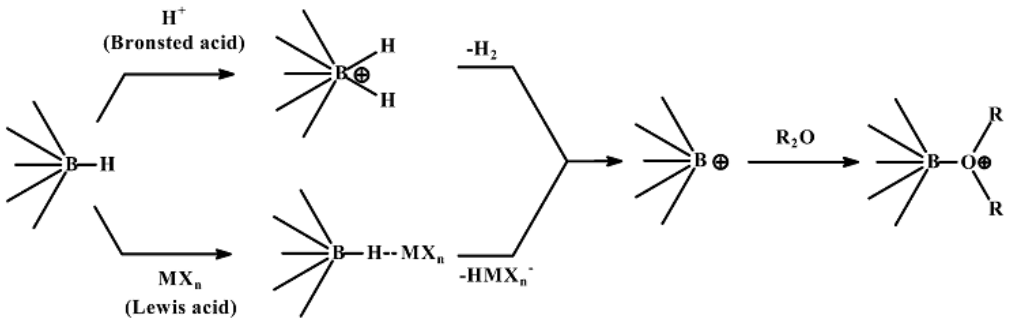

Figure 29: Acid-assisted nucleophilic substitution (AANS) mechanism for polyhedral borane cyclic oxonium deravatives synthesis.[97]

Potential Synthetic Utility

The synthetic applications of cyclic oxonium derivatives of polyhedral boron hydrides has been reviewed in the literature.[95] Various nucleophiles can act as ring-opening reagents to afford corresponding molecules with a reasonable length spacer between the boron cage and the nucleophile (Figure 5). Different types of nucleophiles have been reported and they include: halogen,[98,99] oxygen and sulfur,[52,98] nitrogen and phosphorus,[53,100] and carbon based reactants.[101] For example, the 1,4-dioxane derivative of cobalt bis(dicarbollide) anion and *closo*-dodecaborate anion were reported to be useful synthons for preparation of various functional derivatives for medical application through ring-opening fuctionalizations.[53]

The 1,4-dioxane ring opening gives compounds with the -$(CH_2CH_2O)_2$- chain spacer between the boron cage and the ring opening reagent molecule. This spacer can be considered similar to a short poly(ethylene glycol) (PEG) fragment and has the advantages of a high degree of freedom, biocompatibility, and simple synthetic procedure of its introduction.[97] On the other hand, the THF ring opening gives compounds with the -$O(CH_2)_4$- chain spacer between the boron cage and the ring opening reagent molecule.

For the manganadecaborane THF derivative **1.6**, Gaines and coworkers reported that the refluxing of **1.6** in tetrahydrofuran (THF) with Et_3N produces a good yield of a single product 8-$[(C_2H_5)_3N(CH_2)_4O]$-6-$(CO)_3$-6-MnB_9H_{12} (Figure 30).[102] We, therefore, expect similar ring-opening reactions are possible for the 1,4-dioxane derivative **1.7**.

With these promising prospects, it is expected that the convenient synthesis of these cyclic oxonium derivatives will facilitate the applicability of metallaboranes.

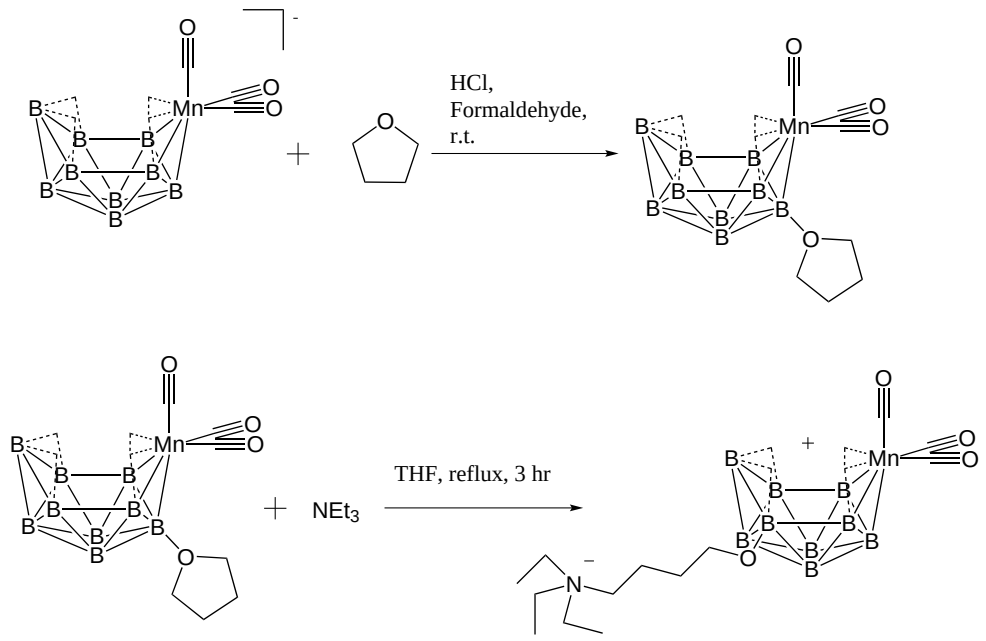

Figure 30: Possible routes for the functionalized manganadecaborane through ring-opening with NEt_3.[102]

1.3.5 Synthesis and Structure of the Rhenium Analogue of the Complex 1.6: [2-$(CH_2)_4$O-*nido*-6-$Re(CO)_3B_9H_{12}$] (1.8)

In order to study differences between metals of the same group on the structures and properties of the metallaborane, we investigated the synthesis of the analogues to the manganadecaborane derivatives.

The rhenium analogy of the complex **1.6** was first reported in the same paper as the synthesis of complex **1.1**.[21] Nevertheless, this complex [2-$(CH_2)_4$O-*nido*-6-$Re(CO)_3B_9H_{12}$] (**1.8**) was not separated and fully characterized in the paper due to the reason that "this material was extremely air and water sensitive".[21]

During our attempted synthesis of this complex **1.8**, a brown-black fraction was obtained by column separation. ^{11}B NMR spectroscopic data showed a similar pattern as the complex **1.6**.

A brown-black crystal was successfully obtained by slow evaporation method for the complex **1.8**. The structure was determined by single-crystal X-ray diffraction

and is shown in Figure 12. The crystal data and structural refinement parameters are presented in Table 11 and selected atomic distances and angles are summarized in Table 12 and Table 13, respectively. The complex **1.8** displays a condensed structure of $ReB_9(CO)_3B_9H_{12}$ and a $(CH_2)_4O$ unit, which is very similar to the manganese analogue, compound **1.6** (Table 17).

Table 17: Selected Bond Distances(Å) for Complexes **1.8** and **1.6** with estimated standard deviations in parentheses (M stands for Mn or Re).

bond	distance	
	1.8	**1.6**
M(6)-B(5)	2.357(5)	2.239(3)
M(6)-B(2)	2.342(5)	2.193(3)
M(6)-C(1)	1.941(5)	1.807(3)
M(6)-C(2)	1.920(5)	1.800(3)
B(1)-B(2)	1.772(7)	1.768(4)
B(1)-B(5)	1.777(7)	1.769(5)
B(4)-B(10)	1.797(7)	1.790(5)
B(4)-B(9)	1.719(7)	1.718(5)
B(1)-B(10)	1.743(7)	1.741(4)
B(1)-B(3)	1.793(7)	1.785(4)
B(5)-B(10)	2.052(7)	2.034(5)
B(2)-B(5)	1.798(7)	1.777(4)
B(9)-B(10)	1.798(7)	1.784(5)
B(1)-B(4)	1.798(7)	1.786(4)
O(1)-C(1)	1.149(6)	1.144(4)
O(2)-C(2)	1.153(6)	1.141(4)
B(2)-O(4)	1.526(5)	1.522(3)
O(4)-C(4)	1.479(5)	1.454(3)

1.4 Conclusion

Photochemical and thermal reaction pathways for a *nido*-6-manganadecaborane **1.1** were reported. The photochemical transformations were found to be solvent dependent. The photoreaction in THF product **1.3** has the general formulation LMB_9H_9 and its ^{11}B NMR spectra confirms its 1:3:3:3 *hypercloso* cluster geometry. It is also the first

of its type containing a group 7 transitional metal. The thermally generated **1.2** is an isomer of **1.1**. It is the first *nido*-5-metallodecaborane which contains a group 7 transitional metal. The structure of **1.2** was determined by single-crystal X-ray crystalography study. The structure has more variations in boron cages compared to **1.1**. This may indicate its different chemistry potential. The possible mechanisms for the generating of *nido*-5 isomer can be described as the skeletal rearrangement through Vertex-swing mechanism or Pentagonal-belt rotation mechanisms. The feasible high yield synthesis of this rare *nido*-5-metalladecaborane facilitates the further examination of their chemistry. The two pathways of this manganodecaborane not only demonstrate the rich chemistry of metallaborane containing group 7 metals but also suggests the possibility for existence of metalladecaboranes containing metals from groups other than 8 and 9.

In addition, using a recent report approach, we successfully synthesized two cyclic oxonium derivatives of this manganadecaborane **1.1**: the previously known THF derivative **1.6** and novel 1,4-dioxane derivative **1.7**. Through the ring-opening functionalization of these compounds a large possibility of functionalized manganadecaborane **1.1** can be easily accessed. It can be therefore expected that these work can be expanded to include many other organometallic borane clusters. Synthetic utility can be expected for this method.

Finally, a stable rhenium analog of complex **1.6**, the complex **1.8** was also synthesized and studied. This suggests the feasibility of group 7 metals to form ether substituted metalladecaboranes. With the fact that the organometallic complexes of a group 7 metal ^{99m}Tc is currently the most widely used radionuclide in diagnostic medicine,[103] the synthesis of technetium analog complex of the decaborane will have potentials for medicine applications.

Chapter 2

Photochemical Investigations of Several Metallaboranes

2.1 Introduction

The study of polyhedral borane clusters is an important branch of modern chemistry. Carboranes are boron hydride clusters in which one or more of the boron vertices are substituted by carbon atoms (Figure 31).[104,105] These main group clusters typically have between three and twelve vertices, with the icosahedral twelve-vertex structure being particularly stable. The synthesis of larger boranes and carboranes with more than 12 vertices (supercarboranes),[104] however, has mostly been the focus of detailed theoretical investigations with exceptionally few experimental examples known.[104,105] The development of this supercarboranes chemistry is well behind that of smaller carborane or metallacarborane chemistry due to the synthetic limitations.[104,105]

In this work, we explored an alternative synthetic approach to the formation of larger borane and carborane clusters with more than 12 vertices using photochemical insertion reactions between metallaboranes and alkynes. We report herein the efficient insertion of one unit of alkyne into the metalladecaborane [*nido*-6-$Mn(CO)_3B_9H_{13}$][NMe_4] (**1.1**) cluster leading to the formation of a series of C_2B_9 cluster species with the general formulation [7-R-8-R'-7,8-*nido*-$C_2B_9H_{10}$][NMe_4] (**2**). The reaction scheme is shown in Table 19. The dark or thermal reaction between the complex **1.1** and alkynes, in contrast, did not produce any products.

In addition to alkynes, the photo-interactions of some unsaturated molecules such as nitriles and ketones with complex **1.1** were also investigated. The complex

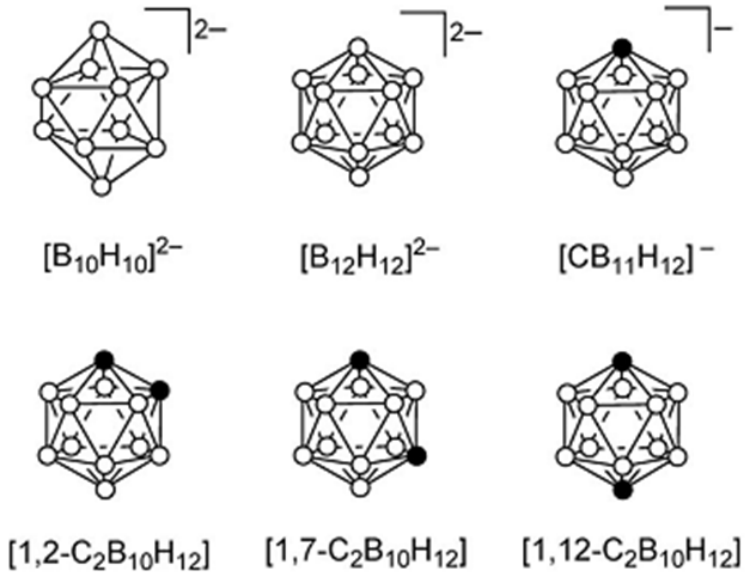

Figure 31: Selected types of borane hydride and carborane (hydrogen atoms are not shown for simplicity, and filled spheres indicate carbon atoms).

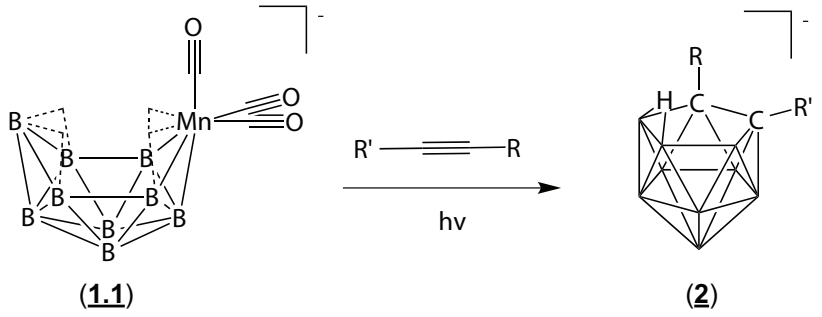

Figure 32: Photoinsertion reactions between alkynes and 6-manganadecaborane **1.1**.

1.1 was found to act as an efficient catalyst for isocyanate cyclodimerization under photo-irradiation conditions.

2.2 Research Significance

The study of larger cluster species is of significant importance to fundamental cluster chemistry as well as to several areas of application chemistry. Boron is generally considered a trivalent, metalloid element that occurs abundantly on Earth and has many properties intermediate between the metals and the electronegative non-metals.[106]Boron has a tendency to form anionic rather than cationic complexes.[25–27,107–115] Boron compounds are used as light structural solid state materials, plant micronutrients, nontoxic insecticides, energetic materials with very high energy densities, and as valuable reagents for chemical synthesis, among many other applications.[109] Boron also has an important ability to form an array of cluster compounds based upon polyhedral structures, three-dimensional multi-faced structures. These clusters, especially 12-vertex boron clusters, have been explored in many areas, such as catalysis,[25–27,112] nanotechnology, nanovehicles,[116] and boron neutron capture therapy (BNCT).[110,117] Thus, the study of boron chemistry is providing promising applications to many technological areas.[25–27,107–117]

The exploration of the organometallic and photochemistry of polyhedral borane clusters will certainly contribute to a better understanding of the mechanisms of inorganic photochemical reactions while providing useful synthetic approaches for boron complexes such as new carboranes, biologically active boron compounds, BNCT agents, and others.

2.3 Background

Boron hydride clusters have traditionally been thought of as deltahedral fragments of *closo*-parents possessing twelve or fewer vertexes. Boron hydride clusters with more

than twelve vertexes would not only benefit the theoretical studies but also potentially benefit the current applications of boron-cluster compounds, for example, in catalysis as weakly-coordinating anions[112,113] and in BNCT of tumors[117] due to larger number of boron atoms in the molecule.

It should be noted that macropolyhedral boranes have been known since the discovery of $B_{18}H_{22}$ (Figure 33) by Hawthorne and coworkers, although these are not formally regarded as polyhedral structures.[118] Recently, a number of macropolyhedral heteroborane clusters in which the heteroatom is a transition metal[119] or a main group atom[120] have also been reported. The studies of macropolyhedral boranes or heteroboranes certainly contributes to the study of boron hydrides. However, due to the fact that these macropolyhedral structures can be thought as two nominally independent cluster fragments that share a single boron atom, an edge or a triangular boron-boron-boron face, marcopolyhedral boranes or heteroboranes are not considered to be traditional polyhedral clusters as deltahedral fragments of *closo*-parents and will not be further discussed in this chapter.

Until recently, the field of polyhedral borane and carborane chemistry has been dominated by the 12-vertex icosahedral geometry, with the predominance of the *ortho*-carborane ($1,2$-*closo*-$C_2B_{10}H_{12}$) structure. Some recent advances in the field have been discussed in several reviews.[14,122] On the other hand, the study of carboranes with more than 12-vertices, often referred to as supercarboranes,[104] was completely limited to theoretical work before 2003.[123]

Theoretical work showed that for borane ion, $[B_nH_n]^{2-}$, as vertex number increases the average stability also increases, with the exception that 12-vertex structure is considerably more stable than the adjacent 13, 14 or 15-vertex structures (Figure 34).[123] This "icosahedral barrier" has been often cited to account for the experimental failures seen in the synthesis of supercarborane compounds.[124–127] Although similar calculations have not been performed for the *closo*-carboranes, the results of these computational

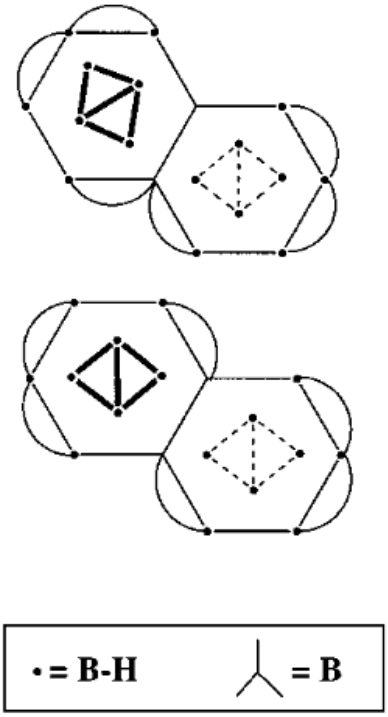

Figure 33: Selected macropolyhedral boron-containing cluster (n-$B_{18}H_{22}$). Stick diagrams representing the structures of *syn*-$B_{18}H_{22}$ (top) and *anti*-$B_{18}H_{22}$ (bottom). The arcs represent bridging hydrogens.[121]

studies on boranes suggest that several stable supercarboranes could also be viable synthetic targets as long as the "icosahedral barrier" can be overcome.

For almost half a century after the discovery of the 12-vertex carborane [1, 2-*closo*-$C_2B_{10}H_{12}$],[128] there were no reports of carboranes which extended the homologous family $C_2B_nH_{2+n}$ beyond $n > 10$ (supercarboranes) nor were there any reports of the parent borane ions $[B_nH_n]^{2-}$ for $n > 12$ (superboranes).[124–127] Although the situation for superboranes remains unchanged in recent years, there have been a few breakthroughs for supercarboranes.

The experimental evidence for the existence of a supercarborane, 1,2-μ-$C_6H_4(CH_2)_2$-3-Ph-1,2-$C_2B_{11}H_{10}$ (**2.1**), was first reported by Welch and coworkers in 2003.[124] To date, carboranes with more than 12 vertices in the supercarborane field are limited

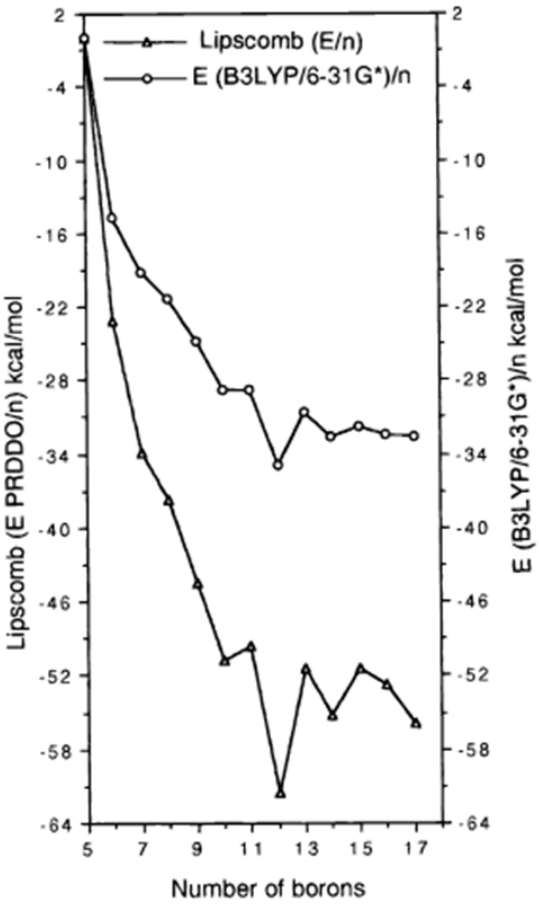

Figure 34: Plots of E_{av} the B3LYP/6-31G total energies per vertex; E_{av}=E/n in kcal/mol, and Lipscomb's PRDDO energy (E/n, kcal/mol) for large *closo*-borane dianions $B_nH_n^{2-}$ $(n = 5 - 17)$ vs number of boron atoms. Note that in both cases, the energy of $[B_5H_5]^{2-}$ is chosen as the reference (adapted from reference 123).

solely to 13 and 14 vertex carboranes. Known supercarborane compounds are given in Table 18. The advances in this field have been reviewed by Xie and coworkers.[104,105]

Thus far, the only synthetic pathways to these supercarborane compounds involves using the "polyhedral expansion" method which was originally developed by Hawthorne.[124,129] In this method, removal of the bridging proton from 7,8-μ-$C_6H_4(CH_2)_2$-7,8-*nido*-$C_2B_{10}H_{11}$ with BuLi or direct two electron (2e) reduction of 1,2-μ-$C_6H_4(CH_2)_2$-1,2-*closo*-$C_2B_{11}H_{10}$ with sodium (Na) yields the [7,8-μ-$C_6H_4(CH_2)_2$-7,8-*nido*-$C_2B_{11}H_{10}]^{2-}$ ion. This *nido*-dianion can then react with $PhBCl_2$ to afford the 13-vertex carborane **2.1** (Figure 35).[124] This method has had only limited success due

Table 18: Selected supercarborane compounds.[104]

Compound
13-vertex:
1,2-Me_2-1,2-$C_2B_{11}H_{11}$
1,6-Me_2-1,6-$C_2B_{11}H_{11}$
μ-1,2-$(CH_2)_3$-1,2-$C_2B_{11}H_{11}$
μ-1,2-o-$C_6H_4(CH_2)_2$-1,2-$C_2B_{11}H_{11}$
μ-1,2-$Me_2Si(CH_2)_2$-1,2-$C_2B_{11}H_{11}$
14-vertex:
μ-2,3-$(CH_2)_3$-2,3-$C_2B_{12}H_{12}$
μ-2,8-$(CH_2)_3$-2,8-$C_2B_{12}H_{12}$

to the fact that it requires not only the carbon adjacent [*nido*-7,8-$R_2C_2B_{10}H_{10}]^{2-}$ compound as the starting material, but it also requires a short *exo*-polyhedral C,C'-linkage that facilitates the capitation reaction by locking the two cage carbon atoms into adjacent positions.[104] In addition, the use of donor solvents, such as tetrahydrofuran and diethyl ether resulted in much lower yields because they presumably complex with the RBX_2 reactant.[104] Moreover, this method has also not been successful for synthesis of supercarboranes with more than two carbon atoms in the skeleton.

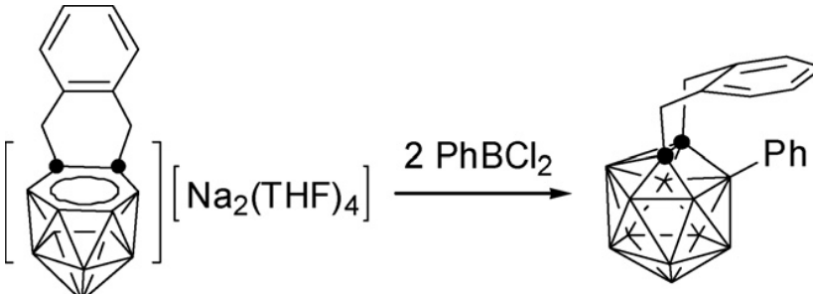

Figure 35: 13-vertex *henicosahedron*-carborane synthesis from [7,8-μ-$C_6H_4(CH_2)_2$-7,8-*nido*-$C_2B_{11}H_{10}]^{2-}$.[124]

These supercarboranes also attract research interest because they have shown to be more reactive than their 12-vertex analogs[104] and they also display properties such as reactivity towards nucleophiles to afford monocarba-*closo*-dodecarborate monoanions by cage-carbon extrusion reaction (Figure 36).[104,126,127] It was also suggested that

supercarboranes should also have other more diverse reactivities than their 12-vertex analogies.[104] In addition, theoretical work has suggested that n rather than n+1 SEP would be the stable configuration.[104]

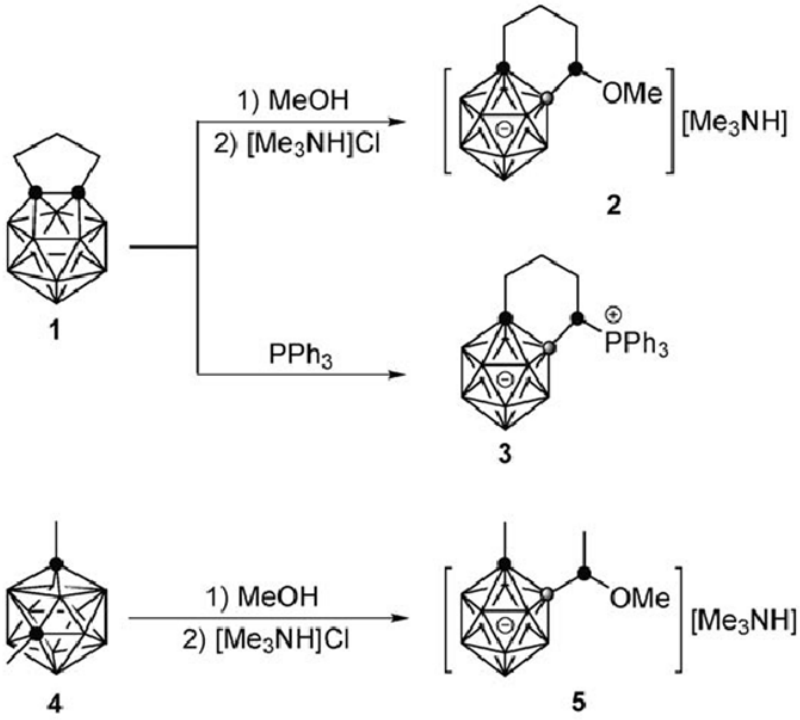

Figure 36: Reaction examples of 13-vertex carboranes with nucleophiles.[127]

In view of this perspective on the interest in supercarborane chemistry coupled with the limitations of present synthetic methods, alternative synthetic approaches to supercarborane formation would greatly benefit the exploration of this field. While most previous studies for preparing boron-containing polyhedral compounds investigated involved thermal methods, we here employed an alternative photochemical approach for the attempted synthesis of these larger boron-containing polyhedral clusters (supercarboranes).

Photochemistry is the study of the interactions between atoms or small molecules and light.[107] As an example, photosynthesis uses the energy of sunlight to convert carbon dioxide into organic compounds, especially sugars. Light has many economic

and ecological advantages over other energy sources: it is usually cheaper, safer, and does not produce industrial wastes. Importantly for our work, photochemical pathways provide options for very low temperature reactions in all three phases with the accessibility of alternate non-thermal pathways. In cluster chemistry, it is common for thermal pathways to provide many products from a single reaction that arise through fragmentation and rearrangement of the cluster fragment components. Photochemical pathways provide the possibility of activating a single reaction manifold to produce a limited number of products in significantly higher yields. Importantly, photochemistry should provide a synthetic pathway that overcomes the icosahedral barrier.[124]

Photochemical transformations are important synthetic strategies for the preparation of new compounds. However, compared to organic and inorganic photochemistry which have been extensively studied and utilized,[108] little work has been reported in the potentially fertile field of main group cluster photochemistry. In the field of the borane clusters, only few mechanistic details and general applications of photochemical processes to the synthesis and transformation of these clusters have been studied.[130,131] Considering the great contribution made by organic and inorganic photochemistry to synthetic and mechanistic chemistry, it can be anticipated that the investigations on borane, carborane and metallaborane cluster photochemistry will make similar contributions. The well-developed organic and inorganic photochemical studies provide the strong precedent for this study.

In particular, we are interested here in the photochemistry of metallaboranes. Metallaboranes are generated when boron centers in the classical binary boron hydrides are replaced architecturally by metal atoms.[132,133] The synthesis and structural features of many metallaboranes have been described in literature[134] as the "first-order chemistry" of metallaboranes, while the reaction chemistry of the metallaboranes was described as the "second-order chemistry".[134] In contrast with the "first-order

chemistry", "second-order chemistry" of metallaboranes is relatively neglected in the literature. This is particularly interesting in view of the electronic redox flexibility of borane clusters. For example, the two-electron redox steps in the well-known *closo-nido-arachno-hypho* sequence (Figure 37),[135] allied with the redox flexibility of transition-element centers,[136,137] should provide a great variety of metallaborane reaction chemistry. One aspect of potential interest concerns reactions between metallaboranes and small unsaturated molecules such as acetylene and isocyanides.[134] Possible reactions include oligomerisation, polymerization, addition, reduction, and incorporation of carbon and/or nitrogen atoms into the metallaborane clusters framework.[134] Isocyanides may additionally be used to insert a single carbon atom or both carbon and nitrogen atoms into borane clusters.[138,139] These various reaction types combined with photochemical tools provide us with the opportunity to potentially study the synthesis of larger borane clusters.

One particularly interesting photoreaction of metallaboranes is the photoinsertion reaction which was communicated by T.P Fehlner.[140,141] In his work, the author found that under UV conditions, two or more alkyne molecules could be inserted into the cluster framework of the starting metallaborane complex $[B_4H_8Fe(CO)_3]$, although these insertion products were very poorly characterized and not isolated. The metallaborane $[B_4H_8Fe(CO)_3]$ itself shows strong absorption in the UV spectral region and, from molecular orbital calculations, it was determined that it is the $Fe(CO)_3$-fragment that accounts for the absorption.[141] Therefore, it was assumed that irradiation of the $[B_4H_8Fe(CO)_3]$ complex would mainly perturb the $Fe(CO)_3$-fragment. By previous work on metal carbonyl systems in general, it has been established that the absorption of a photon by the $M(CO)_3$-fragment results in the dissociation of a labile CO ligand, producing an electronically and coordinatively unsaturated metal center. If other ligands are present, substitution or insertion reactions subsequently can occur at this unsaturated metal center. Therefore, when the $[B_4H_8Fe(CO)_3]$ complex is

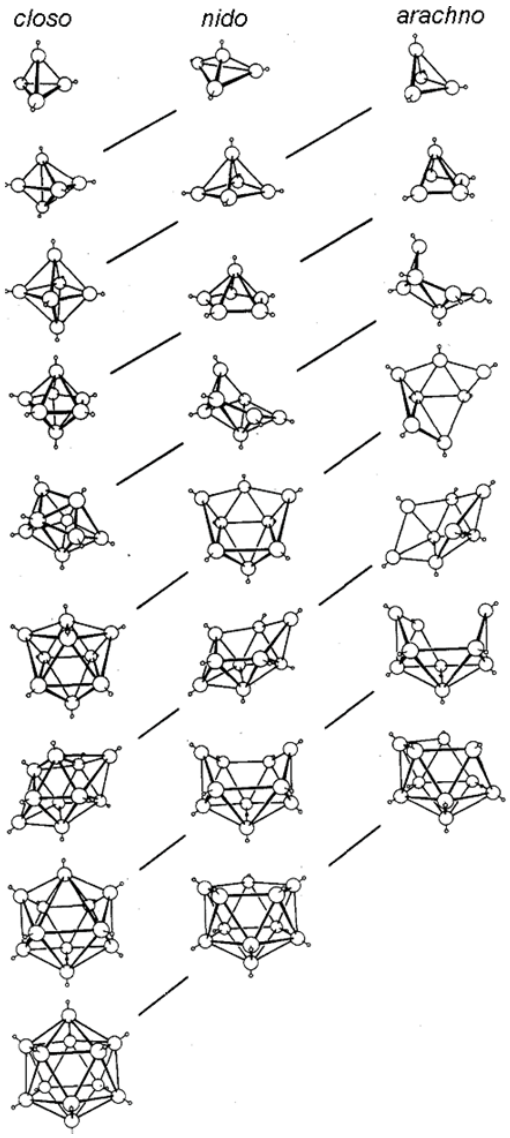

Figure 37: Idealized deltahedra and deltahedral fragments for *closo*, *nido*, and *arachno*-boranes and heteroboranes. From left to right, the vertical columns give the basic *closo*, *nido*, and *arachno* frameworks; bridge hydrogens and BH_2 groups are not shown, but when appropriate they are placed around the open face of the framework (adapted from reference 135).

excited by UV light in presence of 2-butyne, the unsaturated $[B_4H_8Fe(CO)_2]$ fragment might be expected to bind an alkyne ligand initially to the Fe center to form an metallacyclopropene structure. This places the cage ligand and the alkyne ligand in a potentially reactive position that might allow them to undergo insertion of the alkyne's sp-carbons into the open borane-cluster framework to generate the observed new carboranes, proposed by Fehlner as $Me_4C_4B_4H_4$ and $Me_6C_6B_4H_4$. This reaction provides a model example for how a photoreaction might be utilized to generate larger carborane clusters through photoinsertion reactions.[140,141]

In Fehlner's work, the $[B_4H_8Fe(CO)_3]$ complex contains the $M(CO)_3$-fragment which is the key photochemical feature of the compound. So, our first goal was to study the metallaboranes which contain a similarly photoactive $M(CO)_3$-fragment but to instead use photoinsertion to couple alkynes with larger boranes. One compound of particular interest was, therefore, the metalladecaborane **1.1** ([*nido*-6-$Mn(CO)_3B_9H_{13}$][NMe_4]) which was first reported by D.F. Gaines and coworkers in 1973.[21,64] This complex has novel metal-boron bonds which contribute to its high thermal, hydrolytic, and oxidative stability compared to that of other metallaboranes.[64] It was also mentioned by D.F. Gaines and coworkers in their original papers that the carbonyl group in Mn can be substituted by triphenylphosphine ligands under photolytic conditions.[64] Therefore, the metalladecaborane **1.1** was chosen as a suitable polyhedral metallaborane for photochemical transformation studies.

Besides the complex **1.1**, several other metallaboranes such as **1.2** ([*nido*-5-$Mn(CO)_3B_9H_{13}$][NMe_4]) and **2.6** ([$Co(CO)_3B_{10}H_{12}$][NMe_4]) were photochemically studied as well. This study also included an improved synthesis of the complex **2.6** and its first complete ^{11}B NMR characterization.

A common feature of these metallaboranes is that they all contain the $M(CO)_3$-fragment. Using conditions similar to those employed by Fehlner, we treated each

of these metallaboranes with alkynes, isocyanides or other unsaturated molecules under photochemical conditions. In this chapter, we report on the results of these investigations. ^{11}B NMR spectroscopy and mass spectrometry, among other methods, have been employed as our main characterization methods.

2.4 Experimental

2.4.1 Physical Measurements

All NMR spectra were recorded on a Bruker Avance 300 MHz NMR equipped with a 5 mm OXI probe. The ^{11}B NMR spectra were recorded at 96.3 MHz and were referenced at 96.3 MHz. Spectra were referenced to BBr_3 at +40.0 ppm (relative to BF_3Et_2O at $\delta = 0.0$ ppm) with positive chemical shifts indicating downfield resonances. Typical ^{11}B NMR acquisition parameters employed were a relaxation delay of 0.1 ms and a 90° pulse of 10 μs. As previously described, an absolute-value-mode COSY pulse sequence[58] was used to generate the t_1, t_2 data matrix (relaxation delay $-(\pi/2) - t_1 - (\pi/2) - t_2$ in which t_1 was incremented by the inverse of the sweep width in the F_1 dimension and t_2 was the usual acquisition time in a 1D experiment). The t_1, t_2 matrix was collected as 1024×256 data points. Data processing involved the application of a dc offset and first-point correction, shifted sine bell apodization, zero filling, Fourier transformation, and a magnitude calculation to give the 512×512 2D ^{11}B-^{11}B $\{^1H\}$ spectrum.[59,60] Proton (^{1}H) NMR spectra were recorded at 300.15 MHz with chemical shifts referenced to an internal standard of tetramethylsilane at δ=0.0 ppm. Carbon (^{13}C) NMR spectra were obtained at 77.47 MHz. Unit resolution mass spectra were obtained on a Hewlett Packard model 5989B gas chromatograph/mass spectrometer (GC/MS) using an ionization potential of between 11 and 70 eV. FT-IR spectra in the range of 400 to 4000 cm^{-1} were measured on a Mattson Galaxy 2020 spectrometer and were referenced to the 1602.8 cm^{-1} band of polystyrene. The spectra were observed as KBr mulls and are reported in cm^{-1}. UV-Vis spectral data were collected on a Cary 1 UV-Vis spectrophotometer in a quartz cell. All photoreactions were carried under a medium pressure mercury vapor lamp (ACE GLASS, Model: Hanovia, 7825-34, IMMERSION LAMP, Medium Pressure, 450 watt).

2.4.2 Materials

All solvents used were reagent grade or better. Tetrahydrofuran (THF) and hexane were distilled over potassium metal prior to use. TLC plates were purchased from Fisher Scientific. The *nido*-decaborane(14) ($B_{10}H_{14}$), was purchased from the Callery Chemical Company and was purified by vacuum sublimation at 40 °C prior to use. Appropriate care was taken in handling the boron hydrides under inert atmosphere conditions.[61] All reactions were done in an inert atmosphere unless otherwise noted. Deuterated NMR solvents were purchased from Cambridge Isotope Laboratories, Inc. and dried over molecular sieves before use, unless otherwise noted. All other commercially available reagents were used as received. The synthesis of complex **1.1** ([*nido*-6-$Mn(CO)_3B_9H_{13}$][NMe_4]) and **1.2** ([*nido*-5-$Mn(CO)_3B_9H_{13}$][NMe_4]) were described in section 1.2 (Page 9).

2.4.3 Experimental Procedures

[7-n-C_4H_9-7,8-*nido*-$C_2B_9H_{11}$][NMe_4] (**2a**) A solution containing 0.1 g (0.373 mmol) of complex **1.1** and 0.15 g (1.82 mmol) of 1-hexyne in dry dichloromethane was placed in a dry 20 mL Schlenk tube and photolyzed for 3 h using a medium pressure mercury lamp. During irradiation, the homogeneous reaction mixture changed from red to a colorless clear solution with a small amount of a white precipitate in the bottom. The top solution was decanted and the solvent was removed under reduced pressure. The residue was chromatographed on a 10×1 cm column of silica gel eluted with dichloromethane/hexane (3:2) to give 0.04 g (40%) of compound **2a**. ^{11}B NMR (94 MHz, $CDCl_3$, δ(ppm)): -11.06 (2B, J_{BH}=130 Hz), -13.01 (1B, J_{BH}=120 Hz), -17.19 (3B, J_{BH}=175 Hz) -21.44 (1B, J_{BH}=135 Hz), -33.32 (1B, J_{BH}=140 Hz), -37.19 (1B, J_{BH}=135 Hz). ^{1}H NMR (300 MHz, CD_2Cl_2, δ(ppm)): -2.40 (1H, B-H-B), 0.87 (3H, CH_3), 1.25 (6H, CH_2), 1.57 ppm (1H, C_{cage}-H), 3.49 (12H, NMe_3). MS: m/z = 190 ([**2a** − NMe_4]$^-$).

[7,8-Et_2-7,8-*nido*-$C_2B_9H_{10}$][NMe_4] (**2b**) A solution containing 0.1 g (0.373 mmol) of complex **1.1** and 0.15 g (1.82 mmol) of 3-hexyne in dry dichloromethane was placed in a dry 20 mL Schlenk tube and photolyzed for 3 h using a medium pressure mercury lamp. After irradiation, the reaction mixture was found to have changed from a red to a colorless clear solution with a small amount of a white precipitate in the bottom. The top solution was decanted and the solvent was removed under reduced pressure. The residue was chromatographed on a 10 × 1 cm column of silica gel eluted with dichloromethane/hexane (3:2) to give 0.05 g (45%) of compound **2b**. ^{11}B NMR (94 MHz, $CDCl_3$, δ(ppm)): -9.77 (2B, J_{BH}=124 Hz), -10.80 (1B), -17.60 (4B, J_{BH}=144 Hz), -33.58 (1B, J_{BH}=130 Hz), -36.51 (1B, J_{BH}=124 Hz).

[7- n-C_3H_7-7,8-*nido*-$C_2B_9H_{11}$][NMe_4] (**2c**) A solution containing 0.1 g (0.373 mmol) of complex **1.1** and 0.13 g (1.82 mmol) of 1-pentyne in dry dichloromethane was placed in a dried 20 mL Schlenk tube and photolyzed for 3 h, using a medium pressure mercury lamp. After irradiation, the reaction mixture was found to be a colorless clear solution with a small amount of a white precipitate in the bottom. The top solution was decanted and the solvent was removed under reduced pressure. The residue was chromatographed on a 10 × 1 cm column of silica gel eluted with dichloromethane/hexane (3:2) to give 0.06 g (60%) of compound **2c**. ^{11}B NMR (94 MHz, $CDCl_3$, δ(ppm)): -11.85 (2B, J_{BH}=131 Hz), -13.28 (1B, J_{BH}=126 Hz), -17.42 (2B, J_{BH}=120 Hz), -19.48 (1B, J_{BH}=140 Hz), -21.20 (1B, J_{BH}=136 Hz), -33.11 (1B, J_{BH}=132 Hz), -36.78 (1B, J_{BH}=140 Hz). MS: m/z = 178 ([**2a** − NMe_4]$^-$).

[7- PhC_2H_4-7,8-*nido*-$C_2B_9H_{11}$][NMe_4] (**2d**) A solution containing 0.1 g (0.373 mmol) of complex **1.1** and 0.24 g (1.82 mmol) of 4-phenyl-1-butyne in dry dichloromethane was placed in a 20 mL Schlenk tube and photolyzed for 3 h using a medium pressure mercury lamp. After irradiation, the reaction mixture was found to be a colorless clear solution with a small amount of a white precipitate in the bottom. The top solution was decanted and the solvent was removed under reduced pressure.

The residue was chromatographed on a 10 × 1 cm column of silica gel eluted with dichloromethane/hexane (3:2) to give 0.08 g (68%) of compound **2d**. ^{11}B NMR (94 MHz, $CDCl_3$, δ(ppm)): -10.31 (2B, J_{BH}=155 Hz), -12.95 (1B,J_{BH}=127 Hz), -21.23 (3B, J_{BH}=172 Hz), -24.89 (1B, J_{BH}=120 Hz), -32.88 (1B, J_{BH}=134 Hz), -36.98 (1B, J_{BH}=165 Hz).

[7-SiMe$_3$-7,8-*nido*-C$_2$B$_9$H$_{11}$][NMe$_4$] (**2e**) A solution containing 0.1 g (0.373 mmol) of complex **1.1** and 0.18 g (1.82 mmol) of ethynyltrimethylsilane in dry dichloromethane was placed in a dried 20 mL Schlenk tube and photolyzed for 2 h using a medium pressure mercury lamp. After irradiation, the reaction mixture was found to be a colorless clear solution with a small amount of a white precipitate in the bottom. The top solution was decanted and the solvent was removed under reduced pressure. The residue was chromatographed on a 10 × 1 cm column of silica gel eluted with dichloromethane/hexane (3:2) to give 0.06 g (54%) of compound **2e**. ^{11}B NMR (94 MHz, $CDCl_3$, δ(ppm)): -8.00 (2B, J_{BH}=140 Hz), -9.22 (1B, J_{BH}=144 Hz), -11.67 (1B, J_{BH}=134 Hz), -15.39 (1B, J_{BH}=121 Hz), -17.38 (1B, J_{BH}=120 Hz), -20.63 (1B, J_{BH}=126 Hz), -31.52 (1B, J_{BH}=128 Hz), -35.55 (1B, J_{BH}=133 Hz).

[7-C$_5$H$_5$FeC$_5$H$_4$-7,8-*nido*-C$_2$B$_9$H$_{11}$][NMe$_4$] (**2f**) A solution containing 0.1 g (0.373 mmol) of complex **1.1** and 0.19 g (1.82 mmol) of ethynylferrocene $(C_5H_5)Fe(C_5H_4CCH)$, in dry dichloromethane was placed in a 20 mL Schlenk tube and photolyzed for 7 h using a medium pressure mercury lamp. After irradiation, the reaction mixture was found to have become a light yellow clear solution with white precipitate in the bottom. The top solution was decanted and the solvent was removed under reduced pressure. The residue was chromatographed on a 10 × 1 cm column of silica gel eluted with dichloromethane/hexane (3:2) to give 0.10 g (70%) of compound **2f**. ^{11}B NMR (94 MHz, $CDCl_3$, δ(ppm)): -9.69 (2B, J_{BH}=142 Hz), -11.67 (1B, J_{BH}=133 Hz), -15.57 (2B, J_{BH}=153 Hz), -17.98 (1B, J_{BH}=126 Hz), -22.52 (1B, J_{BH}=129 Hz), -32.44 (1B, J_{BH}=123 Hz), -34.77 (1B, J_{BH}=145 Hz).

[7-$C_5H_5FeC_5H_4$-7,8-*nido*-$C_2B_9H_{11}$][NMe_4] (**2g**) A solution containing 0.1 g (0.373 mmol) of complex **1.1** and 0.38 g (1.82 mmol) of phenylacetylene, in dry dichloromethane was placed in a 20 mL Schlenk tube and photolyzed for 7 h using a medium pressure mercury lamp. After irradiation, the reaction mixture was found to have become a light yellow clear solution with white precipitate in the bottom. The top solution was decanted and the solvent was removed under reduced pressure. The residue was chromatographed on a 10×1 cm column of silica gel eluted with dichloromethane/hexane (3:2) to give 0.07 g (84%) of compound **2g**. ^{11}B NMR (94 MHz, $CDCl_3$, δ(ppm)): -7.55 (1B, J_{BH}=142 Hz), -9.16 (1B, J_{BH}=144 Hz), -12.26 (1B, J_{BH}=141 Hz), -15.65 (1B, J_{BH}=140 Hz), -16.82 (1B, J_{BH}=146 Hz), -18.25 (1B, J_{BH}=143 Hz), -21.14 (1B, J_{BH}=144 Hz), -31.47 (1B, J_{BH}=142 Hz), -34.77 (1B, J_{BH}=141 Hz).

[1-$C_5H_5FeC_5H_4$-1,2-*closo*-$C_2B_{10}H_{11}$] (**2.2**) A mixture of $B_{10}H_{14}$ (0.233 g, 1.90 mmol) with 0.95 g (4.5 mmol) of ethynylferrocene and 0.413 g (1.93 mmol) of Proton Sponge in benzene and acetonitrile (v/v = 4/1, 40mL) was refluxed under a nitrogen atmosphere for 5 h. The solvent was evaporated under *vacuo* and the residue was applied to a silica gel column (10×1 cm). Dichloromethane/hexane (8:2) elution gave a dark greyish solution. Removal of the solvent gave 0.218 g (0.665 mmol, 35% yield) of complex **2.2**. ^{11}B NMR (94 MHz, $CDCl_3$, δ(ppm)): -1.26 (1B, J_{BH}=140 Hz), -4.57 (1B, J_{BH}=148 Hz), -8.97 (4B, J_{BH}=153 Hz), -10.61 (2B, J_{BH}=147 Hz), -11.95 (2B, J_{BH}=151 Hz).

[7-$C_5H_5FeC_5H_4$-7,8-*nido*-$C_2B_9H_{11}$]K (**2f'**) Compound **2.2** (0.24 g, 0.7 mmol) and KOH (0.10 g, 1.8 mmol) was stirred in 50 mL degassed EtOH at room temperature for 3 h. After that, the solution was refluxed for 5 h until hydrogen bubbling was stopped and the reaction mixture was cooled to room temperature. 50 ml degassed of EtOH was added and CO_2 was bubbled through the cooled solution. The resulting precipitate of K_2CO_3 was filtered off to afford a clear yellow solution. Removal of the

solvent in *vacuo* afforded an orange powder of analytically pure **2f′** (0.24 g, 0.66 mmol, 94%). ^{11}B NMR (94 MHz, $CDCl_3$, δ(ppm)): -8.99 (2B, J_{BH}=118.06 Hz), -11.33 (1B, J_{BH}=unresolved), -15.10 (2B, J_{BH}=unresolved), -17.47 (1B, J_{BH}=151 Hz), -22.10 (1B, J_{BH}=126 Hz), -31.96 (1B, J_{BH}=unresolved), -34.10 (1B, J_{BH}=170 Hz).

Photoreaction between [KB_9H_{14}] (2.3) and 1-hexyne: Compound **2.3** (0.05 g, 0.33 mmol) and 1-hexyne (0.15 g, 1.82 mmol) in dry DCM were placed in a 20 mL Schlenk tube and photolyzed for 7 h. ^{11}B NMR spectra showed that no reaction occurred.

[$Co(CO)_3B_{10}H_{12}$][NMe_4] (**2.6**) The compound proton sponge, $C_{10}H_6(NMe_2)_2$ (0.426 g, 2 mmol) was added to a stirred solution of $B_{10}H_{14}$ (0.122 g, 1 mmol) in dry and degassed CH_2Cl_2-Et_2O (50:50, 50 ml) at room temperature. The solution became yellow immediately. After 20 minutes, $Co_2(CO)_8$ (0.171 g, 0.5 mmol) together with 50 mL THF was added and stirring was continued for 3 h. The solvent was then evaporated and aqueous Me_4NCl of 100 mL was added to the residue. Filtration gave yellow plates of **2.6** (0.11 g, 72% based on $Co_2(CO)_8$). ^{11}B NMR (94 MHz, $CDCl_3$: +20.7 (1B, J_{BH}=135 Hz), +10.9 (2B, J_{BH}=137 Hz), +7.0 (1B, J_{BH}=133 Hz), -4.5 (1B, J_{BH}=133 Hz), -7.0 (2B, J_{BH}=129 Hz), -23.0 (2B, J_{BH}=127 Hz).

General Procedures for Photoreactions Between (1.1) and Unsaturated Molecules

The unsaturated molecules investigated included: isocyanide, 1,5-dicyanopentane, acetonitrile, methyl cyanoformate, 4-heptanone, 1-indanone, ethyl pyruvate, benzaldehyde, N-benzylidenemethylamine, methyl acrylate and phenyl isocyanate.

A solution containing 0.01 g (0.0373 mmol) complex **1.1** and an excess (5-fold) of the other reactant in dry dichloromethane was placed in a 5 mm NMR tube and photolyzed for 5-15 minutes but stopped when the original color disappeared. The ^{11}B NMR spectrum was immediately taken and recorded. Observed products include

[*arachno*-B_9H_{14}]$^-$ (**2.4**) and [*nido*-B_9H_{12}][NMe_4] (**2.5**) and, other products which were not characterized.

[***arachno*-B_9H_{14}**]$^-$ (**2.4**) ^{11}B NMR (94 MHz, $CDCl_3$, δ(ppm)): -7.15 (d, 3B, J_{BH}=138 Hz), -20.10 (d, 3B, J_{BH}=136 Hz), -23.09 (d, 3B, J_{BH}=136 Hz).

[***nido*-B_9H_{12}][NMe_4]** (**2.5**) ^{11}B NMR (94 MHz, $CDCl_3$, δ(ppm)): -9.86 (d, 3B, J_{BH}=153 Hz), -13.86 (d, 3B, J_{BH}=145 Hz), -33.78 (d, 2B, J_{BH}=138 Hz), -52.05 (d, 1B, J_{BH}=128 Hz).

Photo Interaction of pheynlisocyanate with complex 1.1 in NMR tube

Complex **1.1** (0.001 g, 0.003 mmol) and 0.016 ml (0.15 mmol) phenylisocyanate were placed in a NMR tube and sonicated for 10 min before being put in the photoreactor for 10 min. The solution became colorless. Then this solution was filtered and slow evaporation gave 0.026 g (85 %) colorless crystal of 1,3-diphenyl-urea after filtration.

Photo Interaction of n-butylisocyanate with complex 1.1 in NMR tube

Complex **1.1** (0.001 g, 0.003 mmol) and 0.017 ml (0.15 mmol) of n-butylisocyanate were placed in a NMR tube and sonicated for 10 min before being put in the photoreactor for 10 min. The solution became colorless. This solution was then filtered and slow evaporation gave 0.024 g (91 %) colorless crystal of 1,3-dibutyl-urea after filtration.

2.5 Results and Discussions

2.5.1 Synthesis and Structure of [*nido*-6-$Mn(CO)_3B_9H_{13}$][NMe_4] (1.1)

The starting manganadecaborane employed in this work was the tetramethyl ammonium salt of the anionic [*nido*-6-$Mn(CO)_3B_9H_{13}]^{-1}$ complex, **1.1**. A modified method from literature was used for the synthesis of this complex.[21] Compound **1.1** is an air-stable, reddish-orange crystalline material[21] and stable in dichloromethane (DCM) for several months. However, in the original paper, the authors characterized the compound **1.1** using only spectroscopic methods. In order to gain more insights into its structure, we carried out a crystallographic study of this metallaborane **1.1**. The detailed crystallographic studies are presented in section 1.3.2 (Page 41).

The crystal structure of this metallaborane is shown in Figure 24 and the ^{11}B NMR spectrum in $CDCl_3$ is shown in Figure 38. The reported ^{11}B NMR spectrum for this complex consists of six resonances at 10.8 (2B, B(1), B(3)), 9.2 (2B, B(5), B(7)), 0.1 (1B, B(9)), -1.8 (2B, B(8), B(10)), -27.6 (1B, B(2)), and -34.3 (1B, B(4)) ppm and our data is consistent with these values (Figure 38).

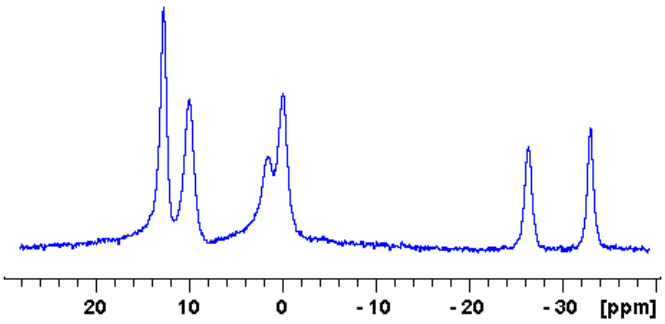

Figure 38: Our experimental ^{11}B NMR spectrum of the complex **1.1** in $CDCl_3$ at 96.3 MHz.

In order to fully characterize this starting complex as required for our subsequent work, we completed the 2-D ^{11}B-^{11}B COSY NMR experiment for the complex **1.1**. The 2-D ^{11}B-^{11}B COSY NMR spectrum is shown in Figure 39. In general, linked boron

atoms in cluster compounds give rise to observable cross peaks in the spectrum.[59,60] Observed cross-peaks in the 2D spectrum of complex **1.1** include: 10.8 with 9.2, -1.8, -27.6 and -34.3; 9.2 with -27.6; 0.1 with -34.3; and -1.8 with -34.3. The peak at 10.8 has a relative intensity of two unit boron atoms and it is linked to all other peaks in the spectrum except the peak at 0.1. From the structure shown in Figure 24, the possible symmetric boron atoms are B1 and B3 and the resonance found at 0.1 ppm can therefore be assigned uniquely to B9. The B9 resonance is shown to be cross-linked with that at -34.3 ppm which can then, therefore, be assigned to B4. In a similar process, the rest of the unique boron atoms can be assigned in the spectrum. It should be noted that, however, the B5 - B10 and B7 - B10 cross-peaks were not observed in the spectrum. This can be explained as a long boron to boron bond (2.025 Å based on the crystal structure) and the B-H-B bridging effect which usually eliminate the cross peaks.[59]

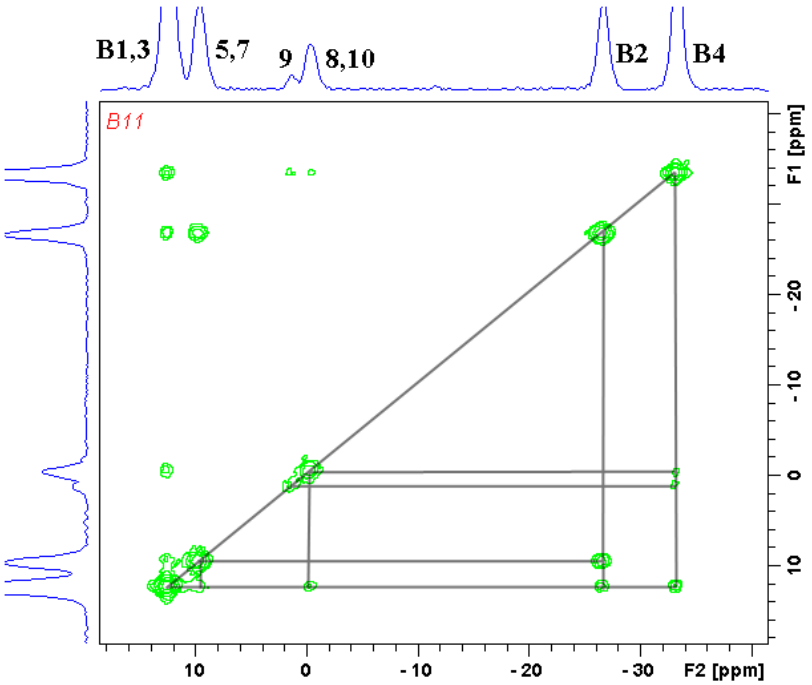

Figure 39: 2D COSY ^{11}B-^{11}B NMR spectrum of the complex **1.1** in $CDCl_3$ at 96.3 MHz.

2.5.2 Photochemical Studies of 1.1 with Alkynes

Synthesis and Characterization of Photoreaction Products 2a-2g

The electronic redox flexibility of borane clusters is illustrated, for example, in the well-known two-electron differences in the *closo-nido-arachno-hypho* sequence shown in Figure 37.[123] When these cage redox features are allied with the redox flexibility of transition-element centers, a very rich metallaborane reaction chemistry is anticipated. This theme has been seen in many aspects of metallaborance cluster chemistry but still presents a vast potential for exploring new science related to cluster-based reactions, especially through photochemical processes.[134]

Several *nido*-6-metalladecaboranes, such as $[(PPh_3)_2HIrB_9H_{13}]$, $[(C_6Me_6)RuB_9H_{13}]$, $[(PPh_3)(Ph_2PC_6H_4)HIrB_9H_{12}]$, $[(MeC_6H_4\text{-}^iPr)RuB_9H_{13}]$ and $[(C_5Me_5)RhB_9H_{13}]$ are known in the literature to react with acetylenes and/or isocyanides to give complete or partial incorporation of carbon and nitrogen heteroatoms into the frameworks of the metallaborane clusters under thermal or room temperature conditions.[134] In contrast, under the same conditions (room temperature or reflux in solvent), we have found that other metallaborane species, including the titled manganadecaborane species **1.1** do not lead to any insertions into the framework of the metallaborane cluster, as monitored by the ^{11}B NMR spectroscopy. This observation demonstrates the exceptional stability of **1.1** framework as compared with some of the other previously investigated metalladecaboranes. This can be partially explained not only by the nature of the different metals but also by the exopolyhedral metal ligands: carbonyl ligands for manganese, phosphines for iridium and cyclopentadienyl for ruthenium and rhodium.

Metal carbonyl groups on metals have been shown to be important for insertion reactions. The known photoinsertion reactions between alkynes and the metallaborane $[B_4H_8Fe(CO)_3]$ to yield carboranes proposed to be two to four vertices larger[140,141]

strongly suggests the importance of the photolytic dissociation of carbonyl ligands in $[B_4H_8Fe(CO)_3]$ by providing an unsaturated site presumably for alkyne coordination prior to insertion (equation (2.1)).

$$[B_4H_8Fe(CO)_3] + CH_3C{\equiv}CCH_3 \xrightarrow{h\nu} (CH_3)_4C_4B_4H_4 + (CH_3)_6C_6B_4H_4 \qquad (2.1)$$

The important role of the metal carbonyl group can also been seen in the $Ru_3(CO)_{12}$-promoted dehydro alkyne insertion reaction of 2-butyne into the neutral $2,3\text{-}Et_2C_2B_4H_6$ (equation 2.2):[142]

$$\begin{aligned} 2,3\text{-}Et_2C_2B_4H_6 + 2\text{-butyne} \xrightarrow{Ru_3(CO)_{12}} 4,5\text{-}Me_2\text{-}7,8\text{-}Et_2C_4B_4H_4 + \\ 5\text{-}[HMeC{\equiv}CMe]\text{-}2,3\text{-}Et_2C_2B_4H_5 + 2\text{-butene} \end{aligned} \qquad (2.2)$$

The important role of the carbonyl groups is not surprising considering the well-studied fact that irradiation of $(arene)M(CO)_3$ complexes can result in the photo-substitution of CO to yield substituted derivatives in the presence of an entering nucleophilic group, X, or oxidative-addition substrate, Y-Z, to yield $(arene)M(CO)_2X$ or $(arene)M(CO)_2(Y)(Z)$ complexes, respectively.[143]

We first studied the absorption spectrum of the metalladecaborane **1.1**. The UV-Vis spectra of **1.1** in dichloromethane is shown in Figure 40. It shows that the compound has a strong absorption band in the 250-400 nm range. We showed earlier in Chapter 1 that, under photo-irradiation conditions, **1.1** in dry dichloromethane is converted to [*hypercloso*-$Mn(CO)_3B_9H_9$][NMe_4] (**1.3**) before finally producing the very stable $[B_9H_{14}]^-$ anion by extrusion of the manganese carbonyl center, promoted by a photoinduced carbonyl loss. This demonstrates the possibility that further photochemical investigations on this complex might be successful in intercepting the *hypercloso*-intermediate to form new complexes. We, therefore, chose to investigate the reactions of **1.1** with unsaturated molecules such as acetylenes and isocyanides

under UV irradiation conditions. We found that under photo-irradiation in dry dichloromethane, **1.1** did not react with isocyanides and only the demetallation product **1.4** ([*arachno*-B_9H_{14}][NMe_4]) was observed. The photoreaction of this complex with alkynes, however, was found to form a variety of photo-insertion products, depending upon the choice of the alkyne employed. Importantly, none of the alkynes or isocyanides examined were found to undergo any observable reactions with **1.1** under dark or thermal conditions.

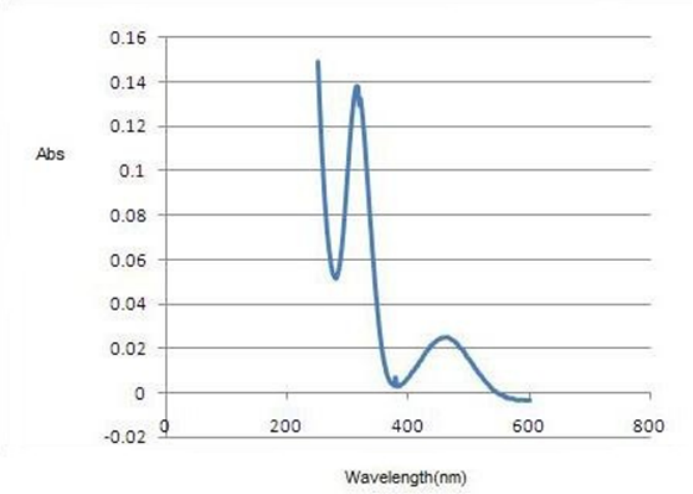

Figure 40: UV-Vis spectrum of the complex **1.1** in dichloromethane at r.t.

In a typical reaction, a solution containing **1.1** and a 10-fold of excess alkyne in dry dichloromethane was photolyzed using a high pressure mercury lamp (max. at 254 nm) until the ^{11}B NMR spectrum indicated that all of the starting manganadecaborane **1.1** was consumed. Standard workup procedures afforded the products **2a**-**2g** in good yields as determined by ^{11}B NMR spectroscopy (Table 19).

The course of the photoreaction of **1.1** with an excess of 1-hexyne was monitored by ^{11}B NMR spectroscopy. Figure 41 shows the ^{11}B NMR spectra for this reaction ranging in time from 0 to 170 min of irradiation. Six new signals were detected from the photoreaction of the **1.1** (one peak overlaps with the starting manganadecaborane complex). It can be observed that these new peaks increased in intensity as the

Table 19: Photoreaction between **1.1** and various alkynes (yield determined by ^{11}B NMR data).

Entry	alkyne	product **2**	%yield
1	$CH_3(CH_2)_3C{\equiv}CH$	**2a**	40
2	$CH_3CH_2C{\equiv}CCH_2CH_3$	**2b**	45
3	$CH_3(CH_2)_2C{\equiv}CH$	**2c**	60
4	$C_6H_5CH_2CH_2C{\equiv}CH$	**2d**	68
5	$Si(CH_3)_3C{\equiv}CH$	**2e**	54
6	$C_5H_5FeC_5H_4$-$C{\equiv}CH$	**2f**	70
7	C_6H_5-$C{\equiv}CH$	**2g**	84

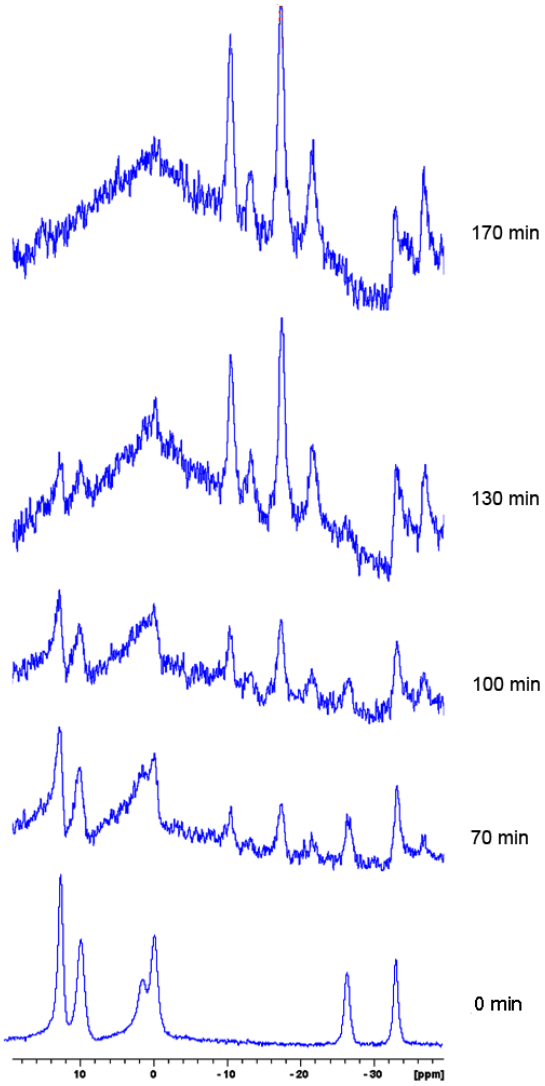

Figure 41: ^{11}B NMR spectrum monitoring of the reaction of 1-hexyne with **1.1**.

peaks of the starting manganadecaborane decreased in intensity, ultimately with the complete disappearance of the starting signals after about 170 min of irradiation. The relative area integrations of the new signals were constant within the reaction course, thus it suggested that the original manganadecaborane cluster was converted to a single boron-containing cluster product. This was confirmed by a 2-D ^{11}B-^{11}B COSY NMR spectrum of the reaction solution (Figure 42). The crosspeaks observed in the 2D experiment included crosspeaks from the resonance at -11.06 ppm with those at -17.19 and -33.32 ppm, a crosspeak from the resonance at -13.01 ppm with that at -37.19 ppm, crosspeaks from the resonance at -17.19 ppm with those at -21.44, -33.32 and 37.19 ppm, and a crosspeak between the resonances at -21.44 and -37.19 ppm. The presence of these crosspeaks provided connectivity between all of the new boron signals indicating the formation of a single product compound.

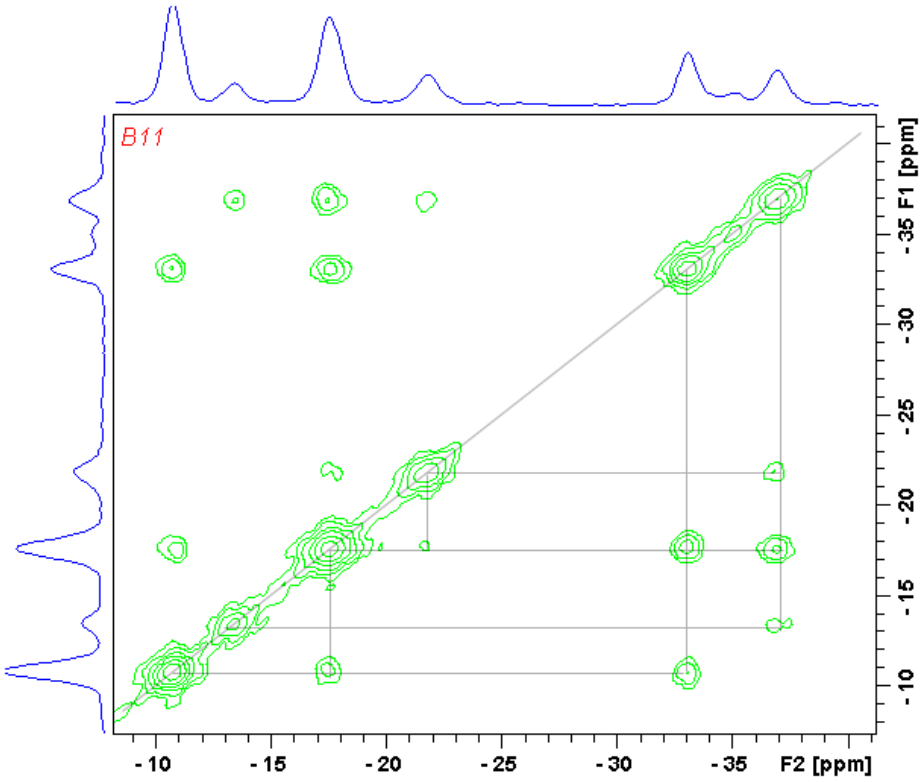

Figure 42: 2-D ^{11}B-^{11}B COSY NMR spectrum of the compound **2a** (no signals in other regions of the spectrum were observed).

The resulting product from the photoreaction was applied to a silica column and one boron-containing product (**2a**) was separated using DCM/hexane (2:1) as eluent. This product was characterized using ^{1}H and ^{11}B NMR spectroscopy, IR spectroscopy, and EI-MS. The ^{11}B NMR spectrum shown in Figure 43 reveals a 2:1:3:1:1:1 pattern of resonances in the region -10 to -40 ppm. The IR spectrum showed a normal boron cluster BH stretch at 2500 cm^{-1}. Based on the ^{11}B NMR (Figure 43) and ^{11}B-^{11}B COSY NMR spectrum (Figure 42), the structure can be proposed as a C_2B_9 boron cluster anion with one butyl group attached to one of the cage carbon atoms.

The structure of **2a** was further confirmed by the EI-MS (Figure 44) which showed a parent envelope at 190 m/z. The MS spectrum also gave the fragments at 175, 160, 145, 131, and 117. This is consistent with the alkyl group attached to the cage carbon in **2a**. ^{1}H NMR spectra (Figure 2.12) shows signals of carborane CH at 1.57 ppm (int 1), and the tetramethylammonium group signal appears at 3.49 ppm (int 12).

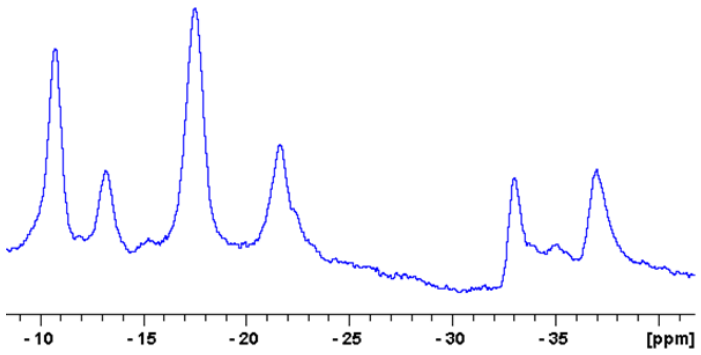

Figure 43: ^{11}B NMR spectrum of the compound **2a**

As shown in Table 19, in addition to 1-hexyne, a number of other alkynes were also found to yield similar products from this type of photoinsertion reaction. We examined a number of alkynes, including a variety of terminal alkynes, such as 1-pentyne, 4-phenyl-1-butyne, ethynylferrocene and ethynyltrimethylsilane. The approximate reaction rate, however, was found to be relatively insensitive to the alkyne substrates investigated. For instance, the highly electron-rich ethynylferrocene reactant (Table 19,

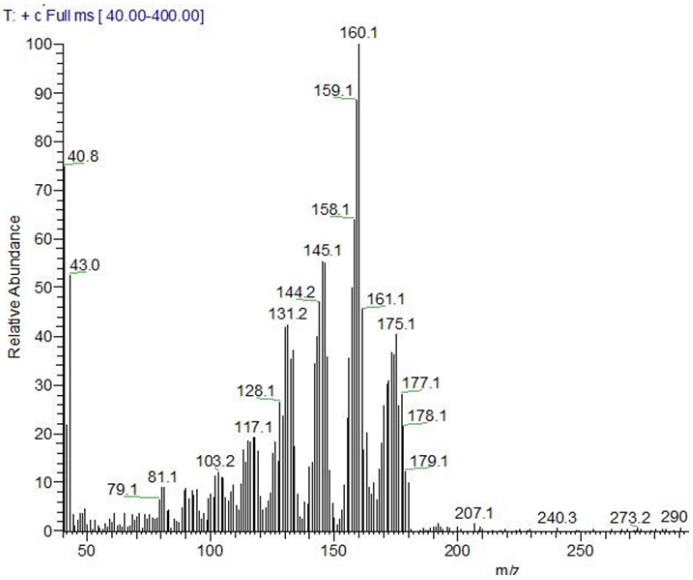

Figure 44: EI-MS spectra for the compound **2a**

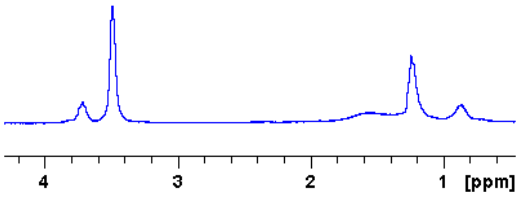

Figure 45: ^{1}H NMR spectra of the compound **2a**

entry 5) and other alkynes reacted at about the same rate and smoothly formed the inserted products. Internal alkynes seemed to be also similarly reactive in comparison with terminal alkynes (Table 19, entry 2 as an example). Comparisons of the ^{11}B NMR spectrum of **2a**-**2g** (Table 20) suggest that the products **2a**-**2g** from these reactions contained the same boron framework cluster structure to that found for **2a** but are simply substituted with different pendant groups. The photoreaction products, therefore, can be used to produce a series of carborane cluster compounds whose general formula can be written as [7-R-8-R'-7,8-*nido*-$C_2B_9H_{10}$][NMe_4] (**2**).

The C_2B_9 cluster is based upon a 12-vertex *closo*-icosahedral framework in which one vertex has been removed. The resulting 11-vertex *nido*-structure is composed of

Table 20: ^{11}B NMR data of photoreaction products **2a**-**2g**.

compound	^{11}B/δ
2a	-11.06 (2B), -13.01 (1B), -17.19 (3B), -21.44 (1B), -33.32 (1B), -37.19 (1B)[a]
2b	-9.77 (2B), -10.80 (1B), -17.6 (4B), -33.58 (1B), -36.51 (1B)
2c	-11.85 (2B), -13.28 (1B), -17.42 (3B), -21.20 (1B), -33.11 (1B), -36.78 (1B)
2d	-10.31 (2B), -12.95 (1B), -21.23 (3B), -24.89 (1B), -32.88 (1B), -36.98 (1B)
2e	-8.0 (2B), -9.22 (1B), -11.67 (1B), -15.39 (1B), -17.38 (1B), -20.63 (1B), -31.52 (1B), -35.55 (1B)
2f	-9.69 (2B), -11.67 (1B), -15.57 (2B), -17.98 (1B), -22.52 (1B), -32.44 (1B), -34.77 (1B)
2g	-7.55 (1B), -9.16 (1B), -12.26 (1B), -15.65 (1B), -16.82 (1B), -18.25 (1B), -21.14 (1B), -31.47 (1B), -34.77 (1B)

[a] ^{11}B chemical shifts (ppm) are relative to BF_3OEt_2 at 96.3 MHz. The peak assignments are shown in Figure 49.

nine BH and two CH units (Figure 46). The carbon atoms are nearest neighbours located along the open pentagonal face of the cage framework. In addition, the structure contains one *endo*-bridging hydrogen along the open face. This analysis is consistent with the well-known relationship between skeletal bonding electrons and observed cluster framework geometry. The electron counting rules developed by Wade,[144,145] Mingos,[146] Williams,[147] and Rudolph[135,148] provide an empirical way for predicting the structure of cluster molecules. Using the general formula proposed for compounds **2a**-**2g**, these clusters consist of two CH units, each giving three framework electrons, and nine BH units, each giving a total of two framework electrons. In addition, the *endo*-hydrogen atoms and the negative charge each provide one additional

electron to the total skeletal electron count. These contributions bring the total framework electron counting for the cluster to $(2 \times 3) + (9 \times 2) + 2$ or 26 skeletal electrons (12 bonding pairs). Since the total number of skeletal bonding electrons of the cluster corresponds to a 2n+4 formulation (n is the vertex number, in this case, n is eleven), according to Wade's Rule,[144,145] the cluster is a *nido*-structure type. We can therefore write the general formula as [7-R-8-R'-7,8-*nido*-$C_2B_9H_{10}$][NMe_4] (Figure 46), which is consistent both with electron counting and spectroscopic information discussed above.

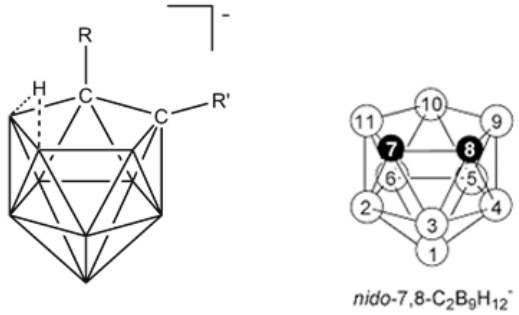

Figure 46: General structure (left) of photoreaction products **2** ($[NMe_4]^+$ cation and hydrogen atoms are omitted except for the endo hydrogen), and the numbering system (right) for the structure (7, 8 are carbons).

Among the compounds **2a**-**2g** produced in this new photochemical pathway, the carborane anions in compounds **2b** and **2g** are previously known compounds, prepared by the conventional route from *ortho*-carborane $C_2B_{10}H_{12}$ (**2.7**) (Figure 47, *vide infra*).[149–151] These compounds **2a**-**2g** are derivatives for a well-known carborane anion in carborane chemistry, the mono-anion [*nido*-7,8-$C_2B_9H_{12}$]$^-$ (**2.8**).[122,138,149,151,152] This mono-anion can be deprotonated by a strong base to form the dicarbollide dianion [*nido*-7,8-$C_2B_9H_{11}$]$^{2-}$ (**2.9**) (Figure 48), which is formally isolobal to cyclopentadienide and thus has formed an important ligand in organometallic and metallacarboane chemistry.[153] Through this **2.9** species, a relatively large numbers of carboranes, metallacarboranes, and heteroboranes have been prepared.[154–158]

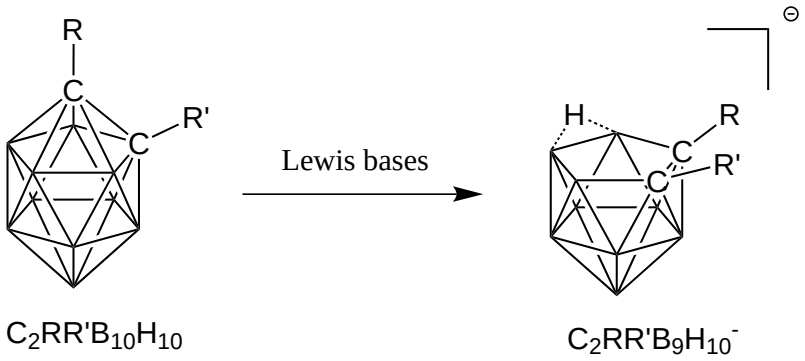

Figure 47: Deboronation of carborane **2.7** by Lewis bases.

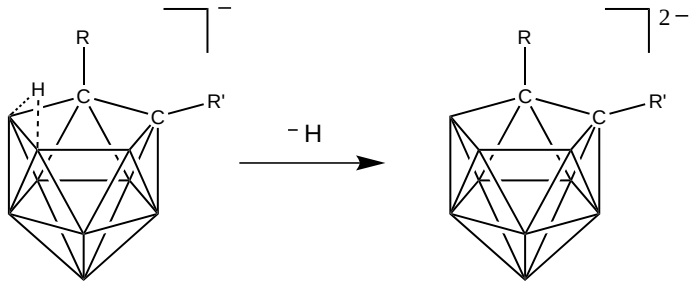

Figure 48: Dicarbollide dianion synthesis.

It is important to note that the previously known synthetic procedures for preparing the *nido*-carborane anion **2.8** are quite different from our photolytic approach. The *nido*-carborane anion **2.8** has been prepared from the easily accessible mono or bis-carbon substituted 12-vertex (icosahedral) **2.7**[159] parent compounds by removing one boron vertex using a variety of Lewis bases (Figure 47).[160–163]

The *nido*-carborane anion **2.8** has been well-characterized by spectroscopic methods.[160–162,164–166] Its structure has also been determined experimentally by X-ray and neutron diffraction as its $[(Me_2SO)_2H]^+$, $[(Me_2N)_3PNH_2]^+$ and PSH^+ salts.[164–166] These structures contain well defined C_2B_9 clusters where all hydrogen atoms were located.

Although crystallization attempts of our compounds **2a**-**2g** did not readily provide a suitable crystal for crystallographic studies, the structures for compounds **2a**-**2g**

as shown in Figure 46 were further confirmed by comparisons with the characterized known 11-vertex *nido*-carboranes anion **2.8** and its derivatives in literature. The stick representations of ^{11}B NMR spectra for compounds **2a**-**2g** and literature compounds **2.8** and its derivatives[149,150,167] are shown in Figure 49. The range and similarities of these NMR patterns further support the identification of the dicarborane cage cluster structure as the same in both our and the literature compounds. The same *nido*-carborane anion in compound **2b** was previously reported by Vinas and cowokers as its $[HNMe_3]^+$ salts using the method of removing one boron vertex from the icosahedral [*closo*-1,2-$(Et)_2$-1,2-$C_2B_{10}H_{10}$] (**2.10**) (complex **2b** and complex [7,8-Et_2-7,8-$C_2B_9H_{12}]^-$ as shown in Figure 49).[149] Similarly, the product **2f** was reported by Weller and coworkers in its K^+ salts by deboronation of [1-$C_5H_5FeC_5H_4$-1,2-*closo*-$C_2B_{10}H_{11}$] (**2.2**) (**2f** and [7-Fc-7,8-$C_2B_9H_{12}]^-$ in Figure 49).[150] Although both of the **2.10** and **2.2** were characterized only by spectroscopic methods,[149,150] as shown in Figure 49, their structures were confirmed by crystallographic studies of their metallacarborane derivatives.[149,150] From Figure 49, although NMR data of our photoproducts **2b** and **2f** are not exactly the same as reported values, the relative positions and intensities in both cases are very similar. The differences can be explained as arising from the different NMR parameters and solvents that were employed in literature and in our work.

To further confirm the structure of the compound **2f**, we used the modified conventional route[150] (Figure 50) to independently synthesize the compound **2f'**. Using Lewis-base or Proton Sponge, ethynylferrocene can be inserted into decaborane in refluxed toluene to generate the ferrocene substituted *ortho*-carborane **2.1**. The ferrocene substituted *o*-carborane **2.1** can then undergo the deboronation reaction in refluxed ethanol to afford the carborane anion [7-$C_5H_5FeC_5H_4$-7,8-*nido*-$C_2B_9H_{11}$]K (**2f'**) in quantitative yield. The ^{11}B NMR spectra comparison for compounds **2f** and

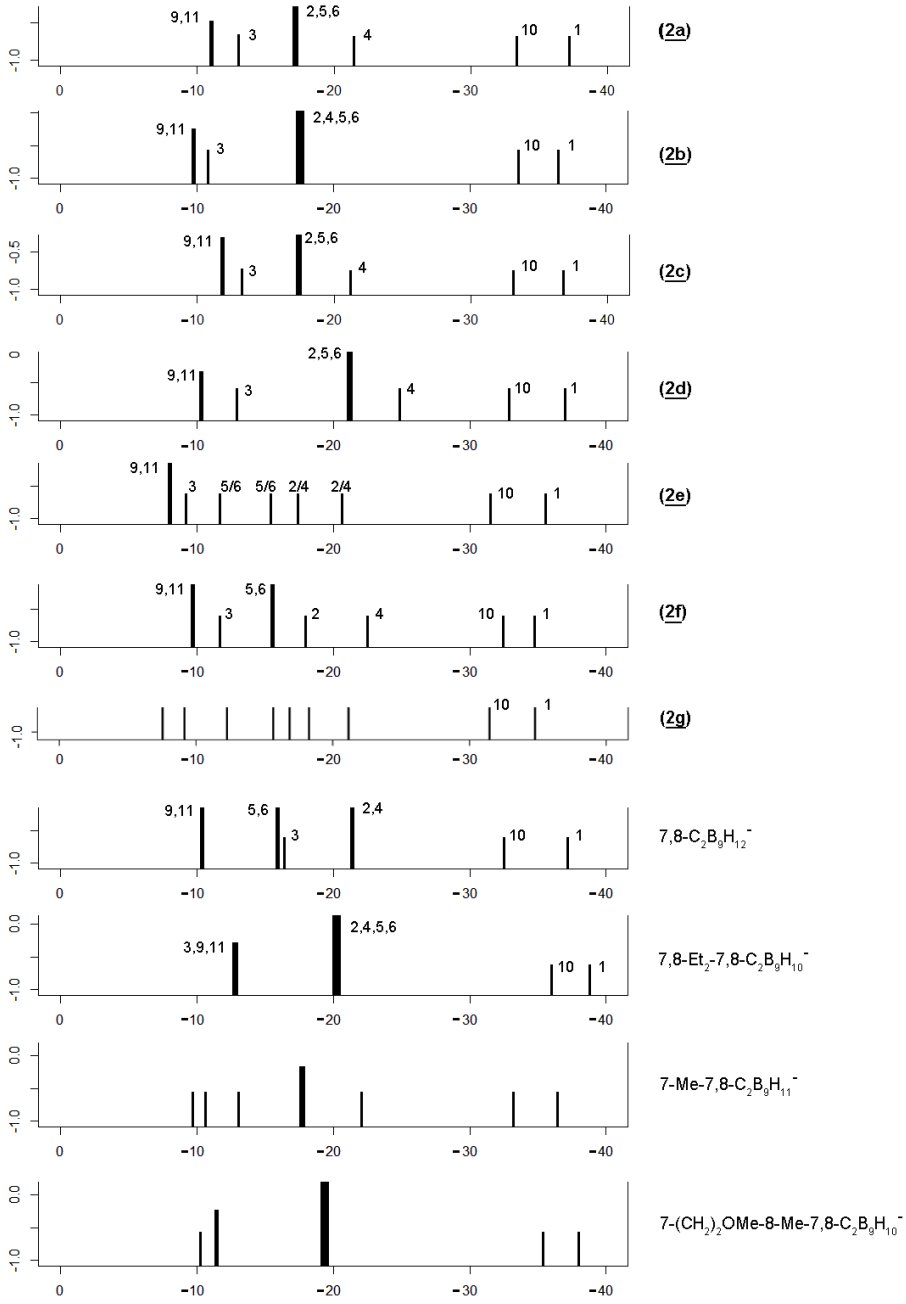

Figure 49: Stick presentation diagram of ^{11}B NMR comparisons for **2a**-**2g** and literature compounds. (Literature compounds data from references 149, 150)

2f' are shown in Figure 51. The almost identical spectra indicate the same boron cluster structure.

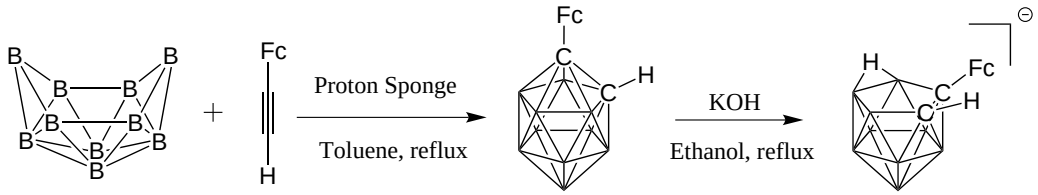

Figure 50: Modified route for the synthesis of compound **2f'**.

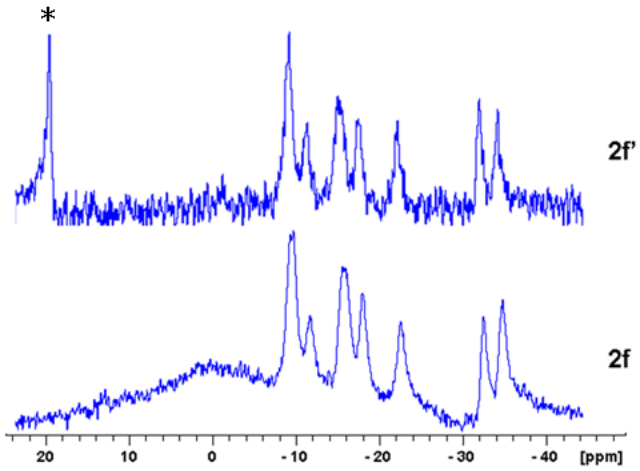

Figure 51: ^{11}B NMR spectra comparison of compounds **2f** and **2f'** in $CDCl_3$ at 96.3 MHz. (The $*$ shows the signal of the borates as a result of the deboronation process).

It was unexpected in our work that only one single alkyne unit would insert into the cage structure to produce the known C_2B_9 monoanion, in contrast to the multi-insertions products mentioned previously in Fehlner's work,[140,141] possibly due to the icosahedral barrier (*vide infra*).

This photoreaction of the complex **1.1** with alkyne is unique when compared with other *nido*-6-metalladecaboranes such as $[(PPh_3)_2HIrB_9H_{13}]$.[2] For other *nido*-6-metalladecaboranes insertion reactions, the metal atoms remain in the final cluster product to generate a new metallacarborane,[2] while for the photoinsertion of **1.1**,

the manganese center was extruded from the cluster to generate a free carborane cluster product. Importantly, this photoreaction of manganadecaborane provides an alternative route to the *nido*-carborane anion **2.8** ([*nido*-7,8-$C_2B_9H_{12}$]$^-$) derivatives synthesis and gives insights into the cage photoinsertion process.

2.5.3 Mechanism Discussion

The reactants and products of the key photoreaction investigated here can be written as shown in Figure 52. This was an unexpected result since, based upon analogy with Fehlner's work,[140,141] where we had anticipated that a more extensive cage expansion process would occur that would involve more than one alkyne unit. Nonetheless, it appears that an insertion reaction does occur leading to a two vertex expansion process and that the reaction mechanism can be compared with the photoinsertion reaction of [$B_4H_8Fe(CO)_3$] and set in the context of other known organometallic photoreactions.[140–142] Although a complete mechanism cannot be defined, consideration of the photoinsertion reaction of [$B_4H_8Fe(CO)_3$] provides some insights for the mechanism.

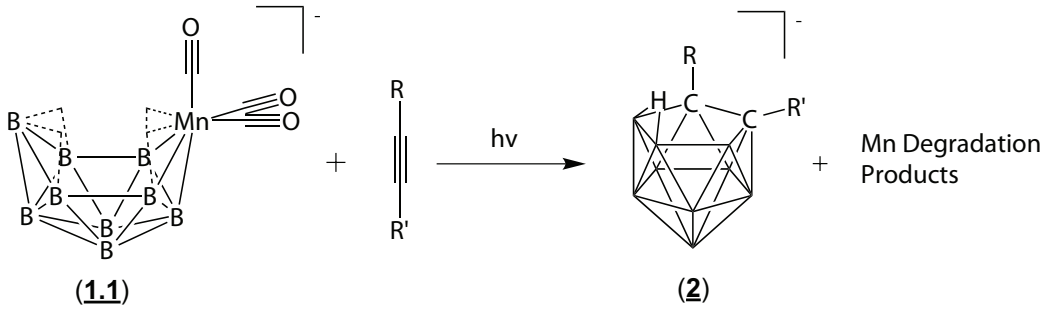

Figure 52: Photoinsertion reaction between alkynes and 6-manganadecaborane **1.1**.

We previously have shown in Chapter 1 that the photolysis of the complex **1.1** is solvent dependent. The products include the complex **1.3** ([*hypercloso*-$Mn(CO)_3B_9H_9$][NMe_4]) in THF, or **1.4** ([*arachno*-B_9H_{14}][NMe_4]) in dichloromethane

(Figure 27). This indicates that the photochemical intermediate may involve in the observed photoinsertion of alkyne into the metalladecaborane **1.1**.

The photoreaction of **1.4** ([*arachno*-B_9H_{14}][NMe_4]) with alkynes was also investigated by us under the same condition as employed in the **1.1** photochemistry studies but this led to no observable reaction. This demonstrates the important role of the manganese center in the photoinsertion reaction and suggests that an intermediate organometallic compound must be formed before the ultimate extrusion of manganese center.

Based on the role of the photoactive manganese carbonyl center and a previous study on the photolysis of the metalladecaborane **1.1**, we propose a plausible mechanism for the photoinsertion of alkyne into the manganadecaborane to form the carborane **2** (**2a**-**2g**) derivatives as shown in Figure 53. Under photo-irradiation conditions, the starting *nido*-manganadecaborane complex is first converted to a *isonido*-manganadecaborane complex through the loss of two hydrogens. Continued irradiation would be expected to result in the loss of a photolabile carbonyl ligand on manganese center to produce a coordinatively unsaturated 16-electron intermediate.[168] Addition of an alkyne ligand to the manganese center then would give the 18-electron manganadecaborane alkyne coordination intermediate. Once formed, the coordinated alkyne ligand may then undergo a migratory insertion into the adjacent M-B bond to give the 12-vertex metallacarborane intermediate (Figure 53).[134,169–171] This insertion leaves a vacant coordination site on the 16-electron manganese complex. At this point, the complex could either coordinate another alkyne ligand to be set up for a second migratory insertion process into the cage framework or undergo a cage elimination reaction to form the C_2B_9 product. Experimentally, further irradiation in the presence of excess alkyne results in liberation of the free carborane [*nido*-7,8-$C_2B_9H_{12}$]$^-$ (**2.8**) derivatives anion. The choice between these two final pathways may be dictated by the effects of the well-known icosahedral barrier, promoting the elimination of the C_2B_9 species,

based upon an icosahedral parent, over the formation of a C_4B_9, thirteen-vertex product, based upon a fourteen vertex parent structure.

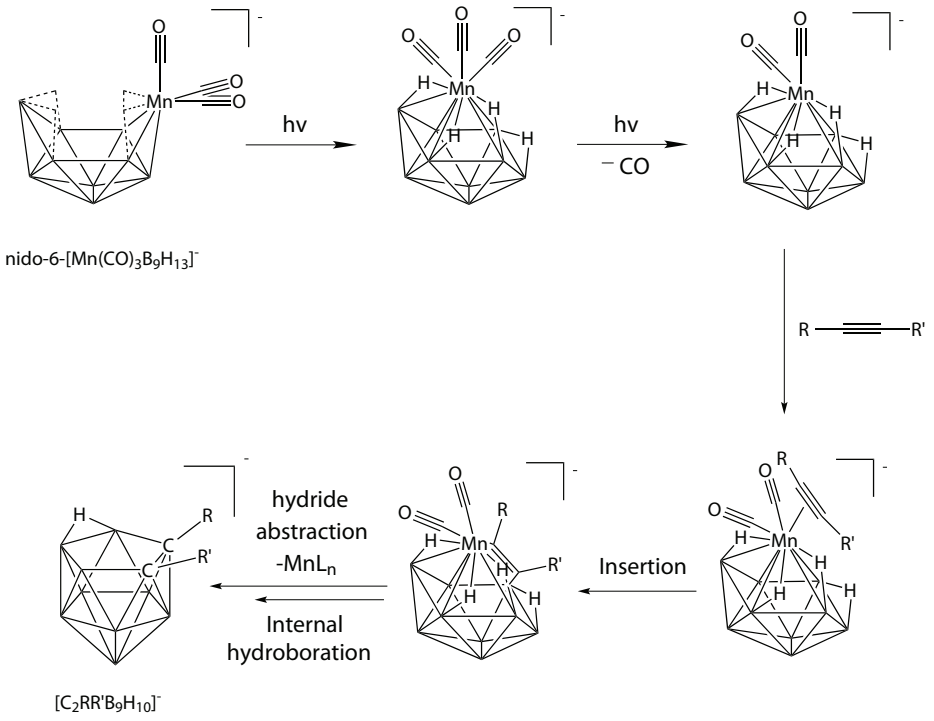

Figure 53: Proposed mechanism for the photoinsertion reaction.

It should be noted that in this mechanism (Figure 53) the steps involving an alkyne insertion into the *isonido*-manganadecaborane framework can be regarded as analogous to the known alkyne insertion into metallacyclopentadiene compounds (MCPs),[172,173] affording benzene derivatives (Figure 54). The latter is a key step in metal catalyzed [2+2+2] cyclotrimerization reactions of alkynes (Figure 55).[174–179] The transition-metal catalyzed [2+2+2] cycloaddition of alkynes is a very powerful method for the construction of substituted arenes in a single operational step (Figure 55). This provides an extremely atom-efficient pathway for arene syntheses.[176] During the past four decades this reaction has been extensively investigated and the topic has been reviewed thoroughly.[174–177] A general reaction pathway was proposed and is represented in Figure 56 by J. A. Varela and C. Saa.[179] Initially, two alkyne partners coordinate to the metal (A) and the resulting complex B forms the metallacyclopentadiene C

by subsequent oxidative coupling. Then, the third unsaturated alkyne or alkene coordinates to the complex to give D, which follows two possible paths: insertion into the MC bond to give cycloheptametallacycle E, which after reductive elimination gives complex G, or intramolecular [4+2] cycloaddition to form bicyclic complex F, which after isomerization affords complex G. On the final stage, decoordination of the metal from the arene produces the final product (Figure 56).[178,179]

Our results of the photoinsertion of alkyne into the metalladecaborane **1.1** to give the substituted carborane **2** can be thought of as an analogous reaction of the cycloaddition of alkyne into the metallacyclopentadiene E in Figure 56. To the best of our knowledge, such a reactivity of metallaborane to mimic the [2+2+2] trimerization of alkyne is unprecedented.

Moreover, one unique feature of the described photoinsertion reaction of the manganadecaborane **1.1** is the involvement of the Group 7 transitional metal manganese. This places it in contrast to the [2+2+2] cycloaddition reaction of alkynes. For [2+2+2] cycloaddition of alkynes, various transitional metal mediated systems have been developed. They include Co, Ni, Pd, Cr, Rh, Fe, Ir, Ru, Ti, Nb, and Ta.[174–177] However, the utilization of the manganese complex $Mn(CO)_5Br$ has only been recently reported.[180,181]

The successful insertion of the alkyne into the manganadecaborane **1.1** implies the importance of polyhedral borane for facilitating the insertion of alkyne into Mn-B bond.

The question arose for this alkyne photoinsertion reaction of why the reaction stops at just one unit alkyne insertion? As mentioned above, theoretical treatments have shown that as vertex number increases, the average stability also increases, with the exception of vertex-12 which is more stable than 13, 14 or 15-vertex (Figure 34).[123] In our proposed mechanism (Figure 53), the reaction proceeds through a 12-vertex

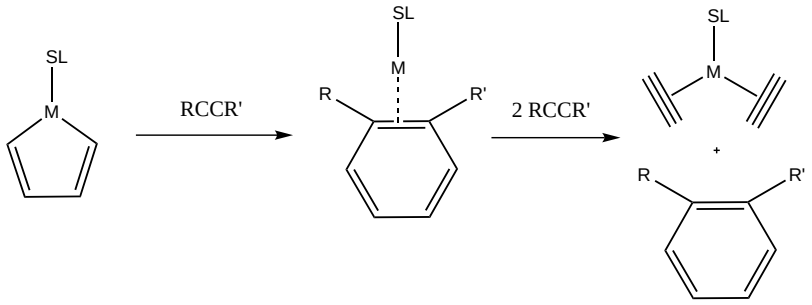

Figure 54: Alkyne insertion into metallacyclopentadiene (SL = spectator ligands).

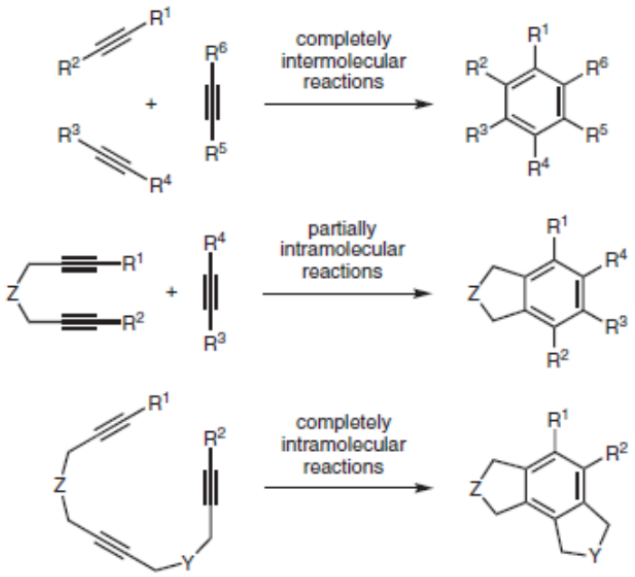

Figure 55: [2+2+2] cycloaddition reactions of alkynes for the synthesis of substituted benzenes.

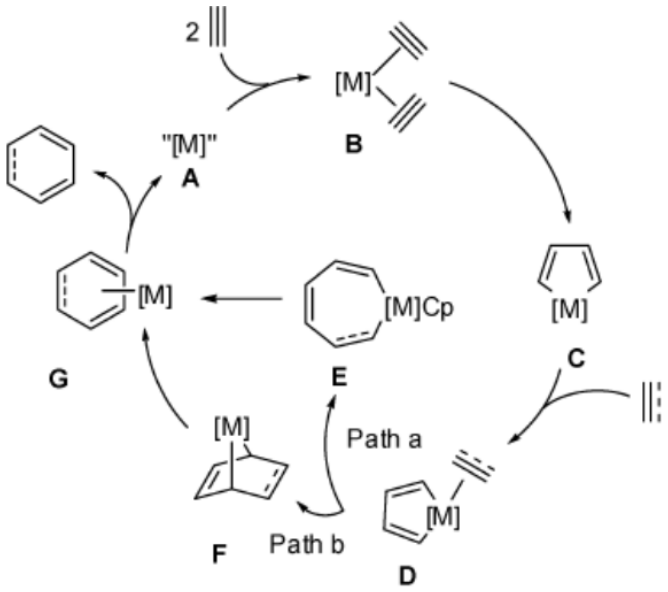

Figure 56: Proposed general pathway for general mechanism proposed for the $CpRuCl^-$ and CpCo-catalyzed [2+2+2] cycloaddition reaction of alkynes.[179]

manganacarborane intermediate which is at the "icosahedral barrier".[124–127] A second alkyne insertion would have exceeded 12-vertex as to produce a 13-vertex product.

The photolytic conditions and manganese carbonyl center play key roles in the formation of the carborane [*nido*-7,8-$C_2B_9H_{12}$]$^-$ (**2.8**) derivatives. This reaction provides an alternative route for carborane synthesis. Based on the reactants, products and the role of manganese, we can call this reaction a Mn mediated [9+2] cycloaddition reaction.

Comparison with Conventional Routes to Carborane C_2B_9 Cluster

The photoinsertion reaction of alkyne into metalladecaborane **1.1** provides an unprecedented route to the mono *nido*-cluster anion, the functionalized C_2B_9 polyhedral borane compound, which is one of the most studied and utilized polyhedral boron containing compounds. This reaction was found to be a general reaction and occurs with various functional groups of the acetylene. Besides thermal reaction, it also has the potential to optimize or develop different reaction conditions.

The similar insertion reaction for alkyne towards the compound **1.1** and metallacyclopentadiene (Figure 54) provides an interesting connection between metallaborane compounds and conventional organometallic compounds. For the traditional polyhedral metallaborane research, this photoinsertion reaction of alkyne into metalladecaborane **1.1** provides a new avenue for polyhedral metallaborane research by indicating that similar reactions could happen for other types of metallaboranes or heteroborane. These polyhedral borane compounds include different hetero atoms and different polyhedral structures. Furthermore, since the discovered photoinsertion reaction of metalladecaborane **1.1** is a stoichiometric reaction, future studies can focus on the possibility of developing the related manganese catalyzed polyhedral borane or carborane reactions.

2.5.4 Photo-interactions of Some Unsaturated Molecules with Manganadecaborane 1.1

In addition to the alkynes and no insertion products observed isocyanides, we also studied the photochemical interactions of some other unsaturated molecules with **1.1**. These unsaturated species investigated include nitriles (1,5-dicyanopentane, acetonitrile, methyl cyanoformate), ketones (4-heptanone, 1-indanone, ethyl pyruvate), aldehyde (benzaldehyde), imines (N-benzylidenemethylamine), alkene (methyl acrylate) and isocyanates (phenyl isocyanate). These unsaturated species represent species which have been found to participate in the metal catalyzed 2+2+2 cycloaddition reaction to form products such as pyridine and 2-pyridone (Figure 57).[182–187]

From our earlier discussion (see section 2.5.3), the metallacyclopentadiene plays a key role in these [2+2+2] cycloaddition reactions. Considering the similar insertion reactivity for alkynes into metalladecaborane **1.1** under photolytic condition, the aim of these investigations for these unsaturated species was to investigate whether insertion reactions can happen similarly for these unsaturated substrates.

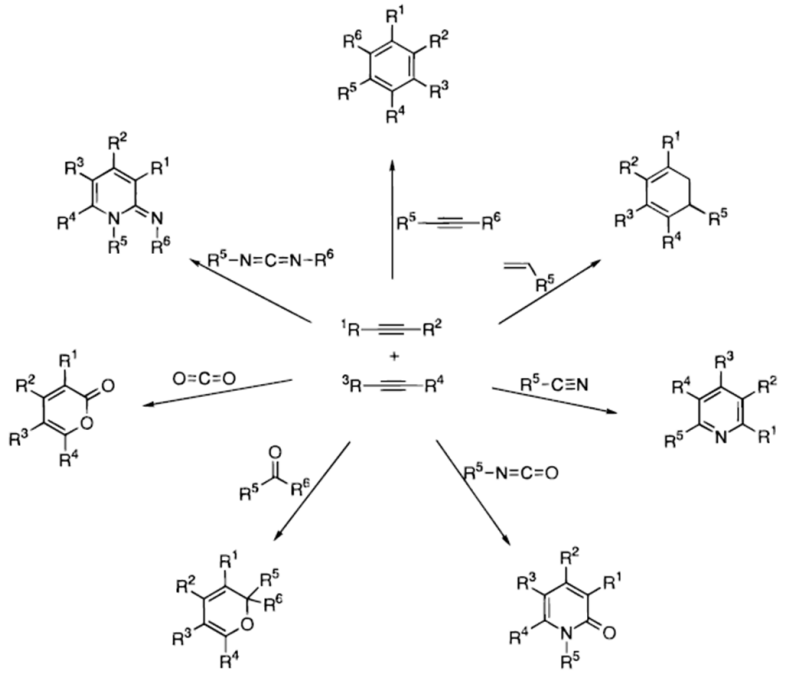

Figure 57: Modified cyclotrimerization involving alkynes and molecules other than alkynes.[188]

For all these investigations, the reaction conditions employed were exactly the same as the conditions employed for the alkyne and isocyanides studies. ^{11}B NMR spectroscopy was employed to monitor these reactions. In most cases, the metallade-caborane **1.1** undergoes a demetallation reaction to give [*arachno*-B_9H_{14}]$^-$ (**2.4**) and [*nido*-B_9H_{12}]$^-$ **2.5** anions (Figure 27). Some preliminary results from these reactions are presented in Table 21. Among all these unsaturated species, N-benzylidenemethylamine was found to not interact with **1.1** under photolytic condition. The only boron containing compound from this reaction was [*arachno*-B_9H_{14}]$^-$ (**2.4**) (Table 21). Three nitriles were studied and, as expected, the observations were very similar. In addition to the complex **2.4**, another boron containing species, [*nido*-B_9H_{12}][NMe_4] (**2.5**) was also detected from the reaction solutions (Table 21). The complex **2.5** was characterized by comparison with literature compounds (Figure 59).[63]

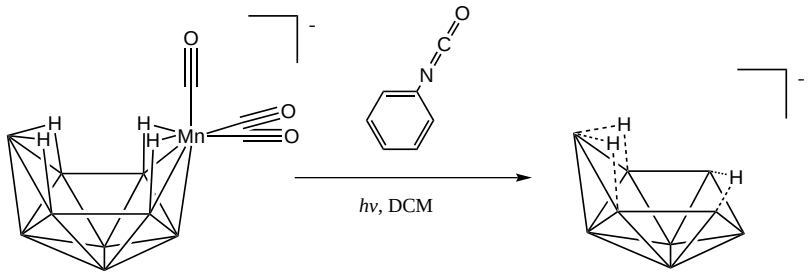

Figure 58: Photoreaction route to the complex **2.5**.

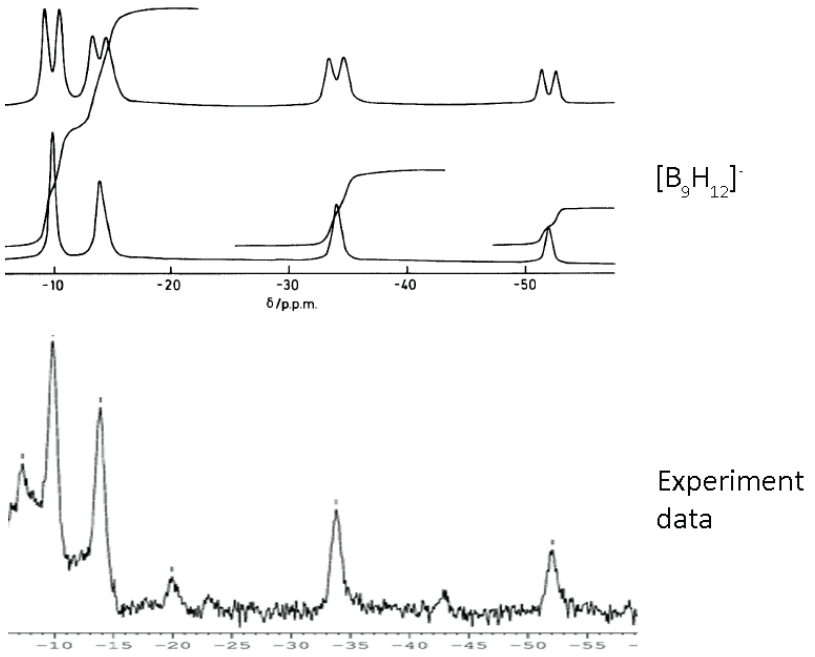

Figure 59: Comparison of ^{11}B NMR spectra for the complex **2.5** (Top: literature data,[63] bottom: experimental data from phenyl isocyanate photoreaction).

Table 21: Photo interactions of some other unsaturated molecules with complex **1.1**.

	Reactants	Observations	products ratio[a]
Nitriles	1,5-dicyanopentane	Colorless solution, White precipitate	1:10
	acetonitrile	Same as above	1:10
	methyl cyanoformate	Same as above	1:5
Ketone	4-heptanone	Same as above	0:0[b]
	1-indanone	Light yellow solution, white precipitate	0:0
	ethyl pyruvate	Colorless solution White precipitate	0:0
Aldehyde	benzaldehyde	Light orange solution	0:0
Imine	N-benzylidenemethylamine	Yellow precipitate	All **2.4**
Alkene	methyl acrylate	Colorless solution White precipitate	1:9
Isocyanates	phenyl isocyanate	Same as above	9:1

[a] Products ratio were **2.5** ($[B_9H_{12}]^-$) to **2.4** ($[B_9H_{14}]^-$), based on ^{11}B NMR spectroscopy.
[b] No signals or very small amount for either **2.5** or **2.4**. The products contain unidentified boron containing compounds, based on ^{11}B NMR spectroscopy.

In the products (Table 21), the ratios of the anion **2.5** to **2.4** in the nitrile reactions were estimated by ^{11}B NMR integration and **2.4** was found to be the favored product (**2.5** to **2.4** ratios are 1:9, 1:8, and 1:6 for 1,5-dicyanopentane, acetonitrile, and methyl cyanoformate, respectively). Thus most of the starting metalladecaborane **1.1** was converted to the $[B_9H_{14}]^-$ anion. Although exact mechanisms remain unclear, the nitrile group may be the key group that interacts with the manganese center in **1.1** and eventually leads to the formation of the **2.5** anion. The different ratios of each anion for the three nitriles can be reasonably explained as the different electronic properties of these nitrile species. Similarly, methyl acrylate was found to lead to the formation of **2.5** and **2.4** with an estimated ratio of 1:8. Similar to nitriles and methyl acrylate, the reaction of phenyl isocyanate with compound **1.1** was found to generate **2.4** and **2.5** as well. Nonetheless, ^{11}B NMR integration showed that in the phenyl isocyanate case, **2.5** was the favored product with a percentage of 89%. However, for the ketones and aldehyde investigated in the photo reactions, there were very little or no **2.5** and **2.4** anions detected in the reaction solutions. Although most of these products were not characterized due to low yields, ^{11}B NMR spectra of them indicated that they may contain insertion products.

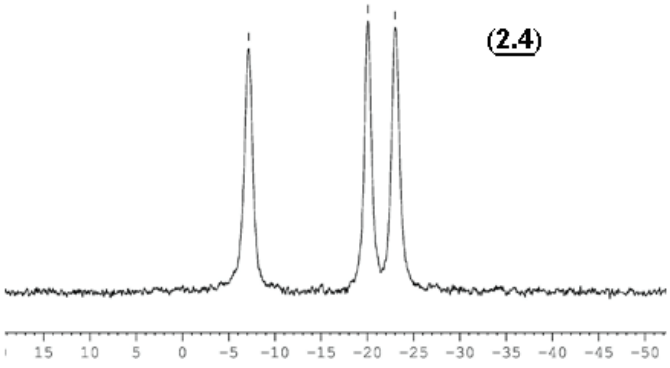

Figure 60: ^{11}B NMR spectra of the photoreaction products between complex **1.1** and N-benzylidenemethylamine in DCM (proton decoupled).

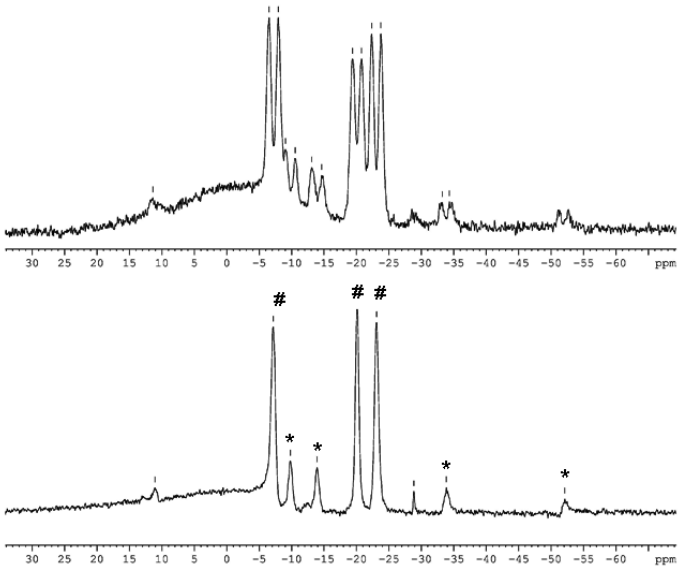

Figure 61: ^{11}B NMR spectra of the photo reaction products between complex **1.1** and methyl acrylate (Top: proton coupled, Bottom: proton decoupled): (#) **2.4**; (∗) **2.5**.

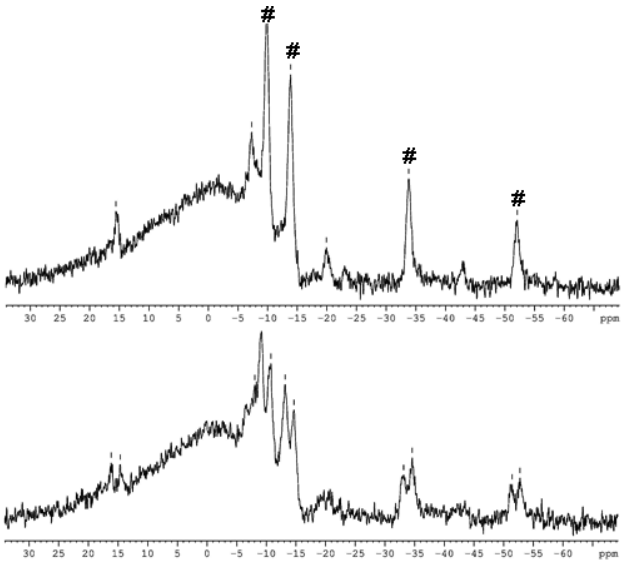

Figure 62: ^{11}B NMR spectra of the photoreaction products between complex **1.1** and phenyl isocyanate in DCM (Top: proton decoupled, Bottom: proton coupled): (#) **2.5**.

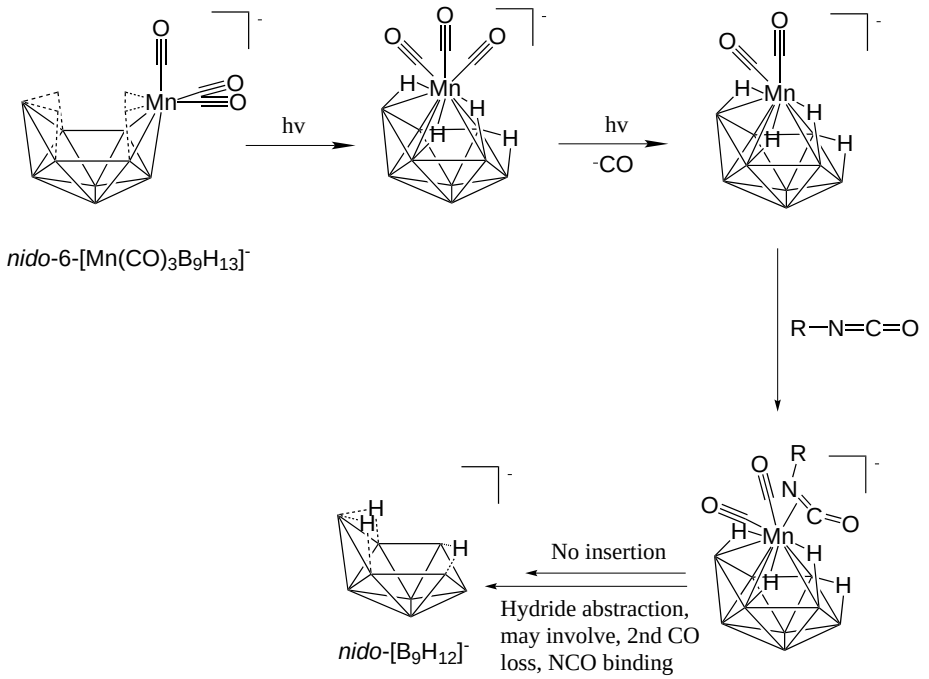

Figure 63: Proposed pathway of isocyanate interaction with the complex **1.1**.

2.5.5 Photo-elimination Versus Photo-insertion

The observed photo-initiated insertion of alkynes to the borane cluster is in contrast to the lack of insertion reactions for isocyanates, nitrile, imine and alkene compounds. It is evident, however, that unsaturated species other than alkynes do coordinate with the coordinatively unsaturated manganese center. These organomanganese complexes, once formed, separate without insertion to form one of two borane cluster products, the **2.4** and **2.5** anions. The ratio of **2.4** and **2.5** anions formed as products varies depending upon the nature of the non-alkyne ligands.

After the photo-assisted loss of the carbonyl group on the manganese center, the unsaturated ligand may coordinate to the vacant site. The key step for insertion to occur is the insertion of the unsaturated bond into the manganese-boron bond. For alkynes, as known in the literature, this insertion into a metal-ligand bond can happen smoothly.[141,142] In contrast, the insertions of non-alkyne unsaturated ligands into the Mn-B bond apparently does not occur readily (see proposed mechanisms in Figure 63).

As examples, counterparts of manganadecaborane can be found in organometallic chemistry. As we have suggested earlier in the chapter, the photo-initiated insertion of alkyne into manganadecaborane **1.1** can be related to the transition metal mediated [2+2+2] cycloaddition reactions in organometallic chemistry. Metal-catalyzed cyclotrimerization of acetylenes to benzene derivatives is well known and can be achieved with many transition metals including Co, Ni, Pd, Cr, Rh, Fe, Ir, Ru, Ti, Nb, and Ta. Mn has also been recently reported where $Mn(CO)_5Br$ was reported to catalyze the coupling reaction of β-keto esters with terminal alkynes by both Nakamura and Tsuji et al. and by Takai and Kuninobu et al.[180,181] Both groups have reported the manganese-catalyzed dehydrative [2+2+2] coupling of 1,3-dicarbonyl compounds with arylacetylenes. The enol form of the β-keto ester mimics the role of an alkyne and undergoes a cycloaddition followed by dehydration to yield *p*-terphenyl derivatives. Takai and coworkers have shown that the cycloaddition between β-keto esters and terminal alkynes is facile under neat reaction conditions at 80 °C in the presence of molecular sieves (4 Å). While the mechanism is not well understood, the authors have suggested that it proceeds *via* one of two metallacycle intermediates (Figure 64). Thus the manganacyclopentadiene intermediate in these reactions represent the counterpart of manganadecaborane in organometallic chemistry.

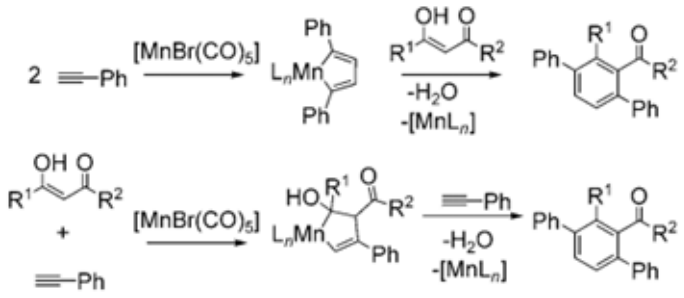

Figure 64: Proposed manganacyclopentadiene intermediate for cycloaddition between β-keto esters and terminal alkynes.[180]

It should also be noted that beside the metal mediated [2+2+2] cycloaddition reaction, the alkyne insertion into the manganadecaborane can also find its counterpart in a light-induced formal [5+2] cycloadditions at manganese. Kreiter and coworkers reported the reaction in Figure 65.[189] This indicates the facile insertion of alkyne to manganese-carbon bond.

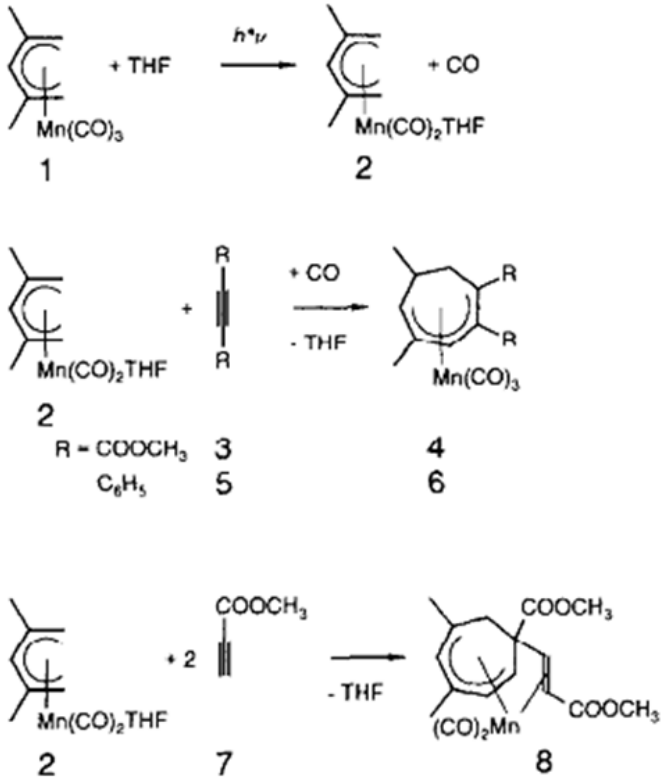

Figure 65: Light-induced formal [5+2] cycloadditions at manganese center.[189]

We have discussed earlier that, besides alkynes, the metal mediated [2+2+2] cycloaddition reactions have been modified to incorporate isocyanates, olefins, nitriles, aldehydes and ketones, carbon dioxide, imines, and di-imides (Figure 57). The transitional metals include Rh, Nb, Ni, Co, Ru, Pd, Ir and others.[182–187,190–193] Nevertheless, to the best of our knowledge, manganese complexes have not been reported for any of these modified [2+2+2] cycloadditions. This is in agreement of our finding of non-insertion of these non-alkyne ligands into the manganadecaborane **1.1**.

Origins for Different Ratios of the Anions 2.4 and 2.5:

From the reaction sequence mentioned above, the coordination to vacant site on manganese and the elimination of the manganese center maybe thought of as two competing processes. The solvent dichloromethane is also involved in the coordination to manganese and can act as a hydrogen pool for the generation of the anion **2.4**.[194]

The literature examples provide us insight into the two processes. The B_9 boron cluster can be considered as an unbound *arachno* nonaborate. It has been documented by Bould and coworkers that in the rhodiumdecaborane reaction with EtNC, the cluster-assimilated EtNC unit can undergo a two-hydrogen reduction on the EtN residue to give an *exo*-cluster NH_2Et moiety.[134] Alvarez and coworkers also reported a 11-vertex *nido-closo-nido* conversion in a metallathiaborane cluster which involves the hydrogen abstraction from the boron cage to the rhodium bounded alkene (Figure 66).[195] Similarly, the Mn coordinated ligands here can also abstract hydride from the boron cluster under the condition that the manganese center with coordinated ligand stays long enough with the boron cluster before elimination, giving birth to the oxidized borane anion **2.5**. On the other hand, if the elimination of the manganese center with coordinated ligand is fast enough, there will be very little or no hydrogen abstraction, and with the coordination of dichloromethane, the main product becomes the anion **2.4**. In other words, rate-limiting step of the coordination and elimination sequence and the position of the transition state on the reaction coordinate leads to the different ratios of the borane anion species in the final products. If the elimination is rate-limiting step, then there will be a greater chance for the hydrogen abstraction from the borane cage to occur. On the other hand, if binding of the unsaturated molecule to metal is rate-limiting step, hydrogen abstraction will less likely occur. Therefore, for the imine N-benzylidenemethylamine, due to the weakly coordinating CN double bond, the elimination of the manganese center should be main process. Accordingly, the only product detected was the anion **2.4**.

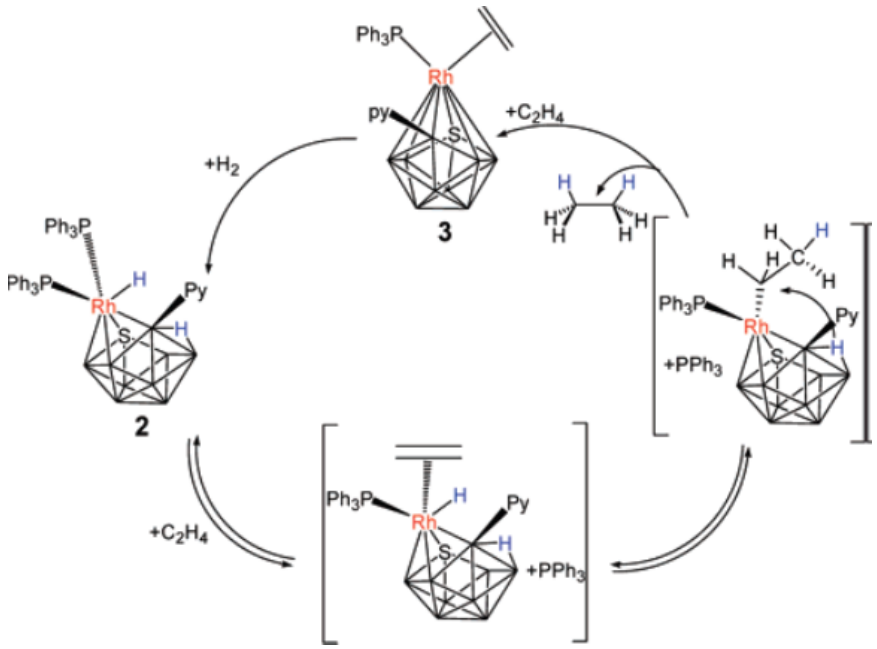

Figure 66: *nido-closo-nido* conversion of a metallathiaborane.[195]

Among the studied three nitriles and the alkene, the methyl acrylate, acetonitrile and 1,5-dicyanopentane give similar ratios of the two anions with the **2.4** being the major product (**2.4** : **2.5** = 10 : 1). While the more reactive methyl cyanoformate gives more **2.5** anion in the products (**2.4**:**2.5**=5:1). This comparison indicates that the more reactive ligand can coordinate to the metal more efficiently and provide a greater chance for hydrogen abstraction to occur.

From these results, a trend can be observed that the stronger the ligand is coordinated, the greater the preference for oxidized anion **2.5** in the products. This trend was further shown in the phenyl isocyanate and *n*-butyl isocyanate cases. The photoreaction involving the activated phenylisocyanate reversed the products ratios, making **2.5** anion the main product (**2.4** : **2.5** = 1 : 9). While the less reactive *n*-butyl isocyanate resulted in less **2.5** anion in the products (**2.4** : **2.5** = 1 : 3).

These arguments can also explain why insertions of the ligands were not observed with these compounds. As mentioned earlier, for most of these compounds the

elimination of manganese center is the dominate process. While for phenyl isocyanate, the facile hydrogen abstraction process possibly circumvents the insertion process.

Considering the fast photo-elimination of the manganadecaborane to anions **2.4** and **2.5**, the photo-irradiation maybe the reason why the elimination process was dominant. This implies that alternative conditions may slow the elimination process so as to possibly encourage the insertion process.

2.5.6 Manganadecaborane 1.1 as an Efficient photo Catalyst for Isocyanate Cyclodimerization

We presented earlier the results of the photo-initiated interaction between some unsaturated molecules and the manganadecaborane **1.1**. For the phenyl isocyanate case, however, it was found that complex **1.1** is able to catalyze the cyclodimerization of phenyl isocyanate under photolytic condition in DCM or THF. The cyclodimerization product readily eliminates one CO molecule to result in the formation of the urea 1,3-diphenyl-urea (**2.11**) which was characterized by X-ray crystallographic studies (Figure 67). Our X-ray structure was identical with the reported structure.[196] It was found that a 2 % mole loading of the complex **1.1** gave a 85 % yield of the 1,3-diphenyl urea.

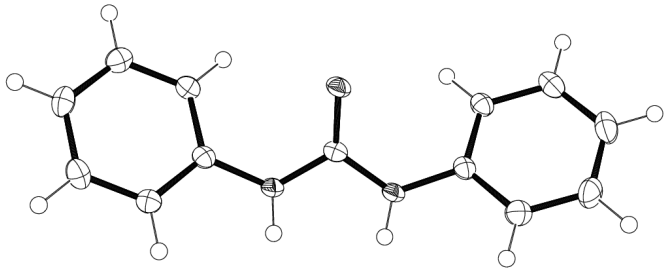

Figure 67: ORTEP drawing of the crystallographically-determined molecular structure of 1,3-diphenyl-urea (**2.11**).

We further studied the reaction of compound **1.1** with *n*-butyl isocyanate. The result was the same as that observed with the phenyl isocyanate case.

The formation of the urea is assumed to proceed through elimination of CO from the phenyl isocyanate cyclodimerization product (Figure 68).[197] The formation of the ureylene ligand RNC(O)NR requires the breaking of a C-N bond with the loss of one equiv of carbon monoxide.

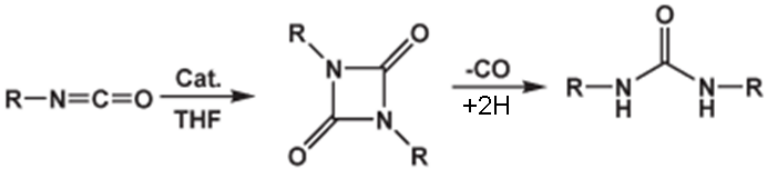

Figure 68: General scheme for the catalyzed cyclodimerization of isocyanates.[197]

Mn has previously been shown to be capable of catalysing the synthesis of hydantoin derivatives from terminal alkynes and isocyanates.[198] This indicates a good affinity of isocyanate towards the manganese center when the manganadecaborane **1.1** is photo-activated. We therefore can propose the mechanism for this metallaborane catalysed isocyanate cyclodimerization as shown in Figure 69. After the photo-activation, the active manganese center can coordinate one isocyanate and enter the catalytic cycle. A second isocyanate molecule would then coordinate to the metal center and the metallacyclic intermediate formed by successive concerted oxidative coupling reactions. This formation of a metallacyclic intermediate resembles those often invoked for the cyclotrimerization of alkynes on metal centers.[199] In the presence of another isocyanate molecule, the isocyanate cyclodimerized product is then released *via* reductive elimination process while the resulting activated metallaborane begins another catalysis cycle.

The readily formed organic ureas (Figure 68) from the isocyanate cyclodimerized products have industrial and academic applications as antioxidants in gasoline, agro-chemicals, resin precursors, dyes for cellulose fibers, and as synthetic intermediates.[200]

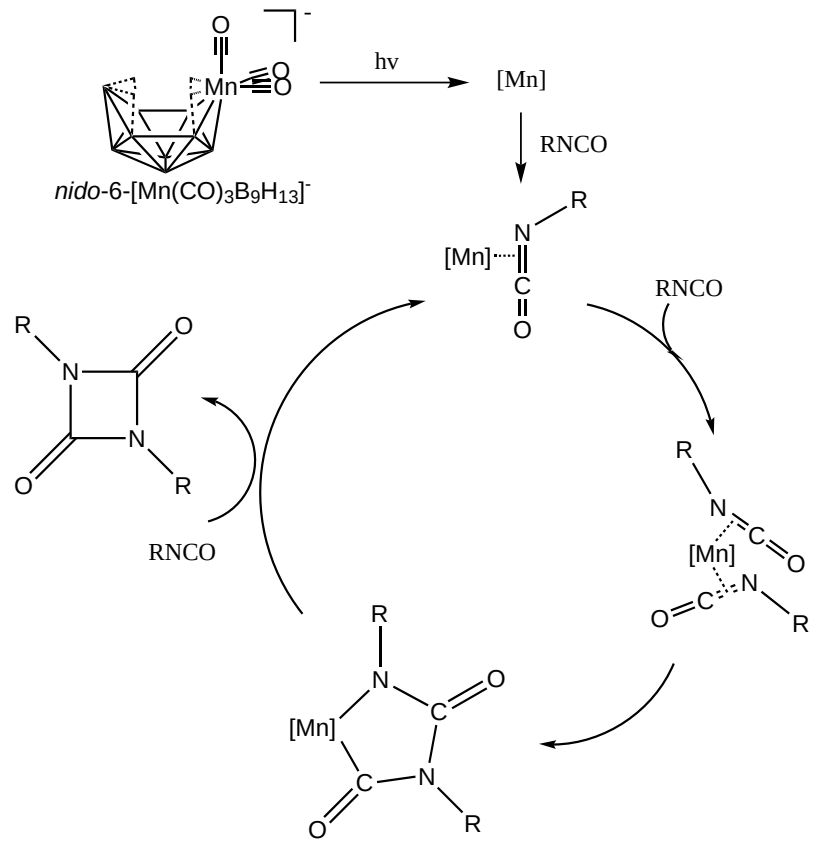

Figure 69: Proposed mechanism for the metallaborane **1.1** catalyzed cyclodimerization with isocyanates.

Therefore, investigation of catalysts that can selectively catalyze the cyclodimerization of isocyanates has become one active topic of organic chemistry.[201] Numerous catalysts have been reported for the cyclodimerization of isocyanates. They include both organic or organometallic compounds.[201] For example, lanthanide(III) 4,6-dimethylpyrimidine-2-thionate complexes have been reported recently for catalysing isocyanate cyclodimerization.[197] To our knowledge, the catalytic activity of the manganadecaborane **1.1** towards the isocyanate cyclodimerization represents the first example employing metallaborane complexes to catalyze the cyclodimerization of isocyanates.

2.5.7 Photoreaction of [*nido*-5-$Mn(CO)_3B_9H_{13}$][NMe_4] (**1.2**) with Alkynes

The complex **1.2** (see chapter 1 for synthesis and structure) is an isomer of **1.1** whose structure we have previously elucidated in chapter 1. The photoreaction between **1.2** and an excess 1-hexyne was investigated as part of our exploration of borane photoexpansion processes. The potential reaction was monitored by ^{11}B NMR and the data are shown in Figure 70. During the course of the reaction, a set of new boron peaks were observed. This suggests that an alkyne insertion reaction occurred for **1.2** to give a carborane insertion product. In view of the structure similarities in the two starting metallaborane isomers, the insertion reactions might proceed by a similar mechanism. Thus far, however, repeated attempts under a variety of conditions have not been successful in fully isolated or characterizing this product from this reaction. Determining the structure of this product will form a useful comparison with the photoreaction of the 6-substituted product and will constitute future work.

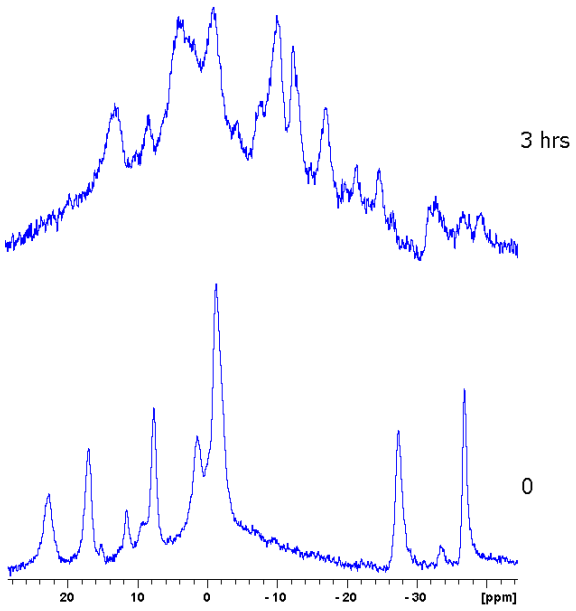

Figure 70: Photoreaction between complex **1.2** and 1-hexyne (bottom: starting solution, and top: after 3 h).

2.5.8 Synthesis and Photochemistry of $[Co(CO)_3B_{10}H_{12}][NMe_4]$ (**2.6**)

The synthesis of $[Co(CO)_3B_{10}H_{12}][NMe_4]$ (**2.6**) was first reported by Muetterties and coworkers[202] and the structure later determined as its $[PhCH_2NMe_3]^+$ salt.[203] The reported yield of 55% of complex **2.6** was obtained by treating $Na[B_{10}H_{13}]$ with $Co_2(CO)_8$ in Et_2O and THF.[202] In this study, we started by treating $B_{10}H_{14}$ together with 1,8-bis(dimethylamino)naphthalene (Proton Sponge, PS, $C_{10}H_6(NMe_2)_2$), and found that the yield was improved to 70%.

Since the complex **2.6** was not spectroscopically fully characterized, the ^{11}B NMR and 2-D ^{11}B-^{11}B NMR data from our experiments are given in Figure 71. One important thing to note here is that the ^{11}B NMR spectra obtained in our work was not the same as reported.[202] However, 2D ^{11}B-^{11}B COSY NMR (Figure 71) and IR spectra (ν_{CO} 2065, 2020, and 2000 cm^{-1}) from our work is consistent with the crystal structure that was reported (Figure 72).[203]

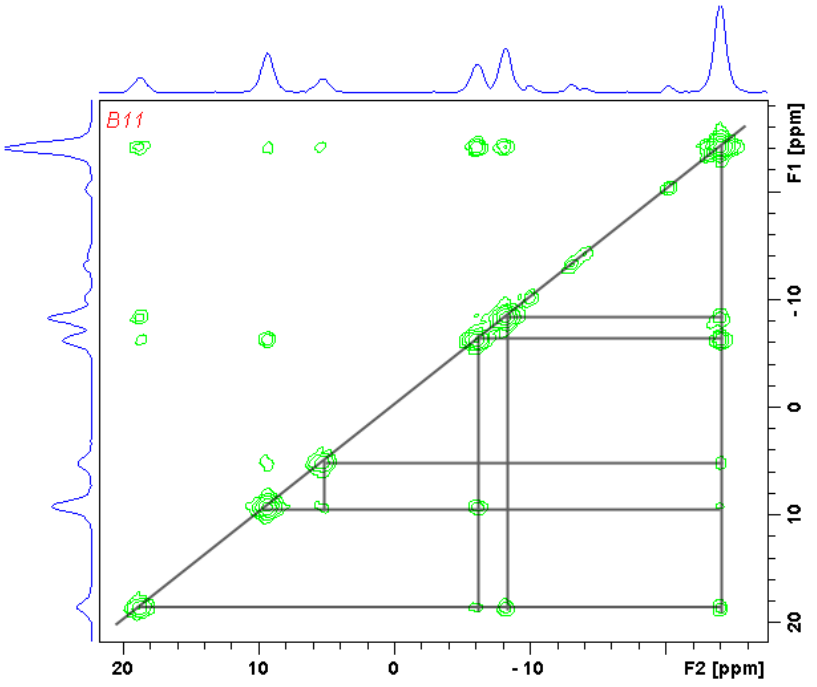

Figure 71: NMR spectrum of the complex **2.6** (1-D ^{11}B and 2-D ^{11}B-^{11}B COSY).

The crosspeaks observed in the 2D ^{11}B-^{11}B COSY experiment (Figure 71) included crosspeaks from the resonance at 20.7 ppm with those at -4.5, -7.0 and -23.0 ppm, crosspeaks from the resonance at 10.9 ppm with those at 6.79, -4.5 and -23.0 ppm, a crosspeak from the resonance at 6.97 ppm with that at -23.0, and a cross peak between the resonance at -7.0 with that at -23.0 ppm. The five peaks can therefore be assigned as +20.7 (B1), +10.9 (B7, B8), +6.97 (B6, B9), -4.5 (B3), -7.0 (B5, B10), -23.0 (B2, B4).(Figure 72) The cross peak between the resonances for B6/9 and B5/10 is missing due to the effect of bridging by the Cobalt atom. Crosspeaks are not to not generally be observable between resonances corresponding to connectivities that involving bonding interations between boron atoms which are bridged by hetero atoms in the two-dimensional COSY ^{11}B-^{11}B NMR spectrum. This has been shown for a variety of known heteroboranes such carboranes and metallasilaboranes.[73,204]

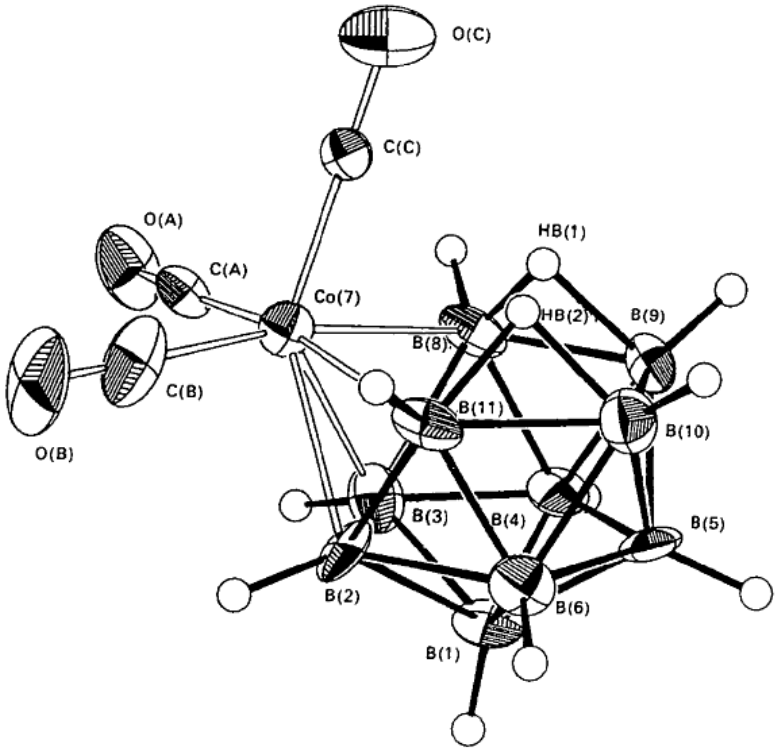

Figure 72: Perspective view of the metallaborane anion in **2.6** (adapted from reference 203).

The carbonyl ligands to the metals are very similar between the **1.1** and **2.6** complexes. This can be observed from the IR data for these complexes: ν_{CO} 2060, 2025, 2005 for **1.1** and ν_{CO} 2065, 2020, and 2000 cm^{-1} for **2.6**. The bond distances from crystal structures also confirms this comparison. In both molecular structures, two of the carbonyl ligands are approximately symmetric. However, the remaining carbonyl ligand shows a longer C-O bond and shorter M-C bond (for **1.1**, Mn-C 1.775 vs 1.800 and C-O 1.169 vs 1.149. for **2.6**, Co-C 1.763 vs 1.816, 1.788, and C-O 1.165 vs 1.133, 1.133). This observation suggests that there is a stronger back donation to this unique metal-carbonyl unit. The similarities around the metal centers between the Mn and Co complexes led us to investigate the photochemical reactions of **2.6**.

The photochemical reaction between complex **2.6** and 1-hexyne was monitored using ^{11}B NMR (Figure 73), however, no changes in the spectra were observed during the reaction. This suggests that the carbonyl groups are less photo-labile for **2.6** under the similar photochemical conditions employed with **1.1**. There may be several reasons for this observation: (a) complex **2.6** did not convert to a *hypercloso*-intermediate structure due to the B(10) boron cluster ligand, (b) the formation of a 13-vertex metallacarborane intermediate is both thermodynamically and kinetically unfavorable, or (c) the carbonyl ligands are less able to photodissociate from the cobalt center. The reactivity comparison of **2.6** and **1.1** towards alkyne suggests the importance of the *hypercloso*-structure and the boron cage structure towards reactivity. Nonetheless, the insertion reaction may take place if we change the ligand environments and we will explore these parameters in the future.

2.6 Conclusion

In this chapter, we studied the photochemical reactions for several metallaborane species.

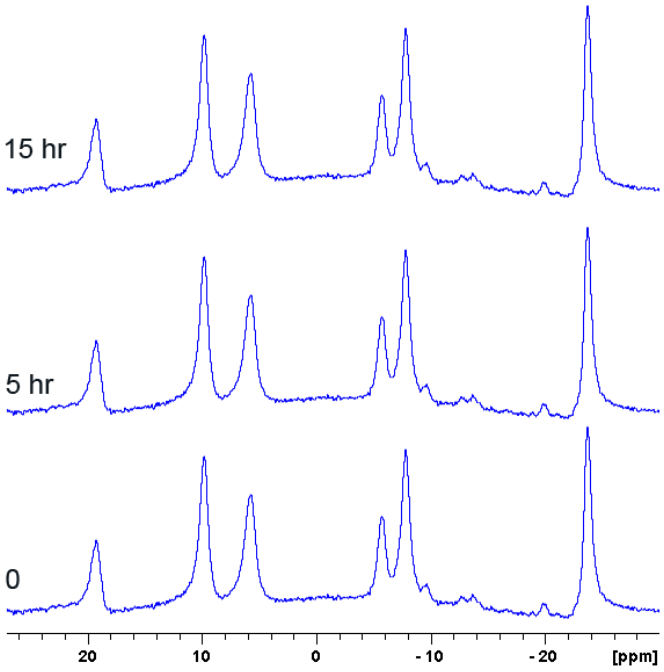

Figure 73: ^{11}B NMR spectra monitoring for photoreaction of **1.6** with 1-hexyne.

We found that under UV photochemical conditions, the *nido*-6 manganadecaborane **1.1** complex reacts with a series of alkynes to afford substituted carborane anion **2** derivatives (**2a**-**2g**) in good yields. These products have been characterized by various spectroscopic methods and by comparison with literature known compounds for **2b** and **2g**. The reaction intermediate in this reaction may involve a *hypercloso*-metallacarborane intermediate coupled with alkyne. This photochemical pathway provides an example of the reaction of a metallaborane to form a larger substituted carborane while also providing an alternative route for substituted carborane synthesis. Due to its similarity to transition metal mediated [2+2+2] alkyne cycloaddition reactions, we can call this Mn mediated [9+2] cycloaddition reaction.

In addition to alkynes, several other unsaturated molecules were also investigated in their interaction with the complex **1.1** under photochemical conditions. Ketones and aldehydes may react with the complex **1.1** to lead to possible insertion products, while the nitriles, alkene, and isocyanate can generate polyhedral borane anions,

the [*arachno*-B_9H_{14}]$^-$ (**2.4**) and [*nido*-B_9H_{12}][NMe_4] (**2.5**). The complex **1.1** was also found to act as an efficient catalyst for isocyanate cyclodimerization under photo-irradiation conditions, representing the first example of a metallaborane complex to catalyse the cyclodimerization of isocyanates.

Besides the complex **1.1**, the complex **1.2** was also found to be reactive under the similar conditions although the products were not able to be characterized.

These results not only imply a rich chemistry between alkyne and metallaboranes but also suggest that the photochemical study of metallaborane can provide important insights to the metallaborane and metallacarborane chemistry. Future photochemically investigations of metallaborane clusters can be expected to be fruitful.

Chapter 3

Thermal Versus Photochemical Pathways for the Rhodadecaborane [6-(η^5-C_5Me_5)-*nido*-6-RhB_9H_{13}] (**3.1**)

3.1 Introduction

A survey of different reaction pathways of metallaboranes is of considerable interest but often shows a limited number of generally applicable reaction pathways of synthetic utility.[1] We have previously shown in Chapter 1 that the *nido*-metalladecaborane **1.1** ([*nido*-6-$Mn(CO)_3B_9H_{13}$][NMe_4]) has two different chemical pathways under thermal and photochemical conditions to give **1.2** ([*nido*-5-$Mn(CO)_3B_9H_{13}$][NMe_4]), **1.3** ([*hypercloso*-$Mn(CO)_3B_9H_9$][NMe_4]) or **1.4** ([*arachno*-B_9H_{14}][NMe_4]) complexes. Compared with the chemical pathways and reactions of some other reported *nido*-6 metalladecaboranes,[3] the large variety of reaction and structural data show that chemical reactions of metalladecaborane compounds are influenced not only by the choice of exopolyhedral metal and ligands, but also by the of valency states and coordination numbers available to different transition metal atom. In this chapter, the chemical behaviors of a *nido*-6-rhodadecaborane [6-(η^5-C_5Me_5)-*nido*-6-RhB_9H_{13}] (**3.1**)[205] is explored.

The synthesis and structural details of the pentamethylcyclopentadienylrhodaborane **3.1**, [6-(η^5-C_5Me_5)-*nido*-6-RhB_9H_{13}], was first reported by Fontaine and coworkers in 1986.[205] It has been shown that a rich chemistry is related to this *nido*-6 rhodadecaborane. For example, the reaction of complex **3.1** with an excess of PMe_2Ph in CH_2Cl_2 solution at room temperature yielded the air-stable, red-orange [5-(η^5-C_5Me_5)-*nido*-5-RhB_9H_{11}-7-$(PMe_2Ph)_2$] (**3.2**) complex with a yield of 35% (Figure 74).[10] Isonitrile

compounds such as MeNC or *p*-MeC_6H_4NC were also reported to react with the *nido*-6 rhodadecaborane **3.1** under mild conditions to give 6-(η^5-C_5Me_5)-6,9-$(MeNC)_2$-*arachno*-6-RhB_9H_{11} (Figure 75).[206]

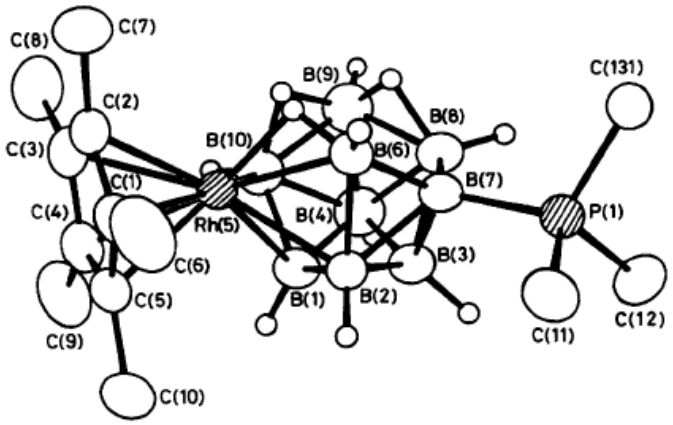

Figure 74: ORTEP drawing of the molecular structure of complex **3.2** (methyl and phenyl hydrogen atoms and P-phenyl carbon atoms other than the *ipso* one omitted for clarity).[10]

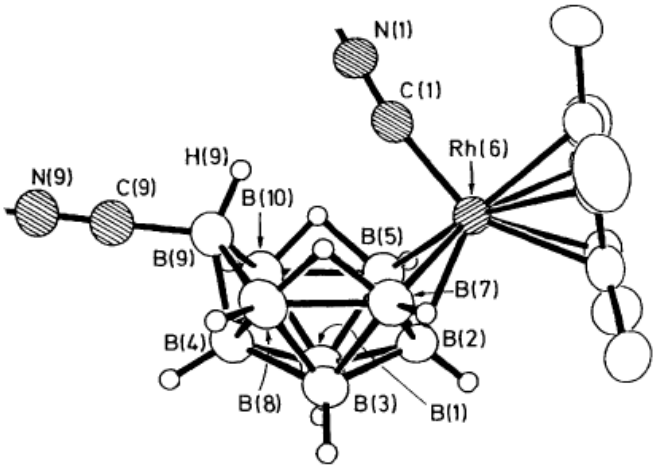

Figure 75: ORTEP drawing of the molecular structure of 6-(η^5-C_5Me_5)-6,9-$(MeNC)_2$-*arachno*-6-RhB_9H_{11}.[206]

Nonetheless, to our knowledge, the reactivity of this *nido*-6 rhodadecaborane **3.1** has not been studied under photolytic condition or at elevated temperatures. Inspired by our previous finding of the thermal isomerization and photochemical

transformation the *nido*-6 manganadecaborane **1.1**, it was of interest to compare the photolytic reactivity with thermal reactivity for this *nido*-6 rhodadecaborane **3.1**.

During our investigations, we found that under relatively mild thermal conditions, the complex **3.1** was converted to [*hypercloso*-(η^5-C_5Me_5)RhB_9H_9] (**3.3**) through the loss of two dihydrogen molecules in toluene. In contrast, under UV irradiation, complex **3.1** undergoes reactions in benzene or diethyl ether to give two previously known compounds [*nido*-5-η^5-C_5Me_5)RhB_9H_{13}] (**3.4**) in benzene and ethoxy-substituted *hypercloso* rhodadecaborane in diethyl ether, respectively (Figure 76).

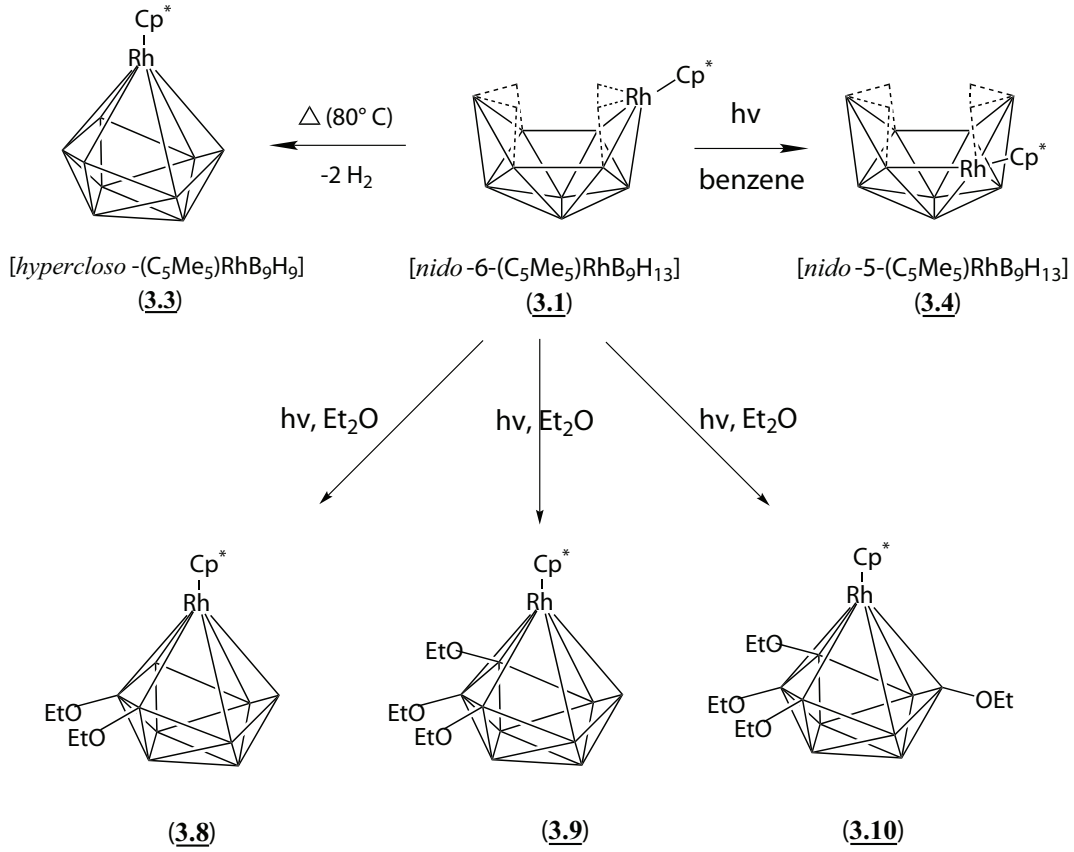

Figure 76: Thermal versus photochemical pathways of the complex **3.1**.

We, therefore, report the synthesis and structural studies of these photochemical and thermal pathways here. The ^{11}B NMR and 2D ^{11}B-^{11}B COSY NMR spectra data were employed as the main characterization methods.

3.2 Experimental

3.2.1 Physical Measurements

All NMR spectra were recorded on a Bruker Avance 300 MHz NMR equipped with a 5 mm OXI probe. The ^{11}B NMR spectra were recorded at 96.3 MHz and were referenced at 96.3 MHz. Spectra were referenced to BBr_3 at +40.0 ppm (relative to BF_3Et_2O at $\delta = 0.0$ ppm) with positive chemical shifts indicating downfield resonances. Typical ^{11}B NMR acquisition parameters employed were a relaxation delay of 0.1 ms and a 90° pulse of 10 μs. As previously described, an absolute-value-mode COSY pulse sequence[58] was used to generate the t_1, t_2 data matrix (relaxation delay $-(\pi/2) - t_1 - (\pi/2) - t_2$ in which t_1 was incremented by the inverse of the sweep width in the F_1 dimension and t_2 was the usual acquisition time in a 1D experiment). The t_1, t_2 matrix was collected as 1024×256 data points. Data processing involved the application of a dc offset and first-point correction, shifted sine bell apodization, zero filling, Fourier transformation, and a magnitude calculation to give the 512×512 2D ^{11}B-^{11}B $\{^1H\}$ spectrum.[59,60] Proton (^{1}H) NMR spectra were recorded at 300.15 MHz with chemical shifts referenced to an internal standard of tetramethylsilane at δ=0.0 ppm. Carbon (^{13}C) NMR spectra were obtained at 77.47 MHz. Unit resolution mass spectra were obtained on a Hewlett Packard model 5989B gas chromatograph/mass spectrometer (GC/MS) using an ionization potential of between 11 and 70 eV. FT-IR spectra in the range of 400 to 4000 cm^{-1} were measured on a Mattson Galaxy 2020 spectrometer and were referenced to the 1602.8 cm^{-1} band of polystyrene. The spectra were observed as KBr mulls and are reported in cm^{-1}. UV-Vis spectral data were collected on a Cary 1 UV-Vis spectrophotometer in a quartz cell. All photoreactions were carried under a medium pressure mercury vapor lamp (Make: ACE GLASS, Model: Hanovia, 7825-34, IMMERSION LAMP, Medium Pressure, 450 watt).

3.2.2 Materials

All solvents used were reagent grade or better. Tetrahydrofuran (THF) and hexane were distilled over potassium metal prior to use. TLC plates were purchased from Fisher Scientific. The *nido*-decaborane(14) ($B_{10}H_{14}$), was purchased from the Callery Chemical Company and was purified by vacuum sublimation at 40 °C prior to use. Appropriate care was taken in handling the boron hydrides under inert atmosphere conditions.[61] All reactions were done in an inert atmosphere (nitrogen) unless otherwise noted. Deuterated NMR solvents were purchased from Cambridge Isotope Laboratories, Inc. and dried over molecular sieves before use unless otherwise noted. All other commercially available reagents were used as received. The compound **3.1** ([6-(η^5-C_5Me_5)-*nido*-6-RhB_9H_{13}]) was synthesized by a modification of a previously described procedure.[205]

3.2.3 Synthesis

[***hypercloso*-η^5-C_5Me_5)RhB_9H_9] (**3.3**) A suspension of 300 mg (0.86 mmol) of complex **3.1** in 10 mL of dry toluene was refluxed under nitrogen for 2 h. After cooling to r.t., the solvent was removed on the vacuum line. The residue was then chromatographed on a 10 × 1 cm column of silica gel, eluting with chloroform. A fast-moving orange-brown band was collected. The product was recrystallized from dichloromethane/ethanol (2:1) and then washed with cold hexane to give 240 mg (81%) of orange-brown complex **3.3**. ^{11}B NMR (CD_2Cl_2, δ (ppm)): +99.73 (d, 3B, B(2,3,4), J_{BH} = 139 Hz), +30.51 (d, 3B, B(8,9,10), J_{BH} = 136 Hz), -7.92 (d, 3B, B(5,6,7), J_{BH}=139 Hz).

Photolysis of complex 3.1 in benzene: [***nido*-5-η^5-C_5Me_5)RhB_9H_{13}] (**3.4**) Complex **3.1** (320 mg, 0.92 mmol) in 10 mL degassed benzene was placed in a quartz tube. The solution was irradiated in a quartz photochemical reactor for 30 min. ^{11}B NMR spectroscopy indicated that the major boron containing product was complex

3.4 (225 mg, yield 75%). ^{11}B NMR for the complex **3.4** ($CDCl_3$, δ (ppm)): +29.4 (d,1B, J_{BH} = 142 Hz) +26.0 (d, 1B, J_{BH} = 138 Hz) +10.2 (d, 1B, J_{BH} = 138 Hz) +5.4 (d, 1B) +2.4 (d, 1B) +1.3 (d, 1B) -3.2 (d, 1B, J_{BH} = 146 Hz) -12.7 (d, 1B, J_{BH} = 143 Hz) -37.6 (d, 1B, J_{BH} = 149 Hz).

Photolysis of complex 3.1 in Et_2O Complex **3.1** (400 mg, 1.15 mmol) in 10 mL Et_2O was placed in a quartz tube. The solution was irradiated in a quartz photochemical reactor for 30 min. The solvent was evaporated *in vacuo* and the residue was applied to a silica gel column (10 × 1 cm). DCM/hexane (v/v=2/8) elution gave a mixture of EtO-substituted *hyperclodo*-rhodadecaboranes.

Stoichiometric reaction of complex 3.1 with phenylacetylene

Complex **3.1** (300 mg, 0.86 mmol) and phenylacetylene (87.7 mg, 0.86 mmol) in 10 mL of dry xylene was refluxed under nitrogen for 2 h. GC-MS method and NMR spectroscopy revealed the disappearance of the complex **3.1** and the cyclotrimerization products of phenylacetylene. ^{11}B NMR showed that the complex **3.1** was degraded.

Alkynes in the presence of catalytic amount (1 mol %) of 3.1: Complex **3.1** (3.0 mg, 0.0086 mmol) and phenylacetylene (87.7 mg, 0.86 mmol) in 10 mL of dry xylene was refluxed under nitrogen for 2 h. All volatile components were then evaporated under reduced pressure at room temperature and the residue was analyzed by GCMS and NMR spectroscopy. The data revealed the conversion of the phenylacetylene to its cyclotrimerization products 1,2,4-triphenylbenzene and 1,3,5-triphenylbenzene. The characterization of the products was completed by a comparison with literature data.[207,208]

Complex **3.1** (3.0 mg, 0.0086 mmol) and 1-hexyne (70.5 mg, 0.86 mmol) in 10 mL of dry xylene was refluxed under nitrogen for 2 hours. All volatile components were then evaporated under reduced pressure at room temperature and the residue was analyzed by GC-MS and NMR spectroscopy. It revealed the conversion of the 1-hexyne to its cyclotrimerization products 1,2,4-tributylbenzene and 1,3,5-tributylbenzene. The

characterization of the products was completed by a comparison with literature data.[207,208]

3.3 Results and Discussion

The starting *nido*-6-rhodadecaborane **3.1** ([6-(η^5-C_5Me_5)-*nido*-6-RhB_9H_{13}]) was synthesized according to the reported literature method.[205] The compound was readily isolated as a blood-orange, air-stable crystalline solid in essentially quantitative yield according to equation (3.1):

$$[\{Rh(\eta^5\text{-}C_5Me_5)Cl_2\}_2] + 2\,[B_9H_{14}]^- \longrightarrow 2\,Cl^- + 2\,HCl + 2\,[6\text{-}(\eta^5\text{-}C_5Me_5)\text{-}nido\text{-}6\text{-}RhB_9H_{13}] \quad (3.1)$$

The compound has a *nido*-$B_{10}H_{14}$ configuration in which the HB(6) vertex is replaced by an isoelectronic and isolobal Rh($\eta^5C_5Me_5$) entity (Figure 77).

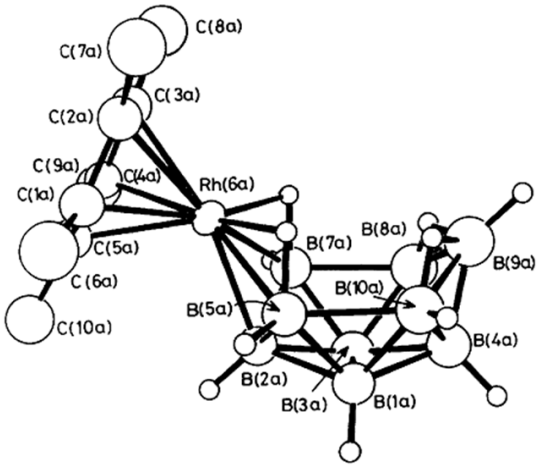

Figure 77: Crystallographically determined molecular structure of complex **3.1** (adapted from reference 205).

3.3.1 Thermal Transformation to *hypercloso*-rhodadecaborane

After refluxing in benzene for 4 days, the starting compound **3.1** was partially converted to *hypercloso*-metalladecaborane **3.3** ([*hypercloso*-(η^5-C_5Me_5)RhB_9H_9]) as

indicated by ^{11}B NMR spectra and shown in equation (3.2):

$$[6\text{-}(\eta^5\text{-}C_5Me_5)\text{-}\textit{nido}\text{-}6\text{-}RhB_9H_{13}] \xrightarrow{\Delta} [\textit{hypercloso}\text{-}(\eta^5\text{-}C_5Me_5)RhB_9H_9] + 2\,H_2 \quad (3.2)$$

This reaction was accelerated when compound **3.1** was refluxed in toluene where the majority of compound **3.1** was converted to compound **3.3** after 2 hours' refluxing. This indicates that solvent and temperature play key roles in the chemical transformation.

The thermal reaction was monitored by ^{11}B NMR spectra. Figure 78 gives the ^{11}B NMR spectra comparison of compounds **3.1** and **3.3**. The thermal reaction product **3.3** was isolated as an orange-brown solid. The ^{11}B NMR spectra of **3.3** is very similar to the few known *hypercloso*-metalladecaboranes (Figure 79).[5,16] As for *hypercloso*-metalladecaboranes, the ^{11}B NMR spectrum (Figure 80) of complex **3.3** shows three doublets of equal intensity with two of the doublets shifted to low field. The doublet at very low field, +100 ppm, is highly indicative of low-coordinate boron atoms directly bonded to a metal and is, therefore, assigned to the four-coordinate B2, B3, and B4 borons. The doublet at +30.4 ppm is assigned to boron B5, B6, and B7, which are also bonded to the metal but which are in five-coordinate positions. The doublet at −8 ppm is assigned to the remaining three boron atoms (B8, B9 and B10) that are not directly coordinated to the metal center. The assignment can be seen in Figure 81.

In addition to the ^{11}B NMR data, 2D ^{11}B-^{11}B COSY NMR spectrum was also measured for complex **3.3** (Figure 80). Cross peaks were observed among all three signals in the spectra. This is consistent with the proposed *hypercloso*-molecular structure (Figure 81).

To our knowledge, the observed formation of this *hypercloso*-rhodadecaborane **3.3** is the first *hypercloso*-metalladecaborane containing the metal rhodium.

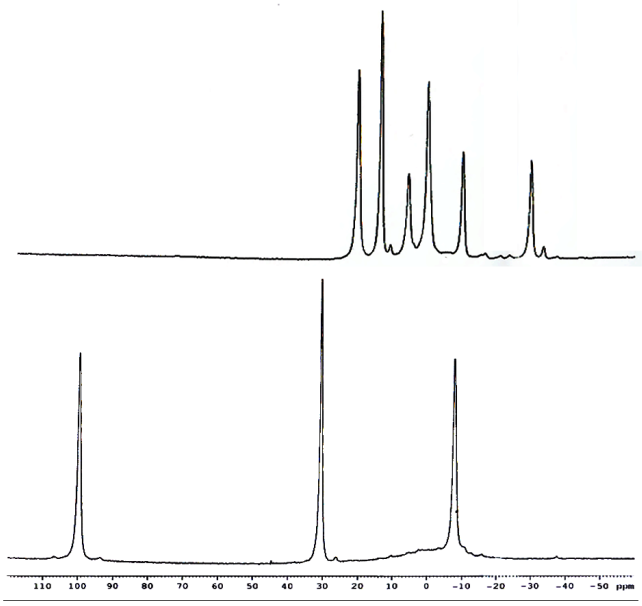

Figure 78: H-decoupled ^{11}B NMR spectra of complex **3.1** (top) and the thermal product **3.3** (bottom).

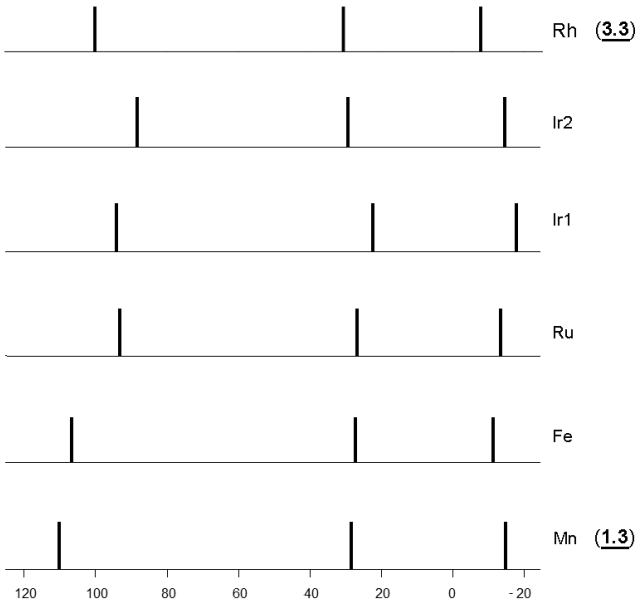

Figure 79: Stick representation diagrams of ^{11}B NMR spectral comparisons for **3.3** (Rh) and some known *hypercloso*-metalladecaborane compounds (Data for literature compounds adapted from references 2, 5, 20).

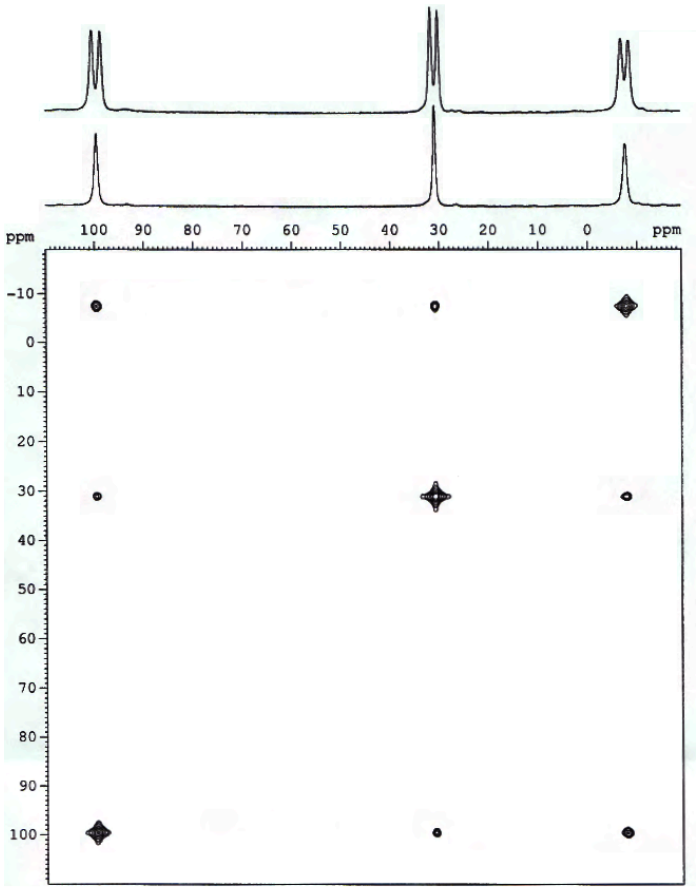

Figure 80: NMR spectra of the thermal product **3.3** (^{11}B and COSY ^{11}B-^{11}B).

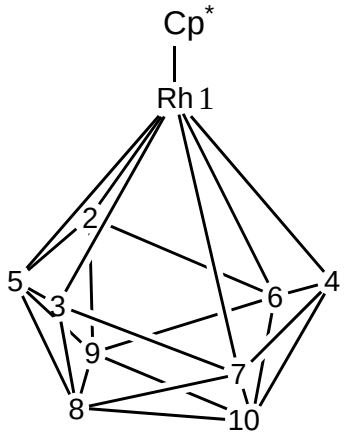

Figure 81: Proposed structure and numbering system for complex **3.3** (each vertex represents a B-H, Cp* =η^5-C_5Me_5)).

The thermally induced conversion from a *nido*-6 to a *hypercloso*- for a metalladecaborane has been previously reported for an iridadecaborane. Bould and coworkers reported that *nido*-metalladecaborane $[(PPh_3)_2HIrB_9H_{13}]$(**3.5**) or $[(PPh_3)(Ph_2PC_6H_4)HIrB_9H_{12}]$ (**3.6**), when heated in solution at ca. 80 °C, quantitatively loses dihydrogen to form the *hypercloso*-iridadecaborane product, $[(PPh_3)(Ph_2PC_6H_4)HIrB_9H_8]$ (**3.7**) (Figure 82).[2] The thermal conversion of the rhodadecaborane compound **3.1** to compound **3.3** indicates a similar reaction course between *nido*-6 rhodadecaborane and *hypercloso*-6 iridadecaborane. The mechanism for the formation of the *hypercloso* compound **3.3** can, therefore, be proposed as in Figure 83. During the first step, the *nido*-6 rhodadecaborane undergoes a thermally initiated cluster shift reaction, together with the loss of the first pair of hydrogen atoms. Although the exact reaction course is unclear, a reasonable path might involve the loss of the first pair of hydrogen atoms, followed by a movement of the 6-vertex rhodium center towards the B(5,10,9) position of the cluster accompanied by the rearranging of the bridging hydrogen atoms (Figure 83). The resulting intermediate $[(\eta^5\text{-}C_5Me_5)RhB_9H_{11}]$ has a formal *closo*-count except that there are two extra bridging hydrogen atoms. The structure can, therefore, therefore be regarded as an *iso-nido* type of metallaborane cluster.[2] This intermediate can then be transformed to the final *hypercloso* product by the loss of a further pair of hydrogen atoms followed by cage closure.[2]

Considering the different *exo*-polyhedral metal ligands, *viz* pentamethylcyclopentadienyl for rhodium and triphenylphosphines and hydride for iridium, the metal center may account for the similarity for both metalladecaborane transformations from *nido*-6 to *hypercloso*-geometry.

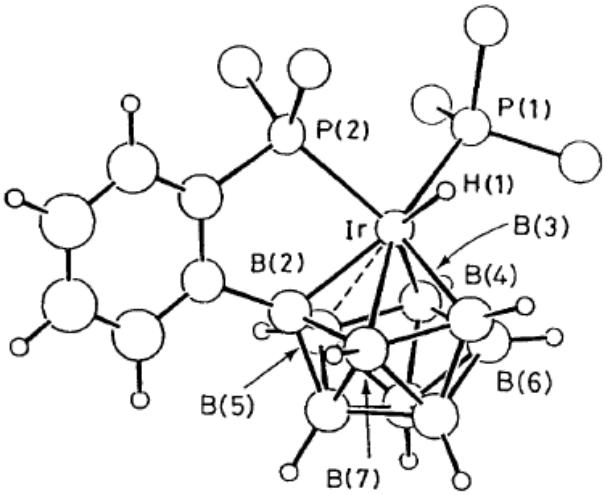

Figure 82: ORTEP drawing of complex **3.7**.[2]

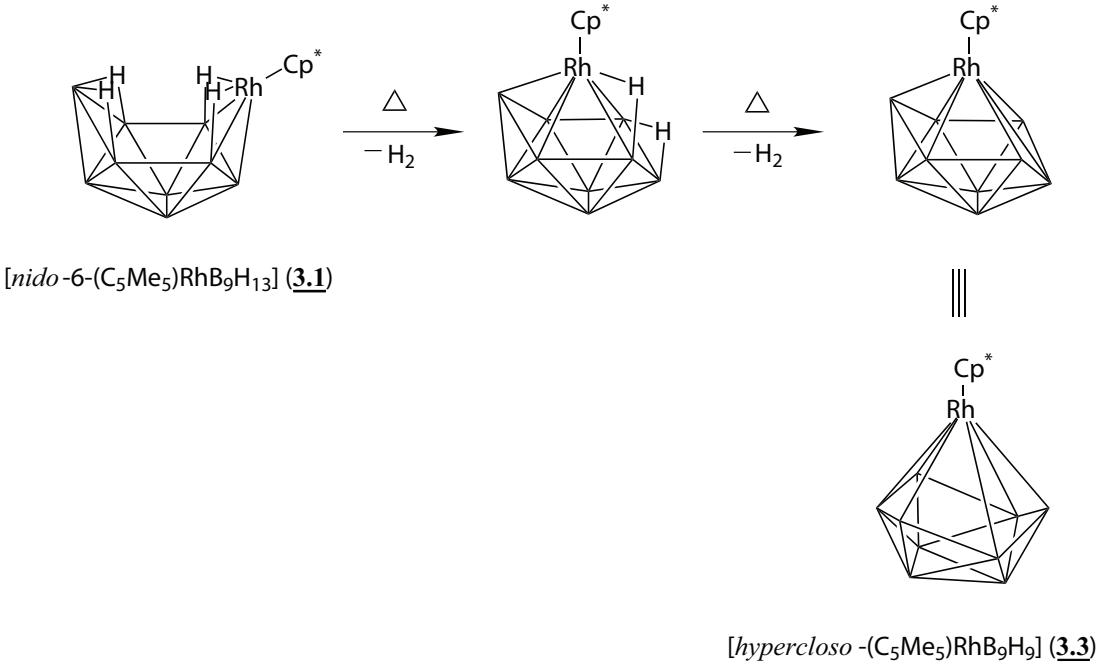

Figure 83: Proposed mechanism for the thermal formation of complex **3.3**.

3.3.2 Photochemical Transformation

Photolysis of Complex 3.1 in Benzene

When UV-irradiated at 254 nm in benzene for 2 hours, the starting *nido*-6-rhodadecaborane **3.1** was found to undergo an isomerization reaction to afford its *nido*-5 isomer, the previously reported *nido*-5-rhodadecaborane **3.4** (Figure 84).[3] A simple stoichiometric reaction can be written for this transformation as in equation (3.3):

$$[6\text{-}(\eta^5\text{-}C_5Me_5)\text{-}\textit{nido}\text{-}6\text{-}RhB_9H_{13}] \xrightarrow{\text{hv,benzene}} [5\text{-}(\eta^5\text{-}C_5Me_5)\text{-}\textit{nido}\text{-}5\text{-}RhB_9H_{13}] \quad (3.3)$$

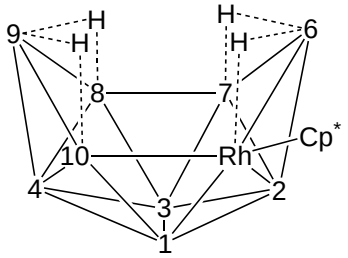

[*nido*-5-(C_5Me_5)RhB_9H_{13}]

Figure 84: Structure and numbering system for the complex **3.4**. (Rh is at 5 position. Terminal hydrogen atoms are omitted for boron 1-4 and boron 6-10. Each vertex represents a B-H. Cp^*= (η^5-C_5Me_5).

In the literature, the *nido*-5 complex **3.4** was prepared through a different method.[3] Bown and coauthor reported that the deprotoned decaborane anion $[B_{10}H_{13}]^-$ reacted with the rhodium dimer complex $[(RhCl_2(C_5Me_5))_2]$ at r.t. to afford the *nido*-5 rhodadecaborane **3.4** in 20.7% yield along with some other *nido*-5 rhodadecaborane derivative compounds. The reaction can be written as in equation (3.4):

$$[B_{10}H_{13}]^- + [(RhCl_2(C_5Me_5))_2] \longrightarrow [5\text{-}(\eta^5\text{-}C_5Me_5)\text{-}\textit{nido}\text{-}5\text{-}RhB_9H_{13}] \quad (3.4)$$

To our knowledge, the photo-irradiation induced *nido*-6 to *nido*-5 geometry conversion of metalladecaborane is unprecedented.[5,70] In contrast, in our previous study of the photolysis of **1.1**, the manganadecaborane either gives the *hypercloso*-manganadecaborane **1.3** or [*arachno*-B_9H_{14}][NMe_4] anion **1.4** depending on the solvent, and its *nido*-6 to *nido*-5 conversion was thermal.

^{11}B NMR spectra were used to monitor the reaction (Figure 85). The spectra showed the formation of the *nido*-5 isomer. This was confirmed by comparison of the ^{11}B NMR data with literature spectroscopic values.[3] Our data was essentially the same as the reported values (Figure 85, Figure 86, and Table 22).

The *nido*-5 rhodadecaborane structure of the complex **3.4** was further confirmed by 2D ^{11}B-^{11}B COSY NMR spectra (Figure 87). All boron-boron crosspeaks were observed in the spectrum except the B6-B7, B8-B9 and B9-B10 which are missing due to the presence of bridging hydrogen.[73]

Table 22: Experimental and literature ^{11}B NMR spectra data for the complex **3.4**.[3]

Experiment	Literature	Assignment
29.4	28.7	B(6)
26.0	25.3	B(1)
10.2	9.5	B(3)
5.4	4.5	B(8)
2.4	1.6	B(7)
1.3	0.6	B(9)
-3.2	-4	B(10)
-12.7	-13.5	B(2)
-37.6	-38.3	B(4)

Mechanism for the formation of compound 3.4

As we suggested earlier, the mechanism for the thermally induced isomerization of manganadecaborane **1.1** to its *nido*-5 isomer **1.2** can be understood through a vertex swing mechanism.[9] Since the isomerization process also applies to the rhodadecaborane

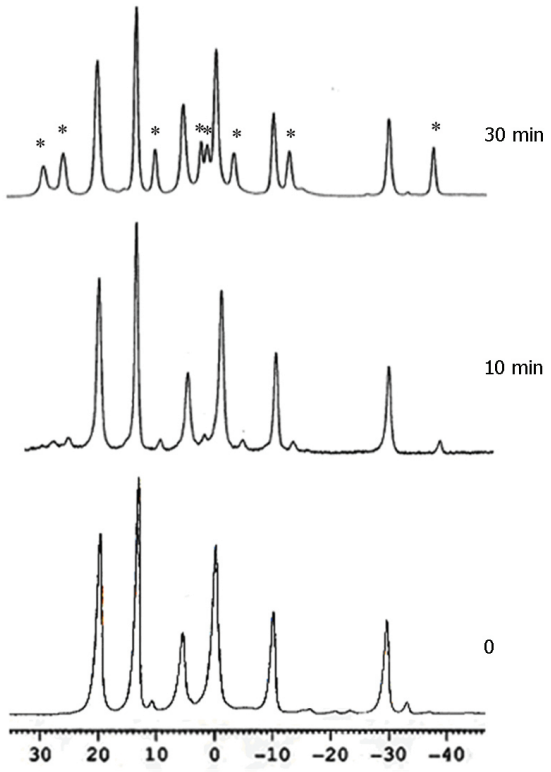

Figure 85: ^{11}B NMR spectra monitoring of photolysis of the complex **3.1** in benzene (Bottom: **3.1**. The (∗) labels: **3.4**).

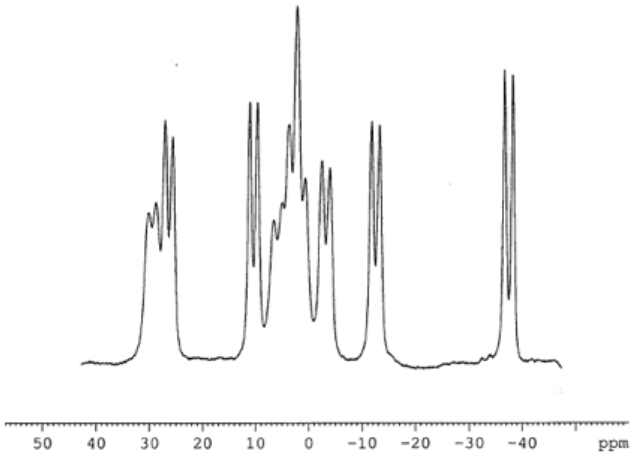

Figure 86: ^{11}B (B-H coupled) NMR spectrum of complex **3.4**.

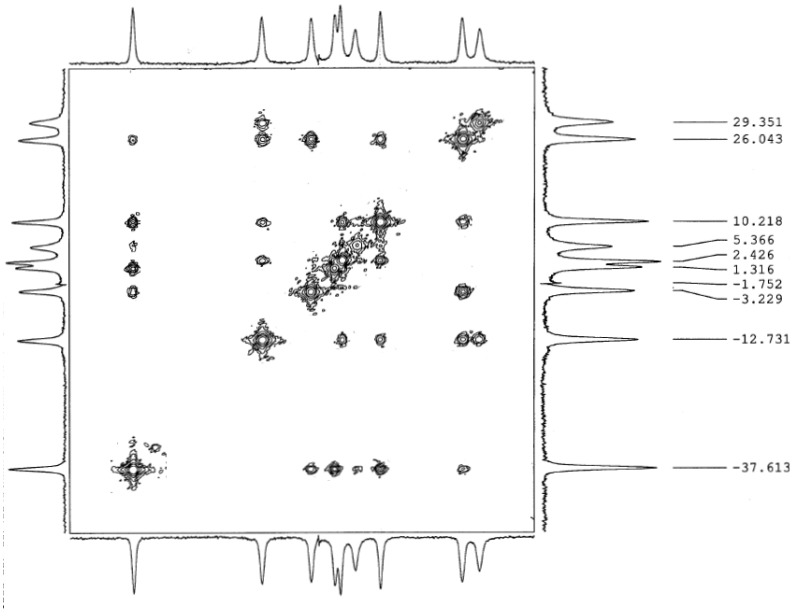

Figure 87: ^{11}B-^{11}B COSY NMR spectrum of the complex **3.4**.

3.4, the isomerization of **3.1** to **3.4** can, therefore, also be reasonably interpreted in terms of the vertex swing of a BH group from B(9) if the vertex is moved to connect across the 6,7,8 position (or the enantiomeric 6,5,10 position) (Figure 88).

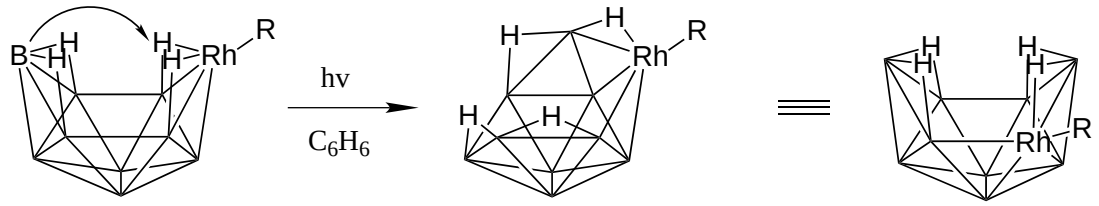

Figure 88: Proposed mechanism for the photochemical formation of complex **3.4**.

It should be noted that although the vertex swing mechanism can be used to rationalize the isomerization process from *nido*-6 to *nido*-5 geometry, the actual processes by which the isomerization proceeds may be much more complex. However, compared with other possible mechanisms, the vertex swing mechanism is the simplest.

Photolysis of Complex 3.1 in Diethyl Ether

Similar to the solvent-dependent behavior of the manganadecaborane **1.1** discussed in Chapter 1, the photolysis of rhodadecaborane **3.1** was also found to be dependent on the choices of solvent system. This supports the general thought that solvent plays an important role in the photoreaction of metallaboranes.

When UV-irradiated at 254 nm in Et_2O, the starting compound **3.1** was found to react with the solvent to afford several EtO-group substituted *hypercloso*-rhodadecaboranes. ^{11}B NMR spectroscopy indicated that 3 different substitution patterns were formed. As shown in Figure 89, these products are [*hypercloso*-2,5-$(OEt)_2$-(η^5-C_5Me_5)RhB_9H_7] (**3.8**), [*hypercloso*-2,3,5-$(OEt)_3$-(η^5-C_5Me_5)RhB_9H_6] (**3.9**), and [*hypercloso*-2,3,4,5-$(OEt)_4$-(η^5-C_5Me_5)RhB_9H_5] (**3.10**). The ^{11}B NMR data for these complexes are also compared with those of the unsubstituted *hypercloso* rhodadecaborane **3.3** in Figure 89. As expected, the chemical shifts of the three compounds can be divided into three regions which are close to the values of complex **3.3**. However, it can be seen from Figure 89 that as the number of substituted vertices increases, the observed chemical shifts generally move upfield. That's the same trend and necessarily true.

3.3.3 Interaction of Complex 3.1 with Alkynes: Catalytic Activity for the [2+2+2] Cycloaddition of Alkynes

Compared to the known syntheses and structures of the metallaboranes, the reaction chemistry of metallaboranes is relatively uninvestigated. Our studies into the chemistry of the complex **3.1** in previous sections indicates a rich chemistry available. In this context, the interaction of complex **3.1** with alkynes is of interest.

Literature examples of acetylene reacting with metallaboranes suggest the possibility of acetylene moieties becoming incorporated into metallaborane cluster frameworks.[134]

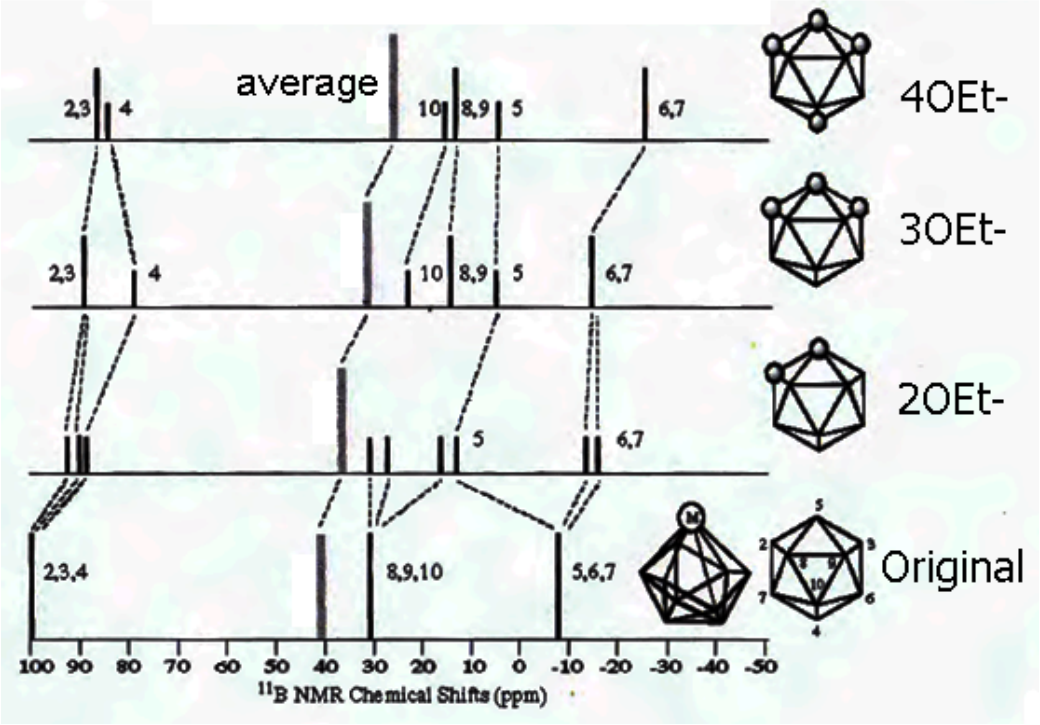

Figure 89: Stick diagram comparison of the products from the photolysis of complex **3.1** in Et_2O.

Using dichloromethane as solvent and when stirred under r.t. for 36 hours, the mixture of complex **3.1** and phenylacetylene showed no sign of reactions. When the mixture was stirred under photolytic condition, surprisingly no reaction was found to occur either. Although the photo-irradiation gives no reaction, it presents some interesting considerations for the metallaborane system. We showed earlier that under photolytic condition, the starting complex **3.1** undergoes an isomerization to the complex **3.4** by a proposed vertex-swing mechanism. However, with the presence of the phenylacetylene, no isomerization was detected by ^{11}B NMR spectroscopy. The prevention of the vertex swing mechanism suggests that the reversible coordination of the alkyne to the rhodium center must occur during the interaction. This suggested interaction of the alkyne with the metal center shows the possibility for further reactions at more forced condition.

Therefore, we monitored the reaction under conditions at elevated temperatures. When the mixture was refluxed in toluene (110 °C) for 2 hours, ^{11}B NMR spectroscopy showed only the starting complex **3.1** and some peaks suggesting the partial degradation of the complex. Since, no complex **3.3** was detected, this indicates the effect on the transformation from the complex **3.1** to complex **3.3** by the alkyne.

We increased the reaction temperature by employing xylene as solvent. When the mixture was refluxed in xylene (138 °C) for 2 hours, ^{11}B NMR spectroscopy showed little or no starting complex **3.1** nor the formation of complex **3.3** or other boron clusters. Although the alkyne insertion into boron cluster was not observed, the analysis of the resulting mixture revealed the presence of trimerization products of the phenylacetylene.

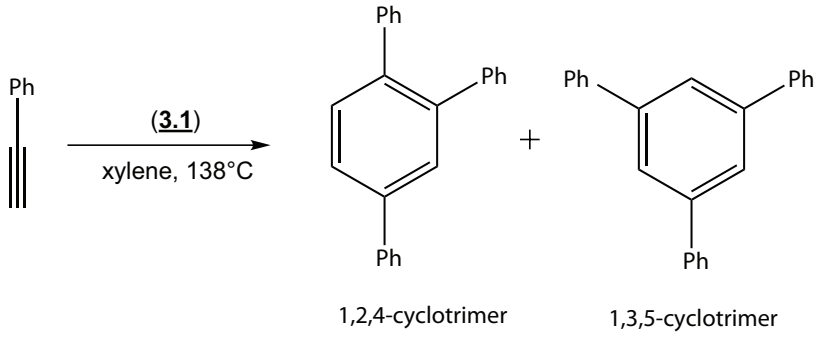

Figure 90: [2+2+2] cycloaddition of phenylacetylene mediated by **3.1**.

The failure in generating the alkyne insertion products implies that insertion of the carbon-carbon triple bond into the rhodium-boron bond may be an unfavorable step. It is also possible, however, that a competing process exists when a second unit of alkyne coordinates the metal and form the more favored metallapentadiene intermediate. The latter intermediate has been showed earlier to be critical in metal catalysed [2+2+2] cycloaddition reactions. Nevertheless, the detection of the alkyne trimerization product indicates the activity of the rhodium center towards catalysis. Since rhodium-based catalysts have been among the most actively pursed catalysts for

the [2+2+2] cycloaddition of alkynes,[209] we briefly investigated whether the observed cycloaddition of alkyne is catalytic.

Catalytic amounts (1 mol%) of the rhodaborane **3.1** were used for the reaction with phenylacetylene. The result confirmed the catalytic role of the rhodaborane for the [2+2+2] cycloaddition of alkynes. A similar result was also observed for an alkyl alkyne, 1-hexyne.

Fehlner and coworkers previously reported that dirhodaboranes such as 2,3-$(C_5Me_5Rh)_2B_3H_7$ are able to catalyze the cyclotrimerization of both terminal and internal alkynes.[169,210] Our results for the larger vertex rhodaborane **3.1** indicates a similar behavior for the larger boron cluster.

To our knowledge, this discovery of the catalytic reactivity of rhodadecaborane **3.1** for [2+2+2] cycloaddition is the first among large vertex metallaboranes.

3.4 Conclusion

The chemical behavior of the titled rhodadecaborane **3.1** was investigated under thermal and photochemical conditions. It was found that thermal condition induces the transformation to the *hypercloso*-rhodaborane **3.3**, while photolysis in benzene affords the isomerization compound **3.4**. It was also found that photolysis of **3.1** in Et_2O gives several EtO substituted *hypercloso*-rhodadecaborane complexes. In addition, the complex **3.1** was found to be catalytic active towards the [2+2+2] cycloaddition of terminal alkynes and this may find synthetic applications for substituted arene synthesis.

These results show the striking differences relative to our previous results with the manganadecaborane **1.1**. The future studies of these metallaboranes can be expected to lead to diverse reactivity.

Chapter 4

Non-covalent Functionalization of Boron Nitride Nanosheets (BNNSs) by Polymers and Application in Dye Sensitized Solar Cells (DSSCs)

4.1 Introduction

Hexagonal boron nitride (*h*-BN) is a graphite-like material in which planar networks of BN hexagons are regularly stacked. *h*-BN powder has been used to prepare a potentially interesting material - hexagonal boron nitride nanosheets (BNNSs).[211,212] Boron nitride nanotubes and nanosheets may be thought of as the isoelectric analog of carbon nanotubes and graphene (Figure 91). Unlike graphene, however, BNNSs do not absorb light in the visible region of the electromagnetic spectrum and thus are sometimes called white graphenes.[213] BNNSs have superb thermal and chemical stabilities. For instance, h-BN is stable up to 900 °C in air and is an intrinsic electrical insulator.[213]

Experiments have suggested that BNNSs may outperform graphene in such applications as field emitters, far ultraviolet light-emitting diodes, and polymer-matrix nanocomposites operated in extreme environments.[214–217]

Thanks to their excellent mechanical strength, chemical inertness and thermal conductivity, BNNSs have recently received increased interest.[212,219–221] Moreover, due to the specific 2-D geometry of the sheets, both sides of a single layer or few layers BNNSs can be used as a substrate for the controlled adsorption of molecules and functional groups. Therefore, BNNSs have the potential advantage of preventing the aggregation of functional materials by distributing them across its surface.

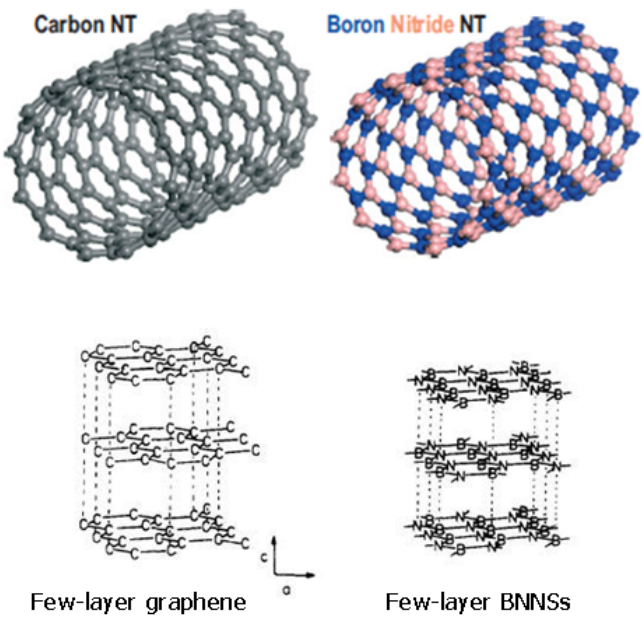

Figure 91: Carbon and boron nitride nanotubes and nanosheets.[218]

Several methods for the preparation of BNNSs have been reported. These methods include liquid-phase sonication, mechanical exfoliation, treating boric acid with urea, and chemical vapor deposition (CVD).[211,214,222]

We have employed the liquid-phase sonication method in the work reported in this chapter. Generally, there are two liquid phase exfoliation based routes empolyed to isolate single or few-layered BNNSs materials from h-BN. One route simply employs a solvent, such as isopropyl alcohol with the assistance of sonication, that exhibits non-covalent polar-polar interactions with the h-BN surface to separate the layered nanosheets.[222] The other route utilizes Lewis bases, such as amines, which can covalently combine with surface boron atoms of h-BN to facilitate the exfoliation of the nanosheets.[211] While the latter method using amine molecules provides higher nanosheets uptake in the dispersion, the former route is attractive since the resultant dispersions are essentially free of reagents other than the weakly-coordinating solvent molecules.[223]

The solvent-based exfoliation method has been shown to prepare BNNSs that are essentially free of foreign materials. Nevertheless, one disadvantage of the solvent-exfoliated BNNSs is that their dispersions in solvent are not stable under normal conditions. For example, aggregates of BNNSs start to form after 36 hours and result in almost complete aggregation after 80 hours. In order to study the functionalization and application of BNNSs, it is, therefore, necessary to find methods that prevent the formation of this aggregation.

Functionalization strategies consist of both covalent and non-covalent methods for nanomaterials.[224] One advantage of the non-covalent functionalization approach is that it usually does not alter the properties of the 2-D nanomaterial sturctures of graphene.[224–226] We, therefore focused on this type of functionalization. The non-covalent functionalization method by π stacking polymers has been reported for solubilizing and/or stablizing boron nitride nanotubes (BNNTs), carbon nanotubes (CNTs) and graphenes.[225,227] The interactions between the polymer and the BNNTs are shown in Figure 92 and Figure 93. The polymer backbone stacks onto the nanotube surface, resulting in enhanced coplanarity of polymer. The parallel stacking shown in Figure 92 and Figure 93 has been experimentally confirmed by atomic force microscopy for a complex of the conjugated polymer and CNTs.[228]

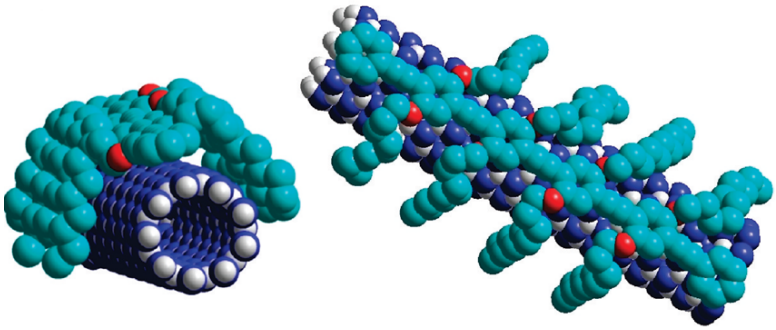

Figure 92: Schematic models of non-covalent functionalization of BNNTs with polymers (adapted from reference 225).

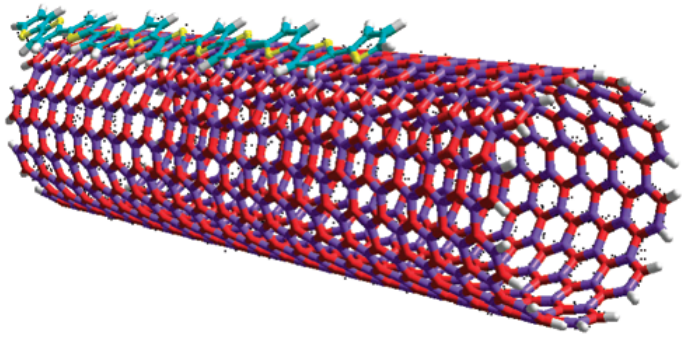

Figure 93: Schematic models of wrapping of BNNTs by polythiophene molecules (adapted from reference 229).

This interaction mode for both BNNTs and CNTs has also been confirmed by simulation studies.[229–231] It has been calculated that the adhesion strength of conjugated polymers to BNNTs is much stronger than that for carbon nanotubes (CNTs).[229] This suggests that the boron nitride structure forms stronger non-covalent interactions with the conjugated polymer. To our knowledge, however, this non-covalent functionalization π-interaction based method has not been reported for BNNSs. Having similar chemical bonding, BNNSs should behave similarly in terms of interacting with polymers. Here, we report the approach of using a polymer based non-covalent $\pi - \pi$ stacking functionalization method to form stable BNNS-polymer dispersions. The polymers employed in this work are based on functionalized polythiophene (PT). A possible arrangement between BNNSs and PT is shown in Figure 94.

Another solvent-based exfoliation strategy employed in this work is based on the non-ionic and non-toxic polymer polyvinylpyrrolidone (PVP). PVP has been reported to detach graphenes from graphite in the aqueous phase under sonication to form stable aqueous dispersions of PVP-coated single layers.[232] The steric or/and depletion stabilization by the non-ionic but largely hydrophilic PVP was reported to be responsible for the exfoliation and stablization.[232] Importantly, the layers are reported to be without oxidation or other structural damages.[232]

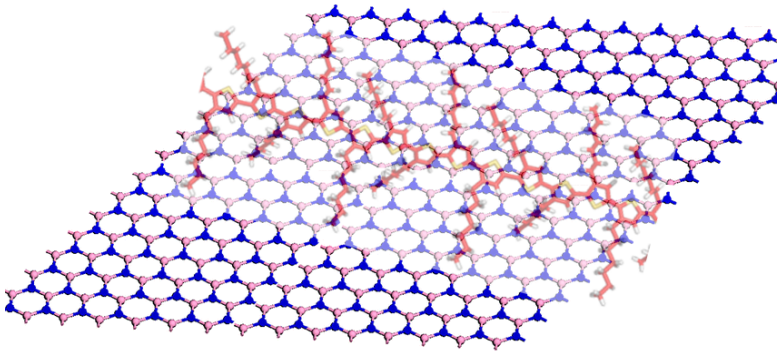

Figure 94: Schematic models for π interactions between BNNSs and polythiophenes (PT).

However, compared with PT, PVP is not very attractive in terms of electronic properties. Due to its unique electronic, optical, and redox properties, as well as their unique self-assembling properties on both solid surfaces and in the bulk, PT is among the most frequently used π-conjugated materials which are investigated as active components in molecular electronics and organic electronic devices.[233,234] For example, polythiophene-sensitized TiO_2 solar cells have been reported.[235,236] However, problems with polythiophene-based solar cells such as the low energy conversion efficiency and low stability, have hindered their further development. We focused on the PT exfoliated BNNSs in this work.

The resultant stable BNNS-polythiophene dispersions can be used as a platform for the conjugation of functional entities, such as semiconducting nanoparticles to form new hybrid systems. The polythiophenes can therefore bridge the BNNSs with other functional entities.

In this study, we also explored the effect of BNNSs on the performance of polythiophene based solar cells by the fabrication of a hybrid system, the BNNS-polythiophene-TiO_2 structure and the investigation of its application in DSSCs construction using BNNS-polythiophene as the "dye" component.

4.2 Experimental

4.2.1 Physical Measurements and Techniques

All NMR spectra were recorded on a Bruker Avance 300 MHz NMR equipped with a 5 mm OXI probe. Proton (^{1}H) NMR spectra were recorded at 300.15 MHz with chemical shifts referenced to an internal standard of tetramethylsilane at δ=0.0 ppm. Carbon (^{13}C) NMR spectra were obtained at 77.47 MHz.

All sonication processes were performed by using a SonorexRK 1028 H (68W) sonicator bath.

UV-Vis absorption and emission analysis was performed to assess the modification of the solubility of the BNNSs following functionalization. The spectum were taken on a Varian Cary 100 Bio UV-Visible UV-visible spectrophotometer or a Horiba Scientific, Fluoromax-4 spectrofluorometer. FTIR spectra in the range of 400 to 4000 cm^{-1} were taken from a Nicolet IR200 FT-IR and were referenced to the 1602.8 cm^{-1} band of polystyrene. The spectra were observed as KBr mulls and are reported in cm^{-1}.

Scanning Electron Microscope (SEM) images were taken using a JEOL JSM-5800 LV low vacuum scanning electron microscope equipped with an EDAX energy dispersive X-ray spectrometer. Transmission electron microscope images were taken using a JEOL JSM-2000EX which has an accelerating voltage of 80-200 kV.

4.2.2 Materials

All solvents used were reagent grade or better. Tetrahydrofuran (THF) and hexane were distilled over potassium metal prior to use. TLC plates were purchased from Fisher Scientific. Appropriate care was taken in handling the boron hydrides under inert atmosphere conditions.[61] All reactions were done in an inert atmosphere unless otherwise noted. Deuterated NMR solvents were purchased from Cambridge Isotope Laboratories, Inc. and dried over molecular sieves before use unless otherwise noted.

Boron nitride was purchased from Strem Chemicals. Poly[3-(4-carboxybutyl)thiophene-2,5-diyl] (PCBT, average MW 30-40 K) and Poly(3-hexylthiophene-2,5-diyl) (H3PT, average MW 28-52 K, regioregularity 97% or greater) were purchased from Rieke Metals, inc. Titanium dioxide was purchased as AEROXIDE TiO_2 P25 with the average particle size of 21 nm. All other commercially available reagents and solvents were used as received.

4.2.3 Synthesis

In order to functionalize the BNNSs using polythiophene, substituted polythiophene structures were needed. The synthesis of polythiophenes containing carboxylic acid groups poly(3-thiophenezoic acid) (PTPA) and poly(3-thiophene acetic acid) (P3TAA) were performed according to reported procedure and characterized accordingly.[237–239]

Poly(3-thiophenezoic acid) (PTPA) Anhydrous ferric chloride (2.46 g, 19.5 mmol), ammonium persulfate (0.89 g, 3.88 mmol) and the monomer 3-thiophenecarboxylic acid (0.5 g, 3.88 mmol) were mixed in 30 mL 1.2 M HCl (aq). The mixture was allowed to stir for 5 h at room temperature. After the reaction was completed, the pH of the reaction mixture was adjusted to 12 with a NaOH solution and the PTPA solution was obtained by filtration.[239] ^{1}H NMR (300 MHz, DMSO$-d_6$, δ(ppm)): 7.43-7.31 (m, 1H, thiophene ring proton). Our data matched reported literature values for PTPA (7.3 ppm for polythiophene ring, non-observable COOH).[238]

Poly(3-thiophene acetic acid) (P3TAA) 3-Thiophene acetic acid (5.0 g, 35.2 mmol) (3TAA) was acidified with concentrated H_2SO_4 (four drops) in dehydrated methanol (50 ml) to protect the carboxylic acid moiety of the monomer from the oxidative decomposition and then refluxed for 24 h. Methanol was then evaporated using a rotary evaporator and diethyl ether was used to extract the organic residue. The extract was thoroughly washed with 200 mL of deionized water and dried with

anhydrous $MgSO_4$ and filtered. 3-Thiophene methyl acetate (3TMA) was recovered after the rotary evaporation of diethyl ether. Anhydrous ferric chloride (5.0 g, 30.8 mmol) was dissolved in dry chloroform (75 mL) under a N_2 atmosphere at 0 °C in a three-necked flask with continuous stirring. The protected monomer 3TMA (1.25 g, 8 mmol) was dissolved in dry chloroform (50 ml) and was added to the ferric chloride solution dropwise under the above conditions. After 24 h, the polymerized brown-red colored poly(3-thiophene methylacetate) (P3TMA) was precipitated by adding the reaction solution to a large excess of methanol (1 L). The residual oxidant and the oligomers were removed by repeated washing with deionized water and fresh methanol. The deprotection reaction was carried out by heating the P3TMA in a 50 mL NaOH (aq) solutions (2.0 M) for 24 h. The mixture was then filtered to remove the insoluble part. The water-soluble portion was neutralized and precipitated by adding a dilute HCl solution. The P3TAA precipitate was carefully washed with deionized water (100 mL) and isolated by high-speed centrifugation before being vacuum-dried for 24 h.[237] ^{1}H NMR (300 MHz, DMSO$-d_6$, δ(ppm)): 12.57 (s, 1H, COOH), 7.55-7.39 (m, 1H), 3.85-3.33 (m, 2H, CH_2). Our data matched reported literature values for P3TAA (12.53 ppm (s, COOH, 1H), 7.49-7.28 ppm (m, 1H), 3.783.35 ppm (m, 2H)).[236]

Exfoliation of Boron Nitride Nanosheets (BNNSs) Following previously reported methods,[222] the BNNSs were prepared by the sonication of h-BN in isopropyl alcohol (IPA) (50 mL) at a concentration of 3 mg/mL in a round-bottomed flask (100 mL) for 48 hours. The suspension was then centrifuged at 1500 rpm for 45 min to remove any aggregated material. The suspension of exfoliated h-BN nanosheets (BNNSs) was left to equilibrate for 24 hours to allow any additional insoluble material or aggregates to precipitate. The translucent supernatant fraction was then retained and the dispersion was used directly for physical measurement. The concentration of the prepared BNNS was determined by UV-Vis absorption spectroscopy by using

the Beer-Lambert law (the extinction coefficient of BNNS in IPA at 300 nm is 2367 mL/mg/m).[222]

Functionalization and stabilization of BNNS in solvent: All polymer-BNNS conjugates were synthesized according to a similar procedure as employed for BNNS-H3PT preparation as described below. To the exfoliated BNNSs dispersion in chloroform (1 mL, 0.04 mg/mL) was added a H3PT chloroform solution (0.2 mL, 4 mg/mL). The resulting mixture was sonicated at room temperature for 4 hours. After 2 hours, the color of the mixture had faded from grey to light yellow. The reaction mixture was then centrifuged at 1500 rpm for 45 min to remove any aggregated material and the supernatant fraction was retained. The obtained supernatant was stable for weeks under normal condition at room temperature. No visible aggregates were observed for at least two weeks. The solvents used for the preparations of other BNNS-polythiophenes conjugates were H_2O for PTPA, DMSO for PCBT and P3TAA (pH adjusted by KOH to 10-12).

Hybrid nanomaterial BNNS-polythiophene-TiO_2 synthesis: To a prepared BNNS-polythiophene solvent dispersion, TiO_2 nanoparticles were added dropwise and the mixture was sonicated for 3 hours. The resultant mixture was then centrifuged (1500 rpm, 45 min) to collect the precipitate BNNS-polythiophene-TiO_2. A control experiment with only the original BNNS-polymer dispersion was processed in parallel and no precipitate was formed. UV-Vis spectra before and after the process were recorded and compared for both samples.

Interaction of Metal Ions with BNNS-P3TAA

To a prepared BNNS-P3TAA DMSO dispersion (1 mL, 0.04 mg/mL) was added $MnCl_2$ aqueous solution (0.01 mL, 1×10^{-3} M). The mixture was sonicated for 2 h at room temperature. UV-Vis and fluorescence spectroscopy was used to monitor the process.

Other heavy metal ions (Ag^{+}, Cd^{2+}, Cr^{2+}, Ca^{2+}, Hg^{2+}, Ni^{2+}, Pb^{2+}, and Zn^{2+}) of the same concentration (0.1 mL, 1×10^{-3} M) were investigated similarly as the Mn^{2+} described above.

4.2.4 Dye Sensitized Solar Cells (DSSCs) Fabrication

The DSSC fabrication methods used have been described in the literature.[235,236,240] The TiO_2 paste Ti-Nanoxide D, purchased from "Solaronix" (Nanoxide-T, Switzerland), contains about 11 % wt. nanocrystalline titanium dioxide mixed with optically dispersing anatase particles. The paste was coated using the "doctor blade" method, a technique also known as slot-coating in its mechanized version. The method uses a hard squeegee, or doctorblade, to spread a portion of titania paste onto the glass. With this technique, the thickness of the titania layer on the transparent conducting glass is determined by the thickness of a spacer placed on both sides. The films were then sintered under N_2 at 500 °C for 45 min. The films were then coated with the dye material by dipping the films in an aqueous polymer dye solution (3×10^{-4} M) for 48 hours and washed either with dry THF or ethanol and dried under N_2 at room temperature. This dye-coated electrode was incorporated into a thin layer sandwich-type cell with a platinum-coated FTO counter electrode, a spacer film and an organic solution containing 0.5 M LiI and 0.05 M iodine in acetonitrile. Photoresponses were measured as described below. All photovoltaic measurements were repeated in three independent devices. A typical fabricated DSSCs device in this study is shown in Figure 95.

Photoelectrochemical Measurement Photoelectrochemical data were measured using a 450 W Xenon light source which was focused to give 1000 W/m^2, the equivalent of one sun at air mass (AM) 1.5 at the surface of the test cell. The performance of the cell was characterized by recording the current-voltage (I-V) behavior.

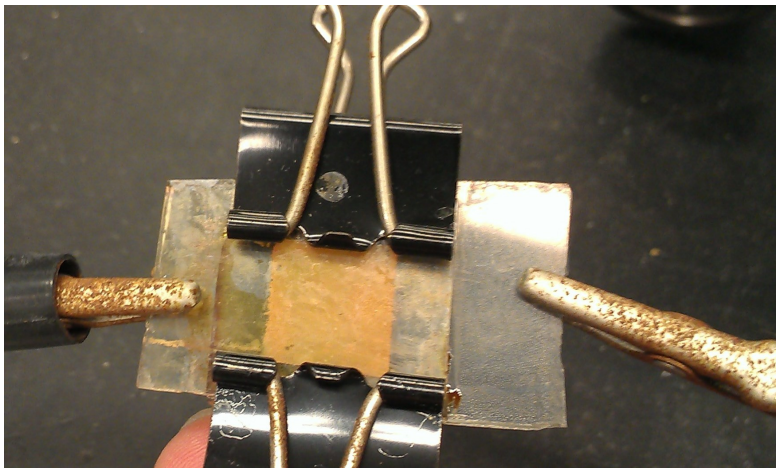

Figure 95: A typical fabricated DSSCs.

The overall power conversion efficiency, η, can be calculated according to equation 4.1 and 4.2:

$$\eta = \frac{\mathrm{FF} \times \mathrm{V_{oc}} \times \mathrm{I_{sc}}}{\mathrm{P_{in}}} \tag{4.1}$$

and the fill factor (FF) is defined as:

$$\mathrm{FF} = \frac{\mathrm{V_{max}} \times \mathrm{I_{max}}}{\mathrm{V_{oc}} \times \mathrm{I_{sc}}} \tag{4.2}$$

where P_{in} is the input power density (i.e., the intensity of incident light, in mW cm^{-2}), V_{OC} is the open-circuit voltage (mV), I_{SC} is the short-circuit current density (mA cm^{-2}), and V_{max} and I_{max} are the voltage and current at maximum power output, respectively.

4.3 Results and Discussion

In this study, we first prepared the BNNSs and demonstrated their non-covalent functionalization by polymers. The BNNSs were successfully solubilized and stablized through this approach. Then we investigated the application of the resultant BNNS-polythiophene conjugates to areas such as metal ion sensing and a platform for TiO_2 nanoparticles. The BNNS-polythiophene-TiO_2 hybrid nanomaterial was further investigated in their potential application in dye sensitized solar cells (DSSCs).

4.3.1 Praparation of BNNSs by Exfoliation of h-BN

The preparation of exfoliated BNNSs were successfully accomplished according to a reported optimized procedure by sonication of *h*-BN in organic solvent.[222] Scanning electron microscopy (SEM) was used to characterize our as-exfoliated BNNSs and typical micrographs of the exfoliates are shown in Figure 96 and Figure 97. From the images, large quantities of two dimensional objects were observed. The flat surface of the sheets can also be observed. Nanosheet size statistics can be generated directly from the SEM images. The average length and width of the nanosheet flakes are 1000 nm and 500 nm, respectively. Most of these nanosheet flakes are 2-6 layered BNNSs, as determined according to the reported procedure.[222]

4.3.2 Non-covalent Functionalization of BNNSs by $\pi-\pi$ Interacting Polymers

The structures of the polythiophenes considered in this study are shown in Figure 98. BNNSs were functionalized and solubilized by mixing the prepared BNNSs with either poly(3-hexylthiophene-2,5-diyl) (H3PT) in chloroform or polyvinylpyrrolidone (PVP) in water. The prepared BNNS-polymers were sonicated and purified by centrifugation.

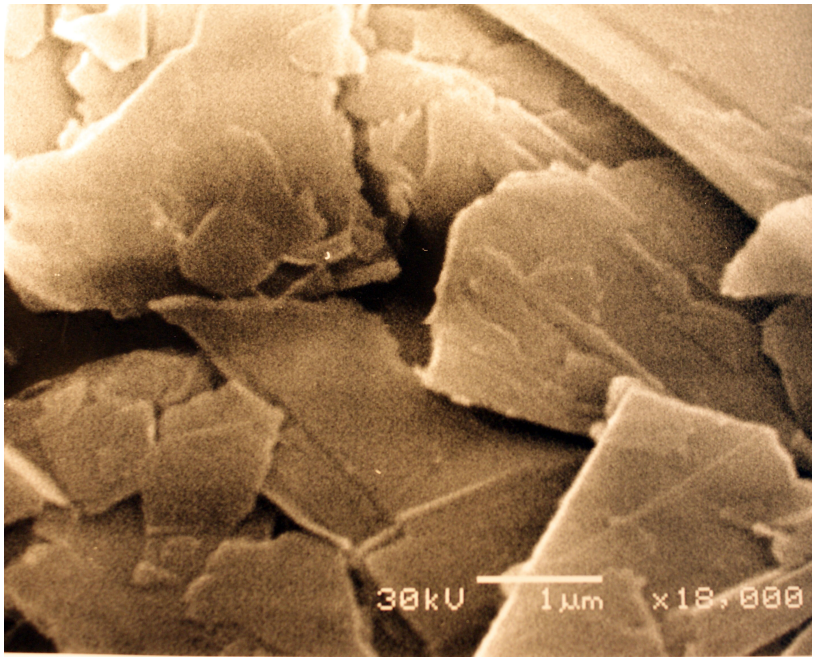

Figure 96: SEM images of exfoliated BNNSs.

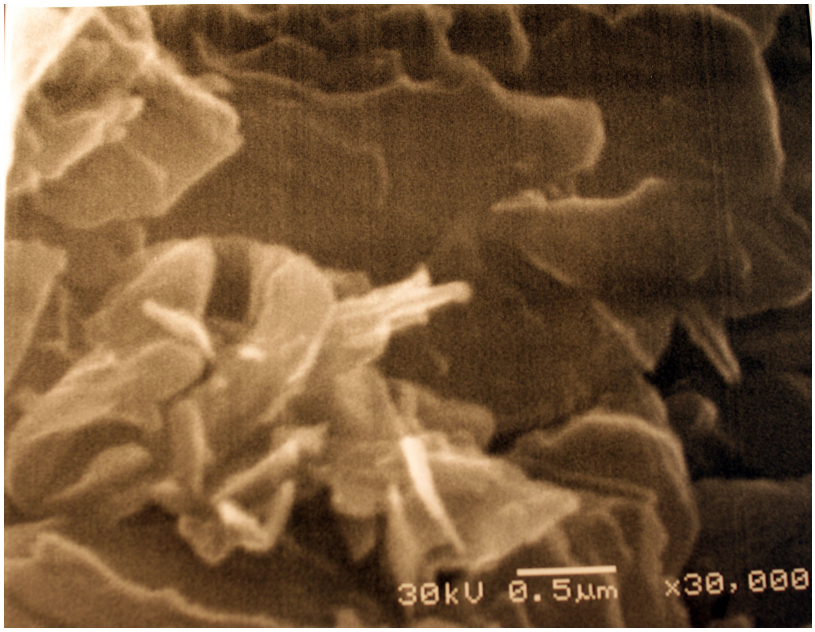

Figure 97: SEM images of exfoliated BNNSs.

The obtained supernatant BNNS-H3PT and BNNS-PVP dispersions in solvent were stable at r.t. for several weeks. No visible aggregates were observed for at least two weeks. In contrast, the unfunctionalized BNNSs quickly form aggregates from the free BNNSs and precipitate from solution. This suggests an effective interaction between the polymers and BNNSs to stabilize individual units.

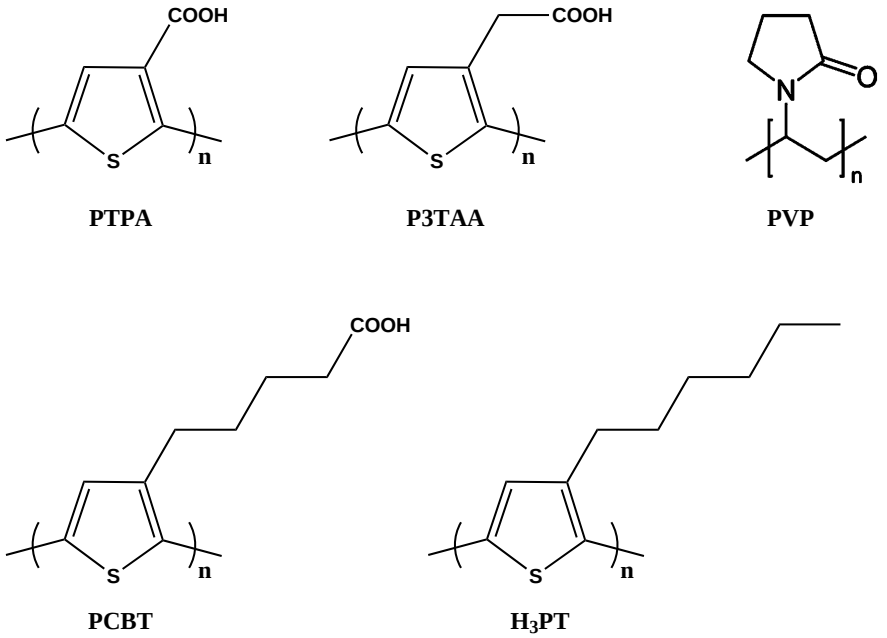

Figure 98: Structures of the polymers considered in this study.

The BNNS-polythiophene dispersions were used directly for physical measurements and further reaction. The UV-Vis and fluorescence spectra for the unreacted BNNSs and BNNS-H3PT in chloroform are given in Figure 100 and Figure 101. The BNNS-H3PT conjugate dispersion was characterized by observing its UV-Vis spectra and fluorescence spectra (Figure 100 and Figure 101). The polymer BNNS-H3PT conjugates displayed a quite significant blue shift of 47 nm in its absorption spectrum and 13 nm blue shift in its emission spectrum compared with the free polymer. The blue shifts indicate that the π-conjugation of the polythiophene is partially disrupted and that the polythiophene polymers are interacting directly with BNNS through

Figure 99: BNNS-H3PT dispersion compared with H3PT polymer in chloroform.

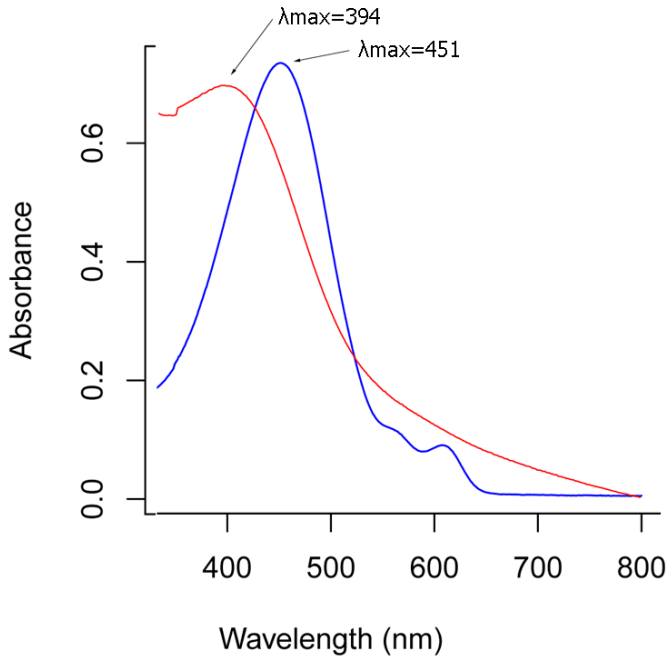

Figure 100: BNNS-H3PT (red line) UV-Vis spectra compared with H3PT polymer (blue line) in chloroform.

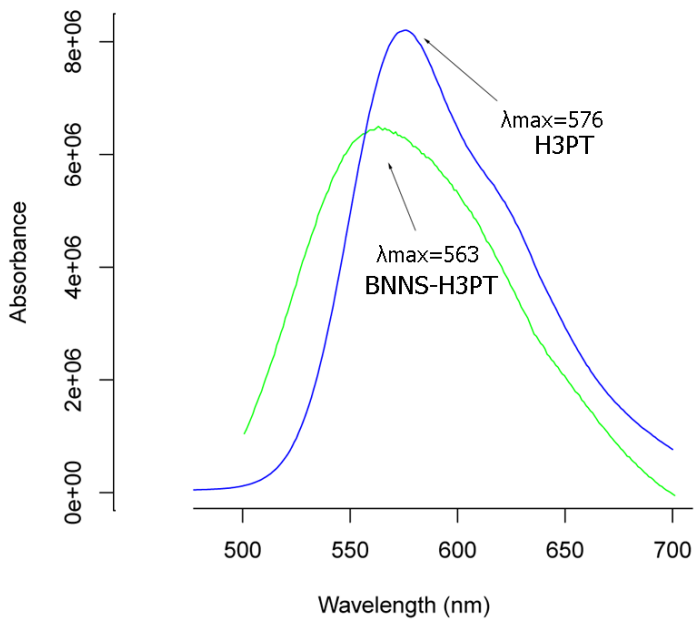

Figure 101: BNNS-H3PT fluorescence spectra compared with H3PT polymer in chloroform.(Blue line: H3PT in chloroform, excitation at 451 nm. Green line: BNNS-H3PT, excitation at 400 nm.)

$\pi - \pi$ stacking interactions.[225] To our knowledge, this is the first report of BNNSs functionalized by the $\pi - \pi$ stacking interaction of polythiophenes.

Energy transfer mechanisms that take place within polymers are typically quite complicated and extensive efforts have been made to relate conformation, excited state dynamics, and energy transfer.[241] In the case of the nanocomposite materials of BNNSs and polythiophene that we prepared, the conformation is clearly different from that of the free polythiophene. This change in conformation results in the observed red/blue shifts in the optical spectra.

The interaction is consistent with literature report of the thiophene polymer functionalization of Boron nitride nanotubes (BNNTs). Velayudham and coworkers reported the composite nanotube material of polymer polythiophene bearing tri-(ethylene glycol) methyl ether side chains and BNNTs displays significant blue shift of 50 and 42 nm in absorption and in emission, respectively.[225] Since the BNNSs

and BNNTs have related chemical structures, the similarity of their interaction with polythiophene (H3PT) is expected.

The TEM images of the resulting BNNS-polythiophene conjugates are shown in Figure 102. This image further confirms the presence of the nanosheets and the shape of these nanosheets remain intact as non-aggregated structures.

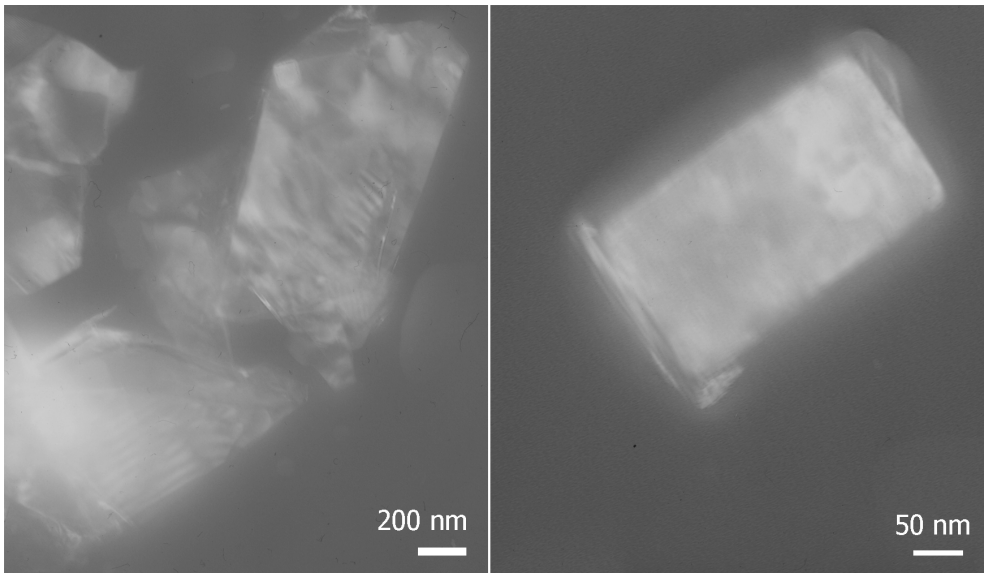

Figure 102: TEM images for BNNS-H3PT dispersion.

The UV-Vis spectra comparison between the polythiophene PTPA and its BNNSs conjugates are shown in Figure 103. Although no significant changes in the absorption pattern was detected, the stablization ability of the PTPA for BNNSs dispersion was found to be quite similar to P3TAA in that the PTPA prevents the aggregation of BNNSs dispersion. This indicates the presence of a $\pi - \pi$ interaction between PTPA and BNNSs.

Besides the polythiophene based system, the polyvinylpyrrolidone (PVP) system was also investigated for its potential ability for functionalizing BNNSs. Stable dispersions were found to be formed after the sonication of the PVP and BNNSs mixture. Although UV-Vis spectra were less useful to monitor concentration, since the

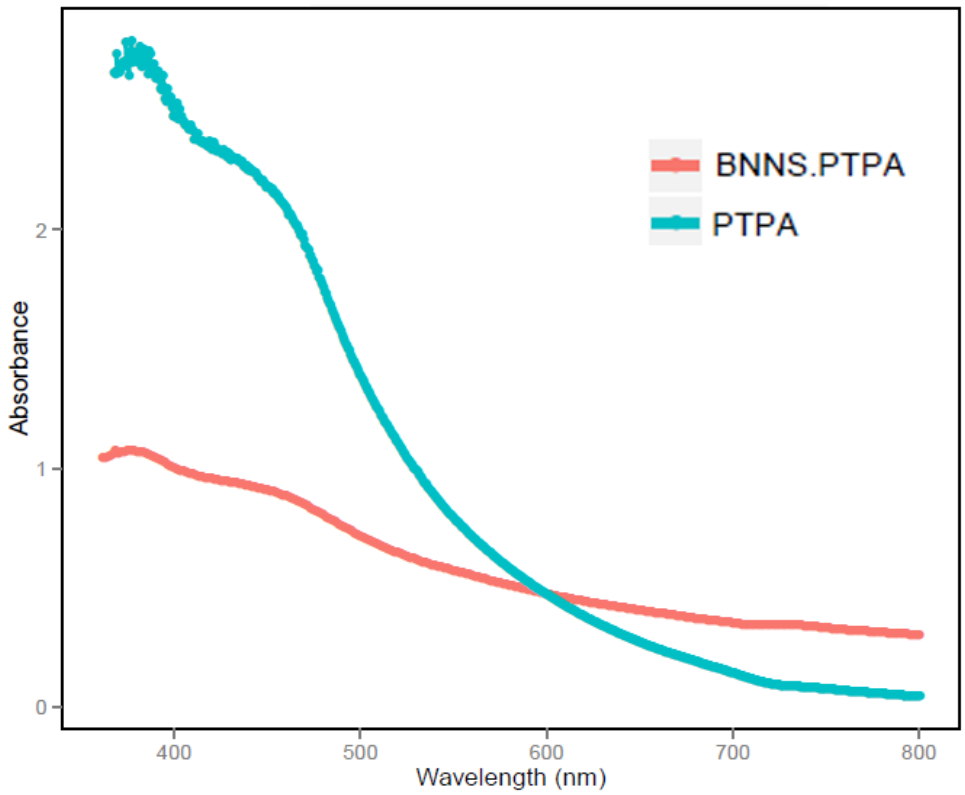

Figure 103: BNNS-PTPA UV-Vis spectra compared with polythiophene PTPA in DMSO.

polymer PVP does not have absorption in visible region, the stablization effect and the TEM images (Figure 104) confirmed the presence of the BNNS-PVP conjugates.

4.3.3 Application of Functionalized BNNSs: BNNS-polythiophene

Investigation of BNNS-polythiophene as a Potential Sensor System for Metal Ions

Due to the close relationship between metal ions in the environment and human health, designing and synthesizing highly sensitive and selective chemosensors for heavy metal ions has become increasingly important.[242,243]

The BNNS-polythiophenes containing carboxylic acid groups in this chapter have both the requisite strong absorption and the binding moieties for metal ion sensing.

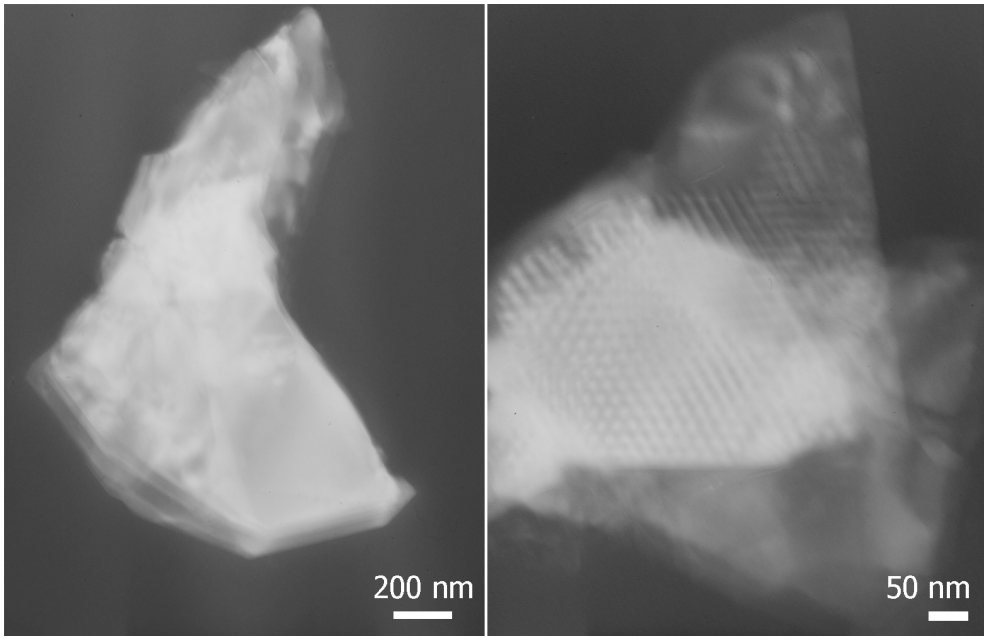

Figure 104: TEM images for BNNS-PVP dispersion.

It also has been reported that metal ions bind exclusively to the carboxylic acid in a number of ferrocene glutamic acid-cystamine conjugates.[244] We therefore evaluated the interactions of metal ions such as Ca^{2+} and Zn^{2+} ions with the BNNS-polythiophenes by monitoring spectral changes in the BNNS-PT-COOH conjuages with metal ions.

An aqueous solution containing 1×10^{-3} M Ca^{2+} was added to the BNNS-P3TAA dispersion and the mixture was sonicated for 2 hours. UV-Vis spectroscopy was used to monitor the process. No significant changes in the spectrum were observed. Other metal ions were added to the BNNS-P3TAA dispersion similarly. These metal ions include Mn^{2+}, Ag^{+}, Cd^{2+}, Cr^{2+}, Hg^{2+}, Ni^{2+}, Pb^{2+}, and Zn^{2+}. UV-Vis spectroscopy was used to monitor the process, however, no significant changes were observed in the UV-Vis absorption spectra. This may due to the insensitivity of the BNNS-P3TAA towards these metal ions under the experimental conditions.

BNNS-functionalized Polythiophene as a Coordination Platform

The stable polymeric non-covalent functionalized BNNSs solvent dispersion might be able to act as a platform for attachment of functional components to form useful hybrid nanomaterials. It has been well known that the carboxylate group can act as an excellent anchor group for functionalizing TiO_2 nanoparticles.[245,246] We have, therefore, investigated TiO_2 nanoparticles for their potential ability to attach to the BNNS-polythiophene to form the BNNS-polythiophene-TiO_2 hybrid nanomaterials.

In our work, several polythiophenes of different lengths with carboxylate group tethers were used for the purpose of connecting the TiO_2 nanoparticles to the polymeric structures (Figure 106). These functionalized polythiophene side chains provide multiple anchoring sites within each polymer to connect to the TiO_2 nanoparticle (Figure 105).

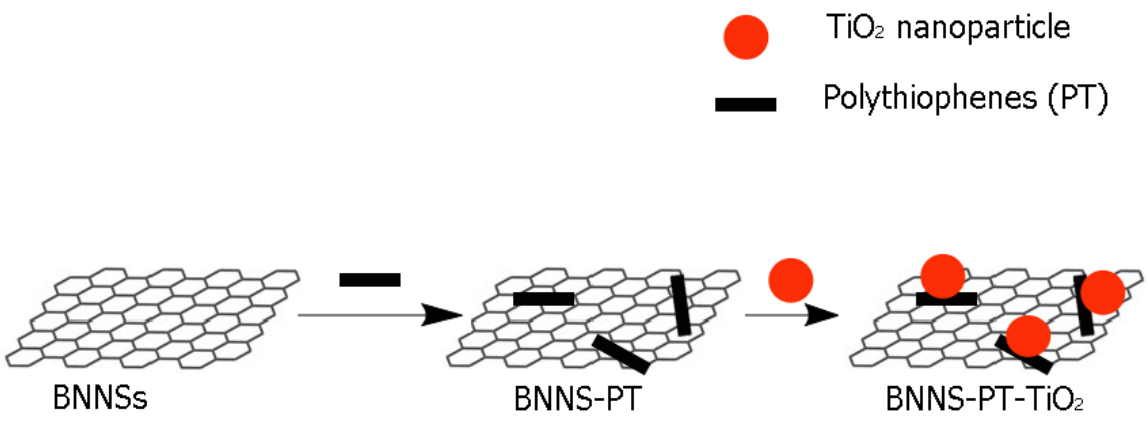

Figure 105: Model for BNNS-polythiophene-TiO_2 hybrid nanomaterial.

BNNS-Poly[3-(4-carboxybutyl)thiophene-2,5-diyl](PCBT)-TiO_2 (m=4)

The dispersion of BNNS-PCBT was prepared using the procedure described in the experimental section from sonication of BNNSs with polythiophenes with carboxylate groups tethers. The UV-Vis spectrum monitoring (Figure 107) showed a significant blue shift in the hybrid material indicating the formation of the non-covalent $\pi - \pi$

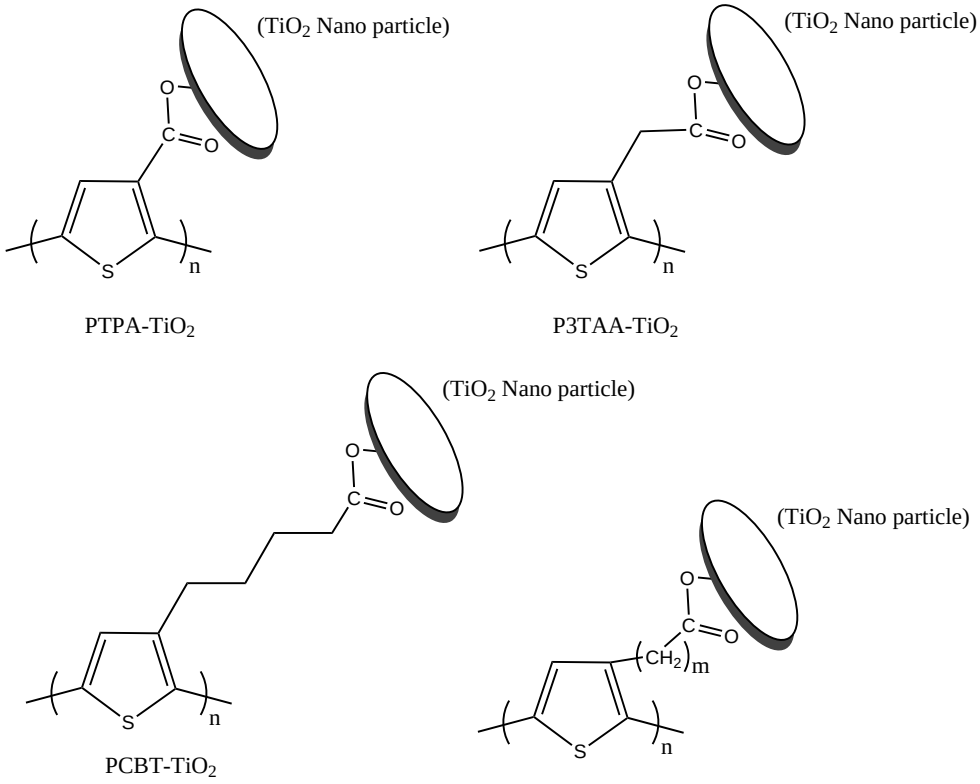

Figure 106: Polythiophene containing carboxylic acid groups and the model for its binding to the surface of TiO_2 nanoparticle (m = 0,1,4).

stacking interaction between the polythiophene and the BNNSs. The blue shift can be observed from the UV-Vis spectrum and is consistent with the blue-shift effects seem for H3PT.

The BNNS-PCBT-TiO_2 hybrid nanomaterial was then synthesized by the sonication of the BNNS-PCBT with TiO_2 nanoparticle in IPA/water. After centrifugation, the supernatant was found to be colorless compared with the control group without the addition of the TiO_2 nanoparticles that was light grey colored. This indicates that the absence of the unreacted BNNS-PCBT after addition the TiO_2 nanoparticles. The UV-Vis spectra of the supernatant from the sample and control sample were compared in Figure 108.

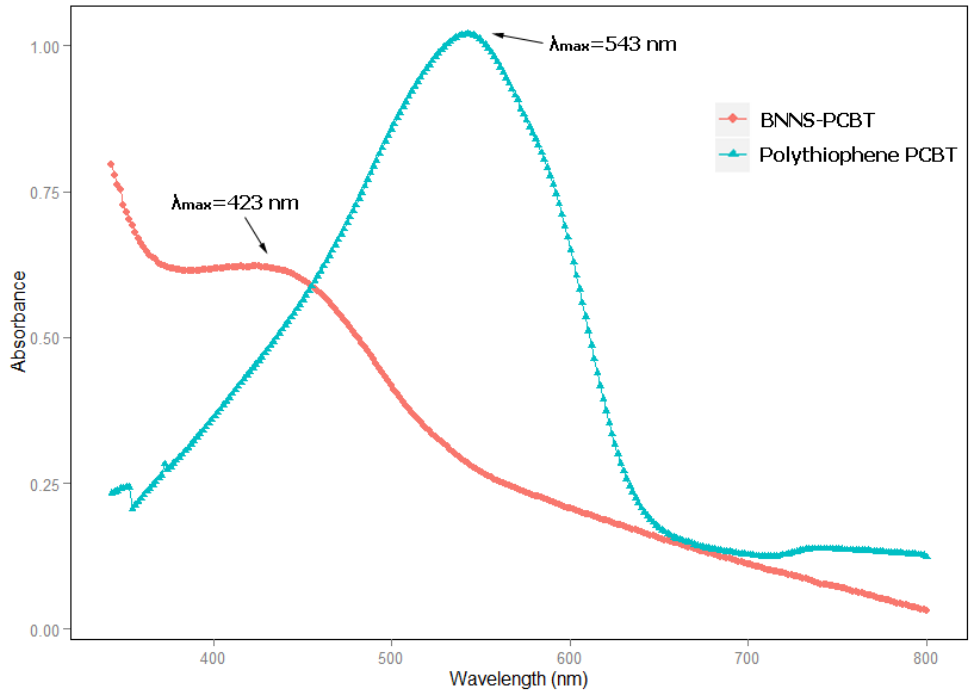

Figure 107: BNNS-PCBT UV-Vis spectra compared with the polymer PCBT in IPA/water (543 nm for PCBT and 423 nm for BNNS-PCBT).

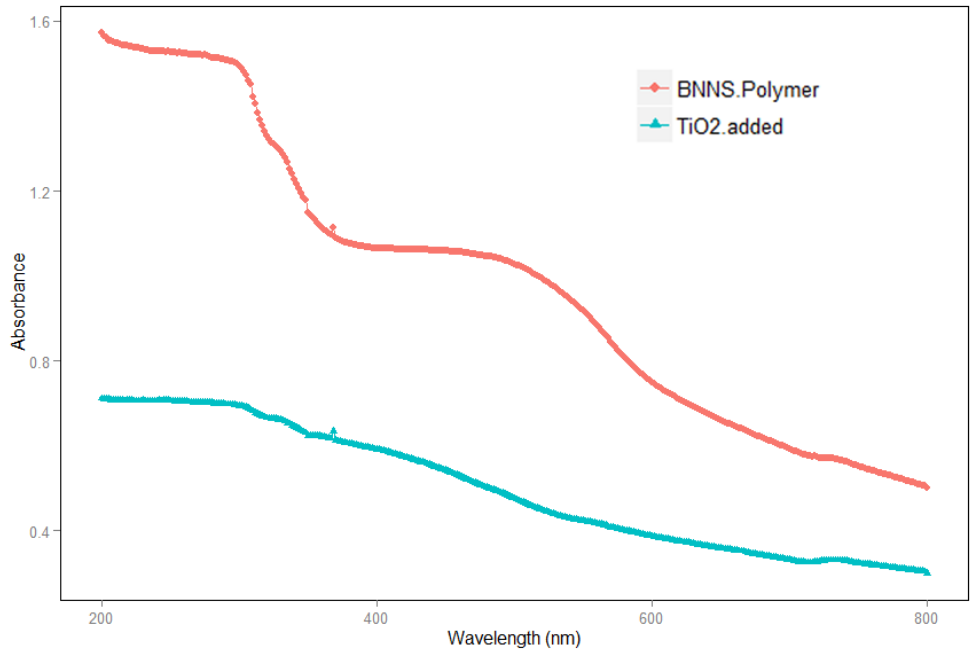

Figure 108: BNNS-PCBT-TiO_2 UV-Vis spectra compared with the polymer PCBT in IPA/water.

The spectral comparison shows that after adding the TiO_2 nanoparticles, the absorption was greatly reduced after centrifugation. This suggests that the binding between the TiO_2 nanoparticle and BNNS-PCBT resulted in a new nanohybrid material that was readily precipitated by the centrifugation.

The precipitates obtained from the centrifugation were powder-like. FTIR spectroscopy has been shown to be a powerful tool for extracting structural information of the molecules adsorbed onto a TiO_2 surface.[247] The IR spectra of the precipitated BNNS-PCBT-TiO_2 showed the presence of the carboxylate asymmetric ν(-COO_{as}) and symmetric ν(-COO_s) bands. These occur at 1632 and 1382 cm^{-1}, respectively, as shown in Figure 109. This supports the binding of the polythiophene to the TiO_2 rather than simple aggregation of the polythiophene on the TiO_2 surface.

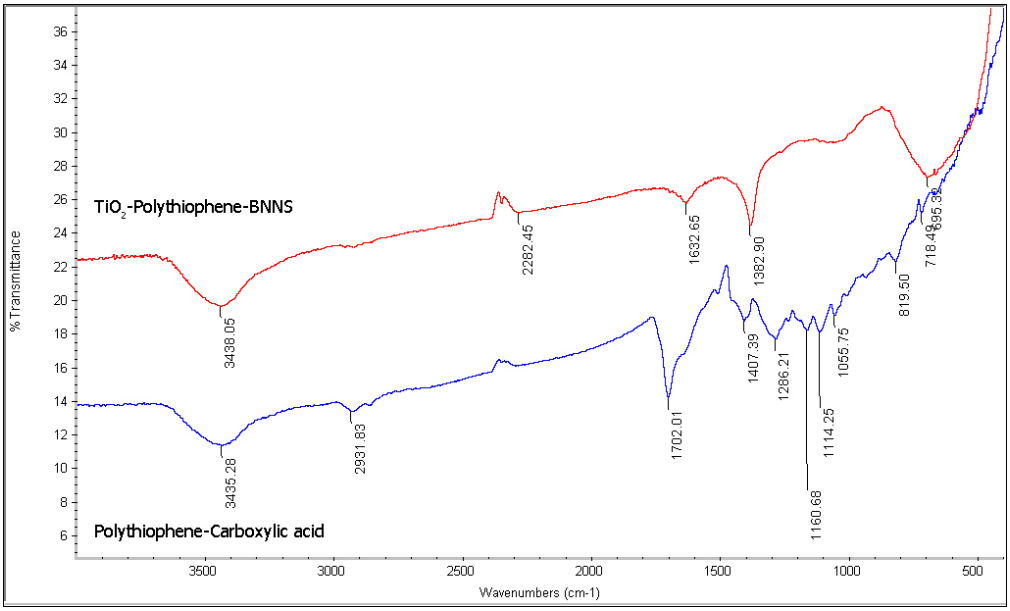

Figure 109: FT-IR spectra comparison of the BNNS-PCBT-TiO_2 and the BNNS-PCBT.

Possible binding modes for polythiophene containing carboxylic acid groups on a TiO_2 surface are shown in Figure 110.[245,246] The unidentate coordination in Figure 110 removes the equivalence of the two oxygen atoms, resulting in an ester type of bond

formation between the TiO_2 surface and the carboxylic acid group. According to the FTIR measurements, this type of coordination can be ruled out, leaving two remaining possibilities of the binding: chelation or bridging bidentate. Similar observations were reported for the binding between TiO_2 surface and porphyrins with carboxylic acid anchor groups and the authors concluded the bridging bidentate mode was responsable for the binding in their paper.[248] Their FTIR spectral data of two strong bands at 1616 and 1372 cm^{-1} is very close to our observed data of two strong bands at 1632 and 1382 cm^{-1}. Therefore, the bridging bidentate mode is most likely responsible for the strong binding in our hybrid nanosystem.

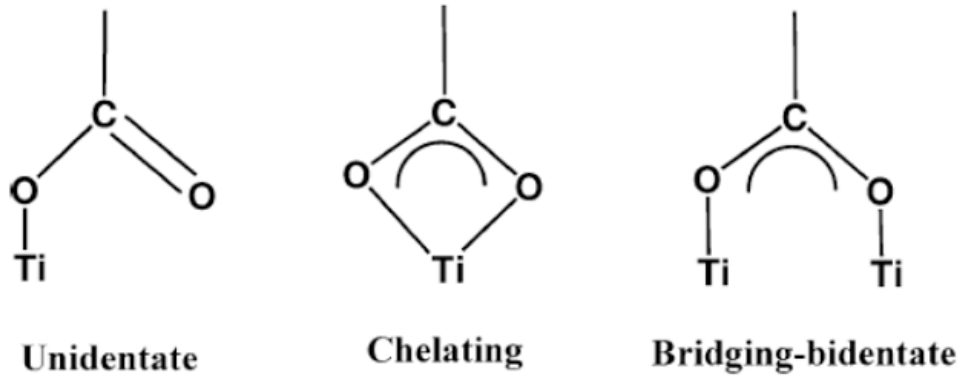

Figure 110: Possible binding modes between carboxylic group and TiO_2 surface.

These results indicate that the BNNSs conjugates of polythiophene with the carboxyl groups coordinate to the TiO_2 nanoparticle under the employed sonication conditions. Thus, boron nanosheets functionalized with polythiophene were combined with TiO_2 nanoparticles to form a new BNNS-polythiophene-TiO_2 material. These resultant nanohybrid materials can be easily precipitated by the centrifugation.

BNNS-poly(3-thiophene acetic acid) (P3TAA)-TiO_2 (m=1)

The polythiophene poly(3-thiophene acetic acid) (P3TAA) with a shorter carboxylic acid side chain was synthesized and characterized according to a reported procedure.[237]

Non-covalent functionalization of BNNSs by the P3TAA was once again confirmed by the UV-Vis spectra. The UV-Vis spectra monitoring of the BNNS-P3TAA is shown

in Figure 111. Surprisingly, however, the resulting BNNSs conjugation shows a red shift of about 40 nm. This can be explained by the steric effects of the different substitution patterns.[249] Upon interaction with the BNNSs surface through the $\pi - \pi$ stacking interaction, the coplanarity of the thiophene backbone would be altered to a differing extent from the various 3-substituents. This is responsible for the observed bandgap and thus the change in the UV-Vis absorption direction.

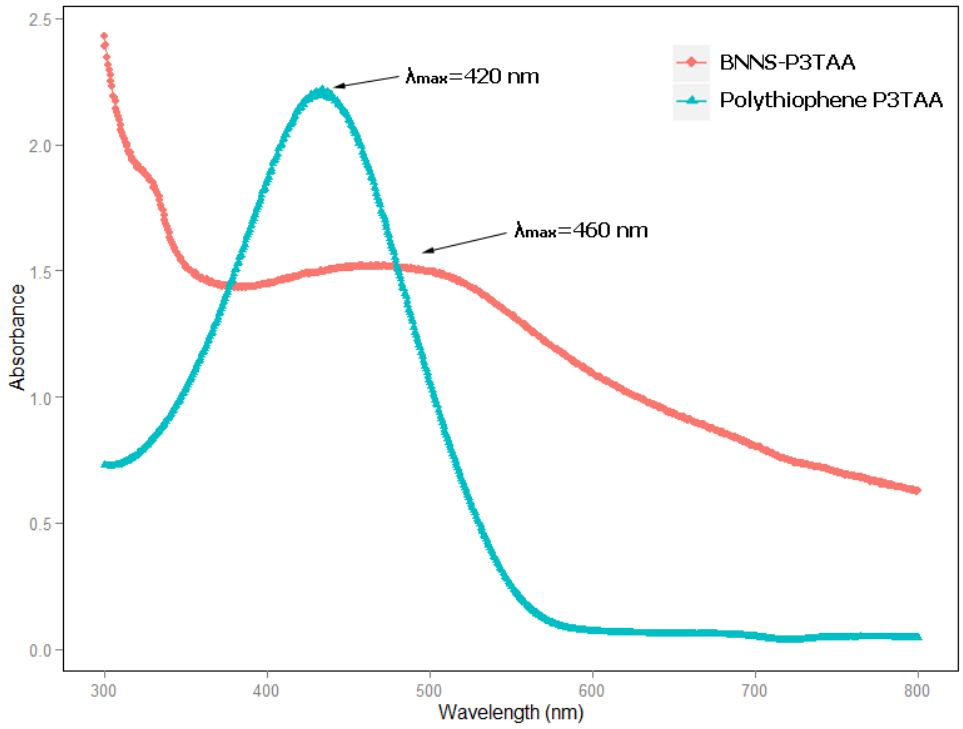

Figure 111: BNNS-P3TAA UV-Vis spectrum compared with the polymer P3TAA in IPA/water (420 peak for Red, while 460 peak for Blue).

The UV-Vis spectra of the supernatant from the sample and control sample are compared in the Figure 112. Similar to the previously showed result for polythiophene with a longer carboxylic acid side chain, these spectra similarly show that, after adding the TiO_2 nanoparticle, the absorption was greatly reduced in solution after the same centrifugation process and the hybrid nanomaterial was obtained as the precipitate after centrifugation.

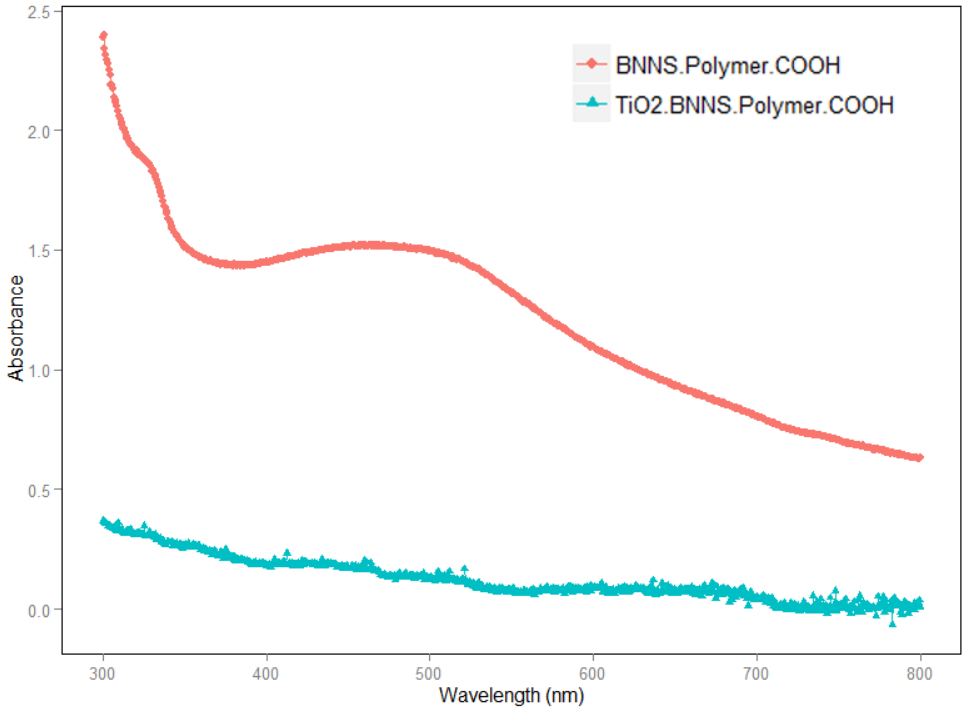

Figure 112: BNNS-P3TAA-TiO_2 UV-Vis spectrum compared with the polymer P3TAA in IPA/water.

In short summary, from these studies of the interaction between BNNSs and the conjugated polythiophene or PVP, the BNNS-polymer conjugates can form stable dispertions in aqueous (DMSO/water) or organic solvent (chloroform). Both blue and red shifts in their absorption spectrum were observed by employing polythiophenes of different length with carboxyl groups. This further show that the noncovalent functionalization of BNNSs with polythiophenes can not only stabilize the BNNSs dispersions in common solvents but also provide an effective approach to tune the band gap of the resulting composite materials by choosing appropriate side chains for the polythiophenes (Table 23). The latter has significant importance as bandgap tuning has attracted research interest for its application in organic electronic devices and molecular electronics.[233,249] We further showed that the BNNS-polythiophene conjugates can act as a platform for other functional moieties by our successful praparation of the BNNS-polythiophenes-TiO_2 hybrid nanomaterials which combine

the BNNS-polythiophene conjugates with another nanomaterial, the TiO_2 nanoparticle. This suggests a potential application for the BNNS-polythiophene in TiO_2 based systems such as the dye sensitized solar cells (DSSCs).

Table 23: Effect of BNNSs conjugation to the absorption of polythiophenes

polythiophenes[a]	number of carbon atoms[b]	effect(Blue or red shift)	Numbers (nm)
H3PT	5	blue	47
PCBT	4	blue	120
P3TAA	1	red	40
PTPA	0	none	0

[a] The structures are shown in Figure 98.
[b] number of carbon atoms for the side chain between thiophene ring and the end carbon atom.

4.3.4 DSSCs using BNNS-polythiophene as Photo Sensitizer

Photovoltaic devices were fabricated to explore the potential application of BNNS-polythiophenes as photo sensitizers in DSSCs. Figure 95 shows a typical fabricated DSSCs. The photovoltaic performance of these cells were measured using simulated sunlight.

The dark current and the photocurrent-voltage curves obtained for the cells sensitized with BNNS-P3TAA are shown in Figure 113. This comparison indicates that the BNNS-P3TAA can effectively act as the photo-sensitizer in the cell.

Figure 114 and Figure 115 show the comparison photovoltaic characteristic for the BNNS-PTPA-sensitized solar cell and BNNS-P3TAA, respectively. The BNNS-P3TAA device exhibits an open-circuit voltage (V_{oc}) of 0.59 V, a short-circuit current density (J_{sc}) of 0.48 mA/cm^2, a fill factor (FF) of 36.6% and a power conversion efficiency (PCE) of 0.10%. In contrast, maintaining the conditions the same, the polythiophene P3TAA device exhibits an open-circuit voltage (V_{oc}) of 0.50 V, a short-circuit current density (J_{sc}) of 0.16 mA/cm^2, a fill factor (FF) of 33.4% and a

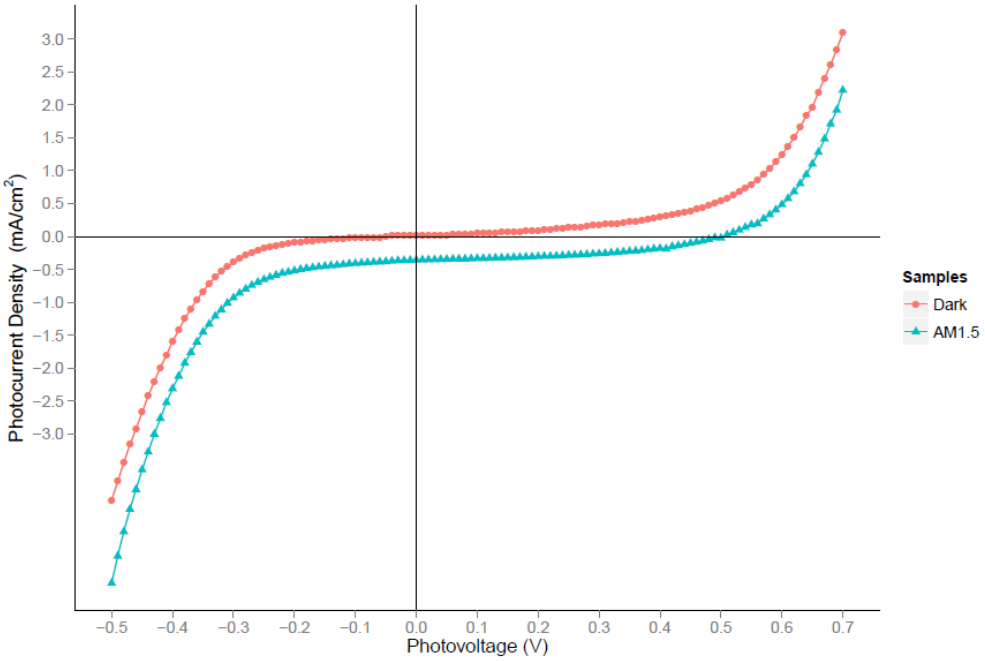

Figure 113: Dark current and photocurrentvoltage (IV) curve comparison for BNNS-P3TAA dyes.

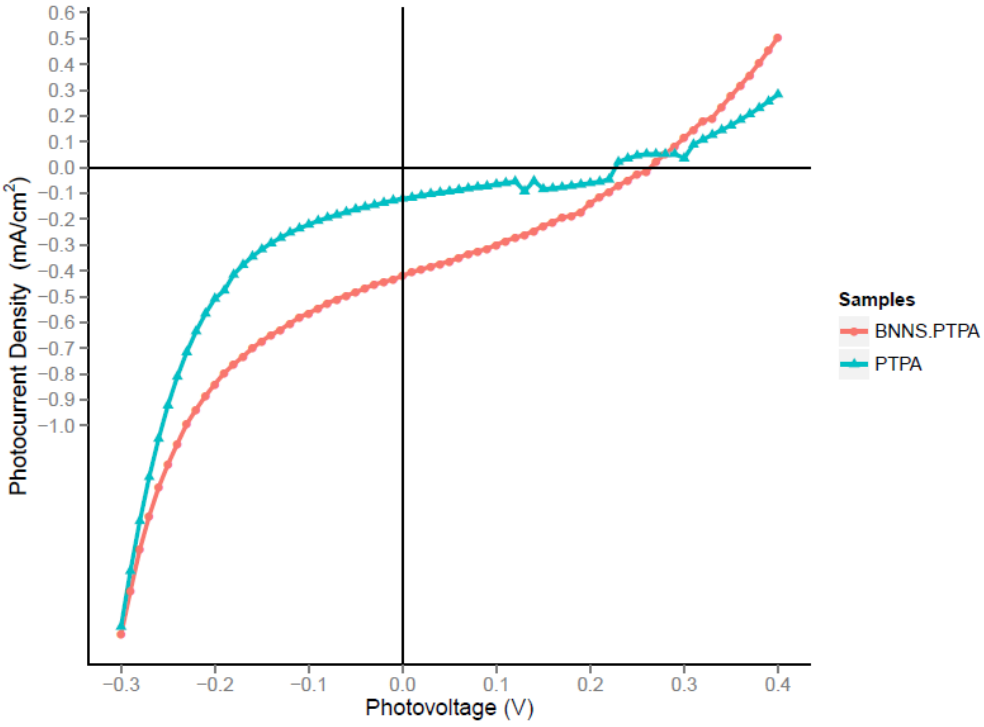

Figure 114: IV curve comparison for DSSCs using BNNS-PTPA and PTPA dyes.

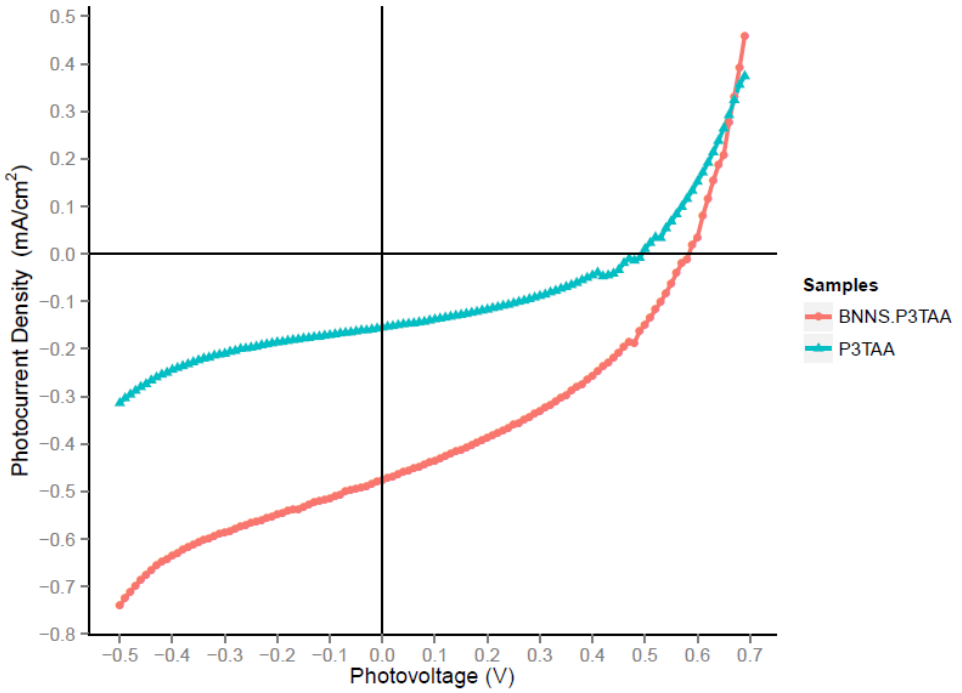

Figure 115: IV curve comparison for DSSCs using BNNS-P3TAA and P3TAA dyes.

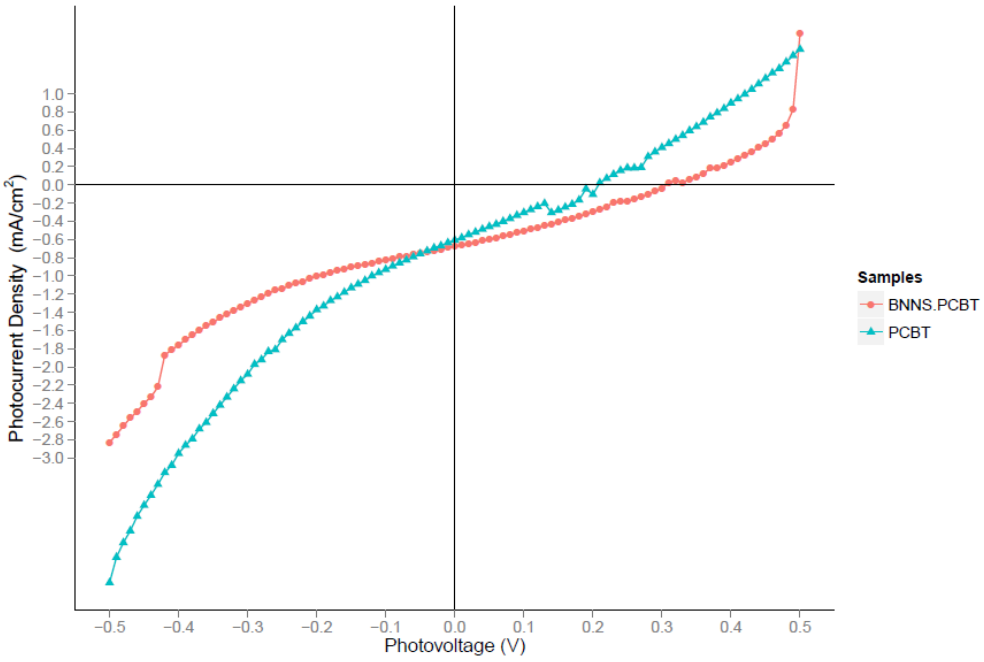

Figure 116: IV curve comparison for DSSCs using BNNS-PCBT and PCBT dyes.

Table 24: Performances of DSSCs using polymer and polymer-BNNS as sensitizers obtained under 100 mW/cm^2 AM 1.5G illumination

	V_{oc} [V]	J_{sc} [mA/cm^2]	FF [%]	η[%]
BNNS-P3TAA	0.59	0.48	36.6	0.100
P3TAA	0.50	0.16	33.4	0.026
BNNS-PTPA	0.27	0.42	30.9	0.035
PTPA	0.23	0.12	47.1	0.013
BNNS-PCBT	0.31	0.68	29.8	0.063
PCBT	0.21	0.61	23.7	0.030

PCE of 0.026%. Compared to the P3TAA based device, a 3.8-fold increased energy conversion efficiency for BNNS-P3TAA based device was observed. The improved efficiency is mainly attributed to the 3-fold increase in J_{sc}. Similar improvements are also observed for BNNS-PTPA over PTPA and BNNS-PCBT over PCBT. For BNNS-PTPA, a 2.7-fold and a 3.5-fold improvement are obtained for energy conversion efficiency and J_{sc}, respectively. For BNNS-PCBT, a 2-fold improvement was obtained for energy conversion efficiency (Table 24).

The best energy conversion efficiency obtained is 0.1%. This is not, however, competitive compared with other reported DSSCs systems. For example, Senadeera and coworkers reported a 2.4% energy conversion for a cell system fabricated by poly 3-thiophenylacetic acid-polymer and either mesoporous TiO_2 or SnO_2-ZnO electrodes and the electrolyte consisting with redox complex (I_3^-/I^-).[250]

There are many device-limiting material properties, such as exciton diffusion length and charge carrier mobility, that are critical to the solar cell performance. The energy transfer and transport characteristics of conjugated polymers depend greatly on their physical conformation.[251] It has been reported that the morphology and aggregation of oligothiophene particles affect not only their optical properties but also their electronic properties.[252] Despite of the low energy conversion efficiency, the

performance comparison between BNNS-polythiophene and polythiophene indicates a potential role for BNNSs in DSSCs systems. The BNNSs has a large flat surface for the π-π conjugation interaction with polythiophenes. This increases the chain planarity of the polythiophenes. Highly planar chains thus extend the effective conjugation length of the polymer and improve absorption, exciton and charge transport by further delocalizing electrons and excited states while reducing the population of carrier trapping sites.[252] Therefore, the improved efficiency in the BNNS-P3TAA can be attributed to the BNNSs' ability to regulate of the morphologies of polythiophene.

Moreover, it also should be noted that practical implementation of polymer based solar cells will require long device lifetimes (5 years by one estimate) in order to be cost-effective.[253] It has been pointed out that combating morphological instability and polymer degradation are key factors for enhancing device lifetime.[251] The BNNSs can possibly contribute to this target due to its inert chemical and mechanical properties.

4.4 Conclusions

In this chapter, BNNSs were prepared by the solvent exfoliation method. An effective and simple noncovalent functionalization and solubilization of BNNSs has been achieved by using polythiophene through strong $\pi - \pi$ stacking interactions between conjugated polythiophene and BNNSs. The BNNS-polythiophene conjugation was characterized by UV-Vis, fluorescence spectroscopy and TEM. In addition, polymer PVP was employed to form stable BNNS-PVP dispersions which were characterized by TEM. To our knowledge, this is the first time that the polymers polythiophene and PVP are used for the functionalization of the BNNSs. It also should be noted that, through our studies of the $\pi - \pi$ interactions between the BNNSs and the polythiophene containing different side chains, we observed that bandgaps of the polythiophenes were tuned according to the side chains. The BNNSs can thus be useful as a bandgap tuning tool for polythiophene derivatives.

By employing the polythiophene containing carboxylic acid groups as the anchor groups for attachment of the TiO_2 surface, the BNNS-polythiophene conjugates can be used for binding TiO_2 nanoparticles. The covalent binding between the TiO_2 surface and the BNNS-polythiophene containing carboxylic acid group was explored by the IR spectroscopy. This novel BNNS-polythiophne-TiO_2 hybrid nano-material was investigated for its applications in DSSCs. Based upon this, DSSCs using BNNS-polythiophenes were fabricated and the performance measurements indicated that the BNNSs can enhance the performance of the DSSCs. The possible reasons include the ability of the planer BNNSs surface to regulate the conformation of the polythiophenes. These results indicate that functionalized BNNSs are suitable for applications such as electronics.

Appendix A

Crystal Data

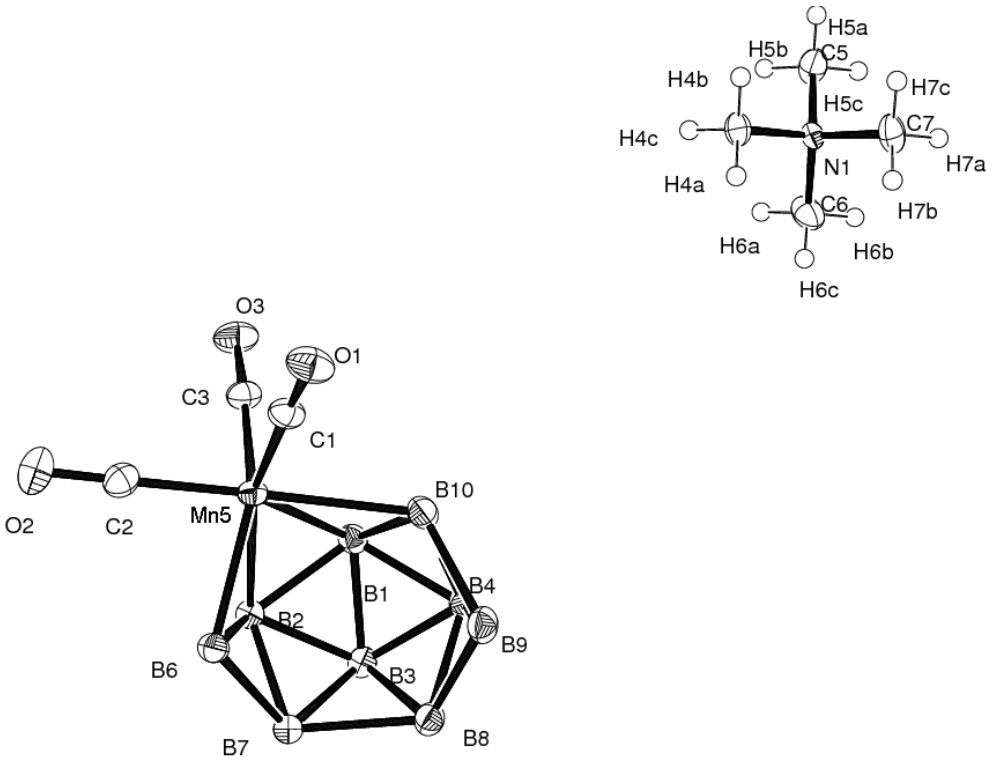

Figure A.1: Crystal data and structure refinement of [*nido*-5-$Mn(CO)_3B_9H_{13}$][NMe_4] (**1.2**).

Table A.1: Atomic coordinates (x10^4) and equivalent isotropic displacement parameters (Å^{2}x10^3) for [*nido*-5-$Mn(CO)_3B_9H_{13}$][NMe_4] (**1.2**)

	x	y	z	U(eq)
Mn(5)	3756(1)	10298(1)	1701(1)	15(1)
O(1)	1100(2)	9192(1)	714(1)	29(1)
O(2)	2527(2)	11789(1)	499(1)	36(1)
O(3)	1889(2)	10940(1)	3218(1)	30(1)
N(1)	1757(2)	6843(1)	9777(1)	17(1)
C(1)	2093(2)	9632(1)	1119(1)	21(1)
C(2)	3016(3)	11213(1)	969(2)	23(1)
C(3)	2600(2)	10672(1)	2630(1)	21(1)
C(4)	1189(3)	7442(1)	8961(1)	24(1)
C(5)	644(3)	6944(2)	10533(2)	29(1)
C(6)	3496(3)	7059(2)	10188(2)	35(1)
C(7)	1693(3)	5933(1)	9428(2)	29(1)
B(1)	5448(3)	9924(2)	3014(2)	18(1)
B(2)	6306(2)	10758(1)	2338(1)	16(1)
B(3)	7625(3)	9946(2)	2935(2)	18(1)
B(4)	6688(3)	8940(2)	3082(2)	21(1)
B(6)	5995(3)	10592(2)	1096(2)	18(1)
B(7)	7947(3)	10274(1)	1785(2)	19(1)
B(8)	8108(3)	9075(2)	2231(2)	21(1)
B(9)	6300(3)	8391(2)	2012(2)	23(1)
B(10)	4626(3)	8988(2)	2425(2)	21(1)

Table A.2: Anisotropic displacement parameters ($Å^2x10^3$) for [*nido*-5-$Mn(CO)_3B_9H_{13}$][NMe_4] (**1.2**). The anisotropic displacement factor exponent takes the form: $-2p^2[h^2a*2U^{11}+...+2hka*b*U^{12}]$

	U^{11}	U^{22}	U^{33}	U^{23}	U^{13}	U^{12}
Mn(5)	14(1)	17(1)	16(1)	-2(1)	3(1)	-1(1)
O(1)	26(1)	32(1)	29(1)	-10(1)	7(1)	-9(1)
O(2)	38(1)	28(1)	39(1)	6(1)	1(1)	9(1)
O(3)	25(1)	37(1)	30(1)	-10(1)	11(1)	1(1)
N(1)	20(1)	14(1)	18(1)	1(1)	2(1)	-2(1)
C(1)	20(1)	22(1)	21(1)	-3(1)	7(1)	-1(1)
C(2)	22(1)	22(1)	25(1)	-3(1)	2(1)	1(1)
C(3)	17(1)	22(1)	24(1)	-4(1)	4(1)	-1(1)
C(4)	30(1)	21(1)	19(1)	5(1)	2(1)	0(1)
C(5)	40(1)	26(1)	24(1)	5(1)	13(1)	9(1)
C(6)	27(1)	36(1)	38(1)	11(1)	-8(1)	-10(1)
C(7)	44(1)	17(1)	27(1)	-2(1)	8(1)	-2(1)
B(1)	20(1)	19(1)	16(1)	0(1)	5(1)	0(1)
B(2)	17(1)	16(1)	15(1)	-1(1)	1(1)	0(1)
B(3)	20(1)	18(1)	18(1)	0(1)	1(1)	2(1)
B(4)	26(1)	18(1)	20(1)	4(1)	5(1)	1(1)
B(6)	17(1)	19(1)	19(1)	0(1)	4(1)	-1(1)
B(7)	17(1)	18(1)	21(1)	2(1)	4(1)	1(1)
B(8)	24(1)	20(1)	20(1)	1(1)	5(1)	4(1)
B(9)	27(1)	16(1)	26(1)	0(1)	5(1)	1(1)
B(10)	24(1)	18(1)	22(1)	1(1)	7(1)	-2(1)

Table A.3: Hydrogen coordinates ($x10^4$) and isotropic displacement parameters ($Å^2x10^3$) for [*nido*-5-$Mn(CO)_3B_9H_{13}$][NMe_4] (**1.2**)

	x	y	z	U(eq)
H(4C)	1224	8024	9192	36
H(4B)	71	7299	8692	36
H(4A)	1907	7385	8477	36
H(5C)	1010	6568	11062	44
H(5A)	-476	6800	10269	44
H(5B)	683	7529	10754	44
H(6B)	3879	6659	10691	52
H(6A)	3531	7632	10446	52
H(6C)	4199	7026	9694	52
H(7B)	2400	5871	8939	43
H(7C)	571	5790	9167	43
H(7A)	2065	5555	9953	43

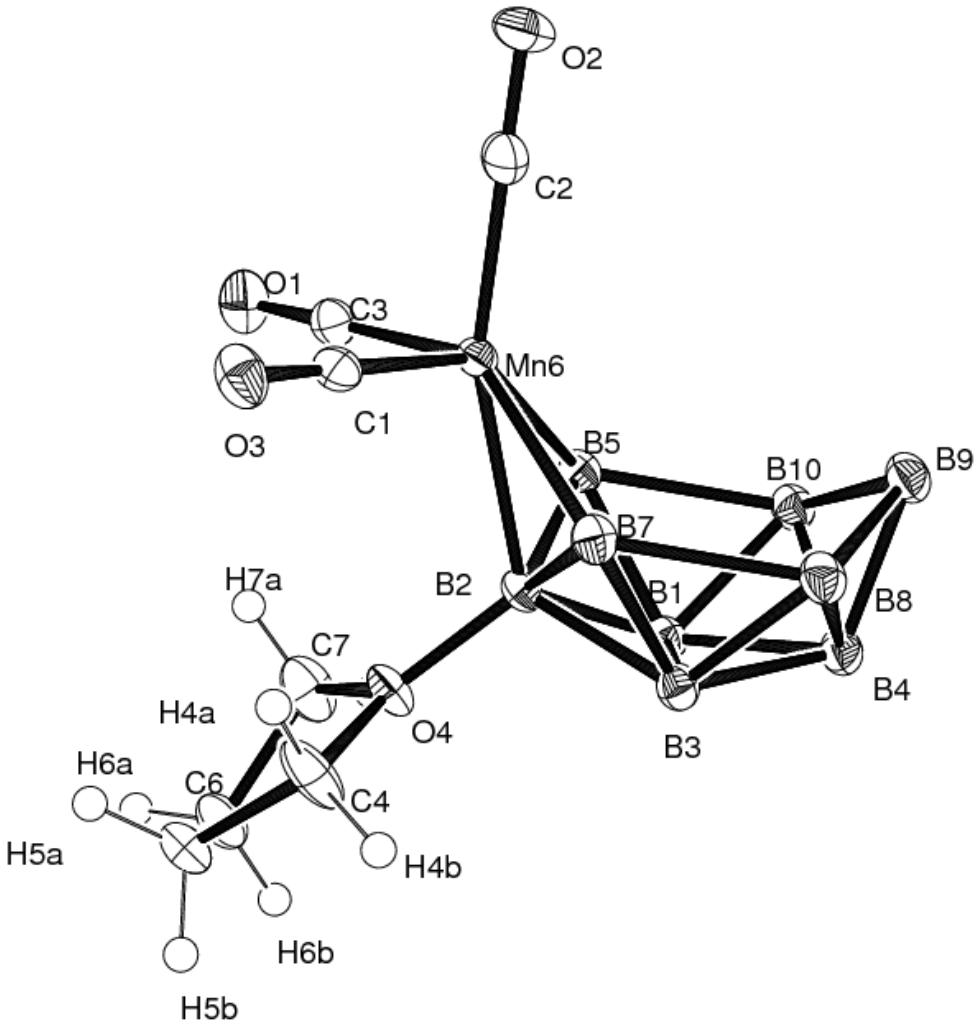

Figure A.2: Crystal data and structure refinement of [2-$(CH_2)_4$O-*nido*-6-$Mn(CO)_3B_9H_{12}$] (**1.6**).

Table A.4: Atomic coordinates (x10^4) and equivalent isotropic displacement parameters (Å^{2}x10^3) for [2-$(CH_2)_4$O-*nido*-6-$Mn(CO)_3B_9H_{12}$] (**1.6**).

	x	y	z	U(eq)
Mn(6)	2715(1)	2687(1)	3947(1)	14(1)
O(1)	4636(3)	5396(2)	3767(2)	28(1)
O(2)	4551(4)	1059(3)	5807(2)	35(1)
O(3)	-617(3)	3416(2)	5666(2)	25(1)
O(4)	775(3)	4767(2)	2037(2)	19(1)
B(1)	2935(5)	2768(3)	1083(3)	16(1)
B(2)	1678(4)	3286(3)	2348(3)	15(1)
B(3)	625(5)	1978(3)	1916(3)	17(1)
B(4)	2371(5)	971(3)	1118(3)	19(1)
B(5)	4231(4)	3070(3)	2047(3)	16(1)
B(7)	423(5)	1756(3)	3421(3)	17(1)
B(8)	975(5)	177(3)	2582(3)	20(1)
B(9)	3460(5)	-250(4)	2069(3)	21(1)
B(10)	4668(5)	1435(4)	1263(3)	19(1)
C(1)	667(4)	3121(3)	5001(2)	18(1)
C(2)	3835(5)	1694(3)	5089(3)	23(1)
C(3)	3911(4)	4340(3)	3827(3)	20(1)
C(4)	-1264(4)	5034(3)	2486(4)	32(1)
C(5)	-1487(4)	6641(3)	2018(3)	21(1)
C(6)	419(4)	7169(3)	1117(3)	24(1)
C(7)	1895(5)	6127(3)	1489(3)	30(1)

Table A.5: Anisotropic displacement parameters ($Å^2x10^3$) for [2-$(CH_2)_4$O-*nido*-6-$Mn(CO)_3B_9H_{12}$] (**1.6**). The anisotropic displacement factor exponent takes the form: $-2p^2[h^2a*2U^{11}+...+2hka*b*U^{12}]$

	U^{11}	U^{22}	U^{33}	U^{23}	U^{13}	U^{12}
Mn(6)	15(1)	14(1)	14(1)	-3(1)	-4(1)	2(1)
O(1)	20(1)	26(1)	36(1)	-13(1)	-2(1)	-3(1)
O(2)	45(2)	36(1)	28(1)	-9(1)	-21(1)	19(1)
O(3)	26(1)	22(1)	20(1)	-4(1)	2(1)	5(1)
O(4)	12(1)	12(1)	26(1)	-1(1)	-1(1)	1(1)
B(1)	17(2)	15(1)	15(1)	-3(1)	-3(1)	1(1)
B(2)	15(1)	11(1)	15(1)	-1(1)	-3(1)	1(1)
B(3)	18(2)	14(1)	18(1)	-4(1)	-4(1)	-1(1)
B(4)	23(2)	15(1)	18(2)	-4(1)	-5(1)	2(1)
B(5)	15(1)	16(1)	17(1)	-3(1)	-3(1)	2(1)
B(7)	18(2)	14(1)	17(1)	-2(1)	-2(1)	-2(1)
B(8)	23(2)	14(1)	20(2)	-2(1)	-4(1)	0(1)
B(9)	26(2)	15(2)	20(2)	-4(1)	-6(1)	3(1)
B(10)	19(2)	18(2)	18(2)	-5(1)	-3(1)	3(1)
C(1)	23(2)	14(1)	16(1)	0(1)	-7(1)	1(1)
C(2)	27(2)	23(1)	22(1)	-9(1)	-6(1)	7(1)
C(3)	15(1)	24(2)	20(1)	-8(1)	-3(1)	4(1)
C(4)	12(1)	20(2)	54(2)	-2(2)	-2(1)	3(1)
C(5)	18(1)	18(1)	24(1)	-2(1)	-4(1)	5(1)
C(6)	22(2)	16(1)	26(2)	1(1)	-2(1)	2(1)
C(7)	26(2)	17(2)	37(2)	0(1)	0(1)	-2(1)

Table A.6: Hydrogen coordinates (x10^4) and isotropic displacement parameters (Å^{2}x10^3) for [2-$(CH_2)_4$O-*nido*-6-$Mn(CO)_3B_9H_{12}$] (**1.6**).

	x	y	z	U(eq)
H(4A)	-1623	4747	3336	38
H(4B)	-2072	4503	2210	38
H(5A)	-1712	7110	2644	26
H(5B)	-2563	6842	1654	26
H(6B)	334	7181	339	29
H(6A)	744	8136	1110	29
H(7B)	2935	6050	822	36
H(7A)	2438	6404	2046	36

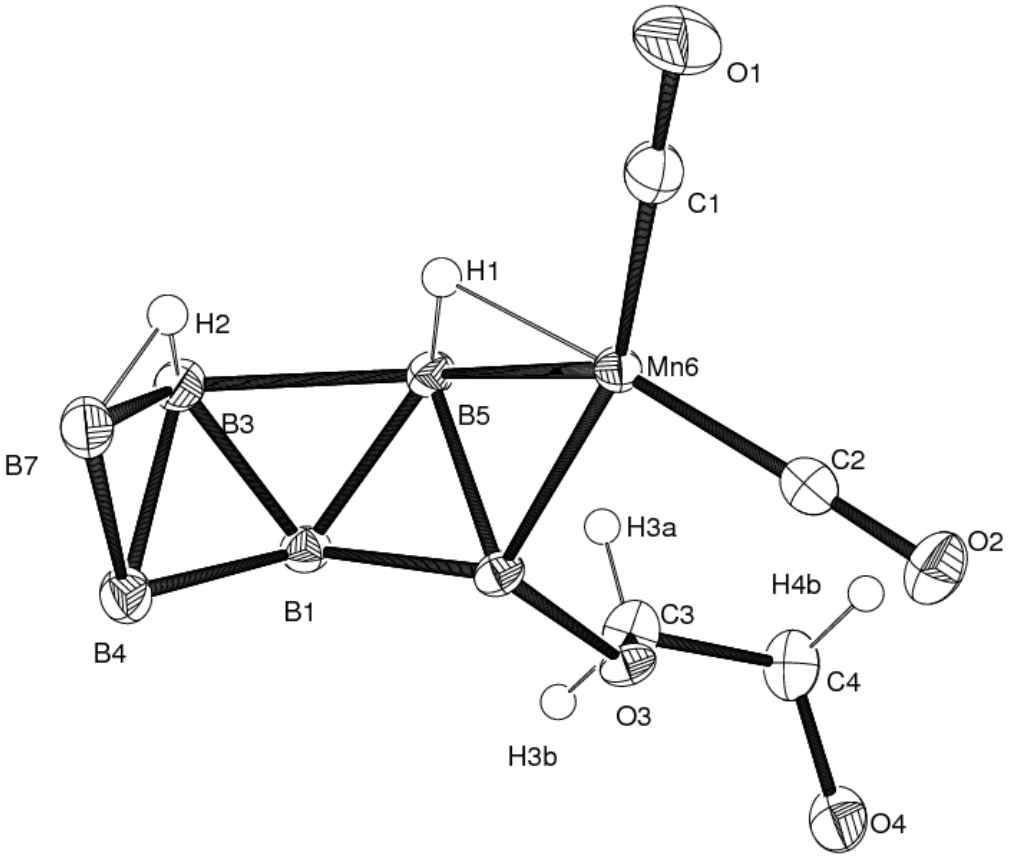

Figure A.3: Crystal data and structure refinement of [2-O(CH_2CH_2)$_2$O-*nido*-6-Mn(CO)$_3$B$_9$H$_{12}$] (**1.7**) (Asymmetric unit only).

Table A.7: Atomic coordinates (x10^4) and equivalent isotropic displacement parameters (Å^{2}x10^3) for [2-O(CH_2CH_2)$_2$O-*nido*-6-Mn(CO)$_3$B$_9$H$_{12}$] (**1.7**).

	x	y	z	U(eq)
Mn(6)	10047(1)	2500	731(1)	14(1)
O(1)	8885(4)	2500	-2799(4)	36(1)
O(2)	12656(3)	4379(2)	1415(3)	26(1)
O(3)	11893(3)	2500	4497(3)	16(1)
O(4)	15198(4)	2500	7121(3)	30(1)
C(1)	9334(5)	2500	-1443(5)	22(1)
C(2)	11621(3)	3655(3)	1109(3)	18(1)
C(3)	12601(4)	1393(3)	5474(4)	24(1)
C(4)	14514(4)	1445(3)	6159(4)	28(1)
B(1)	8528(4)	1686(3)	3391(4)	17(1)
B(2)	10053(5)	2500	3065(5)	15(1)
B(3)	6723(4)	1204(3)	1646(4)	20(1)
B(4)	6571(6)	2500	2730(6)	20(1)
B(5)	9135(4)	1160(3)	1934(4)	16(1)
B(7)	5450(6)	2500	645(6)	21(1)

Table A.8: Anisotropic displacement parameters ($Å^2x10^3$) for [2-O(CH_2CH_2)$_2$O-*nido*-6-Mn(CO)$_3$B$_9$H$_{12}$] (**1.7**). The anisotropic displacement factor exponent takes the form: $-2p^2[h^2a*2U^{11}+...+2hka*b*U^{12}]$

	U^{11}	U^{22}	U^{33}	U^{23}	U^{13}	U^{12}
Mn(6)	14(1)	14(1)	12(1)	0	6(1)	0
O(1)	42(2)	50(2)	16(2)	0	14(1)	0
O(2)	23(1)	22(1)	32(1)	1(1)	12(1)	-5(1)
O(3)	17(1)	12(1)	12(1)	0	2(1)	0
O(4)	19(2)	50(2)	16(1)	0	3(1)	0
C(1)	19(2)	23(2)	22(2)	0	10(2)	0
C(2)	18(1)	19(1)	15(1)	3(1)	8(1)	5(1)
C(3)	22(2)	22(2)	24(2)	12(1)	6(1)	4(1)
C(4)	20(2)	32(2)	26(2)	11(1)	7(1)	6(1)
B(1)	19(2)	17(2)	15(1)	-1(1)	8(1)	-2(1)
B(2)	14(2)	15(2)	12(2)	0	3(2)	0
B(3)	19(2)	26(2)	16(1)	-1(1)	8(1)	-4(1)
B(4)	18(2)	26(2)	18(2)	0	9(2)	0
B(5)	17(1)	15(1)	17(1)	-2(1)	8(1)	-3(1)
B(7)	17(2)	28(3)	20(2)	0	9(2)	0

Table A.9: Hydrogen coordinates ($x10^4$) and isotropic displacement parameters ($Å^2 x10^3$) for [2-O(CH_2CH_2)$_2$O-*nido*-6-Mn(CO)$_3$B$_9$H$_{12}$] (**1.7**).

	x	y	z	U(eq)
H(3A)	12141	659	4790	29
H(3B)	12293	1358	6362	29
H(4A)	15029	711	6826	33
H(4B)	14805	1448	5259	33
H(1)	8570(40)	1440(30)	490(40)	25
H(2)	6070(40)	1660(30)	320(40)	25

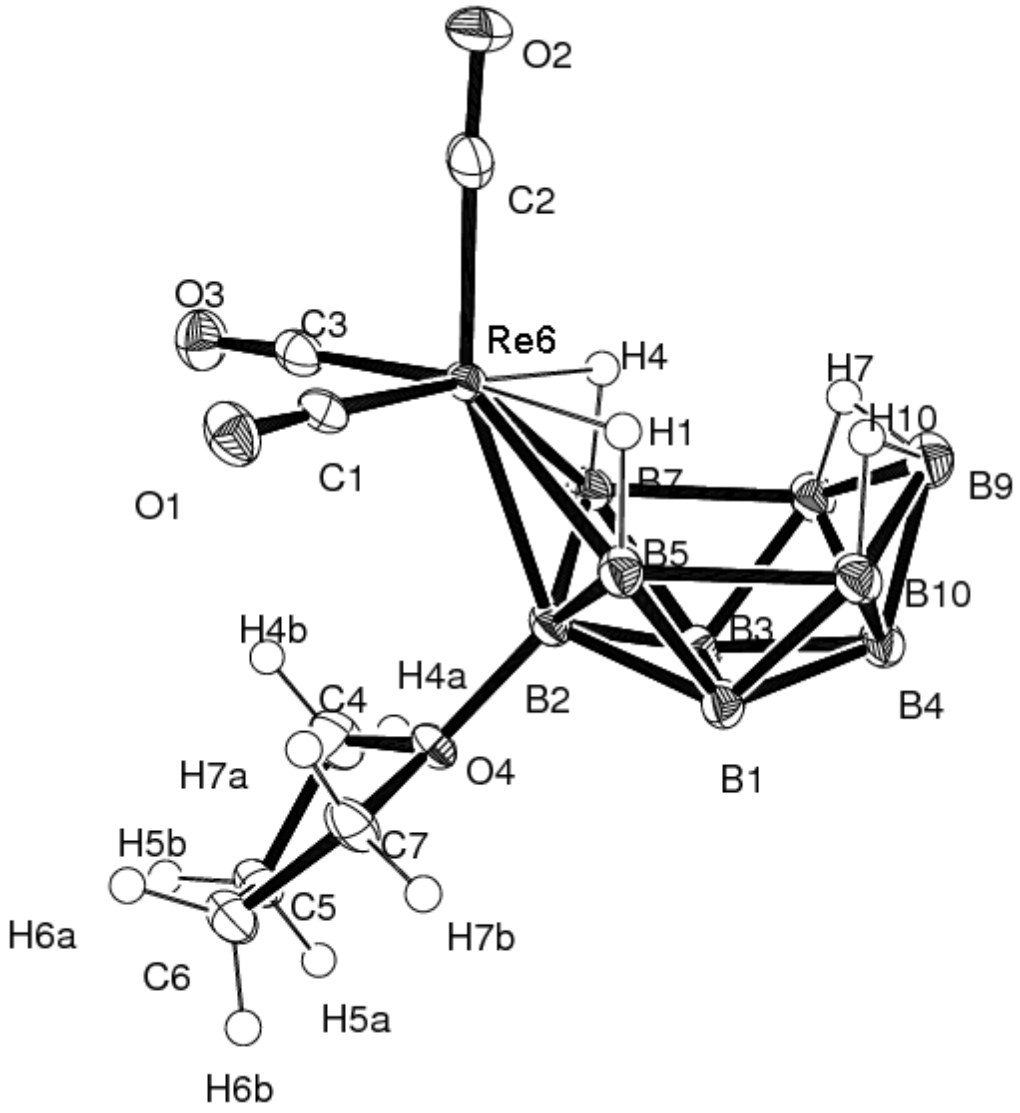

Figure A.4: Crystal data and structure refinement of [2-$(CH_2)_4$O-*nido*-6-$Re(CO)_3B_9H_{12}$] (**1.8**).

Table A.10: Atomic coordinates (x10^4) and equivalent isotropic displacement parameters (Å^{2}x10^3) for [2-$(CH_2)_4$O-*nido*-6-$Re(CO)_3B_9H_{12}$] (**1.8**).

	x	y	z	U(eq)
Re(6)	2751(1)	2708(1)	3948(1)	15(1)
O(1)	-710(5)	3397(3)	5734(3)	25(1)
O(2)	4720(6)	1012(4)	5834(3)	34(1)
O(3)	4796(5)	5509(4)	3780(3)	27(1)
O(4)	756(4)	4740(3)	1895(2)	17(1)
B(1)	584(7)	1962(5)	1858(4)	18(1)
B(2)	1667(7)	3277(5)	2265(4)	16(1)
B(3)	2936(7)	2732(5)	1057(4)	16(1)
B(4)	2338(8)	945(5)	1104(4)	19(1)
B(5)	344(7)	1765(5)	3334(4)	18(1)
B(7)	4269(7)	3075(5)	1974(4)	18(1)
B(8)	4666(8)	1404(5)	1252(4)	20(1)
B(9)	3419(8)	-269(6)	2049(4)	22(1)
B(10)	910(8)	163(5)	2532(4)	20(1)
C(1)	600(7)	3125(4)	5078(4)	19(1)
C(2)	3984(7)	1669(5)	5148(4)	24(1)
C(3)	4061(6)	4448(5)	3846(4)	20(1)
C(4)	1929(7)	6092(5)	1455(4)	26(1)
C(5)	462(7)	7170(5)	1110(4)	22(1)
C(6)	-1443(7)	6644(5)	1994(4)	23(1)
C(7)	-1210(6)	5043(5)	2483(4)	23(1)

Table A.11: Anisotropic displacement parameters ($Å^2x10^3$) for [2-$(CH_2)_4$O-*nido*-6-$Re(CO)_3B_9H_{12}$] (**1.8**). The anisotropic displacement factor exponent takes the form: $-2p^2[h^2a * 2U^{11} + ... + 2hka * b * U^{12}]$

	U^{11}	U^{22}	U^{33}	U^{23}	U^{13}	U^{12}
Re(6)	18(1)	14(1)	13(1)	-3(1)	-5(1)	4(1)
O(1)	28(2)	22(2)	21(2)	-5(1)	0(1)	5(1)
O(2)	46(2)	34(2)	26(2)	-7(2)	-21(2)	16(2)
O(3)	24(2)	25(2)	31(2)	-11(1)	-4(1)	-1(1)
O(4)	18(2)	12(1)	18(2)	-1(1)	-4(1)	2(1)
B(1)	22(2)	14(2)	18(2)	-4(2)	-5(2)	0(2)
B(2)	19(2)	13(2)	14(2)	-3(2)	-3(2)	3(2)
B(3)	18(2)	13(2)	16(2)	-2(2)	-4(2)	2(2)
B(4)	25(3)	15(2)	16(2)	-3(2)	-5(2)	2(2)
B(5)	22(2)	15(2)	18(2)	-4(2)	-4(2)	1(2)
B(7)	17(2)	20(2)	15(2)	-6(2)	-3(2)	5(2)
B(8)	24(3)	19(2)	17(2)	-6(2)	-4(2)	4(2)
B(9)	29(3)	19(3)	18(3)	-5(2)	-4(2)	1(2)
B(10)	26(3)	16(2)	18(2)	-4(2)	-6(2)	3(2)
C(1)	25(2)	12(2)	18(2)	0(2)	-9(2)	4(2)
C(2)	29(2)	21(2)	23(2)	-10(2)	-6(2)	7(2)
C(3)	20(2)	22(2)	16(2)	-5(2)	-3(2)	7(2)
C(4)	26(2)	16(2)	32(3)	-1(2)	-4(2)	-2(2)
C(5)	25(2)	16(2)	24(2)	-2(2)	-8(2)	4(2)
C(6)	26(2)	20(2)	23(2)	-5(2)	-5(2)	7(2)
C(7)	14(2)	22(2)	32(3)	-8(2)	-3(2)	5(2)

Table A.12: Hydrogen coordinates (x10^4) and isotropic displacement parameters (Å^{2}x10^3) for [2-$(CH_2)_4$O-*nido*-6-$Re(CO)_3B_9H_{12}$] (**1.8**).

	x	y	z	U(eq)
H(4A)	3019	6064	793	31
H(4B)	2454	6294	2056	31
H(5A)	339	7217	333	27
H(5B)	835	8137	1117	27
H(6A)	-1668	7138	2603	28
H(6B)	-2557	6825	1632	28
H(7A)	-1348	4796	3319	28
H(7B)	-2198	4485	2333	28
H(1)	1260(80)	1180(60)	4020(50)	28
H(4)	4680(80)	2280(60)	2800(50)	28
H(7)	4600(80)	430(60)	2130(50)	28
H(10)	2200(80)	-350(60)	3020(50)	28

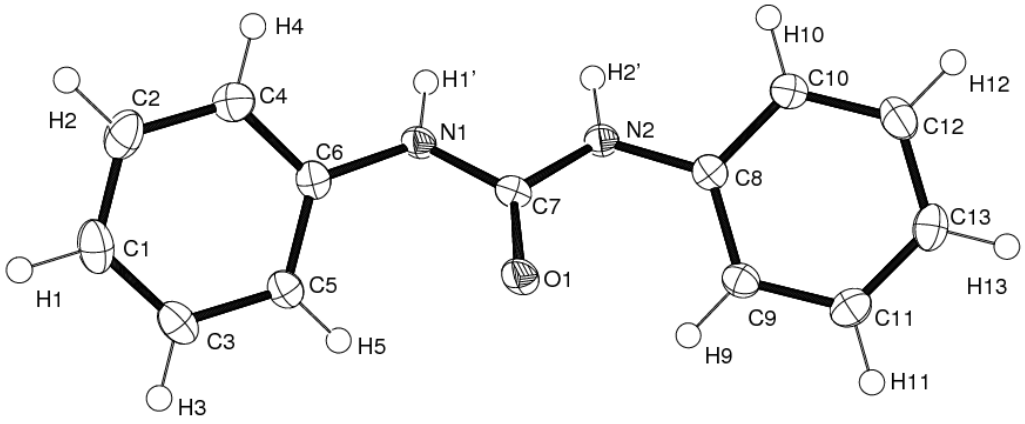

Figure A.5: Crystal data and structure refinement of $C_{13}H_{12}N_2O$ (**2.11**).

Geometry. All esds (except the esd in the dihedral angle between two l.s. planes) are estimated using the full covariance matrix. The cell esds are taken into account individually in the estimation of esds in distances, angles and torsion angles; correlations between esds in cell parameters are only used when they are defined by crystal symmetry. An approximate (isotropic) treatment of cell esds is used for estimating esds involving l.s. planes.

Refinement. Refinement of F^2 against ALL reflections. The weighted R-factor wR and goodness of fit S are based on F^2, conventional R-factors R are based on F, with F set to zero for negative F^2. The threshold expression of F^2>2sigma(F^2) is used only for calculating R-factors(gt) etc. and is not relevant to the choice of reflections for refinement. R-factors based on F^2 are statistically about twice as large as those based on F, and R- factors based on ALL data will be even larger.

Table A.13: Crystallographic Data for $C_{13}H_{12}N_2O$ (**2.11**).

empirical formula	$C_{13}H_{12}N_2O$
formula weight	212.25
crystal system	Orthorhombic
space group	$Pna2_1$
a (Å)	9.0471 (10)
b (Å)	10.3272 (11)
c (Å)	11.7237 (12)
V (Å^3)	1095.4 (2)
Z	4
T (K)	90(2)
D_{calc} (g/cm^3)	1.287
$F(000)$	448
crystal size (mm^3)	$0.34 \times 0.25 \times 0.15$
θ range (deg)	2.3 to 27.1
index ranges	-11≤h≤10,
	-12≤k≤12,
	-13≤l≤14
goodness of fit (GOF)	1.51
no. of reflns collected	9962
no. of independent reflns	2044 [R(int) = 0.016]
no. of parameters	151
wavelength (Å)	0.71073
final R indices [I > $2\sigma(I)$]	$R_1 = 0.024$,w$R_2 = 0.071$

Table A.14: Atomic coordinates (x10^4) and equivalent isotropic displacement parameters (Å^2) for $C_{13}H_{12}N_2O$ (**2.11**).

	x	y	z	U_{iso}*/U_{eq}
O1	0.12357 (8)	0.27778 (8)	0.76271 (7)	0.02178 (18)
N1	-0.09151 (10)	0.21692 (9)	0.67623 (8)	0.0188 (2)
H1'	-0.1838 (14)	0.2043 (13)	0.6906 (12)	0.028*
N2	-0.09524 (10)	0.29949 (9)	0.85699 (8)	0.0188 (2)
H2'	-0.1863 (15)	0.2749 (12)	0.8589 (13)	0.028*
C1	0.06912 (14)	0.09401 (13)	0.35844 (12)	0.0310 (3)
H1	0.1040	0.0660	0.2861	0.037*
C2	-0.03997 (13)	0.02445 (12)	0.41476 (12)	0.0304 (3)
H2	-0.0811	-0.0506	0.3803	0.036*
C3	0.12683 (13)	0.20460 (12)	0.40832 (11)	0.0258 (3)
H3	0.2021	0.2519	0.3702	0.031*
C4	-0.08913 (13)	0.06426 (11)	0.52113 (11)	0.0244 (3)
H4	-0.1620	0.0152	0.5603	0.029*
C5	0.07572 (12)	0.24686 (11)	0.51351 (10)	0.0203 (2)
H5	0.1141	0.3239	0.5464	0.024*
C6	-0.03182 (11)	0.17590 (10)	0.57048 (10)	0.0187 (2)
C7	-0.01198 (11)	0.26602 (9)	0.76413 (10)	0.0169 (2)
C8	-0.03645 (11)	0.34562 (10)	0.96130 (10)	0.0181 (2)
C9	0.08394 (12)	0.42921 (11)	0.96608 (11)	0.0205 (2)
H9	0.1301	0.4576	0.8977	0.025*
C10	-0.10631 (12)	0.30842 (10)	1.06253 (11)	0.0232 (2)
H10	-0.1901	0.2531	1.0599	0.028*
C11	0.13650 (12)	0.47103 (10)	1.07121 (10)	0.0234 (2)
H11	0.2198	0.5270	1.0742	0.028*
C12	-0.05383 (13)	0.35193 (13)	1.16637 (10)	0.0274 (3)
H12	-0.1022	0.3267	1.2348	0.033*
C13	0.06913 (13)	0.43230 (12)	1.17161 (10)	0.0254 (3)
H13	0.1065	0.4603	1.2432	0.030*

Table A.15: Atomic displacement parameters (Å^2) for $C_{13}H_{12}N_2O$ (**2.11**).

	U^{11}	U^{22}	U^{33}	U^{12}	U^{13}	U^{23}
O1	0.0123 (3)	0.0330 (4)	0.0200 (4)	0.0017 (3)	0.0013 (3)	0.0001 (3)
N1	0.0121 (4)	0.0249 (5)	0.0194 (5)	-0.0001 (3)	0.0024 (4)	-0.0007 (4)
N2	0.0122 (4)	0.0248 (5)	0.0193 (5)	-0.0005 (3)	0.0004 (4)	-0.0009 (4)
C1	0.0321 (7)	0.0372 (7)	0.0235 (6)	0.0108 (5)	0.0013 (5)	-0.0073 (6)
C2	0.0316 (6)	0.0255 (6)	0.0341 (7)	0.0041 (5)	-0.0015 (5)	-0.0118 (6)
C3	0.0230 (6)	0.0326 (6)	0.0219 (6)	0.0055 (5)	0.0042 (5)	0.0035 (5)
C4	0.0227 (5)	0.0212 (5)	0.0292 (6)	0.0012 (4)	0.0008 (5)	-0.0002 (5)
C5	0.0182 (5)	0.0232 (5)	0.0196 (5)	0.0039 (4)	0.0006 (4)	0.0011 (5)
C6	0.0153 (5)	0.0222 (5)	0.0186 (5)	0.0057 (4)	-0.0010 (4)	-0.0002 (4)
C7	0.0146 (5)	0.0174 (4)	0.0187 (5)	0.0019 (3)	0.0003 (5)	0.0042 (4)
C8	0.0158 (5)	0.0184 (5)	0.0199 (5)	0.0042 (4)	0.0006 (5)	0.0006 (4)
C9	0.0200 (5)	0.0192 (5)	0.0222 (5)	0.0010 (4)	0.0027 (4)	0.0012 (5)
C10	0.0224 (6)	0.0242 (5)	0.0230 (6)	-0.0033 (4)	0.0023 (5)	-0.0003 (5)
C11	0.0225 (5)	0.0183 (5)	0.0295 (6)	0.0009 (4)	-0.0022 (5)	-0.0022 (5)
C12	0.0334 (6)	0.0289 (6)	0.0200 (6)	0.0006 (5)	0.0052 (5)	0.0014 (5)
C13	0.0314 (6)	0.0233 (6)	0.0215 (6)	0.0041 (4)	-0.0036 (4)	-0.0049 (5)

Appendix B

Some ^{11}B NMR and GCMS data

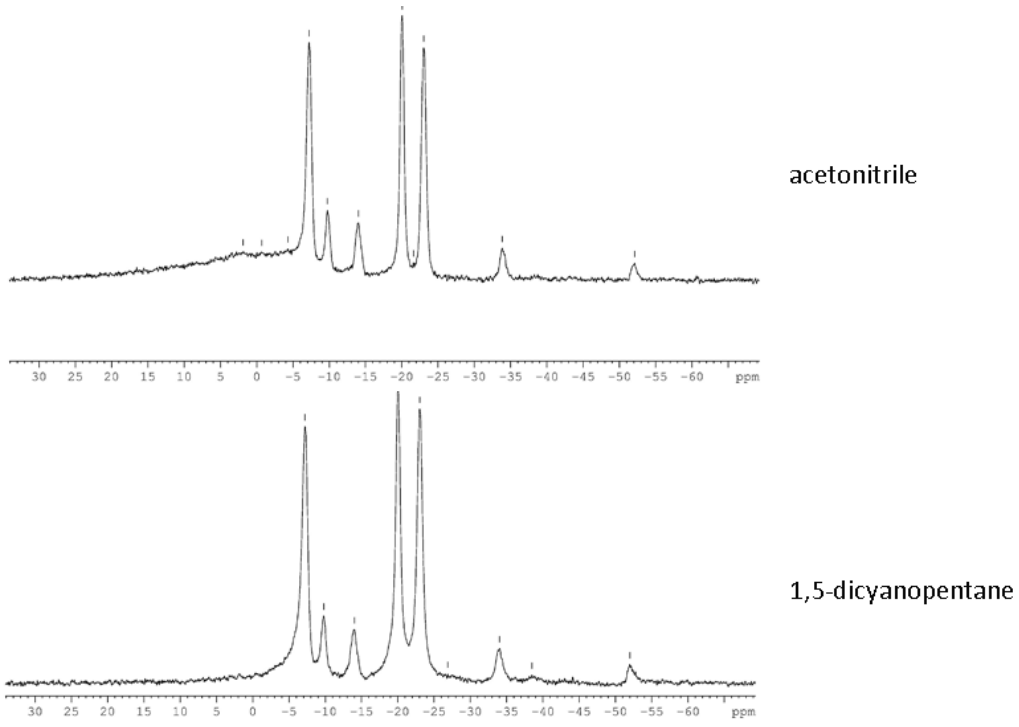

Figure B.1: Photoreaction between **1.1** and acetonitrile or dicyanopentane.

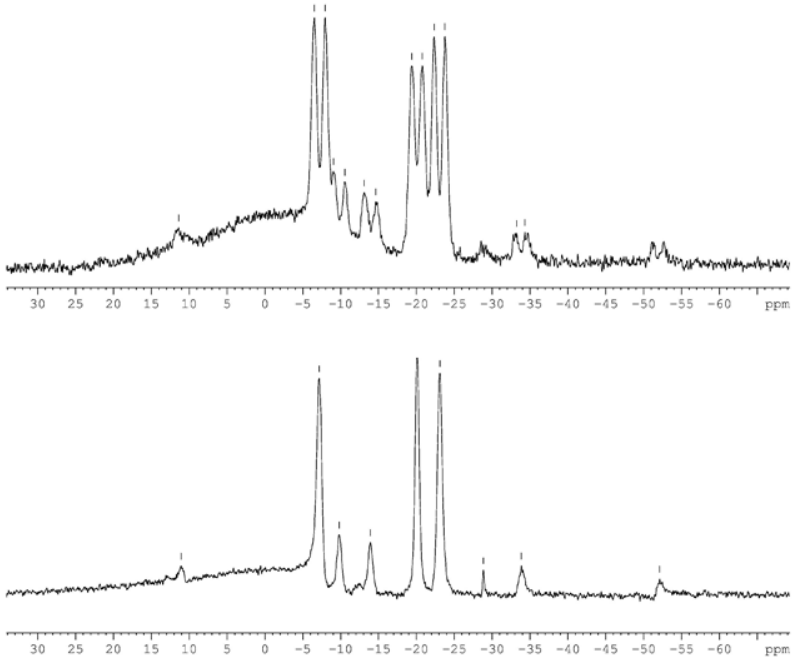

Figure B.2: Photoreaction between **1.1** and methyl acrylate.

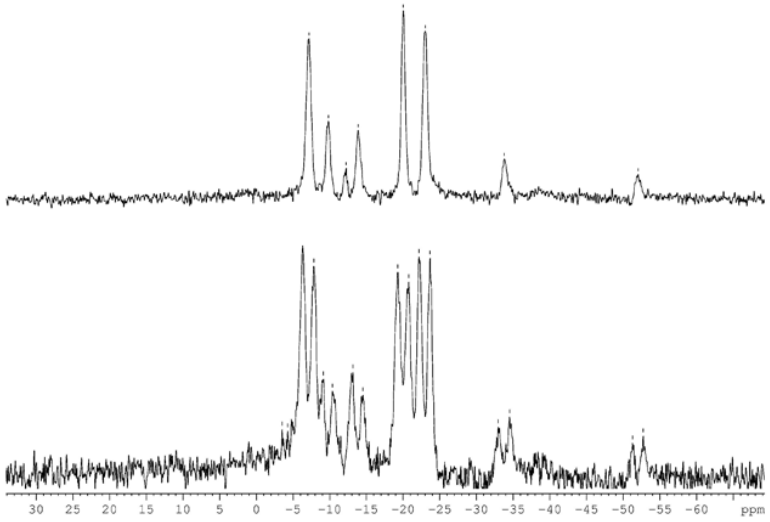

Figure B.3: Photoreaction between **1.1** and methylcyanoformate.

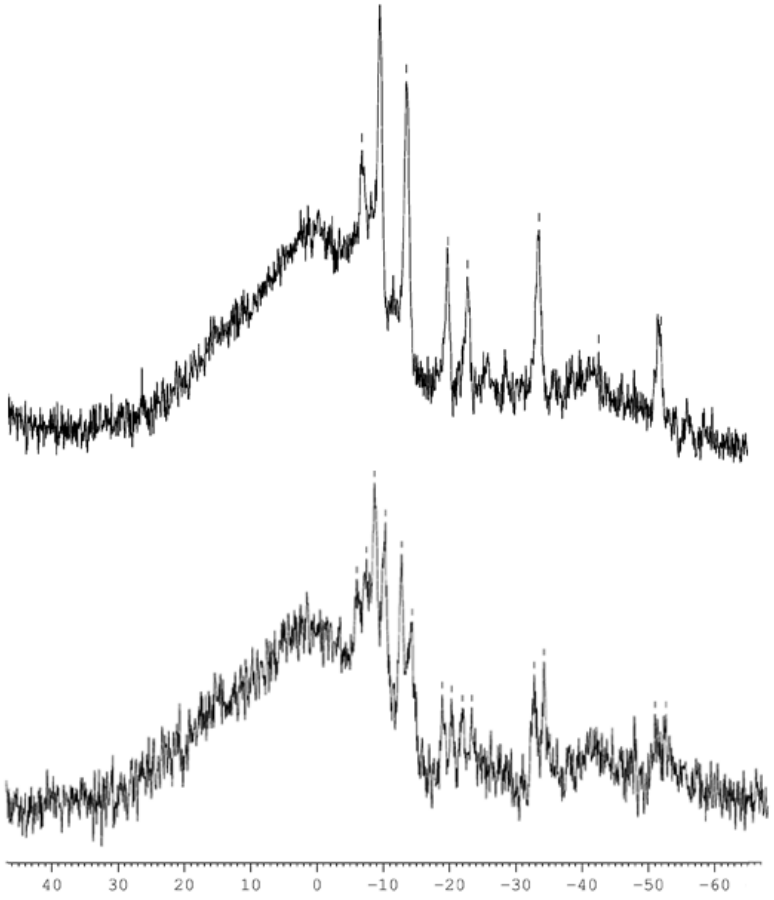

Figure B.4: Photoreaction between **1.1** and ^{n}Bu-isocyanate.

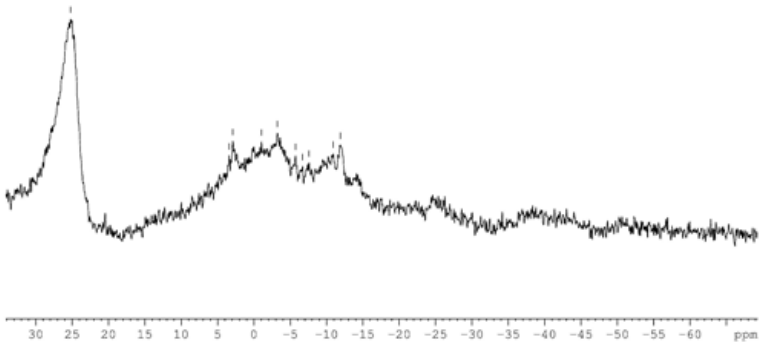

Figure B.5: Photoreaction between **1.1** and benzenaldehyde.

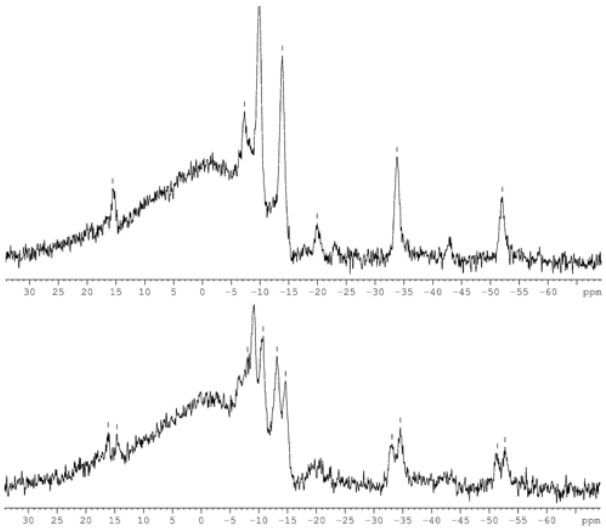

Figure B.6: Photoreaction between **1.1** and phenyl isocyanate.

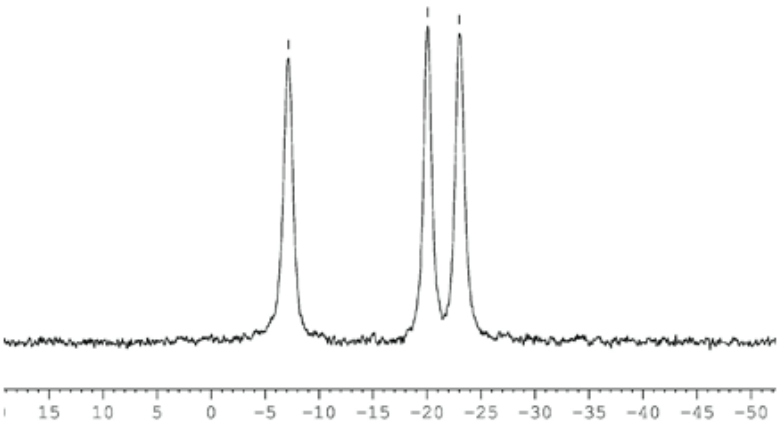

Figure B.7: Photoreaction between **1.1** and N-benzylidenemethylamine.

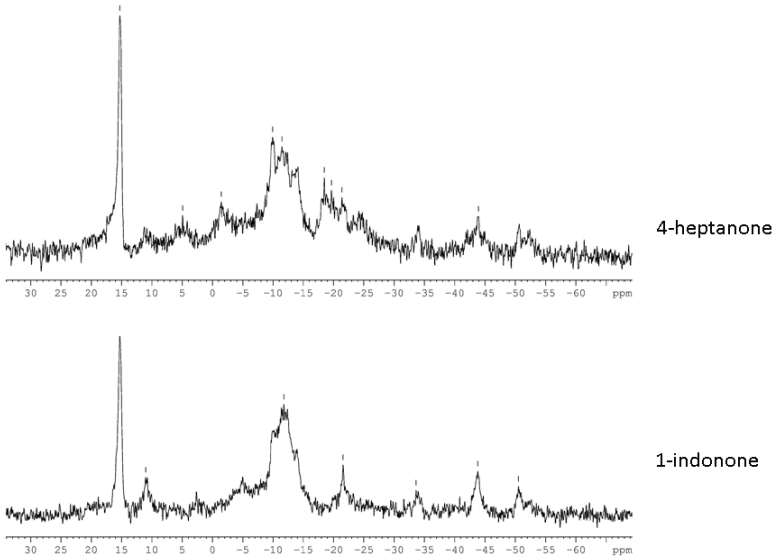

Figure B.8: Photoreaction between **1.1** and ketones.

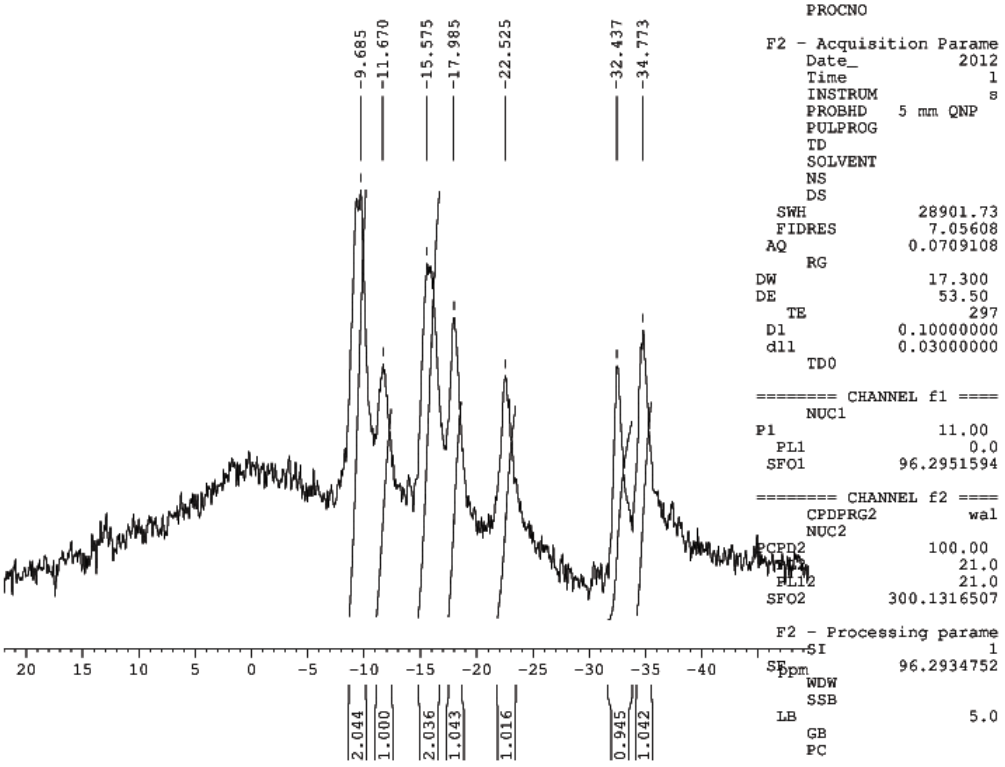

Figure B.9: Photoreaction between **1.1** and ethynylferrocene.

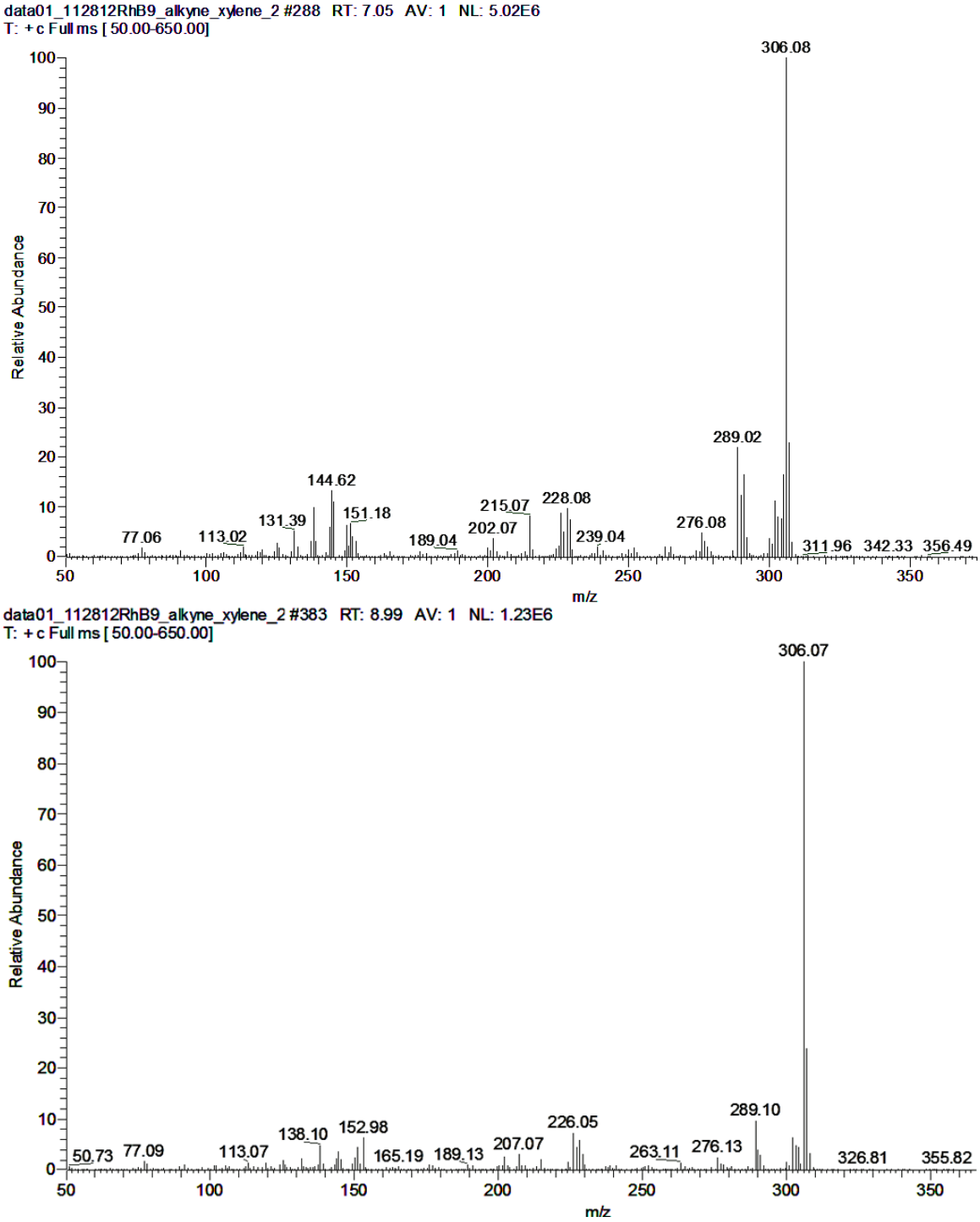

Figure B.10: MS data for phenylacetylene trimerization catalyzed by [6-(η^5-C_5Me_5)-*nido*-6-RhB_9H_{13}] (**3.1**).

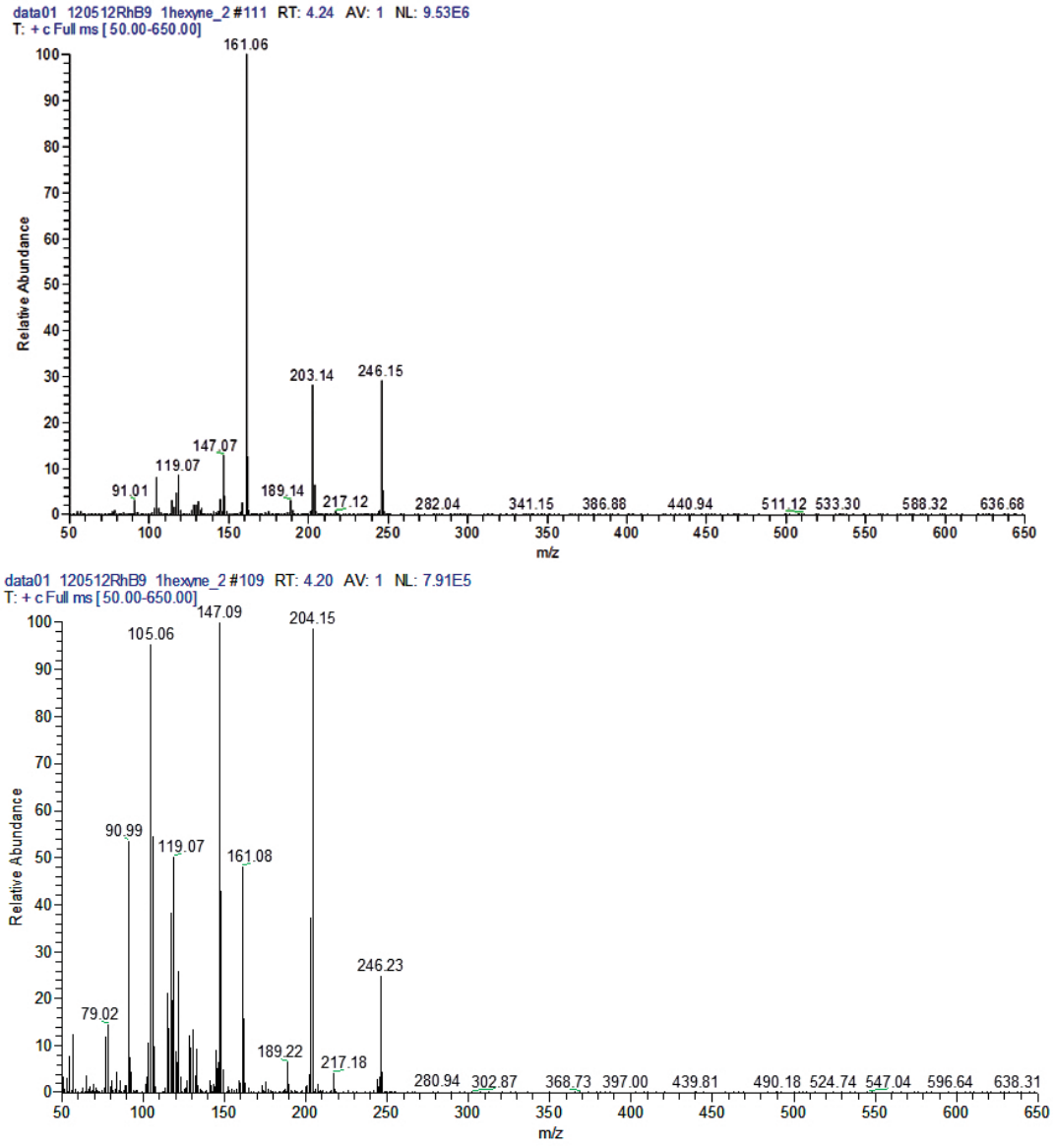

Figure B.11: MS data for 1-hexyne trimerization catalyzed by [6-(η^5-C_5Me_5)-*nido*-6-RhB_9H_{13}] (**3.1**).

References

[1] Kennedy, J. D. *Progress in Inorganic Chemistry, Volume 34.*; 1984; Chapter The Polyhedral Metallaboranes Part II. Metallaborane Clusters with Eight Vertices and More., pp 211–434, and references cited therein.

[2] Bould, J.; Greenwood, N. N.; Kennedy, J. D. *J. Chem. Soc., Dalton Trans.* **1990**, 1451–1458.

[3] Bown, M.; Fowkes, H.; Fontaine, X. L. R.; Greenwood, N. N.; Kennedy, J. D.; MacKinnon, P.; Nestor, K. *J. Chem. Soc., Dalton Trans.* **1988**, 2597–2600.

[4] Bown, M.; Fontaine, X. L. R.; Greenwood, N. N.; Kennedy, J. D.; MacKinnon, P. *J. Chem. Soc., Chem. Commun.* **1987**, 817–818.

[5] Micciche, R. P.; Briguglio, J. J.; Sneddon, L. G. *Inorganic Chemistry* **1984**, *23*, 3992–3999.

[6] Zimmerman, G. J.; Hall, L. W.; Sneddon, L. G. *Inorganic Chemistry* **1980**, *19*, 3642–3650.

[7] Borodinsky, L.; Sinn, E.; Grimes, R. N. *Inorganic Chemistry* **1982**, *21*, 1928–1936.

[8] Borodinsky, L.; Grimes, R. N. *Inorganic Chemistry* **1982**, *21*, 1921–1927.

[9] Bould, J.; Crook, J. E.; Greenwood, N. N.; Kennedy, J. D.; Thornton-Pett, M. *J. Chem. Soc., Dalton Trans.* **1990**, 1441–1450.

[10] Fontaine, X. L. R.; Fowkes, H.; Greenwood, N. N.; Kennedy, J. D.; Thornton-Pett, M. *J. Chem. Soc., Dalton Trans.* **1987**, 1431–1443.

[11] Bown, M.; Fontaine, X. L.; Greenwood, N. N.; Kennedy, J. D. *Journal of Organometallic Chemistry* **1987**, *325*, 233 – 246.

[12] Baker, R. T. *Inorganic Chemistry* **1986**, *25*, 109–111.

[13] Kennedy, J. D. *Inorganic Chemistry* **1986**, *25*, 111–112.

[14] Johnston, R. L.; Mingos, D. M. P. *Inorganic Chemistry* **1986**, *25*, 3321–3323.

[15] Shameema, O.; Jemmis, E. D. *Inorganic Chemistry* **2009**, *48*, 7818–7827.

[16] Ditzel, E. J.; Fontaine, X. L. R.; Greenwood, N. N.; Kennedy, J. D.; Thornton-Pett, M. *J. Chem. Soc., Chem. Commun.* **1989**, 1262.

[17] Kim, Y.-H.; Barton, L.; Rath, N. P.; Kennedy, J. D. *Inorganic Chemistry Communications* **2005**, *8*, 147 – 150.

[18] hee Kim, Y.; Cooke, P. A.; Rath, N. P.; Barton, L.; Greatrex, R.; Kennedy, J. D.; Thornton-Pett, M. *Inorganic Chemistry Communications* **1998**, *1*, 375 – 378.

[19] Ditzel, E. J.; Fontaine, X. L. R.; Greenwood, N. N.; Kennedy, J. D.; Thornton-Pett, M. *Zeitschrift fur anorganische und allgemeine Chemie* **1992**, *616*, 79–85.

[20] Crook, J. E.; Elrington, M.; Greenwood, N. N.; Kennedy, J. D.; Thornton-Pett, M.; Woollins, J. D. *J. Chem. Soc., Dalton Trans.* **1985**, 2407.

[21] Lott, J. W.; Gaines, D. F. *Inorganic Chemistry* **1974**, *13*, 2261–2267.

[22] Littger, R.; Englich, U.; Ruhlandt-Senge, K.; Spencer, J. T. *Angewandte Chemie International Edition* **2000**, *39*, 1472–1474.

[23] Plesek, J. *Chemical Reviews* **1992**, *92*, 269–278.

[24] Dash, B. P.; Satapathy, R.; Maguire, J. A.; Hosmane, N. S. *New J. Chem.* **2011**, *35*, 1955–1972.

[25] Long, J. A.; Marder, T. B.; Behnken, P. E.; Hawthorne, M. F. *Journal of the American Chemical Society* **1984**, *106*, 2979–2989.

[26] Grishin, I. D.; Dyachihin, D. I.; Piskunov, A. V.; Dolgushin, F. M.; Smolyakov, A. F.; Ilin, M. M.; Davankov, V. A.; Chizhevsky, I. T.; Grishin, D. F. *Inorganic Chemistry* **2011**, *50*, 7574–7585.

[27] Hu, P.; Yao, Z.-J.; Wang, J.-Q.; Jin, G.-X. *Organometallics* **2011**, *30*, 4935–4940.

[28] Pleek, J.; Grner, B.; Hemnek, S.; Baca, J.; Marecek, V.; Jnchenov, J.; Lhotsk, A.; Holub, K.; Seluck, P.; Rais, J.; Cisarova, I.; slavsk, J. *Polyhedron* **2002**, *21*, 975 – 986.

[29] Vinas, C.; Gomez, S.; Bertran, J.; Teixidor, F.; Dozol, J.-F.; Rouquette, H. *Inorganic Chemistry* **1998**, *37*, 3640–3643.

[30] Allis, D. G.; Spencer, J. T. *Journal of Organometallic Chemistry* **2000**, *614615*, 309 – 313.

[31] Chetcuti, P. A.; Hofherr, W.; Liegard, A.; Rihs, G.; Rist, G.; Keller, H.; Zech, D. *Organometallics* **1995**, *14*, 666–675.

[32] Taylor, J.; Caruso, J.; Newlon, A.; Englich, U.; Ruhlandt-Senge, K.; Spencer, J. T. *Inorganic Chemistry* **2001**, *40*, 3381–3388.

[33] Yan, Y.-K.; Mingos, D. M. P.; Williams, D. J.; Kurmoo, M. *J. Chem. Soc. Dalton Trans.* **1995**, 3221–3230.

[34] Valliant, J. F.; Morel, P.; Schaffer, P.; Kaldis, J. H. *Inorganic Chemistry* **2002**, *41*, 628–630.

[35] Sykora, D.; Vosmanska, M.; Matejka, P.; Kral, V. *Journal of Chromatography A* **2011**, *1218*, 3029 – 3036.

[36] Hawthorne, M. F.; Varadarajan, A.; Knobler, C. B.; Chakrabarti, S.; Paxton, R. J.; Beatty, B. G.; Curtis, F. L. *Journal of the American Chemical Society* **1990**, *112*, 5365–5366.

[37] Armstrong, A. F.; Lebert, J. M.; Brennan, J. D.; Valliant, J. F. *Organometallics* **2009**, *28*, 2986–2992.

[38] Jelliss, P. A. *Comments on Inorganic Chemistry* **2008**, *29*, 1–25.

[39] Farha, O. K.; Spokoyny, A. M.; Mulfort, K. L.; Hawthorne, M. F.; Mirkin, C. A.; Hupp, J. T. *Journal of the American Chemical Society* **2007**, *129*, 12680–12681.

[40] Singh, A. K.; Sadrzadeh, A.; Yakobson, B. I. *Journal of the American Chemical Society* **2010**, *132*, 14126–14129.

[41] Li, T. C.; Spokoyny, A. M.; She, C.; Farha, O. K.; Mirkin, C. A.; Marks, T. J.; Hupp, J. T. *Journal of the American Chemical Society* **2010**, *132*, 4580–4582.

[42] Bould, J.; Mach?ek, J.; Londesborough, M. G. S.; Macas, R.; Kennedy, J. D.; Bastl, Z.; Rupper, P.; Bae, T. *Inorganic Chemistry* **2012**, *51*, 1685–1694.

[43] Kolb, H. C.; Finn, M. G.; Sharpless, K. B. *Angewandte Chemie International Edition* **2001**, *40*, 2004–2021.

[44] Lutz, J.-F. *Angewandte Chemie International Edition* **2007**, *46*, 1018–1025.

[45] Lutz, J.-F.; Zarafshani, Z. *Advanced Drug Delivery Reviews* **2008**, *60*, 958 – 970.

[46] Moses, J. E.; Moorhouse, A. D. *Chem. Soc. Rev.* **2007**, *36*, 1249–1262.

[47] Li, Y.; Giesbers, M.; Gerth, M.; Zuilhof, H. *Langmuir* **2012**, *28*, 12509–12517.

[48] Nandivada, H.; Jiang, X.; Lahann, J. *Advanced Materials* **2007**, *19*, 2197–2208.

[49] Binder, W. H.; Sachsenhofer, R. *Macromolecular Rapid Communications* **2008**, *29*, 952–981.

[50] Hein, C.; Liu, X.-M.; Wang, D. *Pharmaceutical Research* **2008**, *25*, 2216–2230.

[51] Kurpiers, T.; Mootz, H. *Angewandte Chemie International Edition* **2009**, *48*, 1729–1731.

[52] Sivaev, I. B.; Semioshkin, A. A.; Brellochs, B.; Sjoberg, S.; Bregadze, V. I. *Polyhedron* **2000**, *19*, 627 – 632.

[53] Sivaev, I. B.; Starikova, Z. A.; Sjoberg, S.; Bregadze, V. I. *Journal of Organometallic Chemistry* **2002**, *649*, 1 – 8.

[54] Lesnikowski, Z. J. *Journal of Organometallic Chemistry* **2009**, *694*, 1771 – 1775.

[55] Bernard, R.; Cornu, D.; Perrin, M.; Scharff, J.-P.; Miele, P. *Journal of Organometallic Chemistry* **2004**, *689*, 2581 – 2585.

[56] K. Yu. Zhizhin, E. A. M.-E. Y. M. L. V. G. I. N. P., V. N. Mustyatsa; Kuznetsov., N. T. *Russ. J. Inorg. Chem.* **2005**, *50*, 203209.

[57] Sivaev, I.; Semioshkin, A.; Bregadze, V. *Applied Radiation and Isotopes* **2009**, *67*, S91 – S93.

[58] Goodreau, B. H.; Spencer, J. T. *Inorganic Chemistry* **1992**, *31*, 2612–2621.

[59] James, T. L.; McDonald, G. G. *Journal of Magnetic Resonance (1969)* **1973**, *11*, 58 – 61.

[60] Levy, G. C.; Peat, I. R. *Journal of Magnetic Resonance (1969)* **1975**, *18*, 500 – 521.

[61] Duward F. Shriver, M. A. D. *The Manipulation of Air-Sensitive Compounds, 2nd Edition*; Wiley Interscience, 1986.

[62] Patrick J.Dolan, D. C. M. C. K. N., Donald F.Gaines; by Sheldon G. Shore, R. S. C.; Lawrence, S. H. *Inorganic Syntheses* **1968**, *11*, 1–3.

[63] Jacobsen, G. B.; Meina, D. G.; Morris, J. H.; Thomson, C.; Andrews, S. J.; Reed, D.; Welch, A. J.; Gaines, D. F. *J. Chem. Soc., Dalton Trans.* **1985**, 1645–1654.

[64] Lott, J. W.; Gaines, D. F.; Shenhav, H.; Schaeffer, R. *Journal of the American Chemical Society* **1973**, *95*, 3042–3043.

[65] Hope, H. In *Progress in Inorganic Chemistry, Volume 41*; Karlin, K. D., Ed.; Wiley Interscience, 1994; Chapter X-Ray Crystallography: A Fast, First-Resort Analytical Tool, p 1.

[66] APEX II, Data Collection Software, version 2011.8-0; Bruker AXS Inc.: Madison, WI. 2005-2011.

[67] SAINT Plus, Date Reduction Software, version, 6.45A; Bruker AXS Inc.: Madison, WI. 1997-2002.

[68] Sheldrick, G. M. SADABS; University of Gttingen: Gttingen, Germany. 1996.

[69] SHELXTL PC, version 6.12; Bruker AXS Inc.: Madison, WI. 2002.

[70] Miller, V. R.; Weiss, R.; Grimes, R. N. *Journal of the American Chemical Society* **1977**, *99*, 5646–5651.

[71] Grafstein, D.; Bobinski, J.; Dvorak, J.; Smith, H.; Schwartz, N.; Cohen, M. S.; Fein, M. M. *Inorganic Chemistry* **1963**, *2*, 1120–1125.

[72] Papetti, S.; Heying, T. L. *Journal of the American Chemical Society* **1964**, *86*, 2295–2295.

[73] Venable, T. L.; Hutton, W. C.; Grimes, R. N. *Journal of the American Chemical Society* **1984**, *106*, 29–37.

[74] Carlos, R. M.; Neumann, M. G. *Journal of Photochemistry and Photobiology A: Chemistry* **2000**, *131*, 67 – 73.

[75] Pipal, J. R.; Grimes, R. N. *Inorganic Chemistry* **1977**, *16*, 3251–3255.

[76] Tippe, A.; Hamilton, W. C. *Inorganic Chemistry* **1969**, *8*, 464–470.

[77] Lipscomb, W. N. *Science* **1966**, *153*, 373–378.

[78] Wu, S. H.; Jones, M. *Journal of the American Chemical Society* **1989**, *111*, 5373–5384.

[79] Gimarc, B. M.; Ott, J. J. *Journal of the American Chemical Society* **1987**, *109*, 1388–1392.

[80] Gimarc, B. M.; Warren, D. S.; Ott, J. J.; Brown, C. *Inorganic Chemistry* **1991**, *30*, 1598–1605.

[81] Wales, D. J. *Journal of the American Chemical Society* **1993**, *115*, 1557–1567.

[82] Hart, H. V.; Lipscomb, W. N. *Journal of the American Chemical Society* **1969**, *91*, 771–772.

[83] Kaesz, H. D.; Bau, R.; Beall, H. A.; Lipscomb, W. N. *Journal of the American Chemical Society* **1967**, *89*, 4218–4220.

[84] Edvenson, G. M.; Gaines, D. F. *Inorganic Chemistry* **1990**, *29*, 1210–1216, ,and references cited therein.

[85] Plumb, C. A.; Sneddon, L. G. *Organometallics* **1992**, *11*, 1681–1685.

[86] Graff, J. L.; Sobieralski, T. J.; Wrighton, M. S.; Geoffroy, G. L. *Journal of the American Chemical Society* **1982**, *104*, 7526–7533.

[87] Chung, Y. K.; Williard, P. G.; Sweigart, D. A. *Organometallics* **1982**, *1*, 1053–1056.

[88] Rose-Munch, F.; Marti, A.; Cetiner, D.; Tranchier, J.-P.; Rose, E. *Dalton Trans.* **2011**, *40*, 1567–1575.

[89] Sun, S.; Dullaghan, C. A.; Sweigart, D. A. *J. Chem. Soc., Dalton Trans.* **1996**, 4493–4507.

[90] Eloi, A.; Rose-Munch, F.; Rose, E.; Pille, A.; Lesot, P.; Herson, P. *Organometallics* **2010**, *29*, 3876–3886.

[91] Jaouen, G.; Meyer, A.; Simonneaux, G. *J. Chem. Soc., Chem. Commun.* **1975**, 813–814.

[92] Nechvatal, G.; Widdowson, D. A. *J. Chem. Soc., Chem. Commun.* **1982**, 467–468.

[93] Dubarle-Offner, J.; Rose-Munch, F.; Dtz, K.-H.; Rose, E.; Cuvier, A. S.; Panossian, A. *Organometallics* **2011**, *30*, 6778–6781.

[94] Zhang, J.; Stanciu, C.; Wang, B.; Hussain, M. M.; Da, C.-S.; Carroll, P. J.; Dreher, S. D.; Walsh, P. J. *Journal of the American Chemical Society* **2011**, *133*, 20552–20560.

[95] Semioshkin, A. A.; Sivaev, I. B.; Bregadze, V. I. *Dalton Trans.* **2008**, 977–992.

[96] Jaromr Pleek, F. M., Tom Jelnek; He?mnek, S. *Collect. Czech. Chem. Commun.* **1993**, *58*, 1534–1547.

[97] Sivaev, I. B.; Kulikova, N. Y.; Nizhnik, E. A.; Vichuzhanin, M. V.; Starikova, Z. A.; Semioshkin, A. A.; Bregadze, V. I. *Journal of Organometallic Chemistry* **2008**, *693*, 519 – 525.

[98] Peymann, T.; Kck, K.; Gabel, D. *Inorganic Chemistry* **1997**, *36*, 5138–5139.

[99] Farras, P.; Teixidor, F.; Sillanpaa, R.; Vinas, C. *Dalton Trans.* **2010**, *39*, 1716–1718.

[100] Semioshkin, A.; Nizhnik, E.; Godovikov, I.; Starikova, Z.; Bregadze, V. *Journal of Organometallic Chemistry* **2007**, *692*, 4020 – 4028.

[101] Orlova, A.; Kondakov, N.; Zinin, A.; Kimel, B.; Kononov, L.; Sivaev, I.; Bregadze, V. *Russian Journal of Bioorganic Chemistry* **2006**, *32*, 568–577.

[102] Gaines, D. F.; Lott, J. W.; Calabrese, J. C. *Inorganic Chemistry* **1974**, *13*, 2419–2423.

[103] Jurisson, S. S.; Lydon, J. D. *Chemical Reviews* **1999**, *99*, 2205–2218.

[104] Zhang, J.; Xie, Z. *Chemistry - An Asian Journal* **2010**, *5*, 1742–1757.

[105] Asta Gindulyte, W. N. L., Namby Krishnamachari; Massa, L. *Inorgnic Chemistry* **1998**, *37*, 6546–6548.

[106] Elschenbroich, C.; Salzer, A. *Organometallics*; VCH, 1992.

[107] Suppan, P. *Chemistry and Light*; Royal Society of Chemistry, 1994.

[108] Ninomiya, I.; Naito, T. *Photochemical Synthesis*; Academic Press, 1989.

[109] Hijazi A. A., V. M.; Srebnik, M. *Contemporary Aspects of Boron: Chmistry and Biological Applications(Studies in Inorganic Chemistry 22)*; Elsevier, 2005.

[110] Robert R. Kane, K. D.; Hawthorne, M. F. *Journal of the American Chemical Society* **1993**, *115*, 8853–8854.

[111] Ye Wu, S. O. K., Patrick J. Carroll; Quintana, W. *Inorganic Chemistry* **2003**, *36*, 4753–4761.

[112] Shelly, K.; Reed, C. A.; Lee, Y. J.; Scheidt, W. R. *Journal of the American Chemical Society* **1986**, *108*, 3117–3118.

[113] Douvris, C.; Ozerov, O. V. *Science* **2008**, *321*, 1188–1190.

[114] Guggenberger, L. J. *Inorganic Chemistry* **1970**, *9*, 367–373.

[115] D, E. C.; B, M. T. *Angewandte Chemie International Edition* **2002**, *41*, 2927–2931.

[116] Sasaki, T.; M, J. *Organic Letters* **2008**, *10*, 897–900.

[117] Albert H. Soloway, B. A. B. F.-G. R. R. F. B. I. M. C., Werner Tjarks; Wilson, J. G. *Chemical Reviews* **1998**, *98*, 2389–2390.

[118] Pitochelli, A. R.; Hawthorne, M. F. *Journal of the American Chemical Society* **1962**, *84*, 3218–3218.

[119] Taylor, J. W.; Englich, U.; Ruhlandt-Senge, K.; Spencer, J. T. *Organometallics* **2002**, *21*, 3054–3057.

[120] Jelinek, T.; Cisarova, I.; Stibr, B.; D. Kennedy, J.; Thornton-Pett, M. *J. Chem. Soc., Dalton Trans.* **1998**, 2965–2968.

[121] Dopke, J. A.; Powell, D. R.; Gaines, D. F. *Inorganic Chemistry* **2000**, *39*, 463–467.

[122] Hawthorne, M. F.; Maderna, A. *Chemical Reviews* **1999**, *99*, 3421–3434.

[123] Paul von Rague Schleye, K. N.; Mebel, A. M. *Inorganic Chemistry* **1998**, *37*, 6765–6772.

[124] Burke, A.; Ellis, D.; Giles, B. T.; Hodson, B. E.; Macgregor, S. A.; Rosair, G. M.; Welch, A. J. *Angewandte Chemie* **2003**, *115*, 235–238.

[125] Deng, L.; Chan, H.-S.; Xie, Z. *Angewandte Chemie International Edition* **2005**, *44*, 2128–2131.

[126] Zhang, J.; Zheng, F.; Chan, H.-S.; Xie, Z. *Inorganic Chemistry* **2009**, *48*, 9786–9791.

[127] Zhang, J.; Chan, H.-S.; Xie, Z. *Angewandte Chemie International Edition* **2008**, *47*, 9447–9449.

[128] Bobinski, J. *Journal of Chemical Education* **1964**, *41*, 500.

[129] Hawthorne, M. F.; Evans, W. J. *Journal of the American Chemical Society* **1971**, *93*, 3063–3064.

[130] Goodreau, B. H.; Orlando, L. R.; Spencer, J. T. *Journal of the American Chemical Society* **1992**, *114*, 3827–3835.

[131] Goodreau, B. H.; Orlando, L. R.; Spencer, J. T. *Journal of the American Chemical Society* **1995**, *117*, 11754–11761.

[132] Greenwood, N. N.; Ward, I. M. *Chem. Soc. Rev.* **1974**, *3*, 231–271.

[133] Grimes, R., Ed. *Metal Interactions with Boron Clusters*; Plenum Press, 1982.

[134] Bould, J.; Bown, M.; Coldicott, R. J.; Ditzel, E. J.; Greenwood, N. N.; Macpherson, I.; MacKinnon, P.; Thornton-Pett, M.; Kennedy, J. D. *Journal of Organometallic Chemistry* **2005**, *690*, 2701 – 2720.

[135] Rudolph, R. W. *Accounts of Chemical Research* **1976**, *9*, 446–452.

[136] Coldicott, R. S.; Kennedy, J. D.; Thornton-Pett, M. *J. Chem. Soc., Dalton Trans.* **1996**, 3819–3824.

[137] Young-hee Kim, P. A. C.-R. G. J. D. K., Yvonne M. McKinnes; Thornton-Pett., M. *Collect. Czech. Chem. Commun.* **1999**, *64*, 938–946.

[138] Stibr, B. *Chemical Reviews* **1992**, *92*, 225–250.

[139] Jaromr Pleek, E. D. S. H., Tom Jelnek; tbr, B. *Collect.Czech. Chem. Commun.* **1984**, *49*, 1559.

[140] Fehlner, T. P. *Journal of the American Chemical Society* **1977**, *99*, 8355–8356.

[141] Fehlner, T. P. *Journal of the American Chemical Society* **1980**, *102*, 3424–3430.

[142] Mirabelli, M. G. L.; Carroll, P. J.; Sneddon, L. G. *Journal of the American Chemical Society* **1989**, *111*, 592–597.

[143] Wrighton, M. *Chemical Reviews* **1974**, *74*, 401–430.

[144] Wade, K. *J. Chem. Soc. D* **1971**, 792–793.

[145] Wade, K. In *Structural and Bonding Patterns in Cluster Chemistry*; Emelus, H., Sharpe, A., Eds.; Advances in Inorganic Chemistry and Radiochemistry; Academic Press, 1976; Vol. 18; pp 1 – 66.

[146] MINGOS, D. M. P. *nature physical science* **1972**, *236*, 99–102.

[147] Williams, R. E. *Inorganic Chemistry* **1971**, *10*, 210–214.

[148] Rudolph, R. W.; Pretzer, W. R. *Inorganic Chemistry* **1972**, *11*, 1974–1978.

[149] Vinas, C.; Pedrajas, J.; Bertran, J.; Teixidor, F.; Kivekas, R.; Sillanpaa, R. *Inorganic Chemistry* **1997**, *36*, 2482–2486.

[150] Beckering, C. L.; Rosair, G. M.; Weller, A. S. *Journal of Organometallic Chemistry* **1998**, *556*, 55 – 66.

[151] Busby, D. C.; Hawthorne, M. F. *Inorganic Chemistry* **1982**, *21*, 4101–4103.

[152] Valliant, J. F.; Guenther, K. J.; King, A. S.; Morel, P.; Schaffer, P.; Sogbein, O. O.; Stephenson, K. A. *Coordination Chemistry Reviews* **2002**, *232*, 173 – 230.

[153] Hawthorne, M. F.; Young, D. C.; Andrews, T. D.; Howe, D. V.; Pilling, R. L.; Pitts, A. D.; Reintjes, M.; Warren, L. F.; Wegner, P. A. *Journal of the American Chemical Society* **1968**, *90*, 879–896.

[154] Greenwood, A., N. N.; Earnshaw *Chemistry of the Elements, 2nd ed*; Butterworth-Heinemann: Oxford, 1997.

[155] Pleek, J.; Hemnek, S.; tbr, B.; Waksman, L.; Sneddon, L. G. *Inorganic Syntheses*; John Wiley & Sons, Inc., 2007; pp 231–234.

[156] Grimes, R. N. In *Comprehensive Organometallic Chemistry*; G. Wilkinson, F. G. A. S., Abel, E. W., Eds.; Pergamon, New York, 1982.

[157] Grimes, R. N. In *Comprehensive Organometallic Chemistry II*; E. W. Abel, F. G. A. S., Wilkinson, G., Eds.; Pergamon, New York, 1995.

[158] Saxena, A. K.; Maguire, J. A.; Hosmane, N. S. *Chemical Reviews* **1997**, *97*, 2421–2462.

[159] Li, Y.; Carroll, P. J.; Sneddon, L. G. *Inorganic Chemistry* **2008**, *47*, 9193–9202.

[160] Hawthorne, M. F.; Young, D. C.; Garrett, P. M.; Owen, D. A.; Schwerin, S. G.; Tebbe, F. N.; Wegner, P. A. *Journal of the American Chemical Society* **1968**, *90*, 862–868.

[161] Wiesboeck, R. A.; Hawthorne, M. F. *Journal of the American Chemical Society* **1964**, *86*, 1642–1643.

[162] Hawthorne, M. F.; Wegner, P. A.; Stafford, R. C. *Inorganic Chemistry* **1965**, *4*, 1675–1675.

[163] Tomita, H.; Luu, H.; Onak, T. *Inorganic Chemistry* **1991**, *30*, 812–815.

[164] Buchanan, J.; Hamilton, E. J. M.; Reed, D.; Welch, A. J. *J. Chem. Soc., Dalton Trans.* **1990**, 677–680.

[165] G. Davidson, M.; A. Fox, M.; G. Hibbert, T.; A. K. Howard, J.; Mackinnon, A.; S. Neretin, I.; Wade, K. *Chem. Commun.* **1999**, 1649–1650.

[166] Fox, M. A.; Goeta, A. E.; Howard, J. A. K.; Hughes, A. K.; Johnson, A. L.; Keen, D. A.; Wade, K.; Wilson, C. C. *Inorganic Chemistry* **2001**, *40*, 173–175.

[167] Fox, M. A.; Goeta, A. E.; Hughes, A. K.; Johnson, A. L. *J. Chem. Soc., Dalton Trans.* **2002**, 2132–2141.

[168] Kemnitz, C. R.; Ball, E. S.; McMahon, R. J. *Organometallics* **2012**, *31*, 70–84.

[169] Fehlner, T. P. *Pure Appl. Chem.* **2006**, *78*, 1323–1331.

[170] Bould, J.; Rath, N. P.; Barton, L. *Organometallics* **1996**, *15*, 4916–4929.

[171] Bould, J.; Rath, N. P.; Barton, L.; Kennedy, J. D. *Organometallics* **1998**, *17*, 902–907.

[172] Rausch, M. D.; Genetti, R. A. *The Journal of Organic Chemistry* **1970**, *35*, 3888–3897.

[173] Dolgushin, F. M.; Yanovsky, A. I.; Antipin, M. Y. *ChemInform* **2004**, *35*, 517–540.

[174] Kirchner, K.; Calhorda, M. J.; Schmid, R.; Veiros, L. F. *Journal of the American Chemical Society* **2003**, *125*, 11721–11729.

[175] Agenet, N.; Gandon, V.; Vollhardt, K. P. C.; Malacria, M.; Aubert, C. *Journal of the American Chemical Society* **2007**, *129*, 8860–8871.

[176] Weding, N.; Hapke, M. *Chem. Soc. Rev.* **2011**, *40*, 4525–4538.

[177] Shaaban, M. R.; El-Sayed, R.; Elwahy, A. H. M. *Tetrahedron* **2011**, *67*, 6095–6130, ¡p¿n/a¡/p¿.

[178] Dominguez, G.; Perez-Castells, J. *Chem. Soc. Rev.* **2011**, *40*, 3430–3444.

[179] Varela, J. A.; Saa, C. *Journal of Organometallic Chemistry* **2009**, *694*, 143 – 149.

[180] Tsuji, H.; Yamagata, K.-i.; Fujimoto, T.; Nakamura, E. *Journal of the American Chemical Society* **2008**, *130*, 7792–7793.

[181] Kuninobu, Y.; Nishi, M.; Yudha S., S.; Takai, K. *Organic Letters* **2008**, *10*, 3009–3011.

[182] Varela, J. A.; Saa, C. *Synlett* **2008**, *2008*, 2571–2578.

[183] Tekavec, T. N.; Louie, J. *The Journal of Organic Chemistry* **2008**, *73*, 2641–2648.

[184] Adak, L.; Chan, W. C.; Yoshikai, N. *Chemistry - An Asian Journal* **2011**, *6*, 359–362.

[185] Obora, Y.; Satoh, Y.; Ishii, Y. *The Journal of Organic Chemistry* **2010**, *75*, 6046–6049.

[186] GarcAa-RubAn, S.; Varela, J.; Castedo, L.; SaA, C. *Chemistry - A European Journal* **2008**, *14*, 9772–9778.

[187] Dalton, D. M.; Oberg, K. M.; Yu, R. T.; Lee, E. E.; Perreault, S.; Oinen, M. E.; Pease, M. L.; Malik, G.; Rovis, T. *Journal of the American Chemical Society* **2009**, *131*, 15717–15728.

[188] Lautens, M.; Klute, W.; Tam, W. *Chemical Reviews* **1996**, *96*, 49–92.

[189] Kreiter, C. G.; Koch, E.-C.; Frank, W.; Rei, G. *Inorganica Chimica Acta* **1994**, *220*, 77 – 83.

[190] Yu, R. T.; Lee, E. E.; Malik, G.; Rovis, T. *Angewandte Chemie International Edition* **2009**, *48*, 2379–2382.

[191] Onodera, G.; Shimizu, Y.; Kimura, J.-n.; Kobayashi, J.; Ebihara, Y.; Kondo, K.; Sakata, K.; Takeuchi, R. *Journal of the American Chemical Society* **2012**, *134*, 10515–10531.

[192] Kase, K.; Goswami, A.; Ohtaki, K.; Tanabe, E.; Saino, N.; Okamoto, S. *Organic Letters* **2007**, *9*, 931–934.

[193] Varela, J. A.; Saa, C. *Chemical Reviews* **2003**, *103*, 3787–3802.

[194] Newbound, T. D.; Colsman, M. R.; Miller, M. M.; Wulfsberg, G. P.; Anderson, O. P.; Strauss, S. H. *Journal of the American Chemical Society* **1989**, *111*, 3762–3764.

[195] Alvarez, A.; Macias, R.; Fabra, M. J.; Lahoz, F. J.; Oro, L. A. *Journal of the American Chemical Society* **2008**, *130*, 2148–2149.

[196] Rajnikant, M. B. D., Dinesh; Kamni, *Bulletin of Materials Science* **2006**, *29*, 239242.

[197] Li, H.-X.; Cheng, M.-L.; Wang, H.-M.; Yang, X.-J.; Ren, Z.-G.; Lang, J.-P. *Organometallics* **2011**, *30*, 208–214.

[198] Yoichiro Kuninobu, K. K.; Takai, K. *Chemistry Letters* **2008**, *37*, 740–741.

[199] Canovese, L.; Visentin, F.; Chessa, G.; Uguagliati, P.; Levi, C.; Dolmella, A. *Organometallics* **2005**, *24*, 5537–5548.

[200] Gabriele, B.; Salerno, G.; Mancuso, R.; Costa, M. *The Journal of Organic Chemistry* **2004**, *69*, 4741–4750.

[201] Wang, H.-M.; Li, H.-X.; Yu, X.-Y.; Ren, Z.-G.; Lang, J.-P. *Tetrahedron* **2011**, *67*, 1530 – 1535.

[202] Klanberg, F.; Wegner, P. A.; Parshall, G. W.; Muetterties, E. L. *Inorganic Chemistry* **1968**, *7*, 2072–2077.

[203] Macgregor, S. A.; Yellowlees, L. J.; Welch, A. J. *Acta Crystallographica Section C* **1990**, *46*, 551–554.

[204] Wesemann, L.; Ramjoie, Y.; Trinkaus, M.; Spaniol, T. P. *European Journal of Inorganic Chemistry* **1998**, *1998*, 1263–1268.

[205] Fontaine, X. L. R.; Fowkes, H.; Greenwood, N. N.; Kennedy, J. D.; Thornton-Pett, M. *J. Chem. Soc., Dalton Trans.* **1986**, 547–552.

[206] Fontaine, X. L. R.; Greenwood, N. N.; Kennedy, J. D.; MacKinnon, P.; Thornton-Pett, M. *J. Chem. Soc., Dalton Trans.* **1988**, 2809–2815.

[207] Czelusniak, I.; Kociecka, P.; Szymanska-Buzar, T. *Journal of Organometallic Chemistry* **2012**, *716*, 70 – 78.

[208] Hill, J. E.; Balaich, G.; Fanwick, P. E.; Rothwell, I. P. *Organometallics* **1993**, *12*, 2911–2924.

[209] Shibata, Y.; Tanaka, K. *Synthesis* **2012**, *44*, 323–350.

[210] Yan, H.; Beatty, A. M.; Fehlner, T. P. *Organometallics* **2002**, *21*, 5029–5037.

[211] Lin, Y.; Williams, T. V.; Connell, J. W. *The Journal of Physical Chemistry Letters* **2010**, *1*, 277–283.

[212] Golberg, D.; Bando, Y.; Huang, Y.; Terao, T.; Mitome, M.; Tang, C.; Zhi, C. *ACS Nano* **2010**, *4*, 2979–2993.

[213] Pakdel, A.; Wang, X.; Bando, Y.; Golberg, D. *Acta Materialia* **2013**, *61*, 1266 – 1273.

[214] Zhi, C.; Bando, Y.; Tang, C.; Kuwahara, H.; Golberg, D. *Advanced Materials* **2009**, *21*, 2889–2893.

[215] Wang, Y.; Shi, Z.; Yin, J. *J. Mater. Chem.* **2011**, *21*, 11371–11377.

[216] Yu, J.; Huang, X.; Wu, C.; Wu, X.; Wang, G.; Jiang, P. *Polymer* **2012**, *53*, 471 – 480.

[217] Xu, X.; Sun, B.; Berman, P. R.; Steel, D. G.; Bracker, A. S.; Gammon, D.; Sham, L. J. *Science* **2007**, *317*, 929–932.

[218] Golberg, D.; Bando, Y.; Tang, C.; Zhi, C. *Advanced Materials* **2007**, *19*, 2413–2432.

[219] Chen, W.; Li, Y.; Yu, G.; Li, C.-Z.; Zhang, S. B.; Zhou, Z.; Chen, Z. *Journal of the American Chemical Society* **2010**, *132*, 1699–1705.

[220] Corso, M.; Auwrter, W.; Muntwiler, M.; Tamai, A.; Greber, T.; Osterwalder, J. *Science* **2004**, *303*, 217–220.

[221] Ci, L.; Song, L.; Jin, C.; Jariwala, D.; Wu, D.; Li, Y.; Srivastava, A.; Wang, Z. F.; Storr, K.; Balicas, L.; Liu, F.; Ajayan, P. M. *Nat Mater* **2010**, *9*, 430–435.

[222] Coleman, J. N. et al. *Science* **2011**, *331*, 568–571.

[223] Lin, Y.; Williams, T. V.; Xu, T.-B.; Cao, W.; Elsayed-Ali, H. E.; Connell, J. W. *The Journal of Physical Chemistry C* **2011**, *115*, 2679–2685.

[224] Georgakilas, V.; Otyepka, M.; Bourlinos, A. B.; Chandra, V.; Kim, N.; Kemp, K. C.; Hobza, P.; Zboril, R.; Kim, K. S. *Chemical Reviews* **2012**, *112*, 6156–6214.

[225] Velayudham, S.; Lee, C. H.; Xie, M.; Blair, D.; Bauman, N.; Yap, Y. K.; Green, S. A.; Liu, H. *ACS Applied Materials & Interfaces* **2010**, *2*, 104–110.

[226] Sainsbury, T.; Satti, A.; May, P.; Wang, Z.; McGovern, I.; Gun??o, Y. K.; Coleman, J. *Journal of the American Chemical Society* **2012**, *134*, 18758–18771.

[227] Star, A.; Stoddart, J. F.; Steuerman, D.; Diehl, M.; Boukai, A.; Wong, E. W.; Yang, X.; Chung, S.-W.; Choi, H.; Heath, J. R. *Angewandte Chemie International Edition* **2001**, *40*, 1721–1725.

[228] Steuerman, D. W.; Star, A.; Narizzano, R.; Choi, H.; Ries, R. S.; Nicolini, C.; Stoddart, J. F.; Heath, J. R. *The Journal of Physical Chemistry B* **2002**, *106*, 3124–3130.

[229] Nasrabadi, A. T.; Foroutan, M. *The Journal of Physical Chemistry B* **2010**, *114*, 15429–15436.

[230] Tallury, S. S.; Pasquinelli, M. A. *The Journal of Physical Chemistry B* **2010**, *114*, 4122–4129.

[231] Tallury, S. S.; Pasquinelli, M. A. *The Journal of Physical Chemistry B* **2010**, *114*, 9349–9355.

[232] Bourlinos, A. B.; Georgakilas, V.; Zboril, R.; Steriotis, T. A.; Stubos, A. K.; Trapalis, C. *Solid State Communications* **2009**, *149*, 2172 – 2176.

[233] Fichou, D., Ed. *Handbook of Oligo- and Polythiophenes*; WILEY-VCH Verlag GmbH, 1999.

[234] Klaus Mllen, G. W., Ed. *Electronic Materials: The Oligomer Approach*; Wiley-VCH, 1998.

[235] Warnan, J.; Pellegrin, Y.; Blart, E.; Odobel, F.; Zhang, W.; Liu, B.; Babu, V. J.; Ramakrishna, S. *Macromolecular Rapid Communications* **2011**, *32*, 1190–1194.

[236] Yanagida, S.; Senadeera, G.; Nakamura, K.; Kitamura, T.; Wada, Y. *Journal of Photochemistry and Photobiology A: Chemistry* **2004**, *166*, 75 – 80.

[237] Kim,; Chen, L.; Gong,; Osada, Y. *Macromolecules* **1999**, *32*, 3964–3969.

[238] Xiaoming Sang, L. A. Y. L., Pengcheng Wang; Bu, J. *Advanced Materials Research* **2011**, *284-286*, 1846–1849.

[239] Englebienne, P.; Weiland, M. *Chem. Commun.* **1996**, *0*, 1651–1652.

[240] Klein, C.; Nazeeruddin, M. K.; Di Censo, D.; Liska, P.; Gratzel, M. *Inorganic Chemistry* **2004**, *43*, 4216–4226.

[241] Rose, A.; Tovar, J. D.; Yamaguchi, S.; Nesterov, E. E.; Zhu, Z.; Swager, T. M. *Philosophical Transactions of the Royal Society A: Mathematical, Physical and Engineering Sciences* **2007**, *365*, 1589–1606.

[242] Haiping Hao, J. S., Guangji Wang *Drug Metabolism Reviews* **2005**, *37*, 215234.

[243] Mao, X.; Su, H.; Tian, D.; Li, H.; Yang, R. *ACS Applied Materials & Interfaces* **2013**, *5*, 592–597.

[244] Appoh, F. E.; Kraatz, H.-B. *The Journal of Physical Chemistry C* **2007**, *111*, 4235–4245.

[245] Wang, Z.-S.; Hara, K.; Dan-oh, Y.; Kasada, C.; Shinpo, A.; Suga, S.; Arakawa, H.; Sugihara, H. *The Journal of Physical Chemistry B* **2005**, *109*, 3907–3914.

[246] Nazeeruddin, M. K.; Humphry-Baker, R.; Liska, P.; Gratzel, M. *The Journal of Physical Chemistry B* **2003**, *107*, 8981–8987.

[247] Duffy, N. W.; Dobson, K. D.; Gordon, K. C.; Robinson, B. H.; McQuillan, A. *Chemical Physics Letters* **1997**, *266*, 451 – 455.

[248] Nazeeruddin, M. K.; Humphry-Baker, R.; Officer, D. L.; Campbell, W. M.; Burrell, A. K.; Gratzel, M. *Langmuir* **2004**, *20*, 6514–6517.

[249] Chan, H. S. O.; Ng, S. C. *Progress in Polymer Science* **1998**, *23*, 1167 – 1231.

[250] G. K. R. Senadeera, K. S. L.-K. N. T. K. Y. W., Hantane Road; Yanagidaa., S. *Applied Physics Letters* **2003**, *83*, 5470.

[251] David Bilby, B. G. K.; Kim., J. *Pure Appl. Chem.* **2011**, *83*, 127–139.

[252] Ostrowski, D. P.; Lytwak, L. A.; Mejia, M. L.; Stevenson, K. J.; Holliday, B. J.; Vanden Bout, D. A. *ACS Nano* **2012**, *6*, 5507–5513.

[253] Dennler, G.; Scharber, M. C.; Brabec, C. J. *Advanced Materials* **2009**, *21*, 1323–1338.

Vita

NAME OF AUTHOR	Pei Ma
PLACE OF BIRTH	Danyang, Jiangsu Province, China
DATE OF BIRTH	February 22, 1986
GRADUATE AND UNDERGRADUATE SCHOOLS ATTENDED	Syracuse University, Syracuse, New York, USA. Tianjin University, Tianjin, China.
DEGREES AWARDED	Master of Science in Applied Statistics, 2013, Syracuse University. Bachelor of Science in Pharmaceutical Science, 2007, Tianjin University.
PROFESSIONAL EXPERIENCE	Graduate Research Assistant, Syracuse University, 2009-2013. Graduate Teaching Assistant, Syracuse University, 2008-2013.